ANTI-GONOCOCCAL ACTIVITY OF EXTRACTS FROM SELECTED NAMIBIAN MEDICINAL PLANTS AND COMPUTATIONAL STUDIES OF XERANTHOLIDE, A *NEISSERIA GONORRHOEAE* INHIBITOR

A DISSERTATION SUBMITTED IN FULFILMENT OF THE REQUIREMENTS

FOR THE DEGREE OF

DOCTOR OF PHILOSOPHY IN SCIENCE (MEDICINAL CHEMISTRY)

OF THE UNIVERSITY OF NAMIBIA

BY

MOOLA M. NYAMBE

200028170

APRIL 2023

Main Supervisor: Professor Kazhila C. Chinsembu (University of Namibia)

Co-supervisor: Associate Professor Edet F. Archibong (University of Namibia)

Co-supervisor: Professor Mamello Sekhoacha (University of the Free State, South Africa)

ABSTRACT

Neisseria gonorrhoeae, the causative agent of a sexually transmitted infection, gonorrhea, has developed resistance to all available antibiotics. It is found in humans only and if left untreated can lead to serious complications such as infertility and disseminated gonococcal infections. The search for new effective, affordable, and readily accessible drugs for the treatment of gonorrhea thus continues. Plants have been a good source of structurally diverse lead compounds from which drugs have been developed. Various communities in Namibia commonly use plants in traditional health care for the treatment of sexually transmitted infections (STIs). However, these plants have not yet been evaluated for their anti-gonococcal activity and human safety. Therefore, this study aimed to isolate compounds from plants that are traditionally used to treat gonorrhea, ascertain their anti-gonococcal activity, and elucidate the structures of these compounds in an effort towards searching for selective anti-gonococcal agents. Another aim was to employ computational approaches, including density functional theory (DFT), molecular docking, prediction of activity spectra for substances (PASS) and Quantitative Structure-Property Relationship (QSPR), to model the interaction of xerantholide and its analogues with the active site of *Neisseria gonorrhoeae* carbonic anhydrase (NgCA) and to investigate the geometry, electronic structure, and biological activity spectra.

Agar well diffusion and broth microdilution methods were used to determine the minimum inhibitory concentration (MIC) of extracts. Isolation and characterization of compounds were done using thin layer chromatography (TLC), column chromatography, x-ray diffraction and nuclear magnetic resonance (NMR). Crude extracts from six plants were

confirmed to have anti-gonococcal activity (MIC 2.5-5.0 mg/mL). Xerantholide, with an MIC_{50} = 0.095 mg/mL was isolated from *Pechuel-loeschea leubnitziae* leaves.

Molecular docking analysis revealed that xerantholide and its analogues docked with binding affinities ranging from -5.3 to -7.4 kcal/mol and DFT predicted binding energy of -16.5 to – 43.1 kcal/mol for these sesquiterpene lactones. Based on the docking results, binding of these compounds to NgCA involves hydrogen bonding, ligand-metal-acceptor, and hydrophobic interactions. Using QSPR, a six descriptors model with good predictive ability (R = 0.789, R^2 = 0.623, $AdjR^2$ = 0.578, BIC = 241, AIC = 225) was developed. Finally, a PASS analysis showed that these compounds are potential antibacterial agents. The results in this study suggest that the studied sesquiterpene lactones offer potential anti-gonococcal and inhibitory activity towards NgCA, thus further *in-vitro* studies are recommended.

LIST OF PUBLICATIONS AND CONFERENCE PROCEEDINGS

1. Nyambe, M.M, Archibong, E.F, M., and Chinsembu, K.C. (2022). A DFT and molecular docking study of xerantholide and its interaction with *Neisseria gonorrhoeae* carbonic anhydrase. Journal of Computational Biology and Chemistry. 107779
2. Nyambe, M.M, Archibong, E.F, Sekhoacha, M., and Chinsembu, K.C. (2022). *In-vitro* anti-gonorrheal activity of a sesquiterpene lactone, xerantholide isolated from the leaves of *Pechuel-loeschea leubnitziae*. South African Journal of Botany, 147: 314-318
3. Nyambe, M.M, Archibong, E.F, and Chinsembu, K.C. (2022). Quantitative structure property relationship study of plant-based *Neisseria gonorrhoeae* carbonic anhydrase inhibitor, xerantholide. 1st African Conference on Natural Products and related fields. Cape Peninsula University of Technology – Universidade Lusofona, 24-25 May 2022
4. Nyambe M.M., (2022). CHPC National Conference 2022. Democratisation of Cyber-Infrastructure for sustainable development. 30 Nov – 2 Dec – Gauteng, CSIR ICC/Online
5. Nyambe, M.M, Archibong, E.F, and Chinsembu, K.C. (2021). A density functional theory study of the interaction of xerantholide, an anti-gonococcal agent, with *Neisseria gonorrhoeae* carbonic anhydrase and human carbonic anhydrase II. The Annual Research Conference on Agriculture, Engineering and Natural sciences (ARCAENS), University of Namibia, November 2021
6. Nyambe, M.M, Hakwenye, H., A.K. Ekandjo, and Mukakalisa, C. (2019). Namibian plants for health and nutrition. 7th Science Annual Research Conference, University of Namibia, 13-14 November 2019.
7. Nyambe, M.M, Archibong, E.F, and Chinsembu, K.C. (2017). Characterization and quantitative structure-activity relationship (QSAR) studies of active compounds from selected Namibian medicinal plants used for the treatment of gonorrhea. 5th Annual Science Research Conference, Science today: Global bridge to the future, University of Namibia, November 2017.

TABLE OF CONTENTS

LIST OF TABLES

LIST OF FIGURES

LIST OF ABBREVIATIONS

AIC	Akaike information criterion
ANN	Artificial neutral network
B3LYP	Becke-3-Lee-Yang-Parr
BIC	Bayesian information criterion
CAIs	Carbonic anhydrase inhibitors
CAs	Carbonic anhydrases
CDC	Centre for Disease Control
CO_2	Carbon dioxide
DCM	Dichloromethane
DFT	Density functional theory
DGI	Disseminated gonococcal infection
DM	Dipole moment
DMSO	Dimethylsulfoxide
DNA	Deoxyribonucleic acid
GC	Gas chromatography
GP	Gonorrhea plant
GTO	Gaussian type orbital
HASL	Hypothetical active site lattice

HCO_3^-	Bicarbonate
HF	Hartree-Fock
HOMO	Highest occupied molecular orbitals
HPLC	High performance liquid chromatography
IM	Intramuscular
IR	Infra-red
IV	Intravenous
K_d	Dissociation constant
LMO	Leave many out
LOO	Leave one out
LUMO	Lowest unoccupied molecular orbitals
MD	Molecular dynamics
MeOH	methanol
MIC	Minimum inhibitory concentration
MM	Molecular mechanics
MLR	Multiple linear regression
MS	Mass spectroscopy
NAATs	Nucleic acid amplification tests
NCRST	National Commission on Research Science and Technology

NgCA	*Neisseria gonorrhoeae* carbonic anhydrase
NMR	Nuclear magnetic resonance
OD	Optical density
PASS	Prediction of activity spectrum for substances
PBPs	Penicillin binding proteins
PC	Paper chromatography
PCA	Principal component analysis
Pers. Com.	Personal communication
PID	Pelvic inflammatory disease
PMV	Python molecule viewer
PPNG	Penicillinase-producing *Neisseria gonorrhoeae*
PSA	Polar surface area
QM	Quantum mechanics
QSAR	Quantitative structure-activity relationship
QSPR	Quantitative structure-property relationship
R^2	Correlation coefficient
RNA	Ribonucleic acid
RPM	Rounds per minute
RT	Room temperature

SCF	Self-consistent field
SLs	Sesquiterpene lactones
STIs	Sexually transmitted infections
STO	Slater type orbital
TLC	Thin layer chromatography
TMA	Thayer Martin agar
TMPs	Traditional medicinal practitioners
UV	Ultraviolet
VIF	Variance inflation factor
WHO	World Health Organization
ΔG°	Change in Gibbs free energy

ACKNOWLEDGEMENTS

Jehovah God gave me life, strength, knowledge, and wisdom to be able to complete this project (Proverbs 1:1-9). This study would not have been possible without the financial support from the University of Namibia (Department of Physic, Chemistry and Material Science). I would like to thank my supervisor, Prof K.C Chinsembu for his guidance and support throughout my studies. The encouragements and advice he gave me to keep going despite the challenges helped me to be where I am now. Thank you. I would like to express my gratitude and thanks to Prof E.F. Archibong for teaching me what I know about computational chemistry. I benefited from your patience and immense knowledge and valuable guidance on the wet and computational chemistry work. I appreciate the encouragements too. Prof M. Sekhoacha for the direction and guidance in all the work related to medicinal chemistry in general and the help I received in all my writings throughout my study.

A great thanks goes to the following people for practically helping me in the lab: Klementine K. Kapikara, Dr Jean D. Uzabakiriho, Dr Celine Mukakalisa, Dr Xavier Siwe Noundou, Dr Stefan Louw, Dr Hong Su, Mr Song Wei, Johannes Naimhwaka and Ndapewa Namundjembo. Thanks to research students who worked with me in the lab: Monika Haufiku, Luiise Nghimbwasha, Domingo Kasanga. I am thankful for the emotional support and various kinds of help I got in this work from my friends and acquaintances: Diana Mugaviri, Gracious Masara, Anna Nuugulu, Hilaria Hakwenye, Salatiel Kapofi, David Nanhapo, Prof Petrina Kapewangolo-Nepolo, Dr Celestine Raidron, Dr Ezekiel Kwembeya, Prof Pauline Kadhila. Lastly, thanks go to my family (Nyambe family, Sinkela family and Sangwali-Mbwe family).

DEDICATION

This dissertation is dedicated to my husband Simataa Nyambe and our lovely children (Nasilele, Mukaya and Zayapo), the dearest people to my heart, you mean the world to me. I thank Jehovah for having you to continue giving me the joy through all that we do together. You always motivate me to remember my life's real purpose. I love you.

In memory of my beloved mother (Anna Mbwe-Sinkela): A person whose love, kindness and generosity can never be forgotten. I value and treasure all the life lessons you imparted in me. My grandfather (Mofat Sangwali Mbwe) who contributed to this work in a large way through his immense knowledge of medicinal plants and indigenous knowledge. A large library was lost with your death "Shikura mutwe" as we would call you. I truly loved them and miss them dearly.

DECLARATION

I, Moola M. Nyambe, hereby declare that this study is my own work and is a true reflection of my research, and that this work, or any part thereof has not been submitted for a degree at any other institution. No part of this dissertation may be reproduced, stored in any retrieval system, or transmitted in any form, or by means (e.g. electronic, mechanical, photocopying, recording or otherwise) without the prior permission of the author, or The University of Namibia in that behalf.

I, Moola M. Nyambe, grant The University of Namibia the right to reproduce this dissertation in whole or in part, in any manner or format, which The University of Namibia may deem fit.

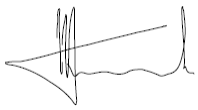

Moola M. Nyambe…	……	……..	03 April 2023...
Name of Student	Signature		Date

CHAPTER 1: INTRODUCTION

1.1 Background of the study

Sexually Transmitted Infections (STIs) are prevalent throughout the world. A report by the World Health Organization (WHO) estimates that some 340 million new cases of curable STIs occur every year worldwide (1). Such a large number of STIs has a strong negative impact on the well-being of the society, including being a cause for acute illness, infertility, long term disability, severe psychological morbidity, and death. The Global Health Data Exchange reported that STIs excluding HIV were one of the three most deadly communicable diseases in Namibia during 2013 (1). Of all STIs, gonorrhea is the second most prevalent bacterial infection worldwide, but it is the least discussed health hazard by society, due to the social stigma associated with STIs (2,3). Gonorrhea is found in humans only and is transmitted by human-to-human contact.

Even though there are antibiotics such as cefixime (oral) and ceftriaxone (injectable) available for the treatment of gonorrhea, studies have shown that *Neisseria gonorrhoeae* has developed resistance to antibiotics that are used as first-line treatments (4–6). The bacterium is also resistant to multiple other standard antibiotics. This resistance is attributed to the worldwide spread of the penicillinase-producing *Neisseria gonorrhoeae* (PPNG) isolates (7,8). The resistance is also as a result of *N. gonorrhoeae*'s ability to change or destroy the antibiotics through production of other enzymes or proteins that break down the drug or alter the receptor targeted by the drug. It also has adaptable antigenic variability which allows it to escape host defences thus persisting and often causing asymptomatic infections. To date, no vaccine is available for gonorrhea. Effective condom use and testing of patients before engaging in sexual activities are currently the

best ways of preventing the spread of the bacteria, since treatment is increasingly becoming ineffective. With such a high rate of resistance by *N. gonorrhoeae* to available drugs, there is a need for a drug that is well tolerated, effective and affordable.

Since plants are commonly used in traditional health care for the treatment of STIs in Namibia, it is possible that these plants contain compounds that are active against gonorrhea, thus making them potential sources of novel compounds for the development anti-gonorrhea drugs. The chemical constituents of such plants need to be studied and their ethnomedicinal uses validated to encourage their use in communities. Additionally, as part of the continuous efforts to solve the problems of antibiotic resistance, at present there are research efforts that focus on the development of drugs that can inhibit or disrupt enzyme processes (9,10). One such line of study is geared towards inhibition of *Neisseria gonorrhoeae* carbonic anhydrase (NgCA), paving the way for the development of potential inhibitors. NgCA is targeted because it plays an important role in the survival of *N. gonorrhoeae* in the host cell as a catalyst for enzymatic activity of carbon dioxide hydration which is essential to meet the metabolic needs of the bacteria (11). Inhibition of NgCA thus disrupt the life cycle of the bacteria.

Computational chemistry is playing an important role in drug screening, design and development, providing deeper insight into the binding mode of new drug molecules with the target receptors. Several computer-aided drug development (CADD) methods are being applied to accelerate the process of drug discovery and cut on cost by reducing wet-lab experiments. The virtual screening technology which encompasses methods such as molecular docking, molecular dynamics simulation, pharmacophore modelling and

quantitative structure-activity/property relationship (QSAR/QSPR) studies are widely used in the field of drug discovery (12, 13). For example, molecular docking is commonly used in structure-based studies to determine the extent and types of interaction between a ligand (drug molecule) with the protein or enzyme receptors. Thus, it identifies correct conformations of both the ligand and the receptor and use a scoring function that correctly ranks candidate compounds that give high binding affinity. QSAR/QSPR studies are very useful to understand the mechanism of action and structure-activity relationship of compounds. QSAR/QSPR approach also has added advantages in that it can reduce the number of animal tests necessary in the assessment of chemical substances, reduce cost of product development and save time (14).

1.2 Problem statement

Although a variety of plants in Namibia have been used traditionally in the treatment of gonorrhea, the plants under study have not yet been evaluated for their anti-gonococcal activity, and human safety. This lack of scientific data impacts negatively on the effort to discover and develop new, cheaper, and more efficacious drugs against gonorrhea. To our knowledge, none of the selected plants have been investigated for their effects against *N. gonorrhoeae*. No computational studies to predict activities of potential drug compounds isolated from Namibian plants used for the treatment of gonorrhea have been conducted. Consequently, the potential of these plants as sources of effective drugs has not been explored fully. It is therefore important that the selected plants be screened for activity, the phytochemical constituents responsible for their antimicrobial activity be isolated, tested

for biological activity and subjected to computational studies, with the aim of discovering potent drug molecules that can be used to manage or treat gonorrhea.

1.3 Objectives of the study

This study aims to contribute to the discovery of drugs from natural products and identification of scaffolds that can be used as templates in the development of anti-infectious agents. The specific objectives of this study are:

a) To do antimicrobial activity screening of crude extracts from 13 selected plant species that are used for the treatment of gonorrhea in Namibia.
b) To isolate and characterize bioactive compounds from extracts that show activity against *N. gonorrhoeae*.
c) To use density functional theory (DFT) method to study the geometry and electronic structure of xerantholide as this compound showed anti-gonococcal activity.
d) To study the interaction of xerantholide and its analogues with *N. gonorrhoeae* carbonic anhydrase via molecular docking and modelling of the active site of NgCA using Zn-tris (imidazole) complex.
e) To develop QSPR models that relate interaction energy with specific descriptors.

1.4 Significance of the study

The chemical analysis of the extracts from selected medicinal plants will contribute to the understanding of the medicinal properties associated with these plants. This will not only encourage the continued use of these plants for management and/or treatment of gonorrhea

but will also pave the way to design and develop new therapeutic agents that are effective, accessible, and affordable. Since natural products have been a source of structurally diverse nucleoside antibiotics, computational studies on compounds isolated from plants associated with gonorrhea could lead to promising scaffolds.

1.5 References

1. World Health Organization. Namibia: State of the Nation's Health Findings from the Global Burden of Disease. Seattle, WA: IHME: Institute for Health Metrics and Evaluation (IHME). 2016: 52 p.

2. Unemo M, Shafer WM. Antimicrobial resistance in *Neisseria gonorrhoeae* in the 21st Century: Past, evolution, and future. Clin Microbiol Rev. 2014;27(3):587–613.

3. Frost DM, Parsons JT, Nanín JE. Stigma, concealment and symptoms of depression as explanations for sexually transmitted infections among gay men. J Health Psychol. 2007;12(4):636–40.

4. Dowell D, Kirkcaldy RD. Effectiveness of gentamicin for gonorrhoea treatment : systematic review and meta- analysis. Sex Trans Infect. 2012;0:1-6.

5. Ekdahl K. Change of guard in Eurosurveillance. Euro Surveill. 2011;16(14):pii=19835.

6. Unemo M, Golparian D, Stary A, Eigentler A. First *Neisseria gonorrhoeae* strain with resistance to cefixime causing gonorrhoea treatment failure in Austria. Euro Surveill. 2011;16(43):19998.

7. Wi T, Lahra MM, Ndowa F, Bala M, Dillon JAR, Ramon-Pardo P, et al. Antimicrobial resistance in *Neisseria gonorrhoeae*: Global surveillance and a call for international collaborative action. PLoS Med. 2017;14(7):1–16.

8. Knapp JS, Ohye R, Neal SW, Parekh MC, Higa H, Rice RJ. Emerging *in-vitro* resistance to quinolones in penicillinase-producing *Neisseria gonorrhoeae* strains in Hawaii. Antimicrob Agents Chemother. 1994;38(9):2200–3.

9. Hewitt CS, Abutaleb NS, Elhassanny AEM, Nocentini A, Cao X, Amos DP, et al. Structure-activity relationship studies of acetazolamide-based carbonic anhydrase inhibitors with activity against *Neisseria gonorrhoeae*. ACS Infect Dis. 2021;

10. Nocentini A, Hewitt CS, Mastrolorenzo MD, Flaherty DP, Supuran CT. Anion inhibition studies of the α-carbonic anhydrases from *Neisseria gonorrhoeae*. J Enzyme Inhib Med Chem. 2021;36(1):1061–6.

11. Angeli A, Carta F, Supuran CT. Carbonic anhydrases: Versatile and useful biocatalysts in chemistry and biochemistry. Catalysts. 2020;10(9):1–11.

12. Lin X, Li X, Lin X. A review on applications of computational methods in drug screening and design. Molecules. 2020;25(6):1–17.

13. Jorgensen WL. The Many Roles of Computation in Drug Discovery. Science (80-). 2004;303(5665):1813–8.

14. Patrick GL. An introdcution to medicinal chemistry. 5th ed. Oxford University Press; 2013.

CHAPTER 2: LITERATURE REVIEW

2.1 Gonorrhea

Gonorrhea is a STI caused by a Gram-negative, non-motile, aerobic, non-sporulating, diplococcus bacterium *Neisseria gonorrhoeae* (Figure 2.1) which usually colonizes the host with or without clinically evident infection (1). Urogenital tract infections are most common (1,2). It is found in humans only (3) and primarily transmitted via vaginal, anal, and oral sex in sexually active people, and there seem to be more efficient transmission from males to females. It can also be transmitted from mother to baby during vaginal childbirth if the mother has an untreated infection. *N. gonorrhoeae* is fastidious in its growth requirement; it survives poorly out of the body, is susceptible to temperature changes and UV-light, and does not survive drying (4). Any sexually active person can contract gonorrhea, but certain people have a higher risk of developing gonorrhea, such as people with multiple sex partners, sex workers, people who have sex without protection, men having sex with other men (MSM), teenagers, and young adults (5).

Diagnosis of this STI is usually by identification of the causative agent *N. gonorrhoeae* at an infected site either by culture or by nucleic acid amplification tests (NAATs) (3). Culture diagnosis is however not reliable as it is affected by the sampling, sample transportation from site to the facility, and handling conditions such as the amount of time between sampling and testing, as well as storage temperature which affects the viability of the bacteria. It can also be diagnosed by Gram stain method in men with urethritis as a cheaper alternative to NAATs. In many countries where laboratory resources are not available,

clinical diagnosis is often done by looking at the symptoms such as vaginal and urethral discharge (6).

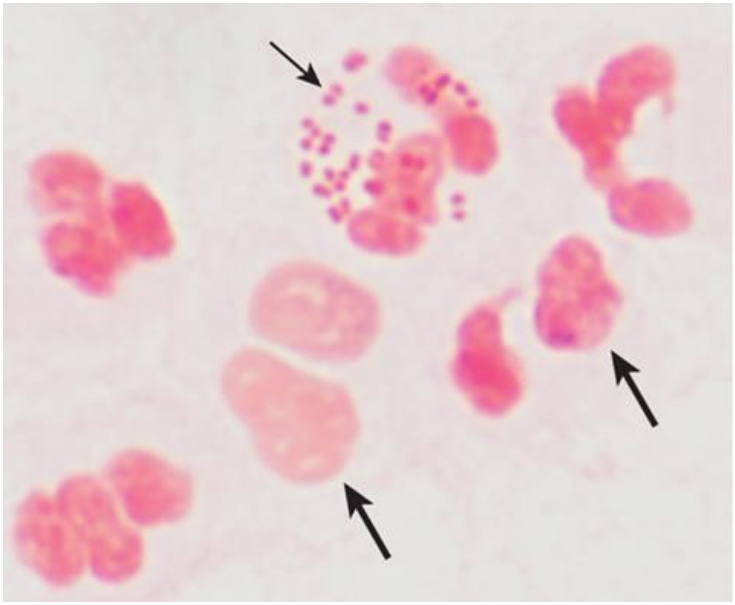

Figure 2.1. Gram-stain of a urethral exudate of a patient with gonorrhea. Nuclei of many polymorphonuclear cells are seen (*large arrows*).

Intracellular gram-negative diplococci *(Neisseria gonorrhoeae*) in one polymorphonuclear cell are marked by the *small arrow*. Adopted from: (7) www.accessmedicine.com

The symptoms and signs of gonorrhea vary depending on the site of infection and the sexual lifestyle of the patient. A high proportion of infections, in women are asymptomatic. The infection may be in the endocervix, Bartholin glands, Skene ducts, vagina, rectum, or pharynx with cervicitis being the most common manifestation (1). Symptoms in women include abnormal vaginal discharge, bleeding between periods, abdominal pain, burning or painful urination and pain during sexual intercourse. About 10 to 20% of untreated case cause pelvic inflammatory disease (PID) in women. Men with gonorrhea are usually symptomatic but at least 10% of men with urethral infections do not show any symptoms.

When symptoms occur, they may appear 2-5 days after infection but may take up to a month to appear. Discharge with dysuria is a common symptom that usually develops 3-10 days after exposure in men with urethral infections. This period can be longer in up to 15% of patients, while many remain asymptomatic. About 95% of untreated symptoms resolve within 6 months but these patients can remain infectious for many months (1,4,8). Rectal infections in both men and women may cause rectal pain, anal itching, anal pain or bloody discharge, constipation, painful bowel movement or tenesmus but are often asymptomatic (8). Anorectal gonorrhea is more prevalent in men who have sex with other men. Rectal gonorrhea in homosexual men is considered indicative of unprotected receptive anal intercourse and is a marker of risk for transmission of other STIs including HIV (9). In women, rectal infection can occur in the absence of anal intercourse (4).

Pharyngeal gonococcal infection also known as oral gonorrhea is another common type of infection in homosexual men but also occurs in all adults. This infection is acquired through direct contact of the oral mucus membrane with discharge containing the *N. gonorrhoeae* bacterium. Transmission is thought to be more efficient through oral-penile contact than oral-vaginal contact (5). Pharyngeal gonorrhea is usually asymptomatic, but can cause symptoms of sore throat, discomfort when swallowing food, fever and tender cervical adenopathy. Purulent conjunctival discharge as a result of autoinoculation can occur in adults with pharyngeal infection. Physical examination may reveal oropharyngeal erythema and exudates. These symptoms are the same for men and women and usually occur a few days after contact. Oral gonorrhea is usually not transmitted via kissing as the bacteria does not infect the tongue or mouth (1,4).

2.1.1 Global epidemiology of gonorrhea

WHO estimated that 78 million new cases of gonorrhea occurred worldwide annually among adolescents and adults aged 15-49 years (10). The highest prevalence is in the WHO African region (1.9%), followed by the region of the Americas (0.9%) and Western Pacific region (0.9%), and lowest in the European region (0.3%). Many factors contribute to the observed differences in prevalence of gonorrhea in these regions, such as availability of healthcare infrastructure, available health care system which cares for screening and treatment, as well as sexual behaviour. Of the 30.6 million global prevalent cases of gonorrhea in 2016, 0.9% is among females and 0.7% among males aged 15–49 years. A pooled prevalence across studies globally, showed that the age group 15-24 years old were of high risk with South Africa and East Africa reporting 4.6% and 8.2% respectively (11). This could be an underestimation as the infection can be both symptomatic and asymptomatic, thus under detection and underreporting is most likely. WHO set a global target of 90% reduction in gonorrhea infection epidemics by 2030 through the Global Health Sector Strategy on STIs 2016-2021. As part of a way to achieve this goal, they have suggested priority actions for countries which include strengthening laboratory capacity, strengthening and/or integrating STI surveillance into the national health information system, identifying populations who are at high risk as well as places where most transmission occurs (12). The actions aim to strengthen the scale of prevention, diagnosis, treatment and care.

2.1.2 Epidemiology of gonorrhea in Africa

The prevalence of gonorrhea in Africa is poorly documented, thus no reliable statistics for the region are available. As a result, many cases remain undiagnosed, unreported and unaccounted for. This lack of data poses a health challenge. Despite those limitations, available data indicates that the African region has the highest rates of gonorrhea infections in the world with high prevalence among youth aged 15-24 years (10). Data that was extracted from several reports on the prevalence of gonorrhea in 16 African countries (Benin, Burkina Faso, Cameroon, Central Republic of Africa, Ethiopia, Ghana, Guinea, Kenya, Madagascar, Mali, Nigeria, South Africa, Sudan, Tunisia, Zambia and Zimbabwe), involving 15734 participants, reported 7.9% prevalence in the study area (13). In South Africa and Southern/Eastern Africa, prevalence of 4.6% and 1.7% respectively, was reported among 15–24-year-olds (14). Moreover, the number of African countries participating in the WHO Gonococcal Antimicrobial Surveillance Programme (GASP) is very low. More effort must be put into monitoring and controlling the spread of gonorrhea infections in Africa.

2.1.3 Epidemiology of gonorrhea in Namibia

In Namibia, the national epidemiological data on gonorrhea infections is not available. STIs in general have been reported to remain a major challenge because of their involvement as co-factor in HIV transmission. STIs prevalence across regions ranged from 3 % in Omusati region to 19 % in Omaheke region of which over 60% reported having sought medical advice or treatment while 29% did not seek any treatment (15). Statistics for STIs may not be accurate especially in rural areas, as those who are infected may not

relate this illness to doctors, while others are asymptomatic. Other factors that contribute to scarcity of data include lack of reporting mechanisms even when diagnosis is done, inadequate facilities for laboratory-based diagnosis, lack of information capturing database and lack of education to increase awareness of the problem in communities. The paucity of data on gonorrhea infections can lead to underestimation of the disease's effects rendering the problem unimportant, leading to reduction in resource allocation that can help in the control and management of the disease as well as monitoring the progress and success of intervention programmes.

A study by Hazel and colleagues in 2014 (16) highlights that *N. gonorrhoeae* infections are very common in the Kunene region affecting 64% of screened participants. Gonorrhea is reported to be one of three bacterial infections with the second highest prevalence of genital infections among HIV-infected adults in Khomas region (16). This study also report that the rate of infections is significantly higher in women compared to men, while Shivute and colleagues (17) observed the opposite in their study with most infections being in men (14.5%) than in women (11.6%) (17). Their study represented 12 regions of Namibia and reported gonorrhea prevalence of 4.3% among 465 patients within the age group of 15-49 years. Consistently across all the regions, majority of infections were among young adults under the age of 34 years and ages of 15-19 years made up 9.1 % of the infections. In this study, age group 35-49 did not test positive for gonorrhea. This could be due to a small population size of the study. Males were more affected than females in seven regions: Erongo, Kavango East, Khomas, Ohangwena, Zambezi, Karas and Hardap. To overcome the problem of lack of epidemiological data in Namibia, more effort is required from

national health services in both public and private health facilities as well as from communities whose involvement is crucial to document accurate incidence and prevalence data on gonorrhea. National and regional surveillance programs which can involve studies of gonorrhea transmission and treatment success and failure, can be introduced.

2.1.4 Complications of gonorrhea

Infants of mothers with gonococcal infection can contract gonorrhea at delivery, and this can result in neonatal conjunctivitis, which may lead to blindness if left untreated. Sepsis, meningitis and arthritis are the most common severe complications that can occur in neonates with few cases of pharyngitis, rhinitis, vaginitis, urethritis and pneumonia (1).

Since gonococcal infection is often asymptomatic in women, it usually results in unrecognized and untreated infections that although usually resolve spontaneously, often lead to serious complications such as PID, inflammation of the bladder, ectopic pregnancy, miscarriage, infertility, and even maternal death. PID is the main cause of infertility associated with gonorrhea infection that results from tubal scarring. Complications in men include prostate inflammation, testicular and scrotal pain, scarred and narrowed urethra which may lead to epididymitis and infertility. *N. gonorrhoeae* infection is also linked to increased susceptibility to HIV. Many of these complications bring about cultural and social implications. There are few studies (5,7) that demonstrate association between *N. gonorrhoeae* and male infertility. Untreated urethral infection in men can lead to epididymitis, urethral stricture, and infertility. Repeated infections increase the risk of complications, whereas early recognition and prompt treatment can prevent complications, reinfection, and transmission of partner (12).

N. gonorrhoeae can spread into the bloodstream resulting in disseminated gonococcal infection (DGI). This is a rare but important complication of mucosal infection that occurs in about 0.4-3% of patients with gonorrhea infection. DGI can develop within 2 to 3 weeks of contracting gonorrhea causing more symptoms including fever or chills, multiple skin lesions including painless or painful petechiae with or without pus and skin discoloration, malaise, joint pains and swelling. These symptoms occur in over 70% of patients with DGI (1,18). Other clinical manifestations that are most common with DGI are syndromes, such gonococcal arthritis and syndromes of tenosynovitis, dermatitis and polyarthralgia without purulent joint infection (19,20). Gonococcal arthritis, that results from DGI causes rashes and inflammation of the joints. Gonococcal endocarditis, can cause damage to the inner lining of the heart muscle, while gonococcal meningitis affects the membranes covering the brain and spinal cord (18). This infection thus affects various tissues and can cause permanent damage. Joints commonly affected include wrists, ankles, hands and feet. DGI is difficult to diagnose as in most cases cultures of synovial fluid and skin lesions test negative while the blood cultures may test positive in patients who present with dermatitis, tenosynovitis or polyarthralgia syndrome (18).

Unlike strains isolated from uncomplicated gonococcal infections, *N. gonorrhoeae* strains that cause DGI are said to be sensitive to penicillin G and tetracycline. It is most common in young women below 40 years than in men but can develop in sexually active persons of any age (18). Asymptomatic mucosal infection is much more likely to results in DGI than symptomatic infections which explains in part, why DGI is more common in women where endocervical gonorrhea may persist without symptoms for extended periods. The epidemiology of DGI is said to be among people of lower socioeconomic status, men who

have sex with men, those with multiple sexual partners and illicit drug users. Other factors that increase the risk of DGI in women with endocervical gonorrhea are: menstruation, pregnancy, the direct postpartum period, compliment deficiencies and systemic lupus erythematosus (20).

2.1.5 Association between gonorrhea and other STIs

Those infected with *N. gonorrhoeae* are at risk for other STIs. Co-infection with *Chlamydia trachomatis* is reported to be detected in 10–40% of people with gonorrhea (12). Due to this common occurrence of co-infection, the CDC treatment guidelines recommend a combination treatment of gonorrhea that includes an antimicrobial agent effective against chlamydia. A study by Mimiaga and colleagues (21) reported that rectal gonorrhea and ulcerated STIs such as syphilis are frequently diagnosed in persons with high-risk sexual exposure and most commonly among men (21). There is a high association between gonorrhea and HIV transmission and acquisition. The increased risk of HIV-gonorrhea coinfection transmission is possibly due to increased viral load in semen or cervico-vaginal fluids and possibly increased CD4 lymphocytes (22). About 16% of tested homosexual HIV positive men in that study were also diagnosed with urethral gonorrhea compared to 12% in HIV uninfected homosexual men. Coinfection with pharyngeal gonorrhea is common in women with cervical gonorrhea and patients with HIV infection (1). Other minor co-infections include *Candida albicans*, *Trichomonas vaginalis*, chancroid, bacterial vaginosis, and herpes (23).

2.1.6 Management of gonorrhea

Over the years, several antibiotics have been developed and used to treat gonorrhea. Initially, *N. gonorrhoeae* was highly susceptible to many antimicrobial agents, but has for the past 70-80 years, shown capacity to develop resistance to all antimicrobial agents introduced for treatment (24,25) . Different studies have suggested many potential virulence factors for *N. gonorrhoeae*, many of them are cell surface proteins that influence pathogenesis and their ability to disseminate from infected mucosa. The presence of pili also enhances bacterial attachment to mucosal and synovial epithelium. Various antibiotics, including β-lactams, cephalosporins, tetracyclines, sulfonamides, and quinolines that target cell membrane, protein (enzyme, receptor) and nucleic acid (DNA, RNA) biosynthesis have thus been used to treat gonorrhea (25–27). The current first line drugs, cefixime and ceftriaxone (Figure 2.2) for treating gonorrhea are both cephalosporins, a type of β-lactam antibiotics, in the same class as penicillin. Other derivatives of cephalosporins that are used for gonorrhea but are not recommended, include; cefuroxime, cefpodoxime, cefoxitin, ceftibuten, cefditoren and celdinir (28). These compounds inhibit the peptidoglycan cross-links in the bacterial cell wall by binding to the major penicillin binding proteins (PBPs) of *N. gonorrhoeae*. Penicillinase-Producing *Neisseria gonorrhoeae* (PPNG) isolates have plasmids that produce β-lactamase, an enzyme which plays a role is the mutation of the bacteria, thereby causing resistance to β-lactam antibiotics. Other drugs that have been reported to be used for the treatment of cephalosporin-resistant infections are azithromycin and erythromycin. These are macrolides that inhibit the protein synthesis thereby causing alterations of ribosomal target (28).

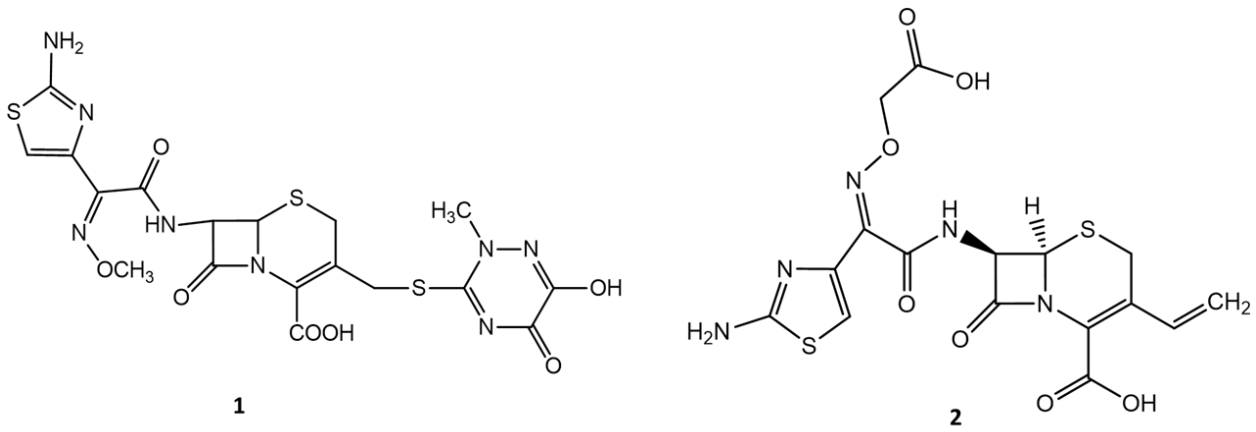

Figure 2.2. Structures of compounds that are *Neisseria gonorrhoeae* inhibitors ceftriaxone (1) and cefixime (2) drawn using ChemDraw

Fluoroquinolones (ciprofloxacin, ofloxacin) is another class of compounds that inhibit *N. gonorrhoeae* through mutation of the enzymes of DNA gyrase (gyrA) and topoisomerase IV (parC) which stops DNA replication (25). Other antimicrobials previously used for treatment are tetracycline, gentamicin, and spectinomycin (29). There is a growing number of failure for gonorrhea treatment reported by various studies (Figure 2.3) (2,30–32). These failures are due to the rapidly changing antimicrobial susceptibility patterns of *N. gonorrhoeae*. Statistics provided by the Word Health Organization's Global Gonococcal Antimicrobial Surveillance Programme (WHO GASP), identified clinical strains of *N. gonorrhoeae* that are resistant to most available antibiotics. As a result, the recommendations for the treatment of gonorrhea are frequently changing (33).

Currently, the recommended treatment of uncomplicated urogenital, anorectal, or pharyngeal gonorrhea is combination therapy of intramuscular (IM) single dose of ceftriaxone (250 mg) with either azithromycin (1 g) oral single dose or doxycycline (100 mg) orally twice daily for 7 days. In the case where ceftriaxone is unavailable, the

alternative treatment regime is with a single dose of cefixime orally with a single dose of azithromycin (1g) orally or doxycycline (100mg) orally twice daily for 7 days. For patients with severe cephalosporin allergy, azithromycin (2 g) in a single oral dose is recommended, followed by a test of cure in one week. For DGI, hospitalization is recommended where ceftriaxone (1 g) IM or IV is given every 24 hours up to 48 hours after improvement begins. Alternatively, 1 g cefotaxime IV or 1 g ceftizoxime IV every 8 hours up to 48 hours after improvement begins after which the patient is switched to cefixime (400 mg) orally twice per day for at at least one week of total antimicrobial treatment (1,8). Other treatments of gonococcal infections are shown in Table 2.1. It is also recommended that patients' sex partners be treated within 60 days. Pharyngeal infections have been reported to be difficult compared to other infections where treatment is not sufficiently effective with lower dose of ceftriaxone.

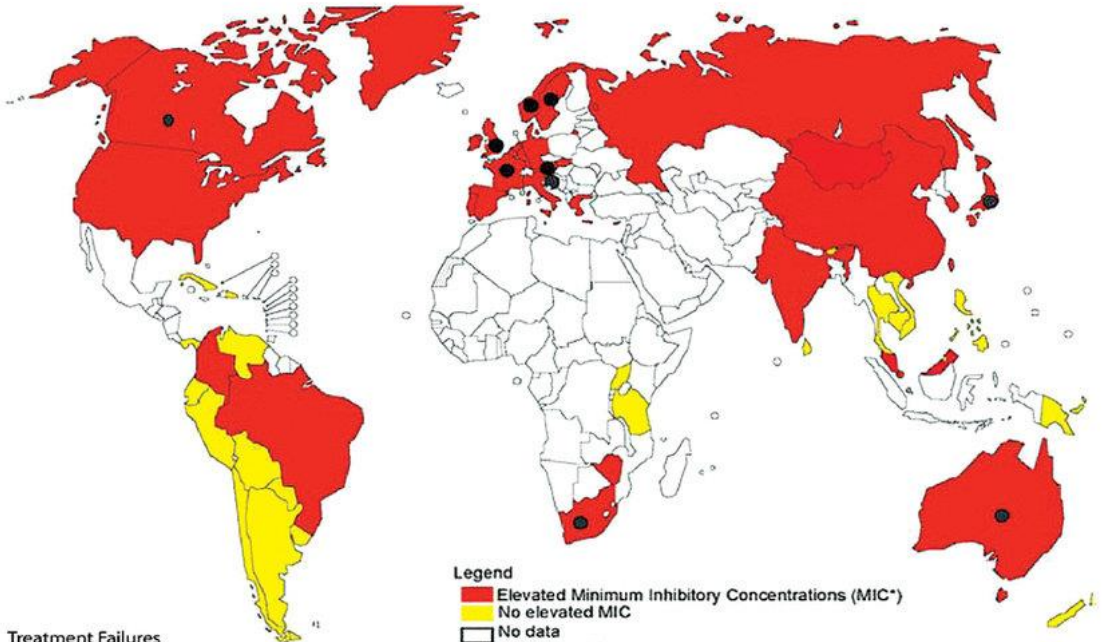

Treatment Failures

Country	Cefixime	Ceftriaxone
Japan	+	+
Norway	+	NV/ND
UK	+	NV/ND
France	+	NV/ND
Austria	+	NV/ND
Australia	NV/ND	+
Slovenia	NV/ND	+
Sweden	NV/ND	+
South Africa	+	NV/ND
Canada	+	NV/ND

Figure 2.3. Global map of reported resistance and treatment failures to extended spectrum cephalosporins. Modification of figure from WHO (26)

Table 2.1 Recommended treatment regimes for *Neisseria gonorrhoeae* infections.

Infection	**Recommended regime**
Urethral, cervical, rectal infection (adults and children > 45 kg)	Ceftriaxone (250 mg) in a single IM dose plus Azithromycin (1 g) orally in a single dose, or doxycycline (100 mg) orally twice per day for 7 days If ceftriaxone is not available, use cefixime (400 mg) orally in a single dose plus Azithromycin (1 g) orally in a single dose, or doxycycline (100 mg) orally twice per day for 7 days plus Test of cure in one week For patients with severe cephalosporin allergy, use azithromycin (2 g) orally in a single dose plus Test of cure in one week
Pharyngeal infection	Ceftriaxone (250 mg) in a single IM dose plus Azithromycin (1 g) orally in a single dose, or doxycycline (100 mg) orally twice per day for 7 days
Pharyngeal infection (children ≤45 kg)	Ceftriaxone (125 mg) IM in a single dose
Pregnant patients	Ceftriaxone (250 mg) IM in a single dose For patients with penicillin allergy, use azithromycin (2 g) orally in a single dose
Conjunctivitis	Ceftriaxone (1 g) IM in a single dose
Ophthalmia neonatorum and Infants born to mother with untreated gonorrhea with no signs of infection	Ceftriaxone (25 to 50 mg) per kg IV or IM in a single dose, not to exceed 125 mg
Meningitis	Ceftriaxone (1 to 2 g) IV every 12 hours for 10 to 14 days
Meningitis (Neonatal)	Ceftriaxone (25 to 50 mg) per kg IV or IM per day for 10 to 14 days or Cefotaxime (25 mg) per kg IV or IM every 12 hours for 10 to 14 days
Gonococcal endocarditis	Ceftriaxone (1 to 2 g) IV every 12 hours for at least 4 weeks
Disseminated gonococcal infection (hospitalization recommended)	Ceftriaxone (1 g) IM or IV every 24 hours until 24 to 48 hours after improvement begins or Cefotaxime (1 g) IV every 8 hours until 24 to 48 hours after improvement begins or Ceftizoxime (1 g) IV every 8 hours until 24 to 48 hours after improvement begins 24 to 48 hours after improvement begins, switch to cefixime (400 mg) orally twice per day, for at least one week of total antimicrobial treatment
Neonatal disseminated gonococcal infection or scalp abscess	Ceftriaxone (25 to 50 mg) per kg IV or IM per day for 7 days or Cefotaxime (25 mg) per kg IV or IM every 12 hours for 7 days

Reference: (1,8), IM = Intramuscular; IV = Intravenous

2.2 Medicinal plants used for the treatment of gonorrhea

Many plant species have been identified and are being used in the traditional systems of medicine because of their perceived medicinal properties. WHO recognize medicinal plants as an alternative in the treatment of various diseases (34). Various communities, thus recognize traditional therapeutic value of plants to treat microbial infections. They use plant extracts to relieve and treat infectious diseases including STIs. A plant is said to be medicinal if it produces active compounds, usually secondary metabolites, which are therapeutically effective and can also be used to promote general health and well-being (35). These active compounds are usually derived from the plant's secondary metabolites which have been shown to be rich sources of antimicrobial agents. An antimicrobial agent is defined as a substance that kills or inhibits the growth or prevents damage due to the action of infectious microorganisms (36). There are various classifications of these agents some of which are based on mechanism of action, organisms affected, spectrum of activity, source or even chemical structure. Modern pharmaceutical industry relies mainly on the diversity of secondary metabolites in medicinal plants for the discovery of new compounds with novel biological properties (35,36). This is an indication that plants are still an important and reliable source of drugs.

2.3 Biological activity testing

2.3.1 Bioassay-guided fractionation

Bioassay-guided fractionation is defined as a step-by-step separation of extracted components based on differences in their physicochemical properties, and their biological activity rather than on a particular class of compound, followed by next round of separation

and assaying (37). There are numerous bioassays available that are used in testing for many different activities. The ideal bioassay is inexpensive, sensitive to small amounts of active material, selective for a specific type of bioactivity and simple to run and maintain. A number of drugs have been developed by isolating compounds from plants or their derivative agents. In many cases, some natural products show biological activity but at the same time displaying either severe toxicity, poor solubility, poor bioavailability due to polarity, or lack of chemical stability, thereby limiting their employment as a drug of choice. To overcome this problem, the toxicity of such a drug must be lowered and the efficacy improved by modifying the molecular structure, identifying the drug target as well as establishment of no adverse effects. Following a bioassay approach, more active analogues that vary slightly from the original isolated compound can be prepared and then study their effects on biological activity or by synthesizing derivatives of a drug with better bioavailability and specificity, preparing new formulations with improved physical properties and combined use with other drugs (38).

2.4 Structure elucidation

2.4.1 Extraction, separation, and isolation of natural products

Extraction is an important step in the analysis of medicinal plants which is usually followed by separation of components and characterization of individual compounds. During this step, care is needed to avoid the loss, distortion or destruction of desired active constituents during the preparation of the extracts. Extraction can be affected by factors such as the quantity and nature of the compound, nature and mixing ratio of solvents, temperature, polarity, pH, and the method used. The extraction of polar compounds uses polar solvents

such as methanol, ethanol or ethyl-acetate, whereas for lipophilic compounds, dichloromethane or a mixture of dichloromethane/methanol in the ratio of 1:1 is commonly used, while hexane is used to remove chlorophyll and fat from the plant materials (39). A good extraction solvent should be easy to remove, inert, non-toxic, not easily flammable and should not form any type of unstable substance during extraction (40). Various methods can be employed for extraction and isolation of a specific class of compounds from a plant source. The commonly used extraction methods are: maceration or percolation of plant material in water or organic solvent, ultrasound extraction (sonification), heating under reflux and Soxhlet extraction. Modern extraction techniques include solid-phase micro-extraction, supercritical-fluid extraction, pressurized-liquid extraction, microwave-assisted extraction, solid-phase extraction, and surfactant-mediated techniques (41).

2.4.2 Chromatographic and spectroscopic methods

Plant extracts usually contain a combination of various types of bioactive compounds with varying degrees of polarity. A number of chromatographic techniques are used to separate, analyze and purify these mixtures. There are various types of chromatography techniques commonly used including paper chromatography (PC), thin layer chromatography (TLC), column chromatography (CC), flash chromatography, gas chromatography (GC), high performance liquid chromatography (HPLC), ion exchange chromatography, and gel permeation chromatography (41,42). Each of them having its advantage and disadvantages. The principle of chromatographic techniques is based on the adsorption of a molecules to a stationary phase and allowed to separate from each with the aid of a mobile phase. Once a pure compound is obtained, spectroscopy techniques are then used to determine the structure of the pure compound. Commonly used spectroscopy techniques include, nuclear

magnetic resonance spectroscopy (NMR), mass spectrometry (MS), infrared (IR), and ultraviolet-visible spectroscopy (UV-Vis).

2.5 Computational chemistry and drug discovery

Drug discovery is one of the challenging areas of medicinal research as it is a long and costly process. As a result, very few new drugs reach the market to be used as effective therapeutics. The rapid development of computer hardware, software and algorithms has led to development of computational methods that are useful in solving chemical problems and greatly reduce the time and cost of drug development (43). The field of computational chemistry applies the fundamental laws of physics, chemistry, and mathematical approximations to study chemical phenomena by running calculations on computers rather than by examining reactions and compounds experimentally as illustrated in Figure 2.4. Essentially, Schrödinger's equation is the basis of computational chemistry aiming at solving this equation for molecular systems. Since the Schrödinger's equation can only be solved exactly for simple systems, approximations are made to solve it numerically for complex systems (many electron atoms/molecules) (44). This involves virtual screening that uses simulations with multiscale models to investigate structural and thermodynamic features of target molecules on different levels. Various models have been developed in computational chemistry which are used to determine the energy and other functions of a molecule by using approximations.

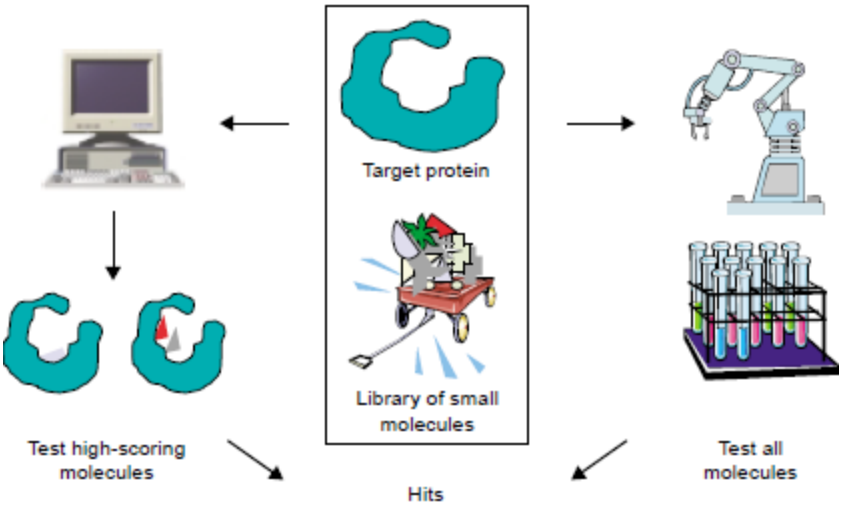

Figure 2.4. Scheme of computational study and experimental way of discovering new leads for drug discovery (45)

Models are expressions and simplifications of real life that contain specific assumptions reliable enough to give chemically meaningful results, and they vary widely in their comprehensiveness, quality, and utility (43). The high level of computer technology has allowed an increase in the size and number of systems that can be studied, as well as the degree of accuracy of the models on a reasonable time scale. Accurate results are obtained with more complex models at the cost of added computational expense. Common methods of virtual screening are molecular docking, pharmacophore modelling and quantitative structure-activity/property relationship (QSAR/QSPR). In computational chemistry, software have been developed for drawing structures, database entry-management-query, 2D to 3D structure conversion, molecular visualization, conformational searching, and biomolecular structure refinement (46). Theoretical methods such as molecular mechanics (MM), molecular dynamics (MD), and quantum mechanical (QM) methods such as *ab initio*, semi-empirical and density functional theory (DFT), are being used.

2.5.1 *Ab initio* and density functional electronic structure calculations

Ab initio is a QM method that is based on the Schrödinger equation using less approximation and is usually used for small molecules. The most common type of *ab initio* calculation is the Hartree-Fock (HF) and DFT calculations. HF, also called self-consistent field method (SCF) is used to calculate properties of multi-electron wavefunction without including electron correlation of a system. Bond length, bond angles, vibrational force constants can be predicted qualitatively with HF theory. With DFT, the energy of a molecule can be determined from the electron density instead of a wave function and this significantly speeds up the calculation. It has become more popular as it has proved to overcome some difficulties experienced with HF method such as bad calculated energies, time consuming iterative solution process and is cost effective to achieve a given level of quantitative accuracy (47).

DFT can be used to calculate the spectroscopic (IR, Raman, UV-vis spectra and ^{1}H and ^{13}C NMR chemical shifts), vibrational frequencies, molecular geometries, linear and nonlinear optical properties (48). It is often a method of choice when dealing with large molecules. Most DFT calculations are done with HF-optimized Gaussian type orbital (GTO) basis sets. The accuracy of results from DFT calculations depends on the choice of basis set and density functional used. The smaller the basis set, the less accurate the results. However, the density functional limits accuracy more than the basis set limitations. Examples of functionals include the Becke-Lee-Yang-Parr (BLYP), Becke-3-Lee-Yang-Parr (B3LYP), Becke-3-Perdew-Wang-1991 (B3PW91), Vosko-Wilk-Nusair-5 (VWN#5), and Becke-88-Lee-Yang-Parr (B88LYP). B3LYP functional is mostly used for many organic molecule

calculations and has been shown to provide an excellent compromise between accuracy and computational efficiency of vibrational spectra for large and medium size molecule (48). Examples of basis sets are: Gaussian type orbital (GTO), Slater type orbital (STO) like STO-3G, STO-nG and the Pople basis sets (6-31G, 3-21G, 4-31G, 4-22G, 6-21G, 6-311G, and 7-41 G.) (49). The Pople basis sets are very common for organic molecules. They can be modified by adding one or two asterisks and one or two plus signs, for example 6-311++G*. Extra set of functions are also added like p and d functions (6-311++G(d,p)) which is synonymous with 6-311++G** (49).

The advantage of *ab initio* methods is that they give accurate qualitative results and can give good quantitative results for smaller molecules. The disadvantage is that they are expensive, often take enormous amounts of computer cpu time, memory and disk space and are limited to smaller systems. Conventional DFT functionals, do not take into consideration long-range dispersion interaction such as van der Waals interactions. There has been advances in the development of DFT methods to account for dispersion, including vdW-DF, semiempirical atom pairwise, dispersion-corrected DFT, parameterized functionals, and dispersion-correcting potentials (50,51).

2.5.2 Semi-empirical methods

Semi-Empirical (SE) methods, like *ab initio* methods are based on the Schrödinger equation with more approximations from experimental values. SE can be used to optimize large molecules even though it is slower than MM but faster than *ab initio* calculations (52). Models for semi-empirical methods include different parameterized models (PM) depending on accuracies (PM3, PM6, PM7) and Austin Model 1 (AM1) are based on

neglect of diatomic differential overlap (NDDO) method. Other models are complete and intermediate neglect of differential overlap (CNDO & INDO), Zerner's intermediate neglect of differential overlap (ZINDO), and Recife model 1 (RM1). AM1 is the most commonly used in many programs. Advantages of SE methods include: simplicity of performance, good compromise between computing time and accuracy, high precision, possibility of subsequent optimization and adaptation to new objects and it can be applied to large molecules (53,54). Though useful, SE has its drawbacks such as poor treatment of dispersion interactions.

2.5.3 Molecular Mechanics (MM)

This is a classical mechanics tool used for optimizing very large molecules in a short period of time. MM uses models such as MM2, MM3, Merck molecular force field (MMFF) for organic molecules, assisted model building with energy refinement (AMBER), and Chemistry at HARvard molecular mechanics (CHARMM) for biomolecules (55). Some components of MM are bond stretching, bond angle bending, dihedral angle rotation (torsion), Van der Waals forces, hydrogen bonding, and electrostatic interactions.

A standard MM force field can be written as:

$$E = E\_stretch + E\_bend + E\_torsion + E\_vdW + \ldots$$

The main advantage of MM is their simplicity, the calculations are fast, and it is a good method for conformational analysis. The disadvantages of MM are that; 1. they are limited to the description of equilibrium geometries and equilibrium conformations, 2. the calculations does not give any information about bonding or electron distributions in molecules, 3. The available force fields cannot handle reaction transition states (55).

2.6 References

1. Mayor MT, Roett MA, Uduhiri KA. Diagnosis and management of gonococcal infections. Am Fam Physician. 2012;86(10):931–8.

2. Jones A, Aro H, Jones A, Jonsson A, Aro H. *Neisseria gonorrhoeae* infection causes a G1 arrest in human epithelial cells. FASEB J. 2007 Mar;21:345–55.

3. Landig CS, Hazel A, Kellman BP, Fong JJ, Schwarz F, Agarwal S, et al. Evolution of the exclusively human pathogen *Neisseria gonorrhoeae*: Human-specific engagement of immunoregulatory Siglecs. Evol Appl. 2019;12(2):337–49.

4. Sherrard J. Gonorrhoea. Medicine (Baltimore). 2010;38(5):245–8.

5. Javanbakht M, Westmoreland D, MSPH, Gorbach P, DrPH. Factors associated with pharyngeal gonorrhea in young people: Implications for prevention. Sex Transm Dis. 2018;45(9):588–93.

6. World Health Organization. Namibia: State of the nation's health findings from the global burden of disease. Seattle, WA: IHME: Institute for Health Metrics and Evaluation (IHME). 2016. 52 p.

7. Riedel S, Hobden JA, Miller S, Morse SA, Mietzner TA, Detrick B, et al. The Neisseriae. In: Riedel S, Hobden JA, Miller S, Morse SA, Mietzner TA, Detrick B, et al., editors. Jawetz, Melnick & Adelberg's Medical Microbiology. 28th ed. McGraw Hill: McGraw Hill; 2019.

8. Workowski K. In the Clinic: Chlamydia and gonorrhea. Ann Intern Med. 2013;158(ITC):1–16.

9. Spencer SE, Bash MC. Extragenital manifestations of *Neisseria gonorrhoeae*. Curr Infect Dis Rep. 2006;8(2):132–8.

10. World Health Organization. Multi-drug resistant gonorrhoea. 2020; (November). Accessed 17 May 2021, <https://www.who.int/news-room/fact-sheets/detail/multi-drug-resistant-gonorrhoea>.

11. Kirkcaldy PD, MD, MPH, Weston E, MPH, Segurado AC, et al. Epidemiology of Gonorrhea: A global perspective. Sex Health. 2019;16(5):401–11.

12. World Health Organization. Global health sector strategy on sexually transmitted infections 2016-2021. Towards ending STIs. Vol. June 2016, WHO/RHR/16.09.

13. Longe BT, Moses O, Osuntoyinbo RT. *Neisseria gonorrhoaea* infections in Africa - Systematic Review and Meta-Analysis. J Microbiol Antimicrob Agents.

2020;5(2):4–9.

14. Torrone EA, Morrison CS, Chen PL, Kwok C, Francis SC, Hayes RJ, et al. Correction: Prevalence of sexually transmitted infections and bacterial vaginosis among women in sub-Saharan Africa: An individual participant data meta-analysis of 18 HIV prevention studies. PLoS Med. 2018;15(2):e1002511.

15. MoHSS. Ministry of Helath and Social Services. Namibia demographic and health survey 2013. Windhoek: Namibia Statistics Agency; 2014. accessed 23 April 2021, <https://dhsprogram.com/pubs/pdf/FR298/FR298.pdf>.

16. Hazel A, Ponnaluri-Wears S, Davis GS, Low BS, Foxman B. High prevalence of *Neisseria gonorrhoeae* in a remote, undertreated population of Namibian pastoralists. Epidemiol Infect. 2014;142(11):2422–32.

17. Shivute S, Omodanisi EI, Okeleye BI, Ntwampe SKO. Incidence of Chlamydia and gonorrhoeae infection among patients at the Namibia Institute of Pathology. In: 17th Johannesburg Int'l Conference on Science, Engineering, Technology & Waste Management (SETWM-19). Johannesburg, South Africa; 2019. p. 215–21. Accessed 23 April 2021.

18. Suzaki A, Hayashi K, Kosuge K, Soma M, Hayakawa S. Disseminated gonococcal infection in Japan: A case report and literature review. Intern Med. 2011;50(18):2039–43.

19. da Cruz M, Palma NZ, Ferraz RV, Oliveira M, Meireles R. Disseminated gonococcal infection: A Case Report of Arthritis-Dermatitis Syndrome. J Med Cases. 2019;10(10):312–4.

20. Ohl CA, Forster D. Gonococcal arthritis. In: Bennett JE, Dolin R, Blaser MJ, editors. Mandell, Douglas, and Bennett's Principles and practice of infectious diseases. 8th ed. Philadelphia, PA: Elsevier Saunders; 2015. p. 171–3.

21. Mimiaga MJ, Helms DJ, Reisner SL, Grasso C, Bertrand T, Mosure DJ, et al. Gonococcal, chlamydia, and syphilis infection positivity among MSM attending a large primary care clinic, Boston, 2003 to 2004. Sex Transm Dis. 2009;36(8):507–511.

22. Ding J, Rapista A, Teleshova N, Mosoyan G, Jarvis GA, Klotman ME, et al. *Neisseria gonorrhoeae* Enhances HIV-1 Infection of Primary Resting CD4+ T Cells through TLR2 Activation. J Immunol. 2010;184(6):2814–24.

23. Bala M, Mullick JB, Muralidhar S, Kumar J, Ramesh V. Gonorrhoea & its co-infection with other ulcerative, non-ulcerative sexually transmitted & HIV infection in a Regional STD Centre. Indian J Med Res. 2011;133(3):346–9.

24. Unemo M, del Rio C, Shafer WM. Antimicrobial Resistance Expressed by *Neisseria gonorrhoeae*: A Major Global Public Health Problem in the 21st Century. Microbiol Spectr. 2016;4(3):1–32.

25. Dillon J-AR, Parti RP, Thakur SD. Antibiotic resistance in *Neisseria gonorrhoeae*: Will infections be untreatable in the future? Culture. 2015;35(1).

26. Patrick GL. An introdcution to medicinal chemistry. 5th ed. Oxford University Press; 2013

27. Walsh C. Molecular mechanisms that confer antibacterial drug resistance. Insight Rev Artic. 2000 Aug;406:775–81.

28. Unemo M, del Rio C, Shafer WM. Antimicrobial Resistance Expressed by *Neisseria gonorrhoeae*: A major global public health problem in the 21st century. Microbiol Spectr. 2016;4(3):1–32.

29. Melendez JH, Hardick J, Barnes M, Page KR, Gaydos CA. Antimicrobial susceptibility of *Neisseria gonorrhoeae* isolates in Baltimore, Maryland, 2016: The importance of sentinel surveillance in the era of multi-drug-resistant gonorrhea. Antibiotics. 2018;7(3).

30. Dowell D, Kirkcaldy RD. Effectiveness of gentamicin for gonorrhoea treatment: systematic review and meta- analysis. Sex Trans Infect. 2012;0:1-6.

31. Ison, CA; Hussey, J; Sankar, KN; Evans, J; Alexander S. Change of guard in Eurosurveillance. Vol. 16, Eurosurveillance. 2011.

32. Unemo M, Golparian D, Stary A, Eigentler A. First *Neisseria gonorrhoeae* strain with resistance to cefixime causing gonorrhoea treatment failure in Austria. Euro Surveill. 2011;16(43):19998.

33. World Health Organization. Emergence of multi-drug resistant *Neisseria gonorrhoeae* – Threat of global rise in untreatable sexually transmitted infections. Dep Reprod Heal Res. 2012;WHO/RHR/11(June).

34. Palhares RM, Drummond MG, Dos Santos Alves Figueiredo Brasil B, Cosenza GP, Das Graças Lins Brandão M, Oliveira G. Medicinal plants recommended by the World Health Organization: DNA barcode identification associated with chemical analyses guarantees their quality. PLoS One. 2015;10(5).

35. Das K, Tiwari RKS, Shrivastava DK. Techniques for evaluation of medicinal plant products as antimicrobial agent: Current methods and future trends. J Med Plants Res. 2010;4(2):104–11

36. Asif M. Antimicrobial agents. J Anal Pharm Res. 2017;4(3):169–75.

37. Malviya N, Malviya S. Bioassay guided fractionation-an emerging technique influence the isolation, identification and characterization of lead phytomolecules. Int J Hosp Pharm. 2017;2:5.

38. Fang W-S, Liang X-T. Recent progress in structure activity relationship and mechanistic studies of taxol analogues. Mini Rev Med Chem. 2005;5(1):1–12.

39. Sasidharan S, Chen Y, Saravanan D, Sundram KM, Yoga Latha L. Extraction, isolation and characterization of bioactive compounds from plants'extracts. African J Tradit Complement Altern Med. 2011;8(1):1–10.

40. Visht S, Chaturvedi S. Review Article Current Pharma Research. Curr Pharma Res. 2012;2(3):584–99.

41. Abdelmohsen UR, Sayed AM, Elmaidomy AH. Natural products' extraction and isolation-between conventional and modern techniques. Front Nat Prod. 2022;1(May):1–4.

42. Bajpai VK, Majumder R, Park JG. Isolation and purification of plant secondary metabolites using column-chromatographic technique. Bangladesh J Pharmacol. 2016;11(4):844–8.

43. Lin X, Li X, Lin X. A review on applications of computational methods in drug screening and design. Molecules. 2020;25(6):1–17.

44. Hermann J, Schätzle Z, Noé F. Deep-neural-network solution of the electronic Schrödinger equation. Nat Chem. 2020;12(10):891–7.

45. Shoichet BK, McGovern SL, Wei B, Irwin JJ. Lead discovery using molecular docking. Curr Opin Chem Biol. 2002;6(4):439–46.

46. Jorgensen WL. The many roles of computation in drug discovery. Science. 2004;303(5665):1813–1818.

47. Amusia MY, Msezane AZ, Shaginyan VR. Density Functional Theory versus the Hartree–Fock Method: Comparative Assessment. Phys Scr. 2003;68(6):C133–40.

48. Abbaz T, Bendjeddou A, Villemin D. Molecular structure, HOMO, LUMO, MEP, natural bond orbital analysis of benzo and anthraquinodimethane derivatives. Pharm Biol Eval. 2018;5(2):27.

49. Feller D. The role of databases in support of computaional chemistry calculations. J Comput Chem. 1996;17(13):1571–86.

50. Andersson MP. Density functional theory with modified dispersion correction for metals applied to self-assembled monolayers of thiols on Au(111). J Theor Chem.

2013;2013.

51. Berland K, Cooper VR, Lee K, Schroder E, Thonhauser T, Hyldgaard P, et al. Van der Waals interactions in DFT. Langmuir. 2014;

52. Cui Q, Guo H, Karplus M. Combining *ab initio* and density functional theories with semiempirical methods. J Chem Phys. 2002;117(12):5617–31.

53. Kozma AA. Advantages of Using Semi-Empirical Methods in Teaching Students at the Faculty of Chemistry of Uzhhorod National University. Int J Educ Sci. 2019;2(2):26697.

54. Filho MAM, Dutra JDL, Rocha GB, Simas AM, Freire RO. Semiempirical quantum chemistry model for the lanthanides: RM1 (Recife Model 1) parameters for dysprosium, holmium and erbium. PLoS One. 2014;9(1).

55. Hehre WJ. A Guide to Molecular Mechanics and Quantum Chemical Calculations. Irvine, CA: Wavefunction, Inc; 2003. 1–796 p.

CHAPTER 3: SCREENING FOR ANTI-GONOCOCCAL ACTIVITY IN PLANTS THAT ARE ETHNOMEDICINALLY USED FOR THE TREATMENT OF GONORRHEA IN THE ZAMBEZI REGION, NAMIBIA

Abstract

The use of plants in traditional medicine is a common practice in the Zambezi region since it is rich in plant diversity. Several plants species are known by indigenous people to treat sexually transmitted infections (STIs) including gonorrhea. Although commonly used, the safety and efficacy of these medicinal plant is not established. This study aimed to evaluate the *in-vitro* antimicrobial activity of extracts from selected plants used to treat gonorrhea and thus validate their traditional medicinal use. Sequential extraction was used. Thin layer chromatography (TLC), preparatory TLC and column chromatography were used to analyse the crude extracts composition. Using well diffusion, extracts were tested on four strains of *Neisseria gonorrhoeae* and 6 strains of non-fastidious microorganisms known to cause various common infections. Antimicrobial analysis revealed that six of the 13 tested plants have anti-gonococcal activity with minimum inhibitory concentration (MIC) range of 2.5 to 10 mg/mL, while four of the plants inhibited *N. gonorrhoeae* with MIC ≥10 mg/mL. These results give basis for supporting the traditional use of these plants to treat gonorrhea as an alternative to modern drugs. Further studies are required to identify the active compounds.

Key words: Traditional medicine, ethnobotany, medicinal plants, gonorrhea, antimicrobial

3.1 Introduction

The Zambezi region, in Namibia, is known for its rich plant diversity with a large portion being covered in plants due to good climatic conditions (1). The rich flora gives a good potential of medicinal plants. Despite the good health care system in Namibia, the Zambezi region community still cling to traditional approaches of plant use. Modern medicine has presented unsolved problems related to drug toxicity, drug resistance and high cost. The increase in noncommunicable diseases such as diabetes, hypertension, cardiovascular disease, asthma, mental illness and cancer are also associated to modern medicine use and food by many (2). Rural population in particular, relate that "our forefathers" lived longer and healthier because they depended on plants and traditional way of living. Therefore, long practiced traditions have led many people in rural areas to still rely on plants to treat STIs. Due to the stigma associated with these infections, many prefer to consult Traditional medicinal practitioners (TMPs) rather than going to western health care facilities. The rural population also cling to traditional approaches rather than approaching health care providers whom they are not familiar with (unknown doctors or nurses). The cost of modern medicine also plays a role (3). These TMPs are considered to be experts in the knowledge of medicinal plants and their use. They use medicinal plants as their primary source of medicinal formulations.

However, ethnomedicinal knowledge has been undermined by factors such as death of resource persons, poor documentation, extinction of plant resources and inadequate scientific research (4). Thus, the safety and efficacy of various traditional medicines still require sufficient support despite continual use of these medicinal plants over many

centuries. Information on medicinal plant species and their traditional uses needs to be collected and find a way to incorporate their use into the national health care system. Due to the side effects and the resistance that pathogenic microorganisms build against antibiotics, more recently, attention has been paid to extracts of biologically active compounds from plant species. Several plants are reported to be used for the treatment of gonorrhea in Namibia, these include *Strychnos cocculoides* Lam. roots, *Ziziphus mucronata* Willd. subsp. mucronata roots, *Tribulus terrestris* (Linn) leaves, fruits and roots, *Talinum sp, Gomphocarpus fruticosa* (L) W.T. Aiton. roots, *Senna occidentalis* (l.) Link roots, *Penchuel-loeschea leubnitziae* (Kuntze) O.Hoffm. roots and leaves, *Ximenia americanum* L., *Ximenia cafra* Sond., *Combretum imberbe* Wawra, *Erythropheum africanum* Afzel., and *Kigelia africana* (Lam.) Benth. roots (5) (Pers. Comm. R. Sinkela and M. Sangwali). Different parts (leaves, bark, roots, and tubers) of these plants are used in the treatment of gonorrhea, either in combination with other plants or as a single plant. Ethnomedicinal uses of many of these plants for other disease models have also been reported among communities in Namibia and other parts of the world. Despite being commonly used, the safety and efficacy of these medicinal plants are not established. This chapter aimed to evaluate the *in-vitro* antimicrobial activity of extracts from selected plants used to treat gonorrhea and thus validate their traditional medicinal use.

3.1.1 *Pechuel-loeschea leubnitziae* (Kuntze) O. Hoffm.

Pechuel-loeschea leubnitziae belongs to the family Asteraceae and is commonly known by various names depending on the region and tribe in Namibia: Runukirizo (Siyeyi), Ekombombo (Sifwe), Edimba, Oshizimba (Oshiwambo), Omundumba (Herero),

Auxan!khâb (Khoekhoegoab), Bitterbos (Afrikaans), Stinky bush (English). It is widely distributed throughout Namibia in sandy areas and disturbed grounds like old gravel pits and along roadsides. It is a multi-stemmed plant characterized by a strong pungent and unpleasant smell. The root and leaf extracts from this plant are commonly used as remedy for gonorrhea (1,6). The plants are also said to be effective for stomach pain, earache, flu, measles, allergies and to disinfect wounds (pers. com. Mbwe M.). It is also an effective mosquito repellent and used by the Ovahimba people to make a powder for cosmetic purposes (1). Dichloromethane leaf extract from this plant has shown strong anticancer activity (7).

Figure 3.1. *Pechuel-loeschea leubnitziae* (A) plant photographed at Sangwali village, Zambezi region in dry stream/riverbed (18°15'32" S, 23°38'17" E [1823BC]), and (B) leaves drying under shade. (Photographer: M.M. Nyambe).

3.1.2 *Ziziphus mucronata* Willd. subsp. *mucronata*

Ziziphus mucronata belongs to the Rhamnaceae family. The common names are: Buffalo thorn (English), Encharo (Sifwe), Blinkblaar-wag-'n-bietjie (Afrikaans), Büffeldorn (Damara Nama), Omukaru (Herero) Omusheshete (Oshiwambo), Mukekete (Rumanyo), Mukalo (Silozi). It is a semi-evergreen (Figure 3.2) small to medium-sized tree with a spreading canopy that is found mostly along moist riverbanks, dams and pan edges but can also be found on plains as it is drought tolerant. Only *Ziziphus mucronata* subsp. *mucronata* is found in Namibia and is widespread throughout Namibia, except in the Namib Desert (1). The plant is used in the management of HIV-AIDS related infections including pneumonia and STIs such as syphilis, gonorrhea, and chlamydia, as well as to treat skin allergy, rash, and sore fingers (8). It is reported to be used for treating diarrhea, piles, dysentery, ringworm, rheumatism, snake bite, vaginal discharge, cough, and fever (9,10). It is confirmed to have antibacterial, antifungal and antioxidant activity (9,11).

Figure 3.2. *Ziziphus mucronata* plant photographed at Sangwali village, Zambezi region (18°00' S, 23°00' E [1823BC]) (Photographer: M.M. Nyambe)

3.1.3 *Tribulus terrestris* (Linn)

Tribulus terrestris is an annual plant with thorny fruits and belongs to Zygophyllaceae family which is widely distributed in both tropical and mild temperate regions around the world (Figure 3.3). It is a common weed, well known as Puncture vine, Land caltrops (English), Nseto (Silozi), Enshonsho (Sifwe). The leaves, roots and fruits are used in form of an infusion to treat gonorrhea and chlamydia (12). It is also traditionally used as an aphrodisiac, as a tonic, analgesic, diuretic, and for treatment of urinary tract infections, cough expectorant, skin pruritus, headache, vertigo, mammary duct blockage, infertility, impotence, erectile dysfunction, and low libido (13,14). The roots and fruits are also used to treat piles, menorrhagia eye problem, edema and rheumatism. Secondary metabolites that have been reported in this plant include phenols, polyphenols, saponins, flavonoids, alkaloids, glycosides, tannins and terpenoids which have antimicrobial function (14). Biological activity that is confirmed for *T. terrestris* is antimicrobial, cytotoxic effect, antiseptic, anti-inflammatory and analgesic activity (15).

Figure 3.3. *Tribulus terrestris* (A) leaves and flowers photographed at Sangwali village, Zambezi region (18°15'39" S, 23°38'35" E [1823BC]), (B) fruits drying under shade. (Photographer: M.M. Nyambe)

3.1.4 *Indigofera hofmanniana* Schinz

Indigofera hofmanniana is a perennial legume, non-climbing, herb or shrub. It belongs to the third largest genus of the Fabaceae family, *Indigofera*. It has curved pods containing more than six seeds (Figure 3.4). Known as lubuna luba Chunga by the people of Linyanti community, in Zambezi region where the shrub grows in abundance. This name, when directly translated means "Mr Chunga's bush" as it is understood that a community member by the name Chunga brought a sample to Linyanti village, from Botswana. It is also found in the northern regions of Namibia where it is known as omikangua in Oshindonga as well as in Etosha area. It grows in Acacia woodlands and alluvial sand in pans or riverbeds (16,17). No literature is available about the chemical composition and biological activity of this plant. The roots are traditionally used to treat gonorrhea and as tonic for women (Pers comm R. Sinkela). The genus *Indigofera* is known for various indigo dye-producing species like *I. Suffruticosa* and *I. Tinctoria* which are closely related to *I. hofmanniana*. Several species from this genus are reported to be traditionally used to treat ailments such as gastrointestinal disorders, inflammation and pain, skin conditions, respiratory problems, and infectious diseases. The genus is rich in terpenes and phenolic compounds (18).

Figure 3.4. (A,B) *Indigofera hofmanniana* plant, and (C) *fruits* (Photographer: M.M. Nyambe)

3.2 Material and methods

3.2.1 Selection of plants

Plants were selected based on information obtained from some herbalists who reported their use in the treatment of gonorrhea/STIs in the Zambezi region, located in the north-eastern part of Namibia. Also based on ethnomedicinal uses reported in literature (SEPASAL database) giving the basis for testing extracts from these plants on other microbes. The identification of species was done by the National Botanical Research Institute of Namibia for the purpose of ensuring correct botanical identification (Appendix 3). Ethical clearance was granted by the University of Namibia (Appendix 1).

3.2.2 Plant collection and identification

A plant collection permit (authorization no: AN20181004 in Appendix 2) for the collection of plant material used in this study was obtained from the Ministry of Environment and Tourism of Namibia through National Commission on Research and Technology (NCRST). Thirteen (13) plants species: *Strychnos cocculoides* Lam., *Ziziphus mucronata* Willd. subsp. *mucronata*, *Tribulus terrestris* (Linn), *Talinum* species, *Gomphocarpus fruticosus* (L.) W.T. Aiton, *Indigofera hofmanniana* Schinz., *Senna occidentalis* (L.) Link, *Pechuel-loeschea leubnitziae* (Kuntze) O.Hoffm., *Kigelia Africana* (Lam.) Benth., *Solanum delagoense* Dunal (Entuntuza), *Aloe maculate* All., *Harpagophytum procumbens* (Burch.) DC.ex Meisn. and one unidentified plant (locally known as kabuna komwisheke) were selected based on previous literature studies that associate these plants to treating gonorrhea (SEPASAL database; (6). In addition, information was provided by one herbalist and other community members in the Zambezi region who gave ethnobotanical data on the use of these plants for treating gonorrhea in the region and surrounding areas (R.K. Sinkela and M.M & M.I Sangwali Pers. Comm.). All 13 plants were collected from the Zambezi region (Sangwali area, Sibbinda area and Ngoma area). A total of 16 plant parts from these species were analysed.

3.2.3 Extraction

Sixteen plant parts from 13 plant species were cleaned with water to remove excess soil and then dried under shade before being ground to a powder (Figure 3.5). About 30 g of the powdered plant material was extracted with 400 mL of dichloromethane (DCM) and methanol (MeOH) mixture (1:1) to allow for the extraction of a variety of polar and non-

polar compounds for 48 hours with occasional stirring. The sample was filtered using a Whatman number 1 filter paper and the residue was rinsed with the same solvent. To make sure that the residue was exhaustively extracted, it was re-extracted with 300 mL of the same solvent for 24 hours, and finally with 300 mL of methanol for 8 hours. The extracts obtained were then combined and concentrated to dryness in a fume hood and the yield determined. Extracts were assigned codes GP1 to GP16 where GP refers to "gonorrhea plant".

Sequential extraction was subsequently done on plant extracts that showed activity against *Neisseria gonorrhoeae*, to group compounds according to their polarity. Maceration technique and solvents of increasing polarity, n-hexane, DCM, ethyl acetate and MeOH were used. The ground plant material (30 g) was first extracted with hexane while placed into the shaking incubator set at 195 RPM speed and extraction was carried out for 24 hours with constant shaking at room temperature (RT). The contents of the flask were then filtered, washed with an additional 250 mL of solvent (n-hexane) and the filtrate was concentrated to dryness by evaporation in a fume hood. The residue was air dried before extraction with the next solvent. The above procedure was then repeated for the remaining three solvents in order of increasing polarity. The percentage yield of extracts was determined.

Figure 3.5. Some of the plant parts that were screened and analysed in this study, (A) *Strychnos cocculoides* roots, (B) *Tallinum* sp. Showing leaves, flower and tuber, (C) *Indigofera hofmanniana* roots, (D) *Tribulus terrestris* leaves (Photographer: M.M. Nyambe)

3.2.4 Microorganisms and growth conditions

To determine the *in-vitro* antimicrobial activity, extracts of the leaves, roots, tubers and bark were screened against four reference strains of *N. gonorrhoeae* (ATCC 19424, ATCC 31426, ATCC 43069 and ATCC 49226) as well as 6 other microorganisms (*Escherichia*

coli ATCC 70928, *Staphylococcus aureus* ATCC 12600, *Candida albicans* ATCC 13933, *Klebsiella pneumonia* ATCC 10556, *Lactobacillus plantarum* and *Streptococcus mutans* ATCC 25175). These microorganisms are known to cause various infections some of which are associated with STIs. The laboratory strains were purchased from American Type Culture Collection through Genmed CC. *N. gonorrhoeae* strains were rehydrated in Brain Heart infusion (BHI) broth and grown at 37 ºC and were grown in Thayer Martin agar (TMA) and BHI broth under anaerobic conditions (candle extinction jar) for all experiments. TMA is a selective medium used for the isolation of *N. gonorrhoeae*. Nutrient agar and broth were used for the growth of other microbes. For each test, overnight bacterial suspension was standardized to 0.5 McFarland standard.

3.2.5 Determination of antimicrobial activity

Growth inhibitory effects of all 16 crude extracts were tested against four strains of *N. gonorrhoeae* and against *E. coli*, *S. aureus*, *C. albicans*, *K. pneumonia*, *L. plantarum* and *S. mutans* using the agar well diffusion method as described by Hanphanphoom et al. (19) with some modification. The microbes were chosen to include a range of microbial types, including the gram positive, gram negative and fungi. Using a micro pipette 1 mL of the microorganism was transferred to 9 mL of BHI broth for *N. gonorrhoae* and nutrient broth for other microbes which was incubated at 37 ºC for 24 hours. Using sterile micro-tips, 20 µL of standardized microbes was placed on the center of the agar plate, spread using a sterile spreader and allowed to stand for 5 minutes. Using a cork borer (No. 3), wells (7 mm diameter) were cut into the inoculated agar and 50 µL at a concentration of 20 mg/mL of the crude extract dissolved in dimethylsulfoxide (DMSO), was filled into the wells

separately. The plates were allowed to stand for 1 hour in the fume hood, to allow the extracts to diffuse into the medium. DMSO was used as a solvent control while ampicillin (10 mg/mL) and tetracycline (5 mg/mL) were used as the reference antibiotic. Plates were incubated for 24 hours at 37 ºC. Clear, distinct inhibition zones around the wells indicated the presence of antimicrobial activity. The diameter of zone of inhibition was measured in millimeter. The extracts were placed in duplicate, and the test was repeated twice, every time using a fresh culture of microbes to avoid contamination and overgrowth and to ensure that the microbes being used are not dead. The strength of activity was classified based on the method described by Nematollahi et al. (20) as strong (zone ≥15 mm), moderate (zone ≥ 10 mm), weak (zone ≥ 9 mm) and inactive (zone ≤ 7 mm).

3.2.6 Minimum inhibitory concentration (MIC)

MIC was determined by the broth microdilution method (21) using the 96 well plates only for the test organisms that had shown ≥10 mm zone of inhibition of the crude extracts. Microbes were standardized by measuring the optical density comparable to that of McFarland standard as described by Wiegand (22). The turbidity of the microbes was assessed by measuring the absorbance of the suspension using a spectrophotometer. The absorbance was accepted when it was in the same range as that of the 0.5 McFarland standard. Microbes were considered standard when their OD value was between 0.08-0.13 at 625 nm which gives microbial count of approximately 1.5×10^8 CFU/mL. Turbidity was adjusted by adding sterile broth. A volume of 150 µL of sterile nutrient broth was placed in the 96 wells, then 50 µL of each extract at the concentration of 20 mg/mL dissolved in DMSO were added to the first-row wells. Serial dilution was done by taking 50 µL of the

solution from the first 9 wells putting it into the next 9 rows, this was done for the next row, until all the 96 wells had broth + extract, which make up 150 µL. Then 50µL of the microbial strains were added to each of the wells separately. Three control wells were maintained for each test batch. The positive control (antibiotic, Mueller-Hinton broth and test organism) and sterility control (Mueller-Hinton broth and DMSO) and organism control (Mueller-Hinton broth, test organism and DMSO). The plates were then read for absorbance before and after being incubated for 24 hours at 37 ˚C. The lowest concentration that showed decline in absorbance value was taken as the minimum inhibitory concentration of the crude extract for the particular organism (23,24).

3.2.7 Isolation, purification, and characterization

3.2.7.1 Thin layer chromatography (TLC)

Commercially available TLC aluminium sheets, coated with silica gel 60 were used. The extracts dissolved in the extraction solvent were spotted on the plate. Different solvent mixtures at various ratios were used to determine the best solvent for separating compounds in the extracts. The mobile phase tested included: (e.g hexane/ethyl acetate, hexane/ethyl acetate/methanol, hexane/acetone, chloroform/methanol, chloroform/methanol/water, chloroform/ethyl acetate/formic acid, methanol/ethyl acetate, acetone/ethyl acetate, petroleum ether/ethyl acetate/methanol, dichloromethane/hexane, dichloromethane/ethyl acetate etc) using several ratios of each solvent mixture. Spots were visualized using a UV lamp (254 and 365 nm) to show any UV-active spots as well as using iodine crystals and a spray reagent p-anisaldehyde/sulfuric acid to try and detect the maximum number of compounds in each extract. The solvent that gave the best separation of compounds for different extracts were selected to be used for separation of compounds on preparative TLC and column chromatography.

3.2.7.2 Preparative TLC

Crude extracts which showed moderate to strong anti-gonococcal activity (GP1, GP2, GP7, GP8, GP9 and GP10) were further separated by Prep-TLC plates coated with Silica gel 60 F24, 2 mm thick, purchased from Mack KGnA, using the mobile phase Chloroform/methanol (10:1 and 5:1). The extracts (60 mg) to be separated were dissolved in 2 mL of DCM:MeOH (1:1) and applied as long streaks, in the sample application zone (Figure 3.6). After the compound separated, the sorbent layers were scrapped off into different beakers, and were then dissolved into DCM:MeOH (1:1) and filtered to remove the silica. The filtrates were dried in the fume hood, weighed, and stored until analysis. The fractions were tested for antimicrobial activity against *N. gonorrhoeae* using the disc diffusion method. The concentration of the fractions used varied depending on the amount obtained after drying. The isolates that gave strong activity were purified further.

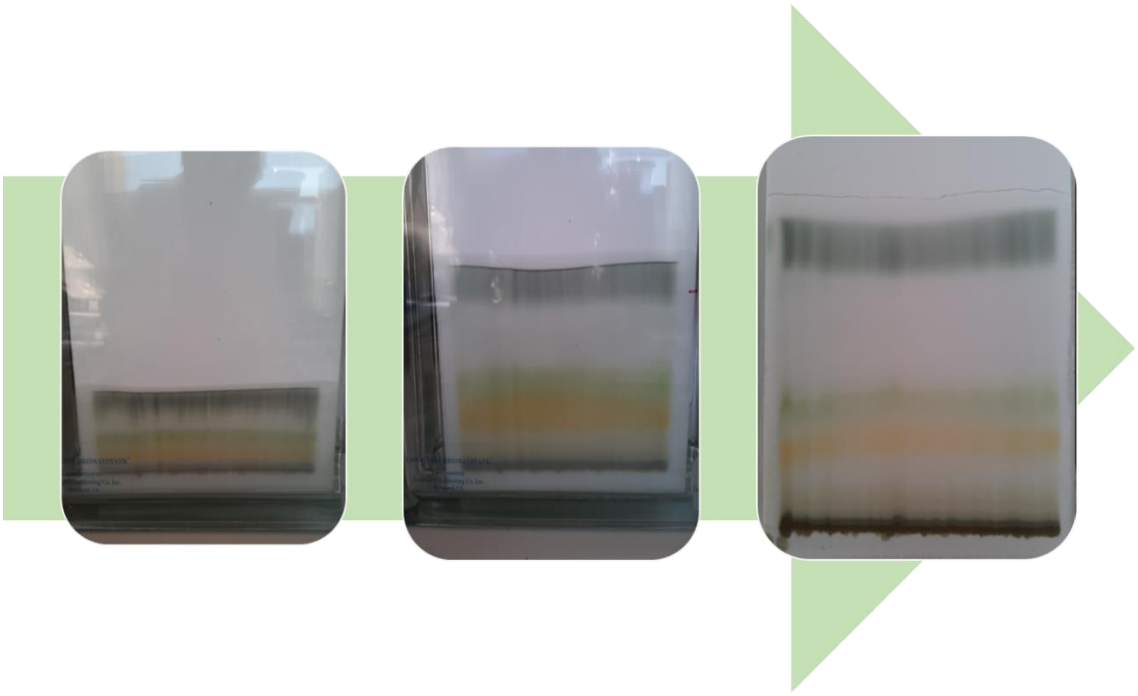

Figure 3.6. Preparative TLC plates of GP1 observed with white light developing in chloroform/methanol (5:1) mobile phase.

3.2.7.3 Column chromatography

To obtain an abundance of compound matrix, column chromatography was used. Extracts of GP1, GP7, GP9 and GP10 were subjected to normal phase column chromatography in silica gel 60 (63 – 200 µm) glass column. The selection of crude extracts for fractionation was based on antimicrobial activity results as well as the TLC profile. Only extracts that were not highly polar were separated on silica gel. About 1.00 - 1.40 g of the crude extracts was dissolved in a solvent of extraction and adhered to 2 grams of silica gel. The adsorbed silica was allowed to air dry and loaded on a column that was wet parked. The column for GP1 and GP7 was packed and eluted with chloroform followed by chloroform:methanol with increasing polarity (99.8:0.2 → 95.0:5.0). GP10 was eluted with [(9:1 → 0:10) Hexane/DCM, (9:1 → 0:10) DCM/ethyl acetate (EA), (9.5:0.5 → 9:1) DCM/MeOH]. While GP9 was eluted with Hex:Ace followed by DCM:Ace. Extracts yielded 86 fractions (GP10), 78 fractions (GP7), 59 fractions (GP9) and 38 fractions (GP1). Following elution, all the collected fractions (Figure 3.7) were qualitatively evaluated using TLC silica gel 60 F254 plate. Fractions with similar TLC profiles were pooled together to get 12, 13, 7 and 6 fractions for GP10, GP7, GP9 and GP1 respectively. Combined fractions were allowed to concentrate slowly in an undisturbed area to allow formation of crystals. Fractions obtained from this analysis were tested against *N. gonorrhoeae* and isolates that shows activity was characterized. The electronic structure, interaction of compound with NgCA active site model and QSPR studies was done on the compound and its analogues.

Figure 3.7. Silica gel column and fractions collected for GP10 dichloromethane extract

3.2.7.4 Nuclear Magnetic Resonance (NMR)

^{1}H, ^{13}C, COSY, HSQC, HMBC NMR spectra with processing, plotting and report was done on two purified fractions (GP7-1 and GP7-2) obtained from GP7 extract (*I. hofmanniana*). Samples were dissolved in 0.45 mL DMSO and transferred to 5 mm NMR tubes. Bruker Ascend NMR spectrometer with a ^{1}H frequency of 600 MHz and a ^{13}C frequency of 150 MHz fitted with a 5 mm CPPBBO probe was used. The default 1D and 2D pulse sequences were optimised according to the sample concentration and 1D ^{1}H NMR spectra. The spectra are referenced to the residual solvent signals and indicated on the spectra. All spectra are processed using Topspin 4.0.7 (25).

3.3 Results and discussion

3.3.1 Extraction

The percentage yield of crude extracts as shown in Table 3.1 was based on the weight of dried and ground plant materials extracted with DCM:MeOH (1:1). The solvent used for extraction was selected based on their polarities which would allow for extraction of a mixture of polar and nonpolar compounds. Henceforth, extracts of different plant parts are represented as GP1-GP16 as presented in Table 3.1, where GP refers to gonorrhea plant. The percentage yield of the crude extracts ranged from 5.7% to 20.2% (Table 3.1) which was relatively high for natural products. The yield of *Kigelia africana* bark was the highest, followed by *P. leubnitziae* leaves, while GP1 and GP12 had the lowest yield. The high extraction yields show that DCM and methanol are good extraction solvents to obtain as many compounds as possible from these plants. Differences in yield percentage are due to various factors such as type of solvent used for extraction in relation to the chemical composition and physical characteristics of the samples (26). Percentage yield of the plant extracts was calculated using the formula:

$$\%\text{Yield} = \frac{Wx}{Wy} \times 100$$

Where *Wx* is the weight of extract after drying and *Wy* is the weight of the plant material before extraction. Based on the antimicrobial screening and TLC profile of the DCM:MeOH crude extracts, 5 extracts were selected for further analysis which involved re-extraction with solvents of increasing polarity (hexane, DCM, EA and MeOH). Application of sequential extraction was an attempt to fractionate compounds according to

polarity. Table 3.2 shows the percentage yield of fractions obtained using solvents of increasing polarity. The results showed that all extraction solvents used were able to extract some components of the plant material but with varying quantities. Methanol extracts had the highest percentage yield for the three out of four plants that were sequentially extracted, suggesting that these plants are rich in polar compounds. DCM had the highest yield of 5% for *P. leubnitziae,* whereas ethyl acetate had the lowest yield for all plants. Hexane being a nonpolar solvent gave good yield compared to DCM and EA for all the samples. This is an indication that these plants contain mixtures of volatile oils, fats and waxes, constituents that easily dissolve in nonpolar solvents like hexane.

Table 3.1 Percentage yield of the 16 extracts of various plant species extracted by maceration with DCM:MeOH (1:1)

Plant name (Family)	**Common name**	**Extract number**	**Plant part used**	**% yield**
Strychnos cocculoides (Loganiaceae)	Kahwi (S), monkey orange (E)	GP1	roots	5.7
Ziziphus mucronata Willd. *subsp. mucronata* (Rhamnaceae)	Encharo (S)	GP2	roots	9.6
Tribulus terrestris (Zygophyllaceae)	Enshonsho (S), nseto (Sl)	GP3	fruits	6.3
Tribulus terrestris (Zygophyllaceae)	Enshonsho (S)	GP4	leaves	7.6
Talinum sp. (Talinaceae)	Libambam (Sy)	GP5	tuber	6.1
Gomphocarpus fruticosus (L.) W.T.Aiton *subsp. fAloe charuticosus* (Asclepiadaceae)	Xhamwa (Sy)	GP6	roots	9.8
Indigofera hofmanniana (Fabaceae)	kabuna kaba Chunga (Mb)	GP7	roots	14.3
Senna occidentalis (L.) Link (Fabaceae)	Enchakancaka (S)	GP8	roots	7.4
Pechuel-loeschea leubnitziae (Kuntze) O.Hoffm. (Asteraceae)	Runukirizo (Sy)	GP9	roots	6.2
Pechuel-loeschea leubnitziae (Kuntze) O.Hoffm. (Asteraceae)	Runukirizo (Sy)	GP10	leaves	18.4
Plant 11 (Unidentified)	kabuna komwisheke	GP11	roots	6.2
Solanum delagoense (Solanaceae)	Entuntuza (S)	GP12	roots	5.7
Kigelia africana (Bignoniaceae)	Bolota (S)	GP13	roots	8.8
Kigelia africana (Bignoniaceae)	Bolota (S)	GP14	bark	20.2
Aloe maculata (Asphodelaceae)	chifurofuro (S)	GP15	roots	15.0
Harpagophytum procumbens (Pedaliaceae)	Maramatwa (S)	GP16	tubers	14.4

Common names are in local languages spoken in Zambezi region. S-Sifwe; Sy-Siyeyi; Sl-Silozi; E-English

Table 3.2 Percentage yield of sequentially extracted plant material

Fractions	*Pechuel leubnitziae* leaves	*Indigofera hofmanniana* roots	*Tribulus terrestris* fruits	*Strychnos cocculoides* roots
Hexane	3.0	0.22	2.5	0.91
Dichloromethane	5.0	4.6	0.76	0.50
Ethyl acetate	0.4	0.10	0.13	0.26
Methanol	4.0	5.2	3.25	3.9

3.3.2 TLC analysis

TLC is a fast and inexpensive method for identifying a number of compounds present in an extract. TLC analysis was done at every stage of extraction and isolation to examine the composition of the 16 crude extracts. TLC was also used to find suitable solvents to separate the compounds. Of the tested mobile phases, chloroform/methanol (10:1 and 5:1) were the best solvent which gave better separation for most of the extracts (Figure 3.8B), while chloroform/ethyl acetate (7:3) was good for GP7 extract. The separation was improper with other solvent mixtures and ratios tried (Figure 3.8A). Appropriate mobile phase was then used to run preparative TLC and CC in order to separate individual compounds from the mixture. As illustrated by Figure 3.8 all extracts consisted of several compounds that require separation. Extracts from GP2 and GP14 appear to have more polar compounds as it remained on the base line with the solvent system that separated other extracts. The five extracts that showed moderate growth inhibition activity against *N. gonorrhoeae* (GP1, GP7, GP8, GP9, GP10) were fractionated further using prepTLC in order to obtain large amounts of compounds of interest. A total of 26 fractions was obtained, GP1 gave five fractions (GP1A-GP1E), GP2 gave three fractions (GP2A-GP2C), GP7 gave five fractions (GP7A-GP7E), GP8 gave seven fractions (GP8A-GP8F) and GP9 gave six fractions (GP9A-GP9F). Some of these fractions were visible with naked eyes on the prepTLC plate while others were only detected under UV light (Figure 3.9). Even though separation was achieved using prepTLC, the purity of these fractions was not determined due to very low yields of the fractions. To improve the quantity of fractions, selected crude extracts were analysed using column chromatography. Figure 3.9 shows that the five compounds seen on TLC for GP1 could be separated successfully on prepTLC

using the same mobile phase used on simple TLC. Preparative TLC is thus a useful technique when isolating compounds in quantities larger than what a usual TLC plate can accommodate.

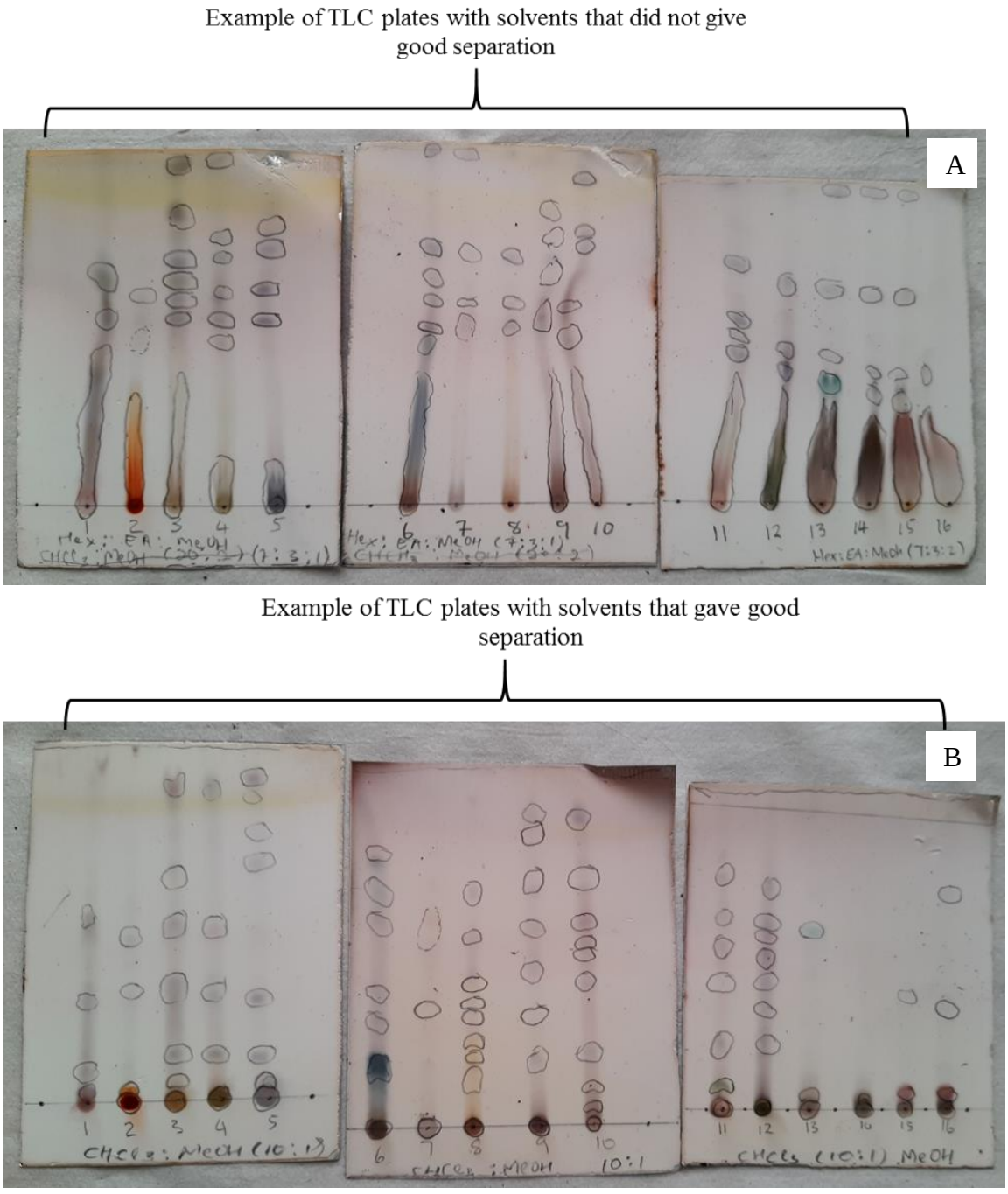

Figure 3.8. TLC plates of 16 extracts illustrating, (A) bad separation and (B) good separation of compounds from a DCM:MeOH extracts sprayed with p-anisaldehyde-sulfuric acid reagent

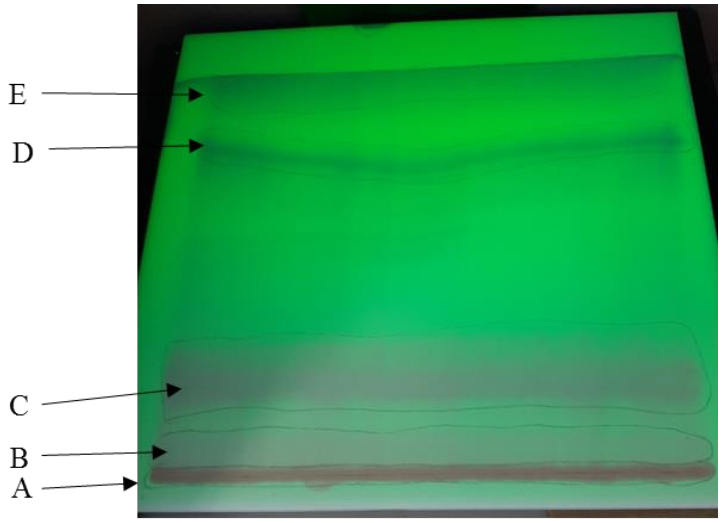

Figure 3.9. Preparative TLC plate showing 5 fractions obtained from extract GP1. The fractions are numbered A-E from the most polar to least polar fraction.

3.3.3 Antimicrobial activity

3.3.3.1 Growth inhibition of crude extracts

People choose plants for medication for reasons such as ease of access, low cost, improved health after use, cultural beliefs and many others. Scientific validation of medicinal use of plants is thus important to increase the trust and acceptability, thus encourage the use of such medicines. In this study, the antimicrobial activity of 16 extracts was studied to determine whether they are effective against Gram-negative and Gram-positive bacteria as well as a fungus. The antimicrobial activity of the 16 extracts is shown in Table 3.3. The results show that 14 (88%) extracts showed some degree of activity against at least two of *N. gonorrhoeae* strains. This indicate that the tested plant extracts have anti-gonococcal activity as well as activity against other microbes with inhibition zones ranging from 8-18 mm. The highest activity, with inhibition zone of 18 mm was observed in the crude root extract from *Z. mucronata* (GP2) against *N. gonorrhoeae* strain ATCC 19424, followed by

I. hofmanniana (GP7) and *S. occidentalis* (GP8) with 16 mm and 15 mm respectively against ATCC 31426. Extracts GP2, GP4 and GP9 exhibited moderate to strong activity against all four tested *N. gonorrhoeae* strains. Extracts GP1, GP2, GP3, GP4, GP7, GP8, GP9 and GP10 inhibited the growth of all *N. gonorrhoeae* strains with varying degree. This suggests that these extracts have antibacterial activity against *N. gonorrhoeae*. The difference in activity can possibly be attributed to the nature of the active ingredients as well as the level of concentration in the extracts.

Extracts GP1, GP3, GP4, GP9 and GP10 inhibited the growth of all microorganisms tested in this study. The observed activity may be indicative of the presence of broad-spectrum antimicrobial compounds or general toxins in the plants. The results obtained in this study for *Tribulus terrestris* leaves (GP4) contrasted the results reported by Murugesan et al. (27) who reported no anti-gonococcal activity of the leaf extract from this plant. DCM:methanol leaf extract of *T. terrestris* showed good anti-gonococcal activity with zone of inhibition of 8-13 mm. The difference in results could be due to the difference in seasonal variation and geographic location of the plants used, the extraction solvents used, types of strains and the assay methods. The result of this study is in agreement with the study by Chhatre et al. (28) who reported the antimicrobial activity of *T. terrestris* parts (leaves, fruits, stem and roots) on both Gram-positive and Gram-negative bacteria (28), as it exhibited growth inhibition for all tested microbes (Table 3.3). Shivani et al. (29) also reported anti-gonococcal activity of *T. terrestris* fruits. Of the four strains of *N. gonorrhoeae*, ATCC 43069 appears to be susceptible to most extracts with weak to moderate growth inhibition activity. ATCC 19424 was more resistant, as it was only inhibited by eight of the extracts.

These effects could be due to the biochemical composition of the strains as they are isolated from different regions in the world. Extracts from unidentified plant (GP11) and *Harpagophytum procumbens* (GP16) did not show any activity against all *N. gonorrhoeae* strains, thus their ethnobotanical use for treating gonorrhea is not supported by the results in this study. *Kigelia africana* bark extract (GP14) showed moderate activity while the root extract (GP13) showed weak activity. This is an indication that different plant parts obtained from the same plant can have different bioactive compounds and thus different activity. The activity of all extracts against *N. gonorrhoeae* were much lower than that of the standard antibiotic, tetracycline. The less potency of the extracts relative to the standard antibiotic could be because the extracts were crude and needed purification or that the concentration of the active compounds was too low. The observed anti-gonococcal activity could be due to presence of biologically active components. The plant extracts that exhibited significant antimicrobial activity (GP1, GP2, GP7, GP8, GP9, and GP10) were subjected to partial fractionation to isolate compounds responsible for the observed activity. Table 3.4 reports the potency of the fractions obtained from these extracts.

The zone of inhibition against the six non fastidious medically important microbial strains ranged from 8-11 mm, which was lower than that observed for *N. gonorrhoeae* strains. *S. aureus* showed resistance to most extract and no inhibition with the reference antibiotic, ampicillin. The activity of the reference antibiotic, ampicillin ranged from 8-27 mm, which in some cases was lower than the activity of the extracts (Table 3.3). This has demonstrated that natural products can be more effective compared to antibiotics that are on the market. *In-vitro* antimicrobial activity of the plant extracts under study against *N. gonorrhoeae* and

other microorganisms showed significant results that confirm the potential of these plants for medicinal use and therefore support their current ethnomedicinal use in treating infectious ailments. The result shows that the extracts possess substances that can inhibit the growth of not only *N. gonorrhoeae* but also other disease-causing microorganisms.

Table 3.3 Zone of inhibition of 16 plant crude extracts against four strains of *Neisseria gonorrhoeae* and 6 other microbes

		Inhibition zone, (mm)									
	Extract #	**ATCC 19424**	**ATCC 31426**	**ATCC 43069**	**ATCC 49226**	***S. aureus***	***S. mutans***	***L. plantensis***	***E. coli***	***K. pneumonia***	***C. albicans***
Plant name		*Neisseria gonorrhoeae* strains				other Gram positive & negative bacteria					
Strychnos cocculoides (r)	GP1	13±2	13±1	9±1	9±2	9±1	9±1	11±1	10±1	9±2	10±1
Ziziphus mucronata (r)	GP2	18±5	13±4	10±7	12±3	-	8±2	10±3	10±1	11±1	11±2
Tribulus terrestris (f)	GP3	13±5	13±3	8±1	10±1	8±1	10±1	8±2	9±1	9±1	10±1
T. terrestris (l)	GP4	11±1	13±2	10±2	11±3	9±1	9±2	10±3	11±1	11±2	10±2
Talinum sp. (t)	GP5	-	8±0	8±1	10±2	-	-	-	9±1	8±1	10±1
Gomphocarpus fruticosus (r)	GP6	-	14±6	9±2	12±2	8±1	8±1	8±2	9±1	8±1	11±1
Indigofera hofmanniana (r)	GP7	12±3	16±6	9±2	9±1	-	9±1	10±2	10±1	8±1	10±1
Senna occidentalis (r)	GP8	12±2	15±4	9±6	11±1	-	10±2	9±2	9±2	8±1	10±1
Pechuel-loeschea leubnitziae (r)	GP9	10±2	13±2	11±1	10±2	9±1	11±1	10±1	11±1	10±0	9±1
P. leubnitziae (l)	GP10	10±2	10±1	11±3	8±0	8±1	11±2	9±1	10±2	10±1	9±1
Plant 11 (unidentified) (r)	GP11	-	-	-	-	8±1	-	-	-	-	8±1
Solanum delagoense (r)	GP12	-	11±1	9±1	-	8±1	11±1	-	11±1	8±1	10±1
Kigelia africana (r)	GP13	-	-	8±0	8±5	8±2	9±2	8±1	10±1	8±1	10±1
K. africana (b)	GP14	-	10±0	9±1	9±2	-	-	8±1	9±1	-	8±0
Aloe maculata (r)	GP15	-	13±2	8±0	10±2	-	8±1	-	9±2	8±1	9±1
Harpagophytum procumbens (t)	GP16	-	-	-	-	-	8±1	-	8±5	-	8±1
Tetracycline*		30±2	29±2	35±2	10±1	NT	NT	NT	NT	NT	NT
Ampicillin		NT	NT	NT	NT	8±0	8±1	8±1	27±2	8±0	16±4
Dimethylsulfoxide		-	-	-	-	-	-	-	-	-	-

Note: Results are expressed as the mean of two replicate experiments measuring 2 wells for each experiment (n=4); mean ± standard deviation; * = Tetracycline concentration is 5 mg/mL; (-) no activity (clear zone of inhibition between 0 and 7 mm); (NT) = not tested. f, l, r, b = fruits, leaves, roots, and bark respectively.

3.3.3.2 Growth inhibition of fractions

Selected crude extracts (GP1, GP2, GP7, GP8, GP9, and GP10) were analysed by prepTLC and column chromatography to isolate compounds with gonococcal activity. Although extract GP2 gave the highest activity, it was not analysed on normal phase column chromatography due to its high polarity nature. The fractions obtained from preparative TLC were subjected to the same strains of *N. gonorrhoeae* to test for antimicrobial activities. As indicated in Figure 3.9, the fractions are numbered starting at the base of the TLC plate (A = base line). Table 3.4 shows the growth inhibition zone of four gonorrhea strains exhibited by the fractions obtained from five extracts whose crude showed activity. The results show that the less polar compounds have moderate to strong activity while polar compounds have weak to moderate activity. Fraction GP1E from *Strychnos cocculoides* exhibited the highest inhibition zone of 15 mm at a concentration of 7 mg/mL, while GP8G also gave strong activity with a zone of 16 mm at a high concentration of 17.6 mg/mL. There was an increase in activity for fraction GP1E giving an inhibition zone range of 10 – 15 mm at 7 mg/mL, compared to the crude extract of GP1 that gave zone of inhibition that ranged from 9 - 13 mm at 20 mg/mL. Other fractions from GP1 gave weak to moderate activity. This indicate that GP1E could be the compound mostly responsible for the activity of GP1 against *N. gonorrhoeae*. Due to low quantity of fractions, purification and isolation could not be done on extract GP1. The activity of GP9's fractions did not improve when compared to the crude extract. Fraction GP7C showed moderate to strong activity with zone of inhibition of 11-14 mm at a concentration of 7 mg/mL.

Based on these results, 3 extracts (GP1, GP7 and GP10) were carried further for column chromatography in order to improve the quantity and quality of the isolated compounds. From GP7 and GP10 crude extracts, three fractions (GP10-F6, GP7-1 and GP7-2) were obtained in abundance and in good purity, thus they were tested for anti-gonococcal activity. The results in Table 3.4 shows that fractions from GP7 have no antibacterial inhibitory effect against the growth of *N. gonorrhoeae* at all concentrations tested in this study. However, fraction F6 from GP10 showed strong anti-gonococcal activity with zone of inhibition ranging from 10 - 24 mm at a concentration of 10 mg/mL. Lack of anti-gonococcal activity from GP7's column chromatography fraction shows that the compound responsible for the crude extracts' activity was not successfully isolated. The preparative TLC fraction shows that GP7C could be the compound of interest.

Table 3.4 The growth inhibition zone of fractions obtained from prepTLC and column chromatography of five extracts (GP1, GP7, GP8, GP9 and GP10)

			zone of inhibition (mm)			
Extracts	**Fractions**	**Concentration (mg/mL)**	**ATCC 19424**	**ATCC 31426**	**ATCC 43069**	**ATCC 49226**
GP1*	GP1A	12	-	-	-	-
	GP1B	6	-	-	-	-
	GP1C	8	-	-	-	-
	GP1D	4	-	-	-	-
	GP1E	7	15±0.7	13±1.4	11±1.4	12±0.7
GP8*	GP8A	15	-	-	-	12±1
	GP8B	10	-	-	13±2	11±1
	GP8C	10	11±4	-	12±1	11±1
	GP8D	15	12±1	11±1	11±1	12±0
	GP8E	16	14±4	13±3	-	13±4
	GP8F	10	-	-	11±1	-
	GP8G	18	16±1	14±2	-	13±3
GP9*	GP9A	13	-	-	-	-
	GP9B	10	-	-	11±1	11±1
	GP9C	12	-	11±5	11±1	-
	GP9D	3	-	-	-	-
	GP9E	14	-	-	-	13±1
	GP9F	24	-	-	-	-
GP7**	GP7-1	10	-	-	-	-
	GP7-2	10	-	-	-	-
GP7*	GP7A	20	-	12±4	11±3	-
	GP7B	9	12±2	-	12±2	-
	GP7C	7	12±1	11±1	14±1	11±1
	GP7D	10	-	-	-	-
	GP7E	18	-	-	-	-

Note: * = extracts analysed using preparative TLC; ** = extracts analysed using column chromatography; n =4

3.3.3.3 Minimum inhibitory concentration (MIC)

The MIC is defined as the lowest concentration of the antimicrobial agent that will inhibit the visible growth of a microorganism after overnight incubation (30). The minimum inhibitory concentration of the crude extracts that showed antimicrobial activity against *N.*

gonorrhoeae and other microbes were determined by looking at the absorbance before and after incubation of the 96 well plate. If absorbance value increase after the incubation period, it is an indication that the extract did not inhibit the growth of microbes and thus turbidity increases. The inhibitory concentration of all crude extracts against *N. gonorrhoeae* strains and other microbes are presented in Table 3.5. As shown, out of the sixteen extracts tested by broth microdilution method, eleven extracts showed MIC of 5 mg/mL for at least one of the *N. gonorrhoeae* strains. The extracts inhibited growth of *N. gonorrhoeae* at a concentration range of 2.5 - 10 mg/mL, while the other microorganisms were inhibited at concentration range of 0.313 – 2.5 mg/mL. This is significant because there has been reports of co-detection of STIs with *C. albicans* (31). Extracts GP1, GP2, GP3, GP7, GP9 and GP10 showed inhibition at a concentration of 5 mg/mL for at least three of the *N. gonorrhoeae* strains. This confirms the results of the preliminary growth inhibition test by well diffusion method that showed that these extracts have moderate to strong anti-gonococcal activity.

These results reveal that six of the 16 plant extracts have *in-vitro* anti-gonococcal activity with MIC of 5 mg/mL. This is good results since confirmation of their anti-gonococcal activity support their traditional use for treating gonorrhea (32,33). In agreement with a previous study on *T. terrestris* extracts, the fruits extract (GP3) showed moderate anti-gonococcal activity with MIC of 2.5 – 5 mg/mL, while the leaf extract (GP4) showed weak activity with MIC over 10 mg/mL (29). *Tribulus terrestris* therefore could have potential as a herbal medicine with scientific evidence for the treatment of gonorrhea. Even though GP8 was one of the extracts that was selected to have moderate anti-gonococcal activity,

the MIC results show that it only inhibits the growth at high concentration of more than 10 mg/mL against all reference strains. Furthermore, the result shows that GP1 is the most active extract as it inhibited all reference strains at a concentration of 2.5 mg/mL and 5 mg/mLwhile other microbes were inhibited by the same extract at 0.313-2.5 mg/mL (Table 3.5). This is an indication that extract GP1 contains high amounts of active compounds that can kill a wide range of microorganisms. GP7 inhibited the growth of all four *N. gonorrhoeae* strains at 5 mg/mL. GP10 gave MIC of 2.5 – 10 mg/mL for *N. gonorrhoeae* strains. Extract GP1, GP2, GP3, GP7, GP9, and GP10 showed a wide range of activity against various organisms with MIC ranging from 2.5 – 5 mg/mL for most microorganisms. This suggest that the extracts have a broad-spectrum antibiotic effect. Extracts GP5, GP13, GP14, and GP15 showed anti-gonococcal activity only at concentration above 10 mg/mL and no or weak activity for non gonorrhea microbes suggesting that compounds in these extracts could be specific to *N. gonorrhoeae*. The antibacterial activity of plant crude extracts depends on the dose and the type of bacterial strains employed. Strain ATCC 43069 was inhibited mostly at high concentrations of extracts.

Table 3.5 Minimum inhibitory concentration (MIC) of crude extracts with inhibition activity against the tested microorganisms

	Microorganisms									
	ATCC 19424	**ATCC 31426**	**ATCC 43069**	**ATCC 49226**	***E. coli***	***S. aureus***	***C. albicans***	***S. mutans***	***L. plantensis***	***K. pneumonia***
Extract #	**MIC (mg/mL)**									
GP1	5	5	5	2.5	1.25	2.5	0.31	2.5	2.5	1.3
GP2	5	5	5	10	10	-	5	2.5	1.3	> 10
GP3	5	5	5	2.5	2.5	-	2.5	2.5	-	2.5
GP4	10	10	10	10	5	-	2.5	2.5	5	5
GP5	-	5	5	10	-	-	5	-	-	-
GP6	-	5	10	10	> 10	-	> 10	> 10	> 10	> 10
GP7	5	5	5	5	> 10	-	2.5	2.5	-	-
GP8	> 10	> 10	> 10	> 10	> 10	-	2.5	> 10	> 10	-
GP9	5	5	> 10	2.5	> 10	> 10	1.25	> 10	> 10	> 10
GP10	5	5	> 10	2.5	> 10	2.5	1.25	5	2.5	2.5
GP11	-	-	-	-	10	-	-	> 10	> 10	> 10
GP12	-	5	> 10	-	> 10	> 10	1.25	5	-	-
GP13	-	-	> 10	> 10	10	-	1.25	> 10	-	-
GP14	-	10	10	5	-	-	-	-	-	-
GP15	-	10	10	5	-	-	-	-	-	-
GP16	-	-	-	-	-	-	-	-	-	-

3.3.4 Isolation from *Indigofera hofmanniana*

Extract from *I. hofmanniana* (GP7) was fractionated on column chromatography and led to the isolation of two other compounds (Figure 3.12). The first one (GP7-1) eluted with 98.8:1.2 → 98.4:1.6 ($CHCl_3$:MeOH) and the second one (GP7-2) eluted with 98.2:1.8 → 97.8:2.2 ($CHCl_3$:MeOH), both of which precipitated out of solution (Figure 3.11). The compound was a white, shiny amorphous powder. The compound's solubility was tested, and it dissolved in acetone and DMS with Rf value of 0.53 for GP7-1 and 0.32 for GP7-2 using DCM:EA (1:1) mobile phase.

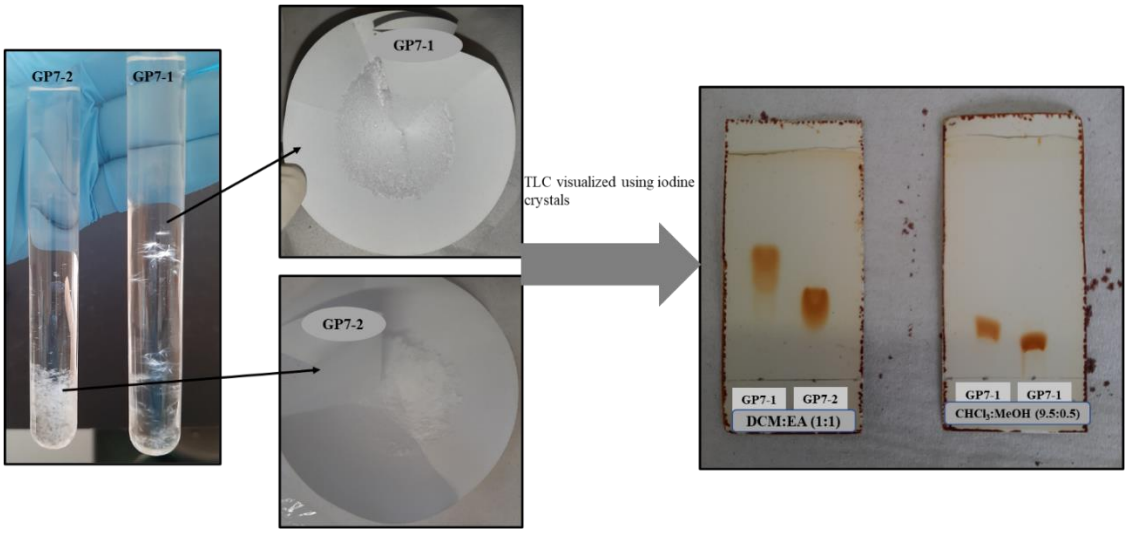

Figure 3.10. Filtered precipitate and TLC profile of compounds isolated from *Indigofera hofmanniana* roots

The structures were determined by NMR and mass spectrometry analysis and identified as [(2R,3S,4S,5R,6S)-4-hydroxy-3,5,6-tris(3-nitropropanoyloxy)oxan-2-yl]methyl-3-nitropropanoate, a known nitropropanoyl glucopyranose, commonly called Hiptagin (PubChem). The mass spectra showed a molecular ion peak at m/z 607.0 corresponding to M + Na^+ ion, which in combination with its ^1H- and ^{13}C-NMR data led to an elemental

composition of $C_{18}H_{24}N_4O_{18}$, a glucopyranose nitro ester. The sugar moiety in the structure elucidated for GP7-1 is the α-anomer of glucopyranose in view of the coupling constant (Figure 3.12). Fragment peaks at m/z 89.5 and 66.6 in this structure indicated the presence of an α-substituted pyranose ring which was confirmed by the ^{1}H NMR spectrum that showed typical signals of an α-monosubstituted pyranose ring at δ 5.23 (t, 4.2). The sugar moiety in the structure of GP7-2 is the β-anomer of glucopyranose in view of the coupling constant (Figure 3.12). Fragment peaks at m/z 92.0 and 70.6 in this structure indicated the presence of a α-substituted pyranose ring which was confirmed by the ^{1}H NMR spectrum that showed typical signals of an α-monosubstituted pyranose ring at δ 5.84 (d, 8.3). NMR spectra are given in Appendix 5.

A bioactivity guided fractionation strategy was followed throughout the separation procedure. However, the quantity of other fractions obtained from CC was not sufficient for bioassay. GP7-1&2 was obtained in large quantity, with percentage yield of 16% of the DCM extract, however it was inactive against *N. gonorrhoeae* strains at 20 mg/mL. The activity of the crude extracts can thus not be attributed to this compound.

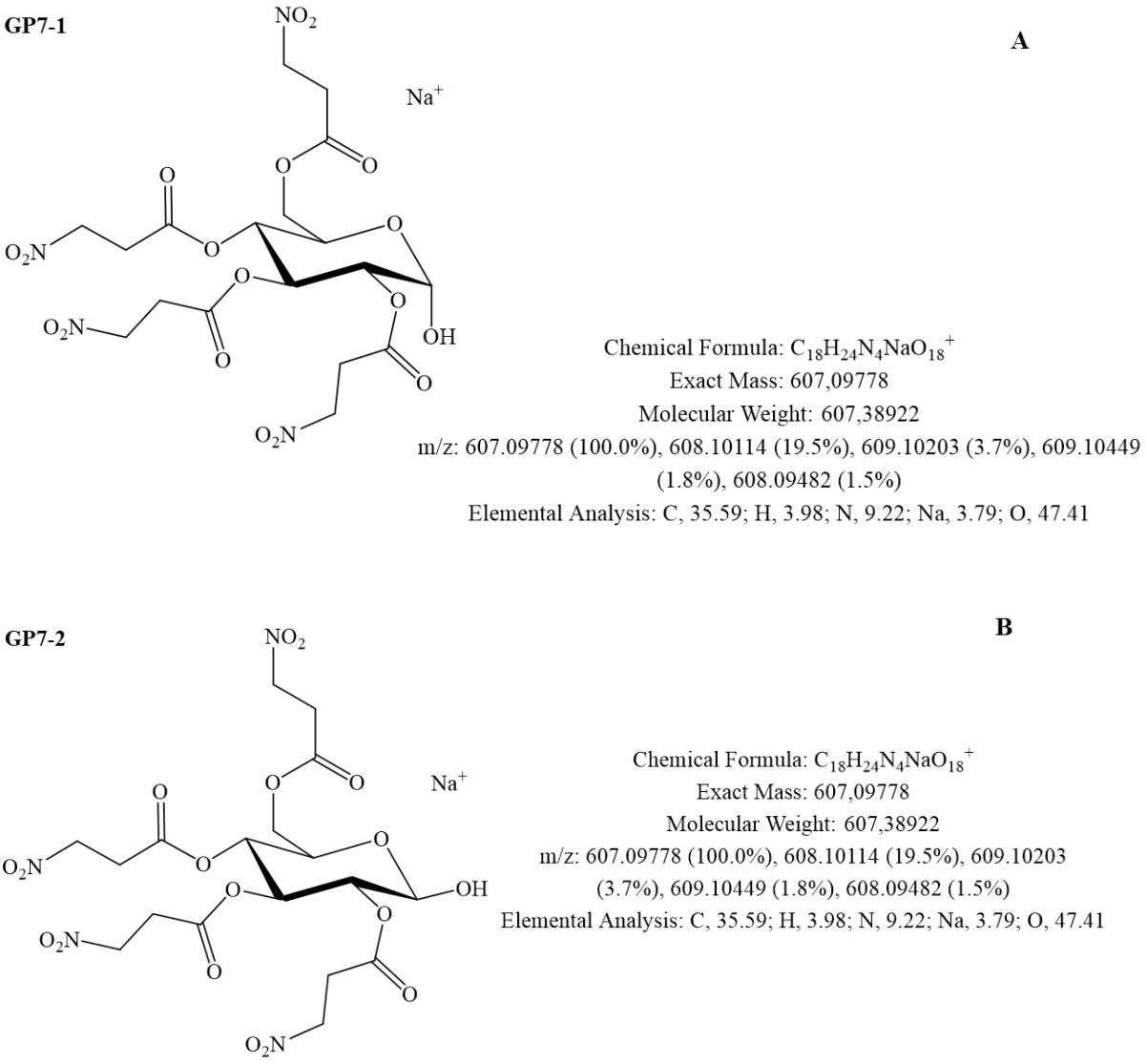

Figure 3.11. Structures of compounds isolated from the roots of *Indigofera hofmanniana*. (A) the α-anomer of glucopyranose, and (B) β-anomer of glucopyranose. On both mass spectra, there are ion peaks at m/z 607.0 corresponding to M+ Na^+

3.4 Conclusion

Antimicrobial analysis results support the traditional use of 10 of the 13 plants for the treatment of gonorrhea as six (*S. cocculoides, Z. mucronata, T. terrestris, I. hofmanniana, P. leubnitziae* and *Tallinum* sp.) of these exhibited anti-gonococcal activity against the four

strains of *N. gonorrhoeae* with MIC ranging from 2.5 -10 mg/mL and the other four extracts showed antimicrobial activity with MIC of ≥10 mg/mL. The results also show that some plants may contain compounds that may have broad spectrum antimicrobial activity as they inhibited Gram-negative, Gram-positive and fungi, for example GP1, GP9 and GP10 that inhibited growth of all tested microorganisms. The result of this study is important considering that *N. gonorrhoeae* is reported to exhibit resistance against currently used modern drugs. However, since crude extracts consist of multiple components mixtures as it was revealed with TLC analysis, further studies to isolate the compounds responsible for this activity and toxicity is recommended. A compound that was successfully isolated from *I. hofmanniana*, namely hiptagin, was not active against *N. gonorrhoeae*, further analysis is thus required to determine the active ingredient in this plant.

3.5 References

1. Le Roux PJ, Müller MAN, Mannheimer C, Curtis B. Le Roux & Müller ' s Field guide to the trees & shrubs of Namibia. 2nd ed. Mannheimer C, Curtis B, editors. Windhoek: Macmillan Education Namibia; 2018.

2. Welz AN, Emberger-Klein A, Menrad K. Why people use herbal medicine: Insights from a focus-group study in Germany. BMC Complement Altern Med. 2018;18(1):1–9.

3. Hossan S, Hanif A, Agarwala B, Sarwar S, Karim M, Taufiq-Ur-Rahman M, et al. Traditional use of medicinal plants in Bangladesh to treat urinary tract infections and sexually transmitted diseases. Ethnobot Res Appl. 2010;8:61–74.

4. Amri E, Kisangau DP. Ethnomedicinal study of plants used in villages around Kimboza forest reserve in Morogoro, Tanzania. J Ethnobiol Ethnomed [Internet]. 2012;8(1):1.

5. Cheikhyoussef A, Shapi M, Matengu K, Mu Ashekele H. Ethnobotanical study of indigenous knowledge on medicinal plant use by traditional healers in Oshikoto region, Namibia. J Ethnobiol Ethnomed. 2011;7:1–12.

6. Chinsembu KC. Green Medicines: Pharmacy of Natural Products for HIV and Five AIDS- related Infections. Africa in Canada Press; 2016. 314 p.

7. Mofolo MJ, Kadhila P, Chinsembu KC, Mashele S, Sekhoacha M. Green synthesis of silver nanoparticles from extracts of *Pechuel-loeschea leubnitziae*: their anti-proliferative activity against the U87 cell line. Inorg Nano-Metal Chem. 2020;50(10):949–55.

8. Mongalo NI, Mashele SS, Makhafola TJ. *Ziziphus mucronata* Willd. (Rhamnaceae): it's botany, toxicity, phytochemistry and pharmacological activities. Heliyon. 2020;6(4).

9. Adamu H, Abayeh O, Ibok N, Kafu S. Antifungal activity of extracts of some *Cassia*, *Detarium* and *Ziziphus* species against dermatophytes. Indian J Nat Prod Resour. 2006;5(5):357–60.

10. Olajuyigbe OO, Afolayan AJ. *In-vitro* antibacterial activities of the methanol extract of *Ziziphus mucronata* willd. subsp. *mucronata* willd. J Med Plants Res. 2011;5(16):3791–5.

11. Lekganyane MA, Matsebatlela TM, Howard RL, Shai LJ, Masoko P. The phytochemical, antibacterial and antioxidant activity of five medicinal plants against the wound infecting bacteria. African J Biotechnol. 2012;11(68):13210–9.

12. Semenya S. Bapedi phytomedicine and their use in the treatment of sexually transmitted infections in Limpopo Province, South Africa. African J Pharm Pharmacol. 2013;7(6):250–62.

13. Durgawale P., Datkhile K. Study of polyphenol content and anti- oxidative potential of *Tribulus terrestris* dry fruit extract. Int J Pharmacogn Phytochem Res. 2017;9(5).

14. Zhu W, Du Y, Meng H, Dong Y, Li L. A review of traditional pharmacological uses, phytochemistry, and pharmacological activities of *Tribulus terrestris*. Chem Cent J. 2017;11(1):1–16.

15. Akram M, Asif HM, Akhtar N, Shah PA, Uzair M, Shaheen G, et al. *Tribulus terrestris* Linn.: A review article. J Med Plants Res. 2011;5(16):3601–5.

16. Schrire BD. Notes Relating to the Genus *Indigofera* (Leguminosae-Papilionoideae) for Flora Zambesiaca: Springer, R Bot Gard Kew. 1998;53(3):651–68.

17. Gillett AJB. Additions to our knowledge of *Indigofera* L . in East Tropical Africa Published by : Springer. R Bot Gard Kew. 1970;24(3):465–506.

18. Gerometta E, Grondin I, Smadja J, Frederich M, Gauvin-Bialecki A. A review of traditional uses, phytochemistry and pharmacology of the genus *Indigofera*. J Ethnopharmacol. 2020;253(July 2019).

19. Hanphanphoom S, Krajangsang S. Antimicrobial activity of *Chromolaena odorata* extracts against bacterial human skin infections. Mod Appl Sci. 2016;10(2):159.

20. Nematollahi A, Aminimoghadamfarouj N, Wiart C. Anti-bacterial, Antioxidant activity and phytochemical study of *Diospyros wallichii* — an interesting Malaysia's endemic species of Ebenaceae. 2011;3(3):1732–6.

21. CLSI. Methods for dilution antimicrobial susceptibility tests for bacteria that grow aerobically; approved standard — 9th Ed. Wayne PC and LSI, editor. Vol. 32. CLSI document M07-A9; 2012. 18 p.

22. Wiegand I, Hilpert K, Hancock REW. Agar and broth dilution methods to determine the minimal inhibitory concentration (MIC) of antimicrobial substances. Nat Protoc. 2008;3(2):163–75.

23. Das K, Tiwari RKS, Shrivastava DK. Techniques for evaluation of medicinal plant products as antimicrobial agent: Current methods and future trends. J Med Plants Res. 2010;4(2):104–11.

24. Green KJ, Dods K, Hammer KA. Development and validation of a new microplate assay that utilises optical density to quantify the antibacterial activity of honeys including Jarrah, Marri and Manuka. PLoS One. 2020;15(12 December):1–25.

25. Bruker. TopSpin AU Progamming user manual, Version 003. 2018.

26. Złotek U, Mikulska S, Nagajek M, Świeca M. The effect of different solvents and number of extraction steps on the polyphenol content and antioxidant capacity of basil leaves (*Ocimum basilicum* L.) extracts. Saudi J Biol Sci. 2016;23(5):628–33.

27. Murugesan K, Rajendran P, Gnanasekaran A, Vikram RE, Anbalagan S. Preliminary studies on activity of *Ocimum sanctum*, *Drynaria quercifolia*, and *Annona squamosa* against *Neisseria gonorrhoeae*. Sex Transm Dis J Pharm Sci. 2013;2(3):1232–7.

28. Chhatre S, Nesari T, Somani G, Kanchan D, Sathaye S. Phytopharmacological overview of *Tribulus terrestris*. Pharmacogn Rev. 2014;8(15):45–51.

29. Shivani N, Pandey A. *In-vitro* antibacterial effect of medicinal plants against *Neisseria gonorrhoeae*. Environ Conserv J. 2009;10(3):97–100.

30. Rakholiya K, Vaghela P, Rathod T, Chanda S. Comparative study of hydroalcoholic extracts of *Momordica charantia* L. against foodborne pathogens. Indian J Pharm Sci. 2014;76(2):148–56.

31. López-Monteon A, Gómez-Figueroa FS, Ramos-Poceros G, Guzmán-Gómez D, Ramos-Ligonio A. Codetection of *Trichomonas vaginalis* and *Candida albicans* by PCR in urine samples in a low-risk population attended in a clinic first level in Central Veracruz, Mexico A. Biomed Res Int. 2013;ID 281892.

32. Ceruso M, Clement JA, Todd MJ, Zhang F, Huang Z, Anastasio A, et al. The inhibitory effect of plant extracts on growth of the foodborne pathogen, *Listeria monocytogenes*. Antibiotics. 2020;9(6):1–13.

33. Bussmann RW, Malca-García G, Glenn A, Sharon D, Chait G, Díaz D, et al. Minimum inhibitory concentrations of medicinal plants used in Northern Peru as antibacterial remedies. J Ethnopharmacol. 2010;132(1):101–

CHAPTER 4: *IN-VITRO* ANTI-GONORRHEAL ACTIVITY OF A SESQUITERPENE LACTONE, XERANTHOLIDE ISOLATED FROM THE LEAVES OF *PECHUEL-LOESCHEA LEUBNITZIAE*

This chapter is published in the South African Journal of Botany

South African Journal of Botany 147 (2022) 314–318

Contents lists available at ScienceDirect

South African Journal of Botany

journal homepage: www.elsevier.com/locate/sajb

In-vitro anti-gonorrheal activity of a sesquiterpene lactone, xerantholide isolated from the leaves of *Pechuel-loeschea leubnitziae*

Moola M. Nyambe[a,*], Edet F. Archibong[b], Mamello Sekhoacha[c], Kazhila C. Chinsembu[d]

[a] Department of Physics, Chemistry and Material Science, School of Science, Faculty of Agriculture, Engineering and Natural Sciences, University of Namibia, P/Bag 13301, Windhoek, Namibia
[b] Department of Pharmaceutical Sciences, School of Pharmacy, Faculty of Health Sciences and Veterinary Medicine, University of Namibia, P/Bag 13301 Windhoek, Namibia
[c] Department of Pharmacology, Faculty of Health Science, University of the Free State, P.O. 339, Bloemfontein 9300, South Africa
[d] Department of Biochemistry, Microbiology and Biotechnology, School of Science, Faculty of Agriculture, Engineering and Natural Sciences, University of Namibia, P/Bag 13301, Windhoek, Namibia

Abstract

Gonorrhea is the second most prevalent sexually transmitted bacterial infection in the world. The global increase in the spread of gonorrhea is due to the fact that *Neisseria gonorrhoeae* has developed resistance to antimicrobials used as first-line treatments. In the search for new anti-gonorrheal agents, this study seeks to validate the use of a medicinal plant, namely, *Pechuel-loeschea leubnitziae*, for which both the root and the leaf extracts are commonly used as a remedy for gonorrhea. Bioassay guided fractionation of dichloromethane and methanol crude extracts (MIC_{50} = 0.730 - 3.07 mg/mL) was carried out. From the most active fraction F6, nearly colorless crystals were isolated and single crystal X-ray diffraction analysis identified the compound as a known sesquiterpene lactone, xerantholide. The compound showed activity against *N. gonorrhoeae* (MIC_{50} = 0.095 mg/mL) comparable with tetracycline, a positive control. This study shows that *P. leubnitziae* extracts have *in-vitro* anti-gonococcal activity and that xerantholide is the active anti-gonorrheal ingredient. The finding supports the traditional use of this plant to treat gonorrhea. This is the first report on the activity of xerantholide isolated from *P. leubnitziae* crude leaf extract against *N. gonorrhoeae*.

Keywords: *Pechuel-loeschea leubnitziae*; *Neisseria gonorrhoeae*; gonorrhea; xerantholide; sesquiterpene lactone

4.1 Introduction

Gonorrhea is the second most prevalent bacterial sexually transmitted infection (STI) worldwide (1). The World Health Organization estimates that 106 million new cases of gonorrhea occur globally every year (2). Gonorrhea is caused by a Gram-negative bacterium, *Neisseria gonorrhoeae*, which affects the mucosal area of the reproductive system, mouth, throat, and eyes (3). Gonorrhea can also be passed from a mother to her baby during childbirth (4). Diagnosing gonococcal infections is a challenge especially in women because a high proportion of these infections are asymptomatic. When symptoms are present in women, the disease is often characterized by nonspecific symptoms that can be mistaken for bladder and vaginal infections. Men with gonorrhea may experience burning sensation when urinating, a white, yellow, or green urethral discharge, and scrotal pain (5). Coinfection with gonorrhea is common in patients with HIV infection (6). If left untreated, gonorrhea can result in critical complications that include infertility and gonococcemia, a blood infection which can result in disseminated gonococcal infection (7).

Neisseria gonorrhoeae has developed resistance to antibiotics, such as, azithromycin and cepharosporins used as first-line treatments (2). This resistance is attributed to the worldwide spread of the penicillinase-producing *Neisseria gonorrhoeae* (PPNG) isolates (8,9). A drug that is well tolerated, effective and convenient is therefore needed. Since plants are commonly used in traditional health care for the treatment of gonorrhea in Namibia, it is worth investigating the therapeutic effect as well as the active constituents of these plants. One of the plants used to treat gonorrhea in Namibia is *Pechuel-loeschea*

leubnitziae (10,11). The plant is characterized by strong pungent and unpleasant smell. It is commonly known by various names depending on the region and tribe in Namibia: Libbobbozo (Siyeyi), Ekombombo (Sifwe), Edimba, Oshizimba (Oshiwambo), Omundumba (Herero), Auxan!khâb (Khoekhoegoab), Bitterbos (Afrikaans), Stinky bush (English). Other ethnomedicinal uses of *P. leubnitziae* include the management of colds, skin diseases including burns in stock, fever, cough, and malaria (11). The traditional use of this plant for malaria treatment was supported by Kadhila et al.'s study (12) which ascribed the leaf extract's antiplasmodial activity to the presence of xerantholide. Different parts of this plants are reported to posses' antimicrobial activities against fungi, Gram-negative and Gram-positive bacteria such as, *Candida albicans*, *Neisseria meningitis*, *Escherichia coli*, *Shigella flexneri*, *Proteus vulgaris*, *Pseudomonas aeruginosa*, and *Staphylococcus aureus* (13). Despite the common use of this plant to treat gonorrhea, no study has confirmed its anti-gonococcal property *in-vitro*. This study reports on the *in-vitro* anti-gonococcal activity of the crude leaf extract and sesquiterpene lactone (xerantholide) of *P. leubnitziae* against *N. gonorrhoeae* strains.

4.2 Materials and methods

4.2.1 Plant material collection

Pechuel-loeschea leubnitziae (Kuntze) O.Hoffm was selected based on ethnobotanical data on the use of the plant for treating gonorrhea in Katima Mulilo and surrounding areas (10). A plant collection permit (authorization no: AN20181004) for the collection of plant material used in this study was obtained from the Ministry of Environment and Tourism of Namibia through National Commission on Research and Technology (NCRST). *P.*

leubnitziae leaves were collected from Sangwali village in Zambezi region of Namibia on 31 December 2019 (GPs coordinates 18°15'32"S, 23°38'17"E). The botanical identification of the plant was confirmed at the National Botanical Research Institute (NBRI) of Namibia under the voucher number WIND102755. The leaves were cleaned with water, air dried under shade at room temperature (RT) and then ground into fine powder.

4.2.2 Extraction of the plant material

Three crude extracts (dichloromethane (DCM), methanol (MeOH) and a mixture of DCM:MeOH (1:1)) of *P. leubnitziae* leaves were prepared by extracting about 30 g using 300 mL. Each extraction was carried out for 48 hours by maceration with occasional stirring at RT. To make sure that the residue was exhaustively extracted, it was re-extracted twice with 200 mL of the respective solvent for 8 hours. The extracts obtained were then concentrated to dryness by air drying in a fume hood and percentage yields were calculated.

4.2.3 Microorganisms and growth conditions

Neisseria gonorrhoeae strains ATCC19424, ATCC31426, ATCC43069 and ATCC49226 were purchased from American Type Culture Collection. The strains were rehydrated in Brain Heart Infusion (BHI) broth and grown at 37 ºC. Bacterial strains were grown in Thayer Martin agar and BHI broth under anaerobic conditions (candle extinction jar) for all experiments. For each test, overnight bacterial suspension was standardized to 0.5 McFarland standard where the turbidity of the suspension was measured spectrophotometrically to be in the range of 0.08-0.13 at OD 625.

4.2.4 Anti-gonococcal activity

Growth inhibitory effects of crude extracts and isolated compound were tested against *N. gonorrhoeae* using agar well diffusion method as described in literature (14) with some modifications. Using sterile micro-tips and a spreader, 20 µL of standardized microbes were spread on the agar plate and allowed to stand for 5 minutes. Using a cork borer (No. 3), wells (7 mm diameter) were cut into the inoculated agar and 50 µL at a concentration 10 mg/mL of the crude extract and pure compound dissolved in dimethylsulfoxide (DMSO), was filled into the wells separately. To allow the extracts to diffuse into the medium, the plates were allowed to stand for 1 hour in the fume hood. Plates were incubated at 37 ºC for 24 hours. The extract was spotted in duplicate, and the experiment was done twice. DMSO was used as the solvent control and tetracycline was used as a reference antibiotic. A clear distinct inhibition zone around the well indicated the presence of antibacterial activity.

4.2.5 Minimum inhibitory concentration

The minimum inhibitory concentration (MIC) of the extracts was determined by broth microdilution method using the 96 well plates. A volume of 50 µL of sterile broth was placed in all the 96 wells, then 50 µL of test samples (extracts, DMSO and antibiotic) in duplicate, at the concentration of 5 mg/mL dissolved in DMSO were placed in the first row (line A) wells. Serial dilution (50 µL) was done up to the last well in each row to obtain concentrations ranging from 0.01 mg/mL to 5 mg/mL of extracts which make up 50 µL. Then, 50 µL of the standardized microbial strains were added to each of the wells except for the last row (row 12) that only had broth serving as a blank, while a well with broth and

microbes only, served as a control. Broth (100 µL) was added to all the wells to make the total of 200 µL in each well. Two other control wells with DMSO and tetracycline were included to serve as negative and positive controls respectively. The absorbance was measured at 625 nm before and after incubating the plate for 24 hours at 37 ˚C in order to measure the reduction of bacterial growth in each well. MIC_{50} was defined as 50% inhibition in growth of the initial bacterial inoculum when compared with the control.

4.2.6 Fractionation and isolation of anti-gonococcal extracts

The DCM crude extract exhibited the highest anti-gonococcal activity and was thus subjected to normal-phase column chromatography (CC) for further fractionation with solvents of increasing gradient polarity: [(9:1 → 0:10) DCM/Hexane, (9:1 → 0:10) DCM/ethyl acetate (EA), (9.5:0.5 → 9:1) DCM/MeOH]. A 1.0013 g sample of crude extract was fractionated over silica gel 60 (63 – 200 µm) to yield 86 fractions. Following elution, fractions were qualitatively evaluated using thin layer chromatography (TLC). Fractions with similar TLC profiles were pooled together to get 12 fractions. Combined fractions were allowed to concentrate slowly in an undisturbed area to allow formation of crystals. Fraction 6 (F6) that eluted with 9:1 → 7:3 (DCM:EA) crystallized, while other fractions dried without crystals. Hence the fraction was further purified by recrystallization and crystals were grown by dissolving F6 in DCM:Hexane (1:1) and allowing for slow evaporation at RT. To remove the colour, crystals were washed with diethyl ether resulting in colourless crystalline compound. A 143.7 mg of the pure compound (GP10) was obtained. TLC analysis of the crystals showed one spot under UV light. The compound's

solubility was tested, and it dissolved in DCM and DMSO. The structure of the isolated compound was elucidated from data obtained from crystallography analysis.

4.2.7 X-ray crystallographic data

Single-crystal X-ray diffraction data were collected on a Bruker D8 Venture diffractometer using graphite-monochromated Mo-Kα radiation (χ = 0.71073 Å). Data collection was carried out at 100 K. Temperature was controlled by an Oxford Cryostream cooling system (Oxford Cryostat). Cell refinement and data reduction were performed using the forementioned program (15). The data were scaled and absorption correction performed using SADABS (16). The structure was solved by direct methods using SHELXS-97 and refined by full-matrix least-squares methods based on F^2 using SHELXL-2014 (16) and using the graphics interface program X-Seed (17,18). The programs X-Seed and POV-Ray were used to prepare molecular graphic images (Persistence of Vision Pty. Ltd. 2014). All non-hydrogen atoms were refined anisotropically. All hydrogen atoms were placed in idealised positions and refined in riding models with U_{iso} assigned 1.2 or 1.5 times U_{eq} of their parent atoms and the C-H bond distances were constrained from 0.95 Å to 1 Å. The structure was refined to R factor of 0.0413. The Flack x parameter is small with large standard uncertainties (s.u.), indicating the absolute structure configuration cannot be determined, probably due to light atom Mo-Kα data.

4.3 Results

4.3.1 Extraction yield

Details of the extracts are shown in Table 4.1. The highest percentage yield was achieved when methanol was used as the extracting solvent, whereas DCM gave the lowest percentage yield, an indication that the majority of compounds in the leaves are soluble in methanol and were polar. TLC profile of the crude extracts showed that the compounds which were isolated from the leaves were found in both DCM and MeOH extract. Compound GP10 was isolated from fraction F6 as clear crystals in good yield (14.3%). This was also subjected to anti-gonococcal activity testing.

Table 4.1 Yield and physical states of *Pechuel-loeschea leubnitzae* crude leaf extract

Solvent	Material (g)	Recovery (%)	Physical state
DCM:MeOH	30.18	18.4	Flaky Blackish green
DCM	30.45	6.82	Sticky dark green
MeOH	30.80	24.8	Sticky dark green

4.3.2 Anti-gonococcal activity

MIC of extracts and fraction obtained from the leaves of *P. leubnitziae* using methanol and DCM were determined against *N. gonorrhoeae* strains using microbroth dilution method. The concentration of crude extracts, isolated compound of *P. leubnitziae* leaves and tetracycline leading to inhibition of 50% of *N. gonorrhoeae* activity (MIC_{50}) is presented in Table 4.2. The isolated compound, GP10 was the most potent growth inhibitor with MIC_{50} ranging between 0.095 - 0.808 mg/mL compared to crude extracts that exhibited anti-gonorrheal activity with MIC_{50} values ranging between 0.730 and >5.00 mg/mL. The strain ATCC49226 showed resistance as none of the crude extracts inhibited its growth

above 50% at a concentration of 5 mg/mL. The isolated compound and tetracycline inhibited this strain with (0.808 mg/mL) 58.2±1.8% and (0.341 mg/mL) 53.1±0.1 inhibition, respectively, while all crude extracts inhibited ATCC49226 activity at less than 30%. From the MIC values, the activity of GP10 (0.095 and 0.096 mg/mL) was close to that of tetracycline (0.019 and 0.013 mg/mL) against the ATCC31426 and ATCC43069 strains, respectively. The activity of GP10 (0.400 mg/mL) is nearly half of that of tetracycline (0.21 mg/mL) against the ATCC19424. Methanol extract only inhibited 42% of *N. gonorrhoeae* strain at a concentration of up to 3.07 mg/mL.

Table 4.2 The percentage inhibition of *Neisseria gonorrhoeae* strains and concentration leading to 50% inhibition (MIC_{50}) of extracts and pure compound from *Pechuel-loeschea leubnitziae* leaves

	MIC_{50} (mg/mL) of *Neisseria gonorrhoeae* strains							
	ATCC19424		**ATCC31426**		**ATCC43069**		**ATCC49226**	
Extracts	MIC_{50} (mg/mL)	% inhibit	MIC_{50} (mg/mL)	% inhibit	MIC_{50} (mg/mL)	% inhibit	MIC_{50} (mg/mL)	% inhibit
GP10[a]	0.400	61.4±3.6	0.095	55.4±6.6	0.096	55.1±1.0	0.808	58.2±1.8
DCM	1.16	51.0±12	0.829	50.0±9.1	0.730	52.7±2.2	>5.00	<30
DCM:MeOH	1.41	50.0±5.6	1.68	49.1±4.3	0.998	50.0±4.3	>5.00	<30
MeOH	3.07	42.0±11	2.00	42.4±2.1	1.56	40.7±2.3	>5.00	<30
Tetracycline	0.21	88.3±0.2	0.019	55.4±2.9	0.013	55.5±3.1	0.341	53.1±0.1

[a] Isolated compound. Results expressed as % mean ± standard deviation (n=4)

4.3.3 Isolation from Pechuel-loeschea leubnitziae

The purity of the isolated compound was tested using TLC before x-ray analysis. Figure 4.1 shows the TLC under UV light at short wavelength (254 nm) for xerantholide crystals. The Rf value of the pure compound was calculated to be 0.6 when DCM:ethyl acetate (7:3) was used as the eluent.

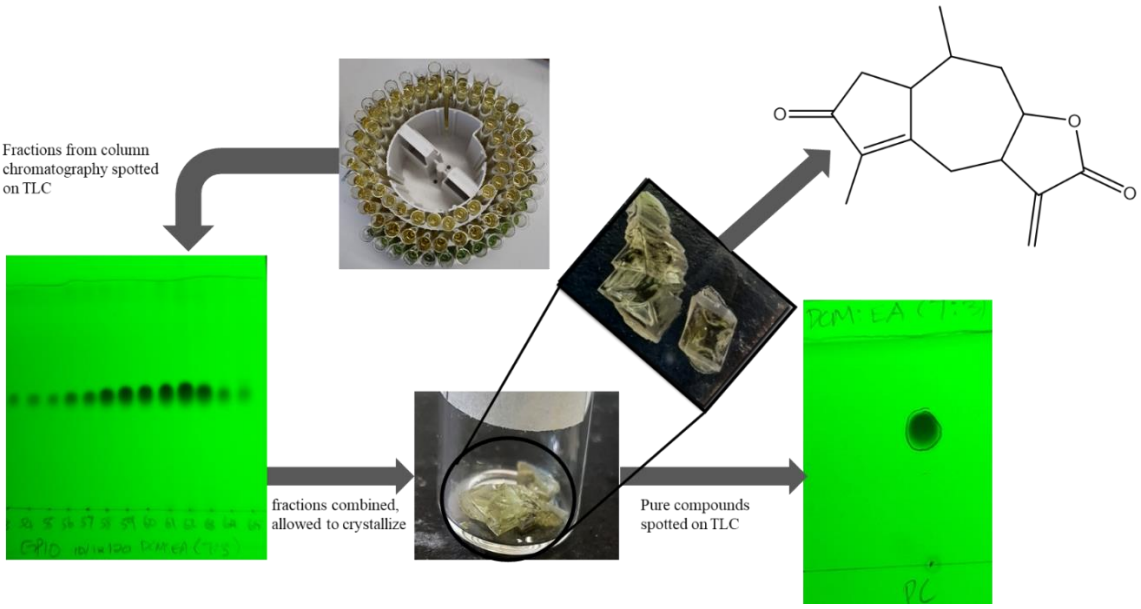

Figure 4.1. TLC profile of *Pechuel-loeschea leubnitziae* leaf fractions collected from column chromatography and the resulting crystals that formed. A single crystal X-ray diffraction was then used to determine the structure of xerantholide

4.3.4 Structure determination of GP10 by X-ray crystallography

Based on the MIC results, the DCM extract was selected for fractionation and purification to identify the active compound/s. A single crystal was selected and subjected to x-ray diffraction (XRD) analysis. XRD measurements of the crystal confirmed the compound as xerantholide (5,8-Dimethyl-3-methylene-3a,7,7a,8,9,9a-hexahydroazuleno[6,5-b]furan-2,6(3H,4H)-dione), with molecular formula ($C_{15}H_{18}O_3$) (Watson et al., 1985). The ball-

stick representation of the structure obtained from the x-ray studies of the isolated compound is shown in Figure 1.1. The XRD results showed that the compound forms colourless orthorhombic crystals, space group P212121. The crystallographic data collection and refinement conditions for the crystal structure are summarized in Tables 4.3 and 4.4. Complete data for the X-ray structure can be found in the supplementary material (Appendix 4).

Table 4.3 Selected geometric parameters of the isolated compound

Bond length (Å)		**Bond Angles (°)**		**Torsion Angles (°)**	
O1-C8	1.478(2)	C8 -O1 -C12	109.20(14)	C8 -O1 -C12 -O2	-170.02(18)
O1-C12	1.355(2)	C2 -C1 -C5	103.03(15)	C5 -C1 -C2 -C3	3.9(2)
O2-C12	1.211(2)	O3 -C3 -C4	126.22(18)	C1 -C2 -C3 -O3	175.24(19)
O3-C3	1.227(3)	O2 -C12 -C11	129.37(	O3 -C3 -C4 -C5	-175.8(2)
C1-C2	1.543(3)	C1 -C10 -C15	112.44(16)	O3 -C3 -C4 -C14	4.4(3)
C1-C10	1.551(3)	C7 -C11 -C13	130.23(18)	C5 -C6 -C7 -C11	179.05(16)
C4-C14	1.486(3)	C7 -C8 -C9	115.96(15)	C7 -C11 -C12 -O2	-169.8(2)
C7-C8	1.528(2)	C12 -C11 -C13	122.76(18)	C13 -C11 -C12 -O1	-167.6(2)
C8-C9	1.507(3)	O1 -C8 -C7	104.45(14)	C13 -C11 -C12 -O2	13.8(4)
C11-C13	1.319(3)	O1 -C8 -C9	109.03(15)	C8 -C7 -C11 -C12	-23.74(19)

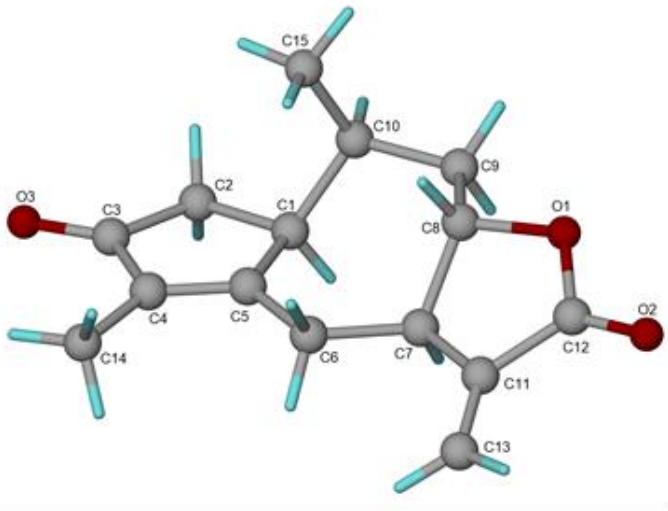

Figure 4.2. Xerantholide (5,8-Dimethyl-3-methylene-3a,7,7a,8,9,9a-hexahydroazuleno[6,5-b]furan-2,6(3H,4H)-dione) isolated from *Pechuel-loeschea leubnitziae* leaves. Compound structure elucidated from crystallography data

Table 4.4 Crystallographic data and structural refinement of the isolated compound, xerantholide

	Xerantholide
Empirical formula	$C_{15}H_{18}O_3$
Formula weight (amu)	246.29
Temperature (K)	173
Wavelength (Å)	0.71073
Crystal system	orthorhombic
Space group	P212121
Unit cell dimensions	
a (Å)	9.6077(6)
b (Å)	10.7727(7)
c (Å)	12.5855(7)
α (°)	90
β (°)	90
γ (°)	90
V (Å^3)	1302.61(14)
Z	4
D_{calcd} (mg/m$^{3)}$	1.256
Absorption coefficient (mm^{-1})	0.086
Absorption correction type	multi-scan
F(000)	528
Crystal description	Colourless, block
Crystal size (mm)	0.24 × 0.40 × 0.41
Θ range for data collection (°)	2.5 - 28.3
Limiting indices	$-12 \leq h \leq 12$ $-14 \leq k \leq -14$ $-16 \leq l \leq 16$
Reflections collected/unique	59247/3230 [R_{int} = 0.176]
Data/restraints/parameters	3230/0/165
Goodness-of-fit	1.029
Final R indices [I>$2\sigma(I)$]	R_1 = 0.0413
	wR_2 = 0.1086
R indices (all data)	R_1 = 0.0467
	wR_2 = 0.1043

4.4 Discussion

The search for effective and safe antimicrobial agents for the treatment of gonorrhea actively continues because of the devastating impact of antimicrobial resistance of *N. gonorrhoeae* globally. In this study, the isolated compound (GP10) which was subsequently identified by X-ray chrystallography as xerantholide and the crude extracts of *P. leubnitziae* leaves were tested against *N. gonorrhoeae* to determine the plant's potential as a source of antimicrobial compounds. The crystallographic parameters in this study were compared with the ones obtained for a xerantholide isolated from *Decachaeta scabrella* (B.L. Rob) R.M. King & H. Rob. var. *scabrella* (19). The atomic distance, angles, and torsion angles of the optimized structures from the current study are very similar to those reported by (19), thereby confirming the identity of the compound as xerantholide, a secondary metabolite that belongs to the group of C15 terpenoids, commonly known as sesquiterpene lactones. Several pharmacological activities of sesquiterpene lactones are documented including antibacterial, antiviral, antifungal and antimalarial. Apart from terpenoids, phytochemicals such as phenolics, alkaloids, saponins, flavonoids and tannins are reported to be present in the leaves of *P. leubnitziae* (20). It is noteworthy that in their case xerantholide was isolated from *P. leubnitziae* (12,21) and the structure determined by NMR analysis. In this study, xerantholide was isolated in very good yields from the leaves of *P. leubnitziae* where it represents about 14% of the total metabolite content of the dichloromethane extract (Table 4.1). Both the DCM and DCM:MeOH crude extracts, as well as xerantholide, showed *in-vitro* anti-gonorrheal activity by inhibiting bacterial growth of tested strains. Although the DCM crude extract inhibited growth of all four test strains, the best anti-gonococcal activity was observed with xerantholide with MIC_{50}

ranging from 0.095-0.808 mg/mL. This shows that the impurities in the DCM crude extract mask the potency of the active ingredients. TLC profiling in DCM:EA solvent system showed the presence of this compound in methanol extract, but weak activity against *N. gonorrhoeae* strains was observed with methanol extract in this study signifying low concentration of the active ingredient. These results thus show that the compound responsible for the anti-gonococcal activity is readily soluble in DCM and slightly soluble in methanol. MIC_{50} results indicated that xerantholide exhibited activity that was favourably close to that of tetracycline with the former showing slightly lower activity against ATCC19424 and ATCC49226. Only xerantholide and tetracycline showed activity against ATCC49226, a strain which displayed resistance to crude extracts. This anti-gonococcal activity of xerantholide is of interest considering the increasing multiple drug resistance of *N. gonorrhea*. The finding, therefore, highlights the potential of this compound as an antimicrobial agent. Tetracycline MIC_{50} values in this study (0.013-0.34 mg/mL) are consistent with values reported in other studies (22,23). Although the activity of the isolated compound and crude extracts from *P. leubnitziae* leaves was observed at MIC values above the breakpoints (22) of other antibiotics currently used for the treatment of gonorrhea such as ceftriaxone and azithromycin, it has potential as an alternative option as a natural medicine because of its potency. Unfortunately, high toxicity (IC_{50} = 2.75 µg/mL) against ovary mammalian cells and insects has been reported for this compound (12,24). Therefore, patients must use this plant with care for the treatment of gonorrhea. Awareness is needed to inform communities that use this plant in traditional treatments in order to avoid bad practices such as overdose or bad method of use. Further, quantitative structure activity relationship (QSAR) studies of this compound is recommended in order

to expand our knowledge about its toxicity while maintaining or improving the anti-gonococcal activity and such studies are ongoing in our laboratory.

4.5 Conclusion

This study shows that *P. leubnitziae* extracts have *in-vitro* anti-gonococcal activity. X-ray crystallography data and antibacterial test point to xerantholide as the active compound against *N. gonorrhoeae*. Although isolation of xerantholide from *P. leubnitziae* has previously been reported, this work reports for the first time on the activity of *P. leubnitziae* extract and xerantholide against *N. gonorrhoeae*. The findings of this work support the use of *P. leubnitziae* traditionally to treat gonorrhea. QSAR studies of xerantholide and its interactions with the target molecule are recommended in order to have a better understanding of mechanism of action and toxicity of the compound.

4.6 References

1. Unemo M, Golparian D, Stary A, Eigentler A. First *Neisseria gonorrhoeae* strain with resistance to cefixime causing gonorrhoea treatment failure in Austria. Euro Surveill. 2011;16(43):pii=19998.

2. World Health Organization. Emergence of multi-drug resistant *Neisseria gonorrhoeae* – Threat of global rise in untreatable sexually transmitted infections. 2012;WHO/RHR/11(June).

3. Jones A, Aro H, Jones A, Jonsson A, Aro H. *Neisseria gonorrhoeae* infection causes a G1 arrest in human epithelial cells. FASEB J. 2007;21(March 2007):345–55.

4. Hewitt CS, Abutaleb NS, Elhassanny AEM, Nocentini A, Cao X, Amos DP, et al. Structure-activity relationship studies of acetazolamide-based carbonic anhydrase inhibitors with activity against *Neisseria gonorrhoeae*. ACS Infect Dis. 2021;

5. Workowski K. In the Clinic: Chlamydia and gonorrhea. Ann Intern Med. 2013;158(ITC):1–16.

6. Hazel A, Ponnaluri-Wears S, Davis GS, Low BS, Foxman B. High prevalence of *Neisseria gonorrhoeae* in a remote, undertreated population of Namibian pastoralists. Epidemiol Infect. 2014;142(11):2422–32.

7. Mayor MT, Roett MA, Uduhiri KA. Diagnosis and management of gonococcal infections. Am Fam Physician. 2012;86(10):931–8.

8. Micaëlo M, Goubard A, La Ruche G, Denamur E, Tenaillon O, Cambau E, et al. Molecular epidemiology of penicillinase-producing *Neisseria gonorrhoeae* isolates in France. Clin Microbiol Infect. 2017;23(12):968–73.

9. Wi T, Lahra MM, Ndowa F, Bala M, Dillon JAR, Ramon-Pardo P, et al. Antimicrobial resistance in *Neisseria gonorrhoeae*: Global surveillance and a call for international collaborative action. PLoS Med. 2017 Jul 1;14(7).

10. Chinsembu KC. Green Medicines: Pharmacy of Natural Products for HIV and Five AIDS- related Infections. Africa in Canada Press; 2016. 314 p.

11. Le Roux PJ, Müller MAN, Mannheimer C, Curtis B. Le Roux & Müller ' s Field Guide to the Trees & shrubs of Namibia. 2nd ed. Mannheimer C, Curtis B, editors. Windhoek: Macmillan Education Namibia; 2018.

12. Kadhila NP, Sekhoacha M, Tselanyane M, Chinsembu KC, Molefe-Khamanga DM. Determination of the antiplasmodial activity, cytotoxicity and active compound of *Pechuel-loeschea leubnitziae* O. Hoffm. (Asteraceae) of Namibia. SN Appl Sci.

2020;2(8).

13. Ndongo D. Antibacterial, antioxidant and phytochemical investigation of *Acacia arenaria*, *Aloe esculenta*, and *Pechuel-loeschea leubnitziae*. University of Namibia; 2017.

14. Hanphanphoom S, Krajangsang S. Antimicrobial activity of *Chromolaena odorata* extracts against bacterial human skin infections. Mod Appl Sci. 2016;10(2):159.

15. SAINT. Bruker AXS Inc. Madison, WI, USA. USA: Madison, WI; 2012. p. 2–5.

16. Sheldrick GM. Crystal structure refinement with SHELXL. Acta Crystallogr Sect C Struct Chem. 2015;71(Md):3–8.

17. Atwood JL, Barbour LJ. Molecular graphics: From science to art. Cryst Growth Des. 2003;3(1):3–8.

18. Barbour LJ. X-seed - A software tool for supramolecular crystallography. J Supramol Chem. 2001;1(4–6):189–91.

19. Watson WH, Kashyap RP, Miski M, Mabry TJ. (1S,7S,8R,10S)-3-Oxoguaia-4,11(13)-dien-8,12-olide, C15H18O3. Acta Crystallogr Sect C Cryst Struct Commun. 1985;41(7):1126–8.

20. Muhongo MN, Kangogo M, Bii C. Qualitative and quantitative phytochemical profiling of crude fractions of *Pechuel-loeschea leubnitziae* leaves. J Med Plants Res. 2021;15(2):64–72.

21. Bohlmann F, Borthakur N. Sesquiterpenes and norsesquiterpenes from *Pechuel-loeschea leibnitziae*. Phytochemistry. 1982;21(5):1160–2.

22. Fiore MA, Raisman JC, Wong NH, Hudson AO, Wadsworth CB. Exploration of the neisseria resistome reveals resistance mechanisms in commensals that may be acquired by *N. gonorrhoeae* through horizontal gene transfer. Antibiotics. 2020;9(10):1–12.

23. Melendez JH, Hardick J, Barnes M, Page KR, Gaydos CA. Antimicrobial susceptibility of *Neisseria gonorrhoeae* isolates in Baltimore, Maryland, 2016: The importance of sentinel surveillance in the era of multi-drug-resistant gonorrhea. Antibiotics. 2018;7(3).

24. Dekic MS, Radulovic NS, Rand Strok Signelovic VN, Stojanovic-Radic ZZ, Veljkovic BP. Essential oils and diethyl ether extracts of Serbian *Xeranthemum cylindraceum* and *X. annum*: Chemical composition, antimicrobial activity, and chemotaxonomic implications. Chem Biodivers. 2015;12(9):1378–97.

CHAPTER 5: A DFT AND MOLECULAR DOCKING STUDY OF XERANTHOLIDE AND ITS INTERACTION WITH *NEISSERIA GONORRHOEAE* CARBONIC ANHYDRASE

This chapter is published in the Journal of Computational Biology and Chemistry

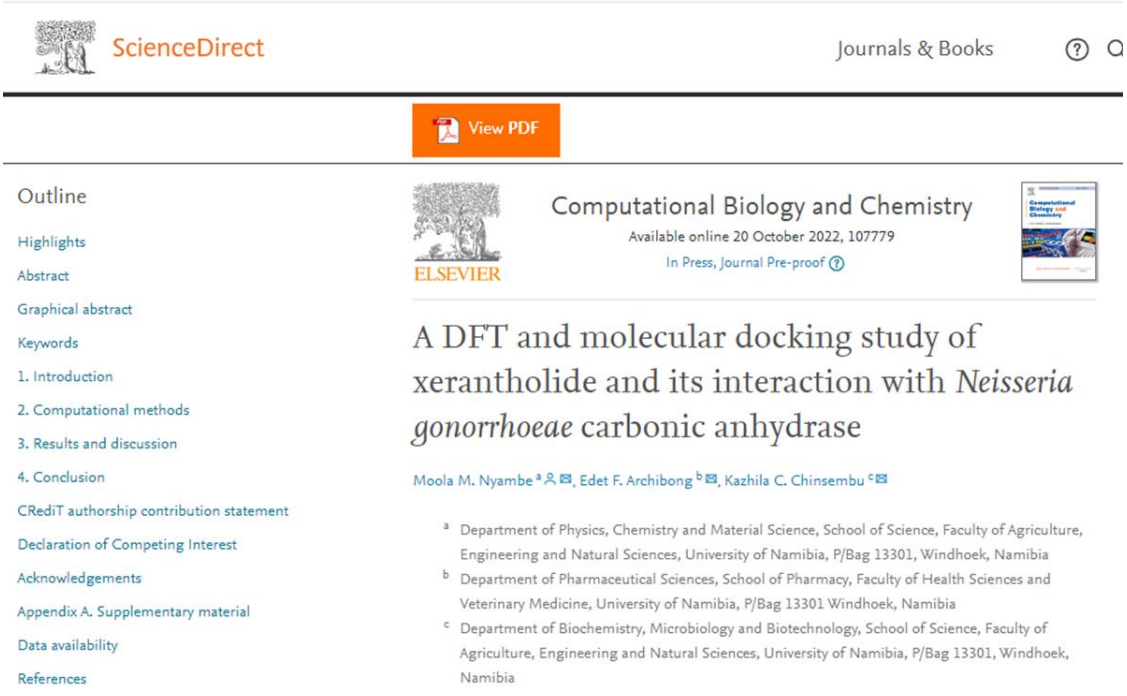

Abstract

Xerantholide is a sesquiterpene lactone that has anti-gonorrhea and anti-plasmodium activities. Gas-phase electronic structure calculations of the equilibrium geometry of xerantholide, its adiabatic electron affinity (AEA), adiabatic ionization energy (AIE) and the energy barrier ($\Delta E^{\ddagger}$) connecting the lowest energy conformers of the sesquiterpene is presented in this chapter. The computations were performed with the B3LYP, M06-2X and ωB97xd variants of the density functional theory (DFT) in conjunction with large basis sets. With the inclusion of the vibrational zero point energy, the computed AEA range from 0.740 eV [B3LYP/Aug-CC-pVTZ] to 0.774 eV [B3LYP/6-311++G(d,p)], and the AIE is roughly 8.6 eV at all theoretical levels. At the B3LYP/Aug-CC-pVTZ level, the barrier ($\Delta E^{\ddagger}$) connecting the two lowest energy conformers is predicted to be 13.9 kcal/mol. Based on the molecular docking analysis, xerantholide interacts with the active site of *Neisseria gonorrhoeae* carbonic anhydrase (NgCA) via hydrogen bonding, metal-acceptor interaction, and non-polar alkyl and pi-alkyl interactions. The predicted binding affinity of -6.8 kcal/mol compares well with those obtained for standard NgCA inhibitors such as acetazolamide (-5.7 kcal/mol). A biomimetic model study involving xerantholide and zinc-tris imidazole ($[ZnIm_3]^{2+}$) ion was also carried out at different theoretical levels to estimate the interaction energy for the formation of the complex formed between the ligand and the active site model of NgCA. The binding free energy (ΔG) has been calculated to be -28.5 kcal/mol at the B3LYP/6-311++G(d,p) level. The interaction mode observed in both the docking and the model calculations involves the lactone ring.

Keywords: Xerantholide, carbonic anhydrase, DFT, docking, binding energies.

5.1 Introduction

Xerantholide is a sesquiterpene lactone (SL) that is commonly found in plant species belonging to the Asteraceae family. Its growth inhibition activity on *Neisseria gonorrhoeae*, the causative agent of the sexually transmitted infection, gonorrhea as well as its anti-plasmodium activity were recently reported by our group (1,2). The bacterial pathogen, *N. gonorrhoeae* has proven to have an extraordinary capacity to develop resistance to all antimicrobial agents that have been used for the treatment of gonorrhea (3,4). The mechanism of action of the current antibiotics is based on altering the DNA, the inhibition of the ribosomal function, and shutting down the biosynthesis of the peptidoglycan layer of the bacterial cell-wall. Recent studies, however, have revealed that carbonic anhydrases (CAs) are also important drug targets that can help to bypass the challenge of antibiotic resistance (5–7). As part of the current efforts to solve the problems of antibiotic resistance, several research efforts are focused on the development of drugs that can inhibit or disrupt enzyme processes. One such line of study is geared towards the inhibition of CAs, thereby paving the way for the development of plant-based drugs as potential carbonic anhydrase inhibitors (CAIs). The anti-gonococcal activity of xerantholide (1) suggests it could be a potential CAI.

CAs are a group of metalloenzymes found in animals, plants, algae, and some bacteria. There are eight classes of CAs, α-. β-, γ-, δ-, ζ-, η-, θ-, and ι-CAs that vary in structural folds but with a common function of catalysing the reversible hydration of carbon dioxide (CO_2) to bicarbonate (HCO_3^-) and a proton (8). The latter is an essential process in the bacteria's life cycle because it is required to maintain CO_2, pH regulation, metabolism, and

assist in acclimation of the bacteria to various niches in which it lives (6,7). CAs also differ in the type of metal ion and amino acids present at the active site. The α-, β-, and δ-CAs consist of Zn^{2+}, while γ-CAs has Fe^{2+} but are also active when bound to Zn^{2+} and Co^{2+}, while ζ-CAs are Cd^{2+} and Zn^{2+} metalloenzymes; η- and θ-CAs are closely related to α-CAs identified as a zinc metalloenzymes and little is known about the ι-CAs (9–11).

The presence of CAs in various pathogenic bacterial species, highlights the important role they play in their transmission and virulence. Of interest is the fact that other bacteria produce the β- and γ-carbonic anhydrase type while *N. gonorrhoeae* produces the α-class carbonic anhydrase called *Neisseria gonorrhoeae* carbonic anhydrase (NgCA) (11). The latter is homologous to a CA produced by humans, specifically the hCA II, with 85% of the residue polypeptides in common and 74 of the 192-sequence positions having identical amino acids (12). The active sites of both hCA II and NgCA consist of a Zn^{2+} ion bound to three rigid imidazole groups belonging to three histidine residues (His-94, His-96, and His-119) with the water molecule completing the tetrahedral coordination geometry (Figure 5.1). The catalytic Zn^{2+} ion is in the centre of the enzyme and the cone-shaped cavity consists of hydrophilic and hydrophobic regions (7,11,13). This similarity makes NgCA a potential target for treating gonorrhea considering that there are FDA-approved CAIs like acetazolamide and ethoxyzolamide that target various human CA isoforms to treat disorders such as glaucoma, congestive heart failure and some cancers and have also shown bacteriostatic or bactericidal effects capability (6, 14). Therefore, finding selective CAIs that are effective in dysregulating NgCA is worth exploring. NgCA is targeted because it plays an important role in the survival of *N. gonorrhoeae* in the host cell as a catalyst for

enzymatic activity of carbon dioxide hydration which is essential to meet the metabolic needs of the bacteria (8). Drugs with mechanisms of action that affect the growth of the bacteria and/or weaken it can also make the bacteria vulnerable to the host defence mechanism.

The cardinal aim of this study is to investigate the CA inhibition potential of xerantholide based on its binding to the active site of NgCA, using molecular docking and density functional theory (DFT). Towards achieving this goal, the geometry and electronic structure of xerantholide was investigated to have a better understanding of its interaction with NgCA. Specifically, we have computed the gas-phase lowest energy structures of xerantholide and the energy barrier for the interconversion of its most stable conformations, the electron affinity and ionization energy of the molecule. More importantly, the binding of the sesquiterpene lactone with NgCA has been investigated using molecular docking, and to complement the molecular docking analysis, the interaction of the molecule with a model of the active site, zinc-tris imidazole ($[ZnIm_3]^{2+}$), has been studied using DFT. To our knowledge, this work represents the first published electronic structure calculation of xerantholide and the molecular docking analysis of the molecule with NgCA. Modelling of the enzyme's active site and its interaction with xerantholide was done using quantum chemical calculations in order to account for some shortcomings of molecular docking, which essentially is based on molecular mechanics force field (15).

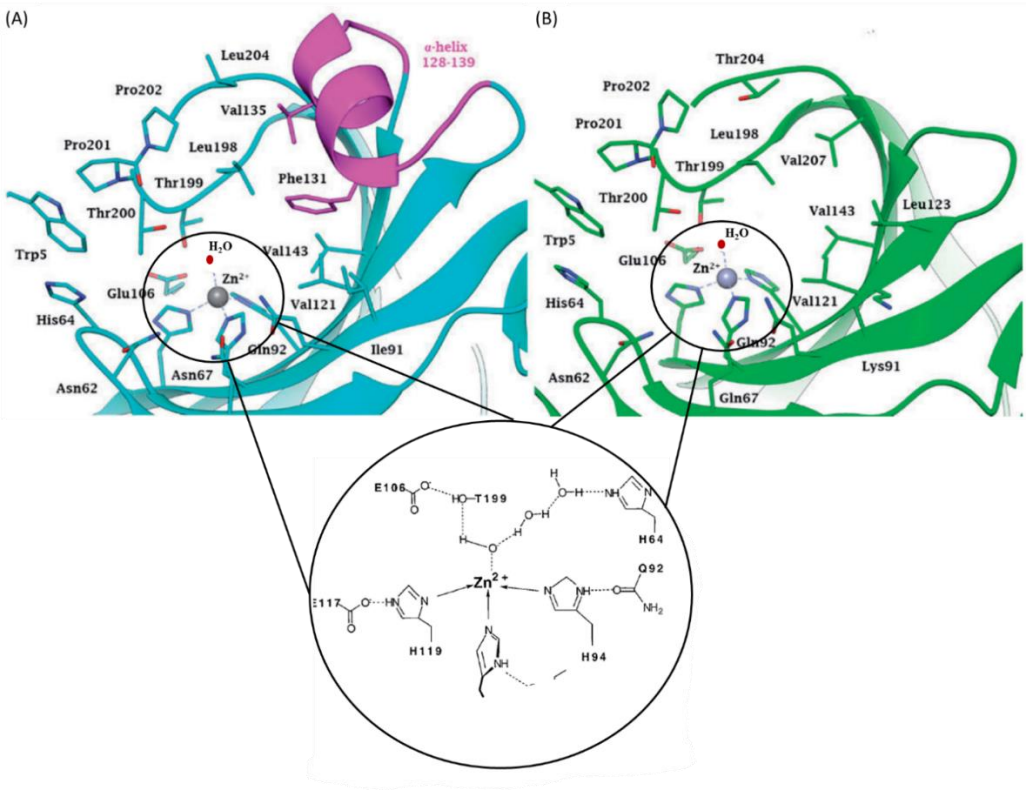

Figure 5.1. Active site structure of (A) hCA II and (B) NgCA.
Amino acid residues of NgCA were renumbered according to the corresponding residues from hCA II. Image adopted from (7) and modified removing the azide anion (N_3^-) and adding water molecule coordinating the zinc ion with three histidine residues to illustrate the active site.

5.2 Material and methods

5.2.1 Computational methods: MMFF, PM3, DFT and CCSD Calculations

The structure of xerantholide was initially obtained from x-ray diffraction analysis (1, 16) of a single-crystal isolated from *Pechuel-loeschea leubnitziae* plant (1). The x-ray structure was then used as an input for an extensive Merck molecular force field (MMFF) and parameterized model 3 (PM3), conformer distribution calculations (17,18). The two lowest energy conformers of xerantholide were then selected based on the total energy and Boltzmann distribution criteria of the conformers generated by MMFF and PM3. Next, the geometry of the two lowest energy conformers of xerantholide predicted by MMFF and

PM3 were fully optimized using B3LYP, B3LYP-D2, M06-2X and ωB97xd functionals (19), and their energies refined using the CCSD//B3LYP approximation (20,21). The 6-31+G(d), 6-311+G(d), 6-311++G(d,p), 6-311++G(2d,p), 6-311++G(2df,2p) and Aug-CC-pVTZ one particle basis sets (22) were employed for the calculations, except for the CCSD//B3LYP calculations where the 6-311++G(d,p) basis set was used. The latter was done within the frozen-core approximation. The transition state structure connecting the two conformers was generated at the PM3 level using the quadratic synchronous transit (QST2) approach, whereby the conformers were used as input. The PM3 transition state structure was subsequently optimized at the B3LYP level using the 6-31+G(d), 6-311++G(d,p), 6-311++G(2df,2p) and Aug-CC-pVTZ basis sets. Frequency calculations on the structure returned one imaginary frequency, thus characterizing it as a saddle point. Further, intrinsic reaction coordinate (IRC) calculation was used to verify that the structure indeed connects the minima. The electron affinity and the ionization energy of xerantholide were calculated, respectively, using the energy computed for the anionic, cationic and neutral forms via the B3LYP, M06-2X and ωB97xd functionals in conjunction with the 6-31+G(d), 6-311+G(d), 6-311++G(d,p), 6-311++G(2d,p), 6-311++G(2df,2p) and Aug-CC-PVTZ basis sets. The theoretical methods used for the computations of the geometry and energy of xerantholide were also used to compute the geometry and energy of zinc-tris imidazole ($[ZnIm_3]^{2+}$). The MMFF and PM3 calculations were done using Spartan 14 (18) while the DFT and CCSD calculations were done using Gaussian 16 revision B01 (23) running on the supercomputer of South Africa Centre for High Performance Computing (CHPC).

The reactivity indices, electron affinity (EA), ionization energy (IE), and interaction energy (ΔE) of xerantholide were calculated as follows:

Chemical hardness $(\eta) = -\frac{1}{2}(E_{HOMO} - E_{LUMO})$ (eqn. 1)

Chemical softness $(\sigma) = \frac{1}{\eta} = \frac{-2}{E_{HOMO} - E_{LUMO}}$ (eqn. 2)

Electrophilicity index $(\omega) = \frac{\mu^2}{2\eta}$ (eqn. 3)

Chemical potential $(\mu) = \frac{E_{HOMO} + E_{LUMO}}{2}$ (eqn. 4)

Electronegativity $(\chi) = -\mu$ (eqn. 5)

Absolute electronegativity is calculated as: $\chi = \frac{IP+EA}{2}$ which measures the molecule's ability to attract electrons.

AEA = E_0 - E_- (eqn. 6)

where E_0 is the energy of the most stable structure of the neutral molecule and E_- is the energy of the most stable structure of the anion.

AIE = E_+ - E_0 (eqn. 7)

where E_+ is the energy of the most stable structure of the cation.

$\Delta G_{bind} = G_{complex} - \left(G_{[ZnIm_3]^{2+}} + G_{xerantholide}\right)$ (eqn. 8)

5.2.2 Molecular docking

To determine the binding patterns of xerantholide to NgCA, the binding affinities were predicted using molecular docking. The AutoDock Vina programme (24,25) using a generic algorithm was used. The enzyme was prepared by modifying the macromolecule file (PDB code: 1KOQ) using the AutoDock Tools 1.5.6. The initial 1KOQ protein structure consisted of two chains (A and B) which are the same; the B chain was deleted to

minimize the structure to a single chain with one active site. All water molecules that were in coordination with A chain were deleted, polar hydrogens and Kollman charges were added. The generated pdbqt file was saved. The docking grid box was defined as to enclose the zinc-tris imidazole, which was defined as the active site (7), with the x, y, z centers as 13.192, -15.534 and 31.999 respectively and the dimensions were determined as 40 Å x 40 Å x 40 Å using 0.375 Å spacing. Modification of the ligand molecules were done using AutoDock Tools and saved as pdbqt file. Schematics representation of interaction of the ligand and residues inside the binding site of the receptor was generated using AutoDock Python Molecule Viewer (PMV), PyMOL and Discovery studio visualizer (24–27).

5.3 Results and discussion

5.3.1 Relative energy and geometry of xerantholide conformers

Starting from the x-ray structure of xerantholide (1), MMFF and PM3 predicted two dominant conformers that were subsequently studied at the B3LYP, M06-2X, and ωB97xd levels, using six basis sets ranging in size from 6-31+G(d) to Aug-CC-pVTZ. Table 5.1 lists the relative energy of the lowest energy conformers, conformer 1 (S1) and conformer 2 (S2) of xerantholide and the transition state (TS) connecting them, calculated at different theoretical levels. The total energies including the thermal energies may be found in the supplementary information Table SP1 (Appendix 6). Conformers S1 and S2 and the TS are depicted in Figure 5.2, together with the atom numbering scheme of xerantholide structure.

Table 5.1 shows that there is consistency between the electronic energies calculated with all the methods and the inclusion of zero-point energy, while stabilizing S1 by 0.2-0.3

kcal/mol, did not change the ordering of the relative energies. The energy difference between S1 and S2 is about 4 kcal/mol for all calculations using DFT, favouring S1 as the most stable structure with the lowest electronic energy. The more accurate calculation at the CCSD//B3LYP using the 6-311++G(d,p) basis set favoured S1 by 3.25 kcal/mol.

The calculated energy barrier($\Delta E^{\ddagger}$) for the interconversion of the two conformers as in Figure 5.2, shows that the barrier in going from S1 to S2 is about 14 kcal/mol for all basis sets used, while the barrier in the opposite direction is about 10 kcal/mol. The visual depiction of the structures in Figure 5.2, the superimposed structures in Figure 5.3 and the geometric parameters in Table 5.2 show that the transition state structure (TS) resembles S2 more than S1. With respect to the similarity between S2 and the TS, the computed value of C4-C5-C6 bond angle for the TS is 126.0˚ compared to S2 which is 126.4˚ while S1 is 123.1˚.

Table 5.1. Total energies (au) and relative energies[a] (kcal/mol) for S1 and S2 computed at the B3LYP, M06-2X, and wB97xd levels using six different basis sets.

	Total Energies		**Relative Energies**		**Relative Energy+ZPE**
Methods	**S1**	**S2**	**S1**	**S2**	**S2**
B3LYP/6-31+G(d)	-808.13041	-808.12402	0.0	4.0	4.2
B3LYP/6-311+G(d)	-808.29989	-808.29369	0.0	3.9	4.1
B3LYP/6-311++G(d,p)	-808.32383	-808.31773	0.0	3.8	4.1
B3LYP/6-311++G(2d,p)	-808.34336	-808.33712	0.0	3.9	4.1
B3LYP/6-311++G(2df,2p)	-808.37057	-808.36428	0.0	3.9	4.2
B3LYP/Aug-CC-pVTZ	-808.39812	-808.39181	0.0	4.0	4.2
M06-2X/6-31+G(d)	-807.78774	-807.78110	0.0	4.2	4.4
M06-2X /6-311+G(d)	-807.97526	-807.96870	0.0	4.1	4.4
M06-2X /6-311++G(d,p)	-807.99244	-807.98595	0.0	4.1	4.3
M06-2X /6-311++G(2d,p)	-808.01440	-808.00781	0.0	4.1	4.4
M06-2X /6-311++G(2df,2p)	-808.03901	-808.03241	0.0	4.1	4.4
M06-2X /Aug-CC-pVTZ	-808.07446	-808.06786	0.0	4.1	4.4
wB97xd/6-31+G(d)	-807.89354	-807.88659	0.0	4.4	4.6
wB97xd/6-311+G(d)	-808.05494	-808.04823	0.0	4.2	4.4
wB97xd/6-311++G(d,p)	-808.07764	-808.07101	0.0	4.2	4.3
wB97xd/6-311++G(2d,p)	-808.09717	-808.09046	0.0	4.2	4.3
wB97xd/6-311++G(2df,2p)	-808.12234	-808.11557	0.0	4.2	4.4
wB97xd/Aug-CC-pVTZ	-808.14911	-808.14236	0.0	4.2	4.4

[a] relative to conformer 1

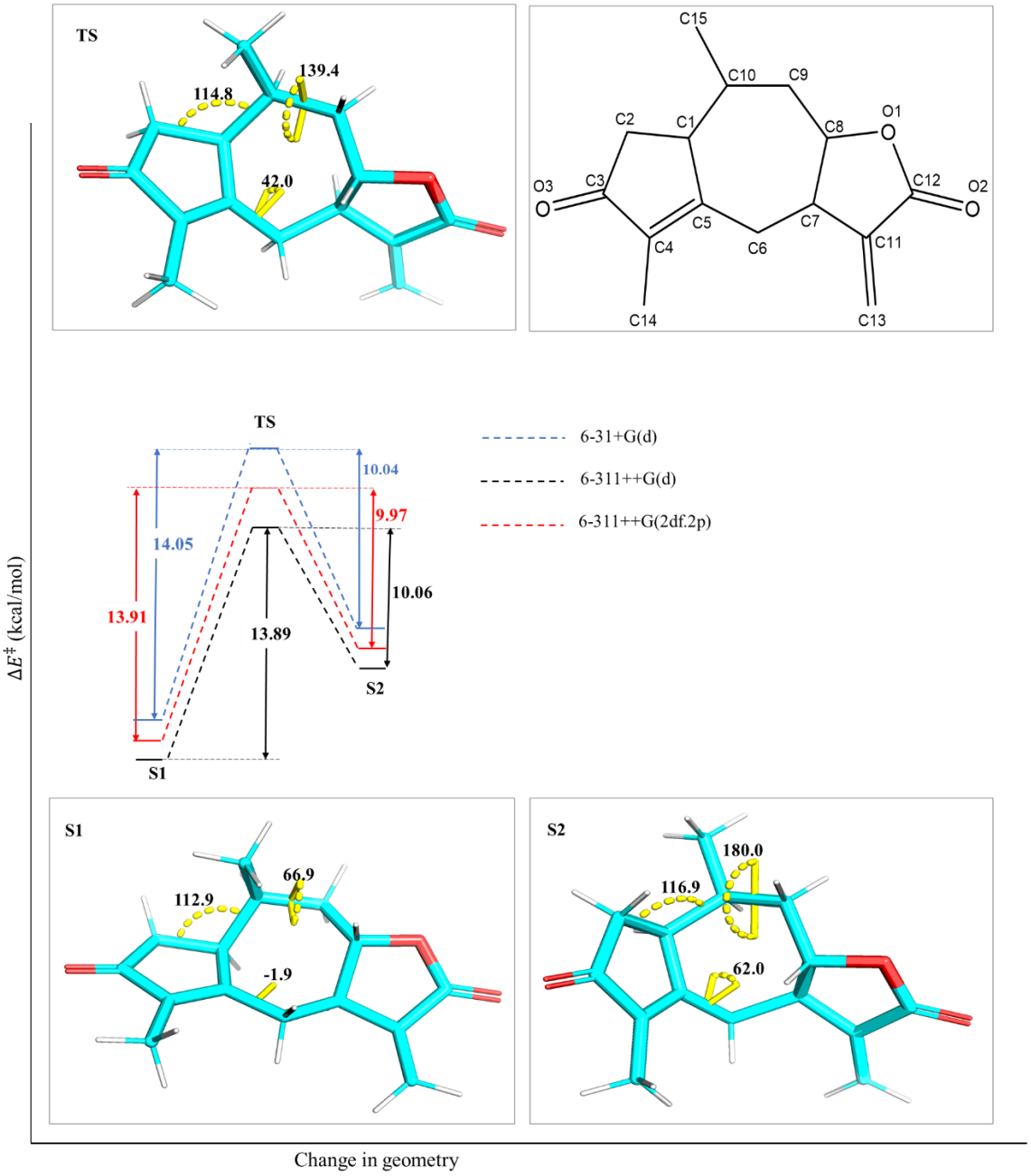

Figure 5.2. Optimized structures of xerantholide's conformer 1 (S1), conformer 2 (S2) and the transition state connecting the two conformers (TS) calculated at DFT/B3LYP/6-311++G(d,p).

Selected geometrical parameters of S1, S2, and TS connecting them are listed in Table 5.2. For comparison purposes, the table also includes corresponding bond distances and angles from the x-ray structure. Overall, the bond distances for both conformers from all three

methods compare well with values from experimental work as determined by x-ray diffraction from a single crystal of xerantholide (1). All the C-C and O-C bonds in the optimized structures for all methods are slightly elongated from 0.001 – 0.036 Å. However, the C-H bond distances are more elongated when compared to the x-ray data (Supplementary material, Table SP2, Appendix 6). Differences in bond angles, contact distance and dihedral angles are noticeable in the two conformers. The geometric parameters listed in Table 5.2 show that some bond angles in S2 are wider compared to reported x-ray diffraction values. For example, the computed C2-C1-C10 bond angle is 117.0˚ compared to 112.0˚ observed experimentally. The comparison between the two conformers indicates that many of S2's bond angles are about 2-4˚ higher relative to x-ray data while conformer 1 have more realistic angles. No significant change in bond length, bond angles and dihedral angles was observed in the lactone rings of both conformers. The obvious difference between the two conformers is a rotation around the C9-C10 bond causing a twist of the 7-membered ring. The big difference in dihedral angles was observed in the 5-membered ring bearing the ketone group and in the 7-membered ring where an increase in dihedral angle value was observed in S2. The dihedral angle through C5-C1-C10-C15 was between -49.79˚ to -52.39˚ for S1 and -176.20˚ to -177.29˚ for S2 and that of C1-C5-C6-C7 was -1.85˚ to 1.36˚ for S1 and 61.96˚ to 65.81˚ for S2. The torsion angles observed in S2 deviates substantially from the ideal geometry estimated experimentally. These changes in torsion angle values caused puckering of the rings thereby altering the bond angles and contact distances that were observed in S2. Good agreement with experimental data in dihedral angles was observed for S1 depicting flattening of the 7-membered ring structure.

Table 5.2. Selected geometric parameters of the optimized structure of xerantholide's two lowest conformers and the transition state calculated at B3LYP, M06-2X, and wB97xd levels

		S1			S2			TS
	x-ray	**B3LYP**	**M06-2X**	**ωB97**	**B3LYP**	**M06-2X**	**ωB97**	**B3LYP**
Bond length (Å)								
O1 - C8	1.478	1.455	1.442	1.442	1.454	1.441	1.441	
O2-C12	1.211	1.199	1.193	1.195	1.199	1.192	1.195	
O3-C3	1.227	1.215	1.206	1.209	1.214	1.206	1.208	
Bond angle (˚)								
C2-C1-C10	111.8	113.0	112.0	112.5	117.0	116.4	116.5	114.8
C5-C4-C14	128.0	128.3	128.4	127.9	130.4	131.0	130.4	130.1
C1-C5-C6	124.2	124.0	123.9	123.9	121.2	120.4	120.6	120.7
C4-C5-C6	122.3	123.1	123.1	123.0	126.4	126.9	126.7	126.0
C5-C6-C7	115.9	115.6	114.9	115.2	112.4	111.4	111.5	112.4
O1-C8-C9	109.0	109.1	108.8	109.1	110.1	110.0	110.2	108.3
O1-C12-O2	121.5	122.8	123.3	123.0	122.8	123.3	123.0	122.8
Dihedral angle (˚)								
C10-C1-C5-C4	121.4	119.7	114.3	115.7	140.4	139.7	139.4	109.7
C10-C1-C5-C6	-60.5	-63.7	-65.2	-64.2	-38.9	-38.1	-38.2	-75.8
C2-C1-C10-C9	-164.3	-164.0	-164.5	-164.3	73.3	69.9	70.5	139.7
C5-C1-C10-C9	77.8	77.2	78.7	78.4	-49.1	-51.5	-51.1	19.9
C5-C1-C10-C15	-50.9	-52.4	-49.8	-50.6	-176.2	-177.2	-177.3	-108.8
C1-C2-C3-O3	175.2	176.4	171.9	173.2	-168.5	-167.5	-168.3	165.7
C1-C5-C6-C7	-1.5	-1.9	1.4	0.5	62.0	65.8	65.6	42.0
C4-C5-C6-C7	176.4	176.6	-178.1	-179.4	-117.2	-111.6	-111.7	-144.3
C5-C6-C7-C8	62.7	64.7	64.2	64.3	16.6	12.0	12.1	47.9
C7-C8-C9-C10	70.9	66.9	66.5	66.7	33.3	35.7	35.8	39.0

For numbering of atoms in Table 5.2 and 5.3, refer to Figure 5.2

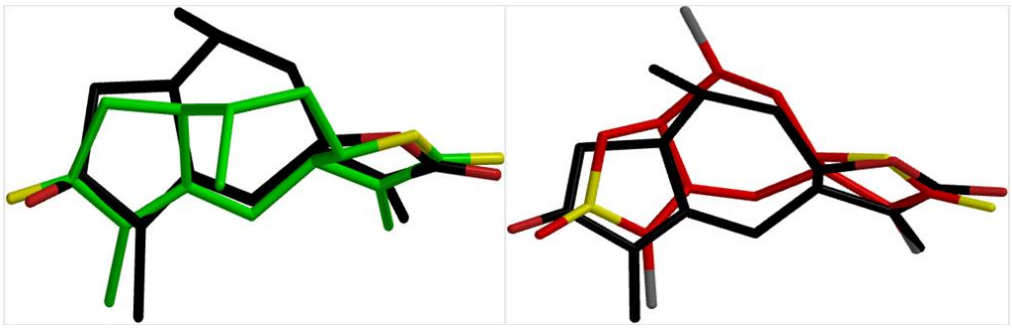

Figure 5.3. An overlay of the optimized structures of the transition state (black) with S1 (green) and S2 (red)

Conformational freedom of xerantholide is limited by the 3-ring structure which imparts a strong restricted bond rotation thus allowing only a certain degree of conformational changes. This strong restricted bond rotation explains the limited number of conformers observed. The difference in bond strain between the conformers was also reflected in their total electronic energies. There was consistency in the results calculated using different DFT methods and a good match of geometric parameters with experimental data, thereby validating the accuracy of the methods used and the results obtained.

The energies of the frontier molecular orbitals (FMO) are related to the chemical reactivity of a molecule. Energy of the highest occupied molecular orbital (E_{HOMO}) is associated with the electron donating ability of the molecule and the energy of the lowest unoccupied molecular orbital (E_{LUMO}) is related to the ability of a molecule to gain electrons. The active site of a molecule can be described by the distribution of frontier orbitals (28). Soft molecules have a small HOMO-LUMO gap (ΔE_{H-L}) and can easily donate electrons, while hard molecules have a large ΔE_{H-L} (29). The HOMO-LUMO graphic surface and energies computed using M06-2X and the 6-311++G(d,p) basis set is shown in Figure 5.4. HOMO

has a major orbital contribution from the 5-membered ring bearing the carbonyl group and no contribution from the lactone ring. In contrast, the LUMO shows main contributions from the orbitals on the lactone ring, which is a region of interest, with some minor contributions from the other 5-membered ring.

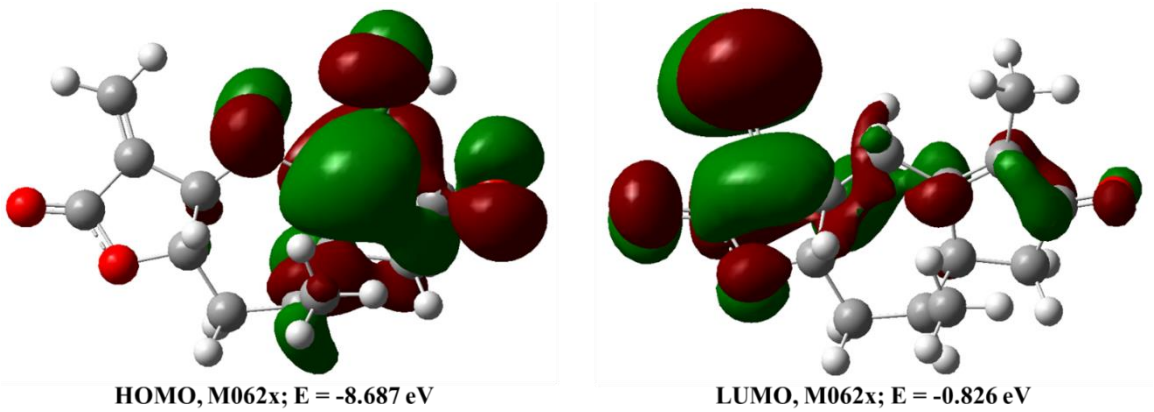

Figure 5.4. Contour surfaces of frontier molecular orbitals of xerantholide at M06-2X/6-311++G(d,p)

Table 5.3 presents the results which give more insight into the chemical reactivity of xerantholide. The HOMO-LUMO energy gap signifies that xerantholide is a soft molecule and may easily react with biomolecules with attendant biological activity (30). When compared to some molecules that have been classified as soft molecules, the calculated chemical parameter values of xerantholide are in the same range (30–32). The molecule's softness is thus depicted by the lower value of 2.52 eV for the chemical hardness (η), high value of 0.3953 eV for chemical softness (σ) and high negative value of -4.458 eV for the chemical potential (μ). The η describes the charge transfer of a system, while the σ describes the capacity of an atom or group of atoms to receive electrons (31). The

calculated η and σ values reveal that xerantholide is a soft electrophile, which is consistent with the high electrophilicity index (ω) of 3.93 eV that indicate the molecule's capacity to accept electrons from the environment, thus signifying good binding capacity to biomolecules (30,32). Additionally, the good electron accepting ability is also indicated by the high electronegativity value of 4.458 eV.

Electron affinity is an indicator of a molecule's ability to gain electrons while IP describe the minimum energy required to remove an electron from a neutral molecule. The B3LYP adiabatic electron affinity (AEA) of S1, including ZPE correction, was computed to be 0.752 eV, 0.774 eV and 0.740 eV using the 6-31+G(d), 6-311++G(d,p) and Aug-CC-pVTZ basis sets, respectively. The electron affinity of xerantholide may be compared to those of coumarins which are similarly characterized by a lactone ring. Previous computational studies suggested that these molecules have EA values ranging from 0.49 – 1.09 eV, and they were considered to have a great electron acceptor capacity (33). The added electron goes into the LUMO of the neutral molecule resulting in changes in some geometric parameters in the lactone ring. For instance, O1-C12 and C11-C13 bond lengths increased by 0.04 Å while C11-C12 bond length was shortened by 0.05 Å in the anion molecule. The bond angles O1-C12-O2 and C7-C11-C13 reduced from 122.8˚ to 119.6˚ and 130.95˚ to 127.07˚ respectively in the anion. Most of the geometric parameters did not show significant differences between the anion and the neutral molecule. Additional data on geometric parameters for the neutral and anionic structure of xerantholide can be found in supplementary Table SP2 (Appendix 6). These results show that the bonds in the lactone ring are mostly affected by the added electron. Removal of an electron from the HOMO of

S1 gives the cationic form and the adiabatic ionization energy (AIE), corrected for ZPE, was computed to be 8.63 eV, 8.66 eV and 8.62 eV using the 6-31+G(d), 6-311++G(d,p) and Aug-CC-pVTZ basis sets, respectively. This value may be compared to IE value of 8.72 eV of coumarin lactones (33). It is noteworthy that the AEA and AIE obtained from the Koopman's approximation using energies of the LUMO and HOMO are 0.6437 eV and 8.73 eV respectively. The values of $\Delta E_{H-L,}$ EA, and IP as shown in Table 3 all indicate that this compound is a reactive compound.

The molecular electrostatic potential (MEP) of xerantholide is presented in Figure 5.5 where the blue regions indicate the positive regions at which nucleophilic attack is more possible, while red indicate the most negative areas where electrophilic attack is more likely. The carbonyl oxygen atoms of the two 5-membered rings are the sites with the largest negative potential, not surprising due to pi electrons on the oxygen atoms. The positive potential sites are scattered around the C6, C7 and the hydrogen atoms. The regions marked by green colour are neutral.

Table 5.3. Quantum chemical parameters of xerantholide calculated using B3LYP/6-311++G(d,p)

Function	**value**
E_{HOMO} (eV)	-6.998
E_{LUMO} (eV)	-1.928
ΔE_{HOMO} - E_{LUMO} gap (eV)	5.060
Chemical hardness (η) (eV)	2.530
Chemical softness (σ) (eV)	0.3953
Electronegativity (χ) (eV)	4.458
Ionization potential (IP) (eV)	8.730
Electron affinity (EA) (eV)	0.6437
Electronic chemical potential (μ) (eV)	-4.458
Electrophilicity index (ω) (eV)	3.928

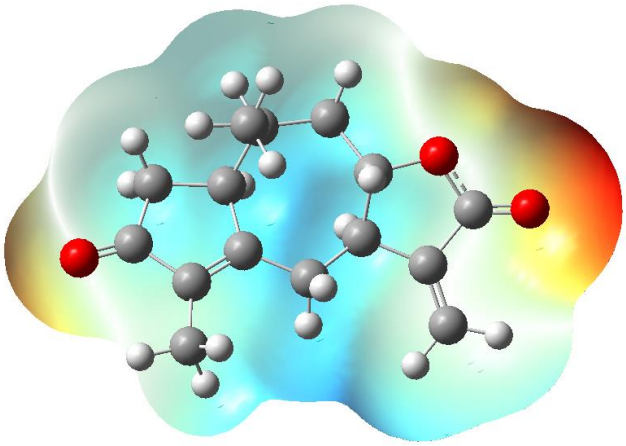

Figure 5.5. Molecular electrostatic potential surface of xerantholide showing electron rich region (red) and electron poor region (blue)

5.3.2 Molecular docking studies

Molecular docking approach is used to predict the preferred binding orientation of a ligand to a target receptor. It is a useful computational technique in drug development process. The binding features of xerantholide and NgCA were predicted, and the binding scores are presented in Table 5.4. The results show that xerantholide docked with binding affinity of -6.8 kcal/mol. This value is lower than the binding affinity obtained for known NgCA inhibitors, acetazolamide (AZM) and ethoxzolamide (EZM) that exhibited -5.7 and -5.3 kcal/mol, respectively. Note that the lower the binding energy value, the higher the affinity. These results suggest that the inhibition of xerantholide is comparable or probably higher than that of reference NgCA inhibitors AZM, EZM and that of a reference antibiotic, tetracycline. Consequently, it may be inferred that xerantholide has the ability to inhibit the activity of NgCA and could be a good candidate to be explored for *in-vitro* studies. Docking analysis given in Table 5.4 and Figure 5.6 - 5.8 shows xerantholide's mode of interaction

with NgCA indicating that there is a network of interactions with several amino acid residues participating in nonpolar or close van der Waals contacts.

Table 5.4. Binding score and interaction of xerantholide with NgCA as determined by molecular docking analysis.

	Binding score (kcal/mol)	**Zn^{2+} & Amino acids interactions**	**H-bond(s)**
Xerantholide (S1)	-6.8	Thr-177, Thr-178, His-92, His-111, Val-113, Val-123, Leu-115, Leu-176, Pro-121 Zn^{2+}	1
Xerantholide (S2)	-5.9	His-92, His-111, Val-113, Leu-176	0
Acetazolamide	-5.7	Gln-69, Asn-64, Thr-177, Thr-178, Trip-7, His-92, His-111, Zn^{2+}	4
Ethoxzolamide	-5.3	Asn-64, Thr-177, Thr-178, His-92, His 111, Zn^{2+}	3
Tetracycline	-6.6	Gln-69, Gln-90, Asn-64, Trp-7, Pro-179, Pro-180, Thr-178, His-92	4

As depicted in Figure 5.6 (A), only in two of the generated poses do xerantholide interacts with NgCA inside the binding pocket, others are attached outside. Figures 5.6 and 5.7 shows that xerantholide is coordinated to Zn^{2+} in NgCA active site at a distance of 2.6 Å through the carbonyl oxygen of the lactone ring, a group that has been shown to be responsible for some of the biological activities reported for SLs. The interaction with Zn^{2+} is possible because of the heterocyclic ring system of xerantholide which acts as zinc binding group, a feature that can make it an effective NgCA inhibitor (9). Additionally, Zn^{2+} interaction is specifically at the carbonyl of the lactone ring because the α-methylene-γ-lactone group contains a reactive α, β-unsaturated carbonyl group which is a strong

alkylating agent of bionucleophiles (34). This metal acceptor interaction stabilizes the ligand. This is supported by the ESP-map in Figure 5.5 which indicates that the lactone group has higher electron density than the other carbonyl group. The 2D analysis given in Figure 5.7 shows that there are about 12 hydrophobic interactions with xerantholide involving six amino acids, Val-123, Leu-176, Leu-115, Val-113, Pro-121(alkyl), and His-92 (π-alkyl) indicating that xerantholide can interact deep into the hydrophobic pocket region of NgCA. The surface representation of NgCA and xerantholide in Figure 5.8 shows that the lactone ring interaction with the enzyme is dominantly in the hydrophobic region. The affinity of the ligand for this hydrophobic region can inhibit the activity of the enzyme. The pi-alkyl interaction observed with His-92 is significant as this type of interaction helps in inserting the ligand to the binding site of the receptor and assists the stability of the complex.

Figures 5.6 and 5.7 also show that xerantholide interacts with the active site of NgCA by establishing one conventional hydrogen bond between threonine (Thr-178) and oxygen group in the lactone ring with a bond distance of 2.397 Å. This interaction increases the stability of the ligand-receptor complex. It is also an important interaction because threonine is one of the essential amino acids required for the bacteria's growth and survival as it is required in the activation of enzymes to perform metabolic events necessary for the bacteria to cope with anaerobic conditions (35,36). The affinity of xerantholide to threonine suggests a possibility of disrupting NgCA's activities thus diminishing its activity.

When the binding profile of xerantholide is compared to that of known NgCA inhibitors, AZM and EZM, Thr-178 is a common residue, forming a H-bond (Figure 5.7) and they all

involve Zn^{2+} interaction. Both ligands display the same interaction mode as CO_2, the substrate molecule of NgCA, which involve a nucleophilic attack of Zn^{2+} by either the N atom of the sulfonamide moiety in the case of AZM and EZM or carbonyl group in xerantholide. This suggests competitive inhibition by these molecules. The chemical structure of xerantholide is however very different from the two sulfonamides (RSO_2NH_2) that form Zn-N bond via the sulfonamide group (6,37) while xerantholide form Zn-O bond via the lactone ring at the active site. These three compounds have been shown to have anti-gonococcal activity (1,38), thus the docking results presented in the current work, which shows good affinity of xerantholide to NgCA, supports the potential of xerantholide to be a NgCA inhibitor of different chemical structure. Since docking of xerantholide with NgCA produced docking scores comparable to known active CAIs, it is an indication that xerantholide indeed can bind to the active site of NgCA. Though less H-bonds are observed with xerantholide compared to AZM, the high binding scores can be attributed to the additional amino acid residue interactions observed for xerantholide-NgCA complex that keeps the ligand inside the binding pocket as depicted in Figure 5.7 and Figure 5.8.

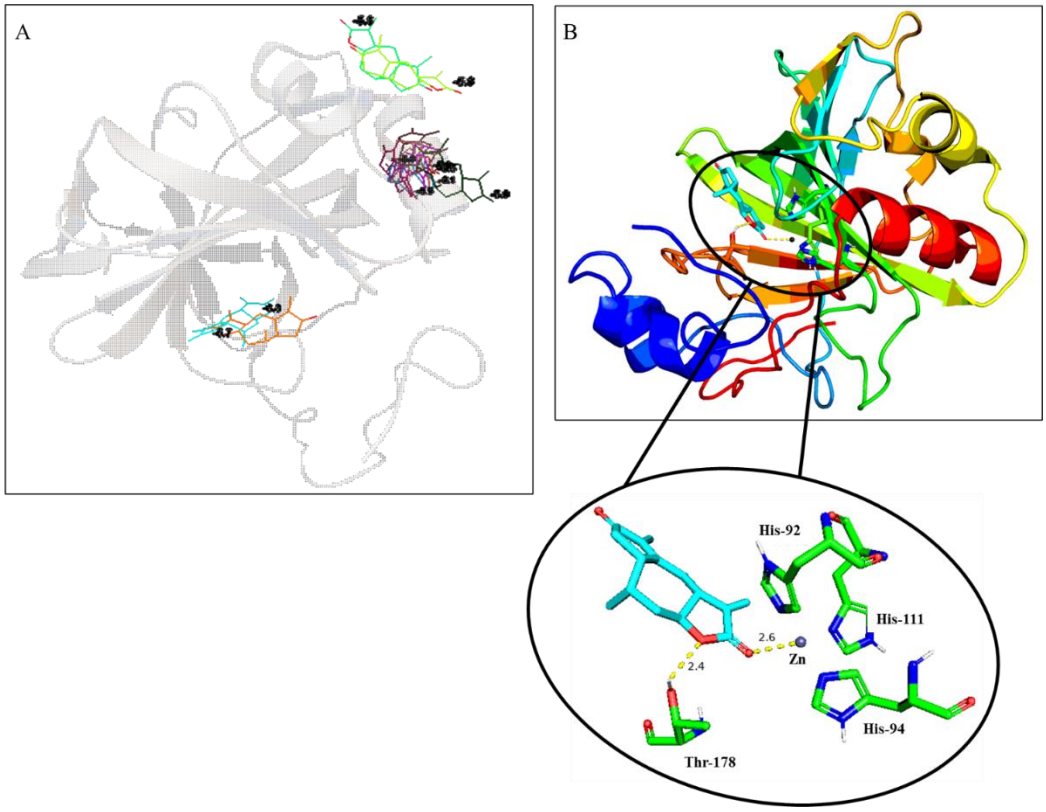

Figure 5.6. Ribbon structure of *Neisseria gonorrhoeae* carbonic anhydrase depicting, (A) the binding position of the 10 generated poses of xerantholide on NgCA; (B) the best pose (pose 1) of xerantholide ligand interaction with NgCA, showing polar interaction in the active site as well as the protein backbone.

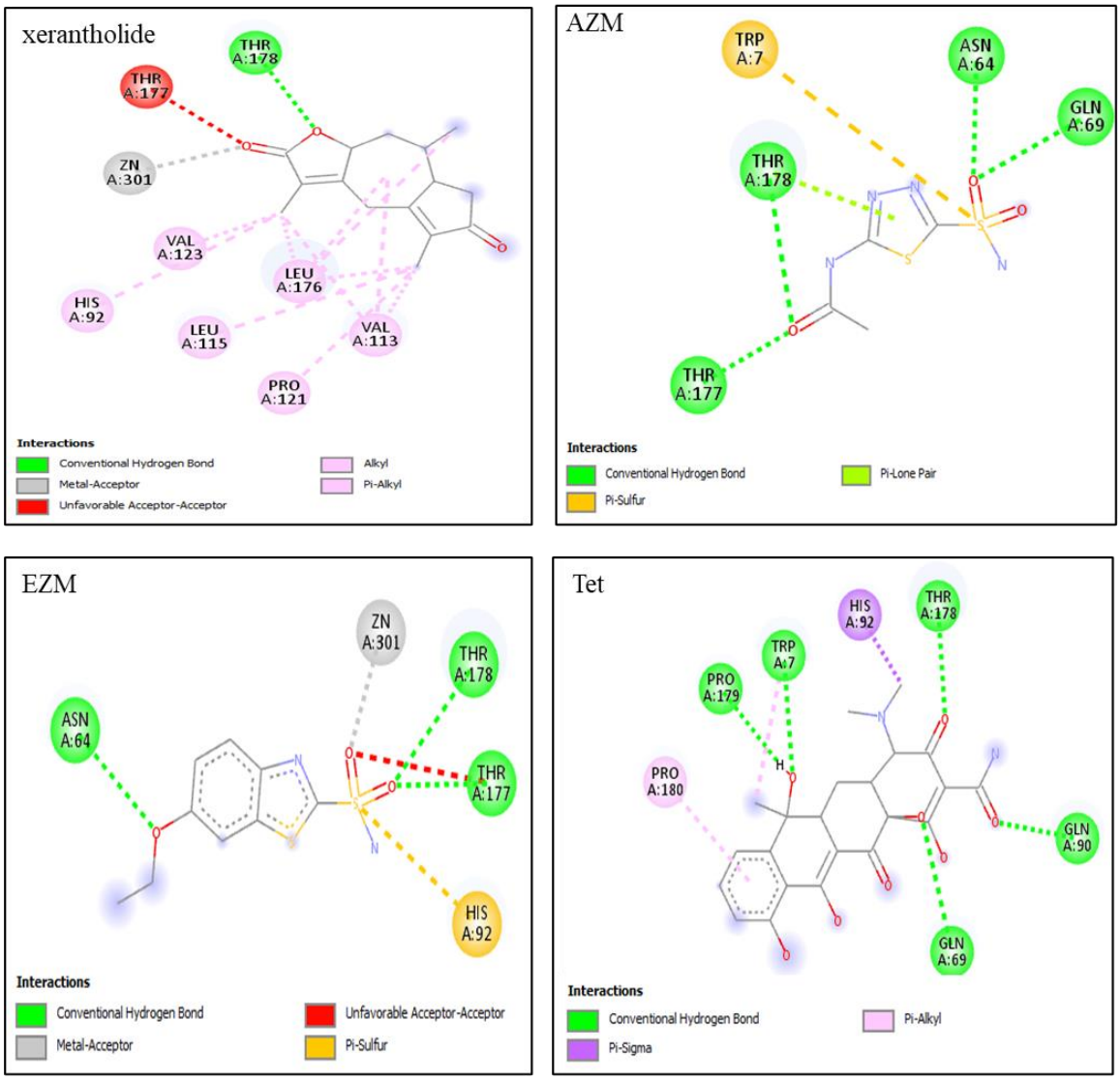

Figure 5.7. 2D view of binding mode and amino acid residues involved in the interaction of xerantholide with NgCA at the active site, in comparison to established inhibitor AZM and anti-gonococcal agents EZM and tetracycline.

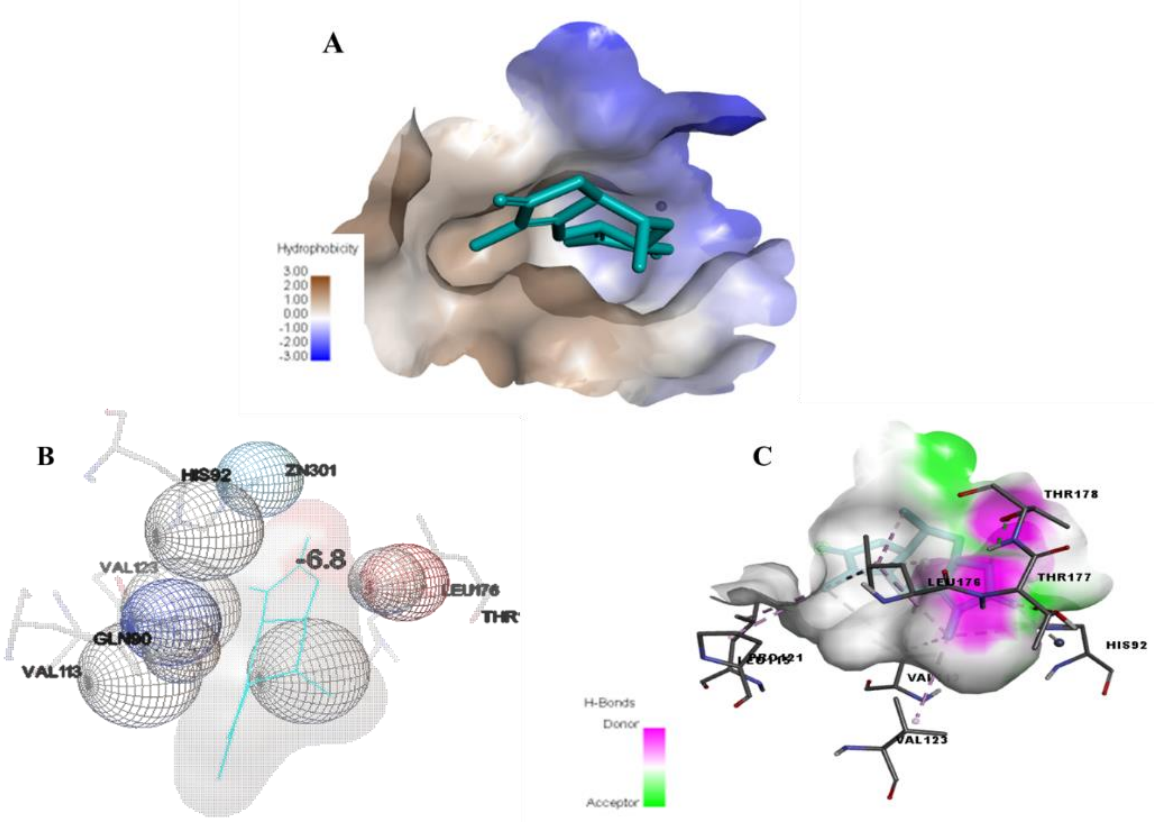

Figure 5.8. Docked pose 1 of xerantholide with NgCA showing (A) hydrophobic surface at the active site; (B) amino acids in close proximity with the ligand; (C) hydrogen bond surface

5.3.3 Interaction of xerantholide with model of NgCA active site, Zn-tris imidazole ion ($[ZnIm_3]^{2+}$)

In addition to the docking study in section 5.3.2, the interaction of xerantholide with $[ZnIm_3]^{2+}$, the active site model of NgCA was investigated using DFT. The structures of $[ZnIm_3]^{2+}$ and the xerantholide-$[ZnIm_3]^{2+}$ complexes are shown in Figure 5.9. The gas-phase structure of $[ZnIm_3]^{2+}$ was fully optimized and characterized as minimum at different levels of theory. The B3LYP/6-311++G(d,p) Zn-N bond lengths (roughly 1.97 Å) in $[ZnIm_3]^{2+}$ lowest energy structures are shown in Figure 5.9 and they are in excellent

agreement with 1.986 Å previously reported (15). The most stable conformer of xerantholide was employed in the formation of xerantholide-$[ZnIm_3]^{2+}$. In addition to B3LYP, the B3LYP-D2, M06-2X, and ωB97xd functionals were specifically used for geometry optimization and frequency calculations in order to account for dispersion effects (20,39) which are often found in weakly interacting systems.

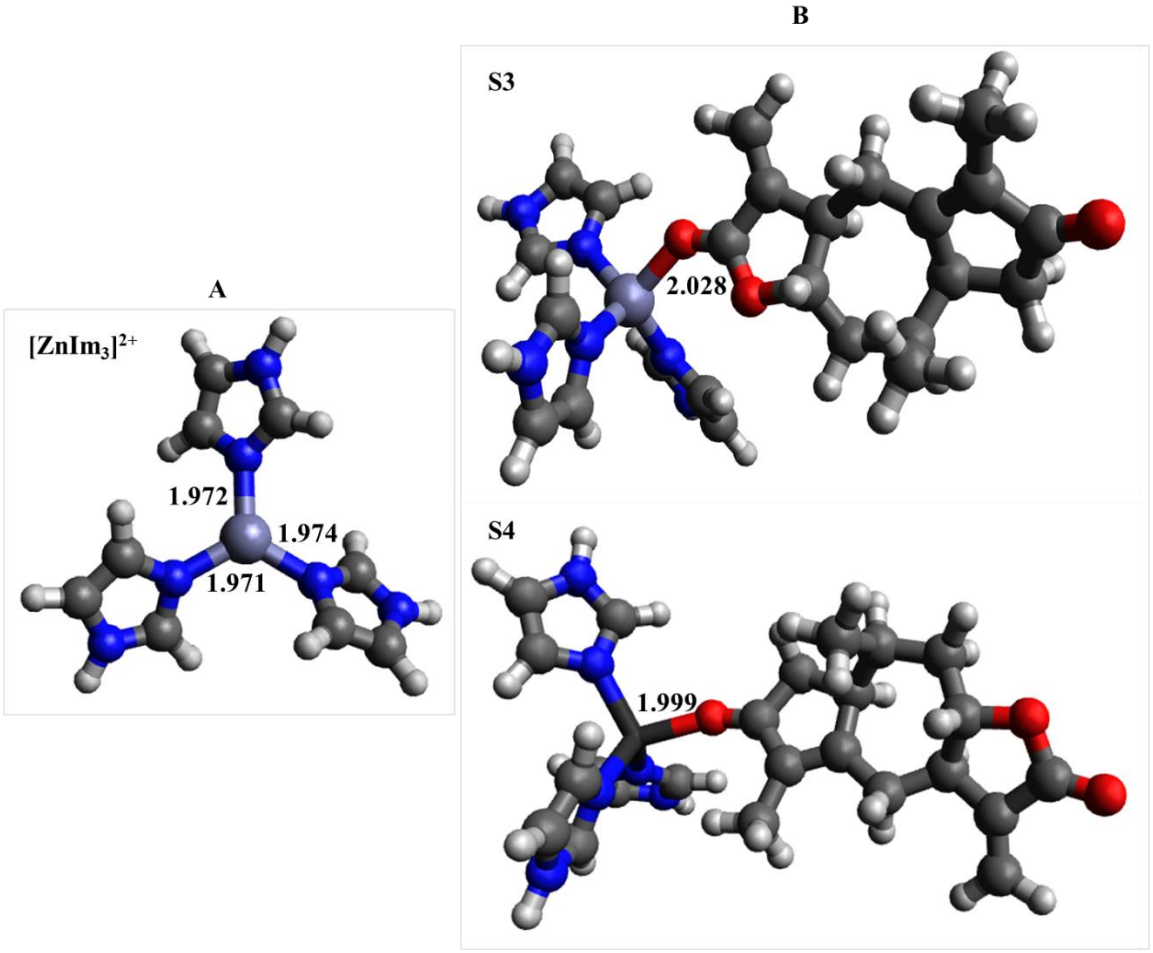

Figure 5.9. (A) Optimized structure of the carbonic anhydrase active site model $[ZnIm3]^{2+}$, depicting 3 imidazole molecules bound to Zn^{2+} ion, (B) xerantholide-$[ZnIm3]^{2+}$ complexes calculated at the B3LYP/6-311++G(d,p) level

Two structures of the xerantholide-$[ZnIm_3]^{2+}$ complexes are reported in this study (Figure 5.9). Structure S3 represents the interaction of xerantholide with $[ZnIm_3]^{2+}$ through the

lactone moiety as observed in the docking calculations reported in section 5.3.2. Structure S4 shows the interaction of xerantholide with $[ZnIm_3]^{2+}$ through the carbonyl group positioned in the second 5-membered ring of xerantholide. Vibrational frequency analysis indicated that both S3 and S4 are genuine minima. The total energies of the two xerantholide-$[ZnIm_3]^{2+}$ complexes computed at different theoretical levels are listed in supplementary information Table SP1 (Appendix 6). The interaction energies can be found in Table 5.5. Using the 6-311++G(d,p) basis set, the results in the table shows that S3 and S4 are nearly isoenergetic with S3 slightly more stable by 3.2, 1.4, 2.2 and 1.6 kcal/mol at the B3LYP, B3LYP-D2, M06-2X and ωB97xd levels, respectively. It is noteworthy that S4 is more stabilized by roughly 1.0 to 1.8 kcal/mol by functionals that include the dispersion corrections. These results suggest that accurate theoretical analysis of xerantholide interacting with Zn^{2+} containing CA should take into account dispersion effect. Including correction for zero-point vibrational energy affects the energy difference between S3 and S4 by less than 0.4 kcal/mol. The interaction energy computed for the S3 xerantholide-$[ZnIm_3]^{2+}$ complex ranged from -37.1 to -49.5 kcal/mol. Basis set superposition errors (BSSE) lowered the interaction energies by roughly 2.1 kcal/mol and the inclusion of zero-point energy (ZPE) increased the interaction energies by less than 0.9 kcal/mol at all levels of theory considered in this study. These values suggest that xerantholide has a good binding affinity with the model of the NgCA active site.

Figure 5.9 shows that xerantholide interacts with $[ZnIm_3]^{2+}$ through the oxygen atom in the lactone ring. The Zn-O bond length of the optimized S3 calculated using 6-311++G(d,p) basis set were very similar, B3LYP (2.028 Å), M06-2X (2.024 Å) and ωB97xd (2.018 Å). The Zn-O bond showed longer distance of 2.613 Å in molecular docking analysis

compared to Zn-O bond in xerantholide-$[ZnIm_3]^{2+}$ complex in DFT calculations. This could be attributed to intermolecular interactions present in the docking studies but neglected in the active site model study.

Table 5.5. Interaction energies calculated using 3 methods and 6 basis sets

	Interaction Energy (kcal/mol)	
Method	**S3**	**S4**
B3LYP/6-31+G(d)	-40.7	
B3LYP/6-311+G(d)	-40.3	
B3LYP/6-311++G(d,p)	-40.3	-37.1
B3LYP/6-311++G(2d,p)	-39.8	
B3LYP/6-311++G(2df,2p)	-39.7	
B3LYP/Aug-CC-pVTZ	-39.7	
B3LYP-D2/6-311++G(d,p)	-47.1	-45.7
B3LYP-D2/6-311++G(2df,2p)	-46.4	
M06-2X/6-31+G(d)	-49.5	
M06-2X /6-311+G(d)	-48.8	
M06-2X /6-311++G(d,p)	-48.8	-46.6
M06-2X /6-311++G(2d,p)	-48.2	
M06-2X /6-311++G(2df,2p)	-48.0	
M06-2X /Aug-CC-pVTZ	-48.5	
ωB97xd/6-31+G(d)	-46.9	
ωB97xd/6-311+G(d)	-46.8	
ωB97xd/6-311++G(d,p)	-46.7	
ωB97xd/6-311++G(2d,p)	-46.3	-45.1
ωB97xd/6-311++G(2df,2p)	-46.1	
ωB97xd/Aug-CC-pVTZ	-45.8	

5.4 Conclusion

The two lowest energy conformers of xerantholide have been computed. These conformers are nearly isoenergetic and separated by less than 4 kcal/mol. The computed geometry of the lowest energy structure of xerantholide agrees well with previously reported x-ray data.

Computed electronic properties indicate that xerantholide is a soft molecule with high capacity to react with biomolecules. Molecular docking studies suggest the potential of xerantholide as an NgCA inhibitor. The results show that xerantholide has a high binding affinity to NgCA as demonstrated by the low docking score. Xerantholide interact with NgCA's active site through various bond types such as hydrogen bond (Thr-178), metal-acceptor interaction through (Zn^{2+}), alkyl interaction (Val-123, Leu-176, Leu-115, Val-113, Pro-121), and pi-alkyl interactions (His-92), thus making ligand-receptor complex stable. The calculated binding energy, binding score and binding mode observed *in-silico*, is indicative of xerantholide's potential to inhibit NgCA. This study thus gives basis for future *in-vitro* studies aimed at identifying novel anti-gonorrheal agents with mechanism of action targeting the disruption of essential enzyme activity. B3LYP-D2, M06-2X and ωB97xd methods that include dispersion corrections appear to give higher interaction energy compared to B3LYP.

5.5 References

1. Nyambe MM, Archibong EF, Sekhoacha M, Chinsembu KC. *In-vitro* anti-gonorrheal activity of a sesquiterpene lactone, xerantholide isolated from the leaves of *Pechuel-loeschea leubnitziae*. South African J Bot. 2022;147:314–8.

2. Kadhila NP, Sekhoacha M, Tselanyane M, Chinsembu KC, Molefe-Khamanga DM. Determination of the antiplasmodial activity, cytotoxicity and active compound of *Pechuel-loeschea leubnitziae* O. Hoffm. (Asteraceae) of Namibia. SN Appl Sci. 2020;2(8).

3. Unemo M, del Rio C, Shafer WM. Antimicrobial Resistance Expressed by *Neisseria gonorrhoeae* : A Major Global Public Health Problem in the 21st Century. Microbiol Spectr. 2016;4(3):1–32.

4. Dowell D, Kirkcaldy RD. Effectiveness of gentamicin for gonorrhoea treatment: systematic review and meta- analysis. Sex Trans Infect. 2012;0:1-6.

5. Mishra CB, Tiwari M, Supuran CT. Progress in the development of human carbonic anhydrase inhibitors and their pharmacological applications: Where are we today? Med Res Rev. 2020;40(6):2485–565.

6. Hewitt CS, Abutaleb NS, Elhassanny AEM, Nocentini A, Cao X, Amos DP, et al. Structure-activity relationship studies of acetazolamide-based carbonic anhydrase inhibitors with activity against *Neisseria gonorrhoeae*. ACS Infect Dis. 2021;

7. Nocentini A, Hewitt CS, Mastrolorenzo MD, Flaherty DP, Supuran CT. Anion inhibition studies of the α-carbonic anhydrases from *Neisseria gonorrhoeae*. J Enzyme Inhib Med Chem. 2021;36(1):1061–6.

8. Angeli A, Carta F, Supuran CT. Carbonic anhydrases: Versatile and useful biocatalysts in chemistry and biochemistry. Catalysts. 2020;10(9):1–11.

9. Cuffaro D, Nuti E, Rossello A. An overview of carbohydrate-based carbonic anhydrase inhibitors. J Enzyme Inhib Med Chem. 2020;35(1):1906–22.

10. Lomelino CL, Andring JT, McKenna R. Crystallography and Its Impact on Carbonic Anhydrase Research. Int J Med Chem. 2018;2018:1–21.

11. Supuran CT, Capasso C. An overview of the bacterial carbonic anhydrases. Metabolites. 2017;7(4).

12. Huang S, Xue Y, Sauer-Eriksson E, Chirica L, Lindskog S, Jonsson BH. Crystal structure of carbonic anhydrase from *Neisseria gonorrhoeae* and its complex with the inhibitor acetazolamide. J Mol Biol. 1998;283(1):301–10.

13. Bottoni A, Lanza CA, Miscione GP, Spinelli D, Calhorda MJ, Mora M. New model for a theoretical density functional theory investigation of the mechanism of the carbonic anhydrase: How does the internal bicarbonate rearrangement occur? Chemtracts. 2004;17(7):366–70.

14. Mahmudov I, Demir Y, Sert Y, Abdullayev Y, Sujayev A, Alwasel SH, et al. Synthesis and inhibition profiles of N-benzyl- and N-allyl aniline derivatives against carbonic anhydrase and acetylcholinesterase – A molecular docking study. Arab J Chem. 2022;15(3):103645.

15. Lagutschenkov A, Lorenz UJ, Dopfer O. IR spectroscopy of isolated metal-organic complexes of biocatalytic interest: Evidence for coordination number four for Zn2+(imidazole) 4. Int J Mass Spectrom. 2011;308(2–3):316–29.

16. Watson WH, Kashyap RP, Miski M, Mabry TJ. (1S,7S,8R,10S)-3-Oxoguaia-4,11(13)-dien-8,12-olide, C15H18O3. Acta Crystallogr Sect C Cryst Struct Commun. 1985;41(7):1126–8.

17. Al-Swaidan IA, El-Azab AS, Alanazi AM, Abdel-Aziz AAM. Synthesis and conformational analysis of sterically congested (4 R)-(-)-1-(2,4,6-trimethylbenzenesulfonyl)-3- n -butyryl-4- tert -butyl-2-imidazolidinone: X-ray crystallography and semiempirical calculations. J Chem. 2014;2014.

18. Spartan'14V1.1.0. Tutorial and User ' s Guide Preliminary Edition. Irvine: Wavefunction, Inc; 2013.

19. Fang C, Durbeej B. Calculation of Free-Energy Barriers with TD-DFT: A Case Study on Excited-State Proton Transfer in Indigo. J Phys Chem A. 2019;123(40):8485–95.

20. Grimme S. Density functional theory with London dispersion corrections. Wiley Interdiscip Rev Comput Mol Sci. 2011;1(2):211–28.

21. Ryzhkov AB, Ariya PA. A theoretical study of the reactions of parent and substituted Criegee intermediates with water and the water dimer. Phys Chem Chem Phys. 2004;6(21):5042–50.

22. Feller D. The role of Databases in support of computaional Chemistry calculations. J Comput Chem. 1996;17(13):1571–86.

23. M. J. Frisch et al., Gaussian 16, Revision B.01, Gaussian, Inc., Wallingford CT, 2016.

24. Morris GM, Ruth H, Lindstrom W, Sanner MF, Belew RK, Goodsell DS, et al. Software news and updates AutoDock4 and AutoDockTools4: Automated docking with selective receptor flexibility. J Comput Chem. 2009;30(16):2785–91.

25. Trott O, Olson AJ. Software News and Update-AutoDock Vina: Improving the speed

and accuracy of Docking with a new scoring function, efficient optimization, and multithreading. J Comput Chem. 2009;31(2):455–61.

26. Schrödinger L, DeLano W. PyMOL Molecular Graphics System. Schrödinger, LLC; 2020. Accessed 8 June 2022, <http://www.pymol.org/pymol>.

27. BIOVIA DS. Discovery Studio Visualizer,. San Diego: Dassault Systèmes; 2019.

28. Dege N, Gökce H, Doğan OE, Alpaslan G, Ağar T, Muthu S, et al. Quantum computational, spectroscopic investigations on N-(2-((2-chloro-4,5-dicyanophenyl)amino)ethyl)-4-methylbenzenesulfonamide by DFT/TD-DFT with different solvents, molecular docking and drug-likeness researches. Colloids Surfaces A Physicochem Eng Asp. 2022;638(January).

29. Miar M, Shiroudi A, Pourshamsian K, Oliaey AR, Hatamjafari F. Theoretical investigations on the HOMO–LUMO gap and global reactivity descriptor studies, natural bond orbital, and nucleus-independent chemical shifts analyses of 3-phenylbenzo[d]thiazole-2(3H)-imine and its para-substituted derivatives: Solvent and subs. J Chem Res. 2021;45(1–2):147–58.

30. Banuppriya G, Sribalan R, Padmini V. Synthesis and characterization of curcumin-sulfonamide hybrids: Biological evaluation and molecular docking studies. J Mol Struct. 2018;1155:90–100.

31. Saranya M, Ayyappan S, Nithya R, Sangeetha RK, Gokila A. Molecular structure, NBO and HOMO-LUMO analysis of quercetin on single layer graphene by density functional theory. Dig J Nanomater Biostructures. 2018;13(1):97–105.

32. Mohammad AM, Tarun KP, Md Ashraful A, Md Al-Amin-Al-Azadul I, Subrata P, Md Chanmiya S. DFT studies on vibrational and electronic spectra, HOMO-LUMO, MEP, HOMA, NBO and molecular docking analysis of benzyl-3-N-(2,4,5-trimethoxyphenylmethylene)hydrazinecarbodithioate. J Mol Struct. 2020;128715(1220).

33. Kumar A, Baccoli R, Fais A, Cincotti A, Pilia L, Gatto G. Substitution effects on the optoelectronic properties of coumarin derivatives. Appl Sci. 2020;10(1).

34. Possart K, Herrmann FC, Jose J, Costi MP, Schmidt TJ. Sesquiterpene lactones with dual inhibitory activity against the trypanosoma brucei pteridine reductase 1 and dihydrofolate reductase. Molecules. 2022;27(1):1–14.

35. Amorim Franco TM, Blanchard JS. Bacterial Branched-Chain Amino Acid Biosynthesis: Structures, Mechanisms, and Drugability. Biochemistry. 2017;56(44):5849–65.

36. Létoffé S, Chalabaev S, Dugay J, Stressmann F, Audrain B, Portais JC, et al. Biofilm

microenvironment induces a widespread adaptive amino-acid fermentation pathway conferring strong fitness advantage in Escherichia coli. PLoS Genet. 2017;13(5):1–20.

37. Di Fiore A, Capasso C, De Luca V, Monti SM, Carginale V, Supuran CT, et al. X-ray structure of the first "extremo-α-carbonic anhydrase", a dimeric enzyme from the thermophilic bacterium Sulfurihydrogenibium yellowstonense YO3AOP1. Acta Crystallogr Sect D Biol Crystallogr. 2013;69(6):1150–9.

38. Abutaleb NS, Elhassanny AEM, Seleem MN. In vivo efficacy of acetazolamide in a mouse model of *Neisseria gonorrhoeae* infection. Microb Pathog. 2022;164:105454.

39. Kasende OE, Nziko VDPN, Scheiner S. Interactions of nucleic acid bases with temozolomide. stacked, perpendicular, and coplanar heterodimers. J Phys Chem B. 2016;120(35):9347–61.

CHAPTER 6: MOLECULAR DOCKING AND THE ACTIVE SITE MODEL CALCULATIONS FOR THE INTERACTION OF XERANTHOLIDE SESQUITERPENE LACTONE ANALOGUES WITH *NEISSERIA GONORRHOEAE* CARBONIC ANHYDRASE

Abstract

Carbonic anhydrase inhibitors (CAIs) have the potential to cure diseases, and they are becoming very popular as a means of overcoming the problem of antibiotic resistance. This study evaluated the ability of 83 sesquiterpenes lactones (SLs) analogues of xerantholide to inhibit *Neisseria gonorrhoeae* carbonic anhydrase (NgCA), an enzyme that catalyses an essential reaction in the growth and survival of the bacterium. Screening of sesquiterpene lactones for NgCA inhibition potential was done using molecular docking with the NgCA as a receptor. Further, the active site of NgCA was modelled with zinc-tris imidazole, ($[ZnIm_3]^{2+}$) and the binding energy of the 83 SL-$[ZnIm_3]^{2+}$ complexes computed at the B3LYP/6-311++G(d,p) level. All structures docked with binding affinities ranging from -5.3 to -7.4 kcal/mol and the computed DFT binding energy ranged from -16.5 to – 43.1 kcal/mol. Analysis of the results shows that the binding of these compounds to the active site of NgCA involves both hydrogen bonding, van der Waals, and hydrophobic interactions. The lactone ring is essential for strong binding which is enhanced by substituent groups such as epoxides, ketones and esters. This study thus revealed the possible binding mode and factors that affect the observed binding energies. Eleven structures (**22**, **40**, **65**, **69**, **70, 71, 72, 73, 74, 76**, **80**) gave lowest ligand-receptor binding score between -7.0 to -7.4 kcal/mol suggesting higher binding affinity than the lead structure.

Key words: Molecular docking, sesquiterpenes, Zinc imidazole, active site, *Neisseria gonorrhoeae*, NgCA

6.1 Introduction

Sesquiterpene lactones (SLs) are 15-carbon terpenoids which are one of the most widespread and biologically important classes of secondary metabolites in plants. They are characterized by the presence of an α-methylene-γ-lactone ring (Figure 6.1), formed from condensation of three isoprene units followed by cyclization and oxidative transformation which results in either cis or trans-fused lactone (1). There are several classes of SLs including: germacranolides, haliangolides, guaianolides, pseudoguaianolides, hypocretenolides and eudesmanolides. Some of the biological activities reported for SLs are: anticancer, fungicidal, antimicrobial, antiplasmodial, trypanocidal, antidiabetic, analgesic, anti-inflammatory, antioxidant, antiprotozoal, herbicidal, and allergenic effects, however, they are also very toxic (1–3). Some SLs have also been reported to have enzyme inhibition activity (4–6). Besides the medicinal benefits of SLs, they also have nutritional benefits. They are found in herbs and vegetables such as celery, parsley, spinach, sunflower, lettuce, and carrots (7). The biological effect of SLs is attributed to the α-methylene-γ-lactone group, which has been shown to be necessary for activity. For example, a study by Fisher et al. (1998), showed that the reductive opening of the lactone ring showed no activity against *Mycobacterium tuberculosis* (8). However, other studies have shown that though the α-methylene-γ-lactone group is essential for activity, it is not sufficient. Other functional groups neighbouring the α-methylene-γ-lactone such as epoxides, chlorohydrin, unsaturated ester, unsaturated lactones, aldehydes, and ketones

may enhance activity by either chemical or steric effects (7). Other factors such as number of alkylating structural elements and lipophilicity, may also influence the potency of SLs (1).

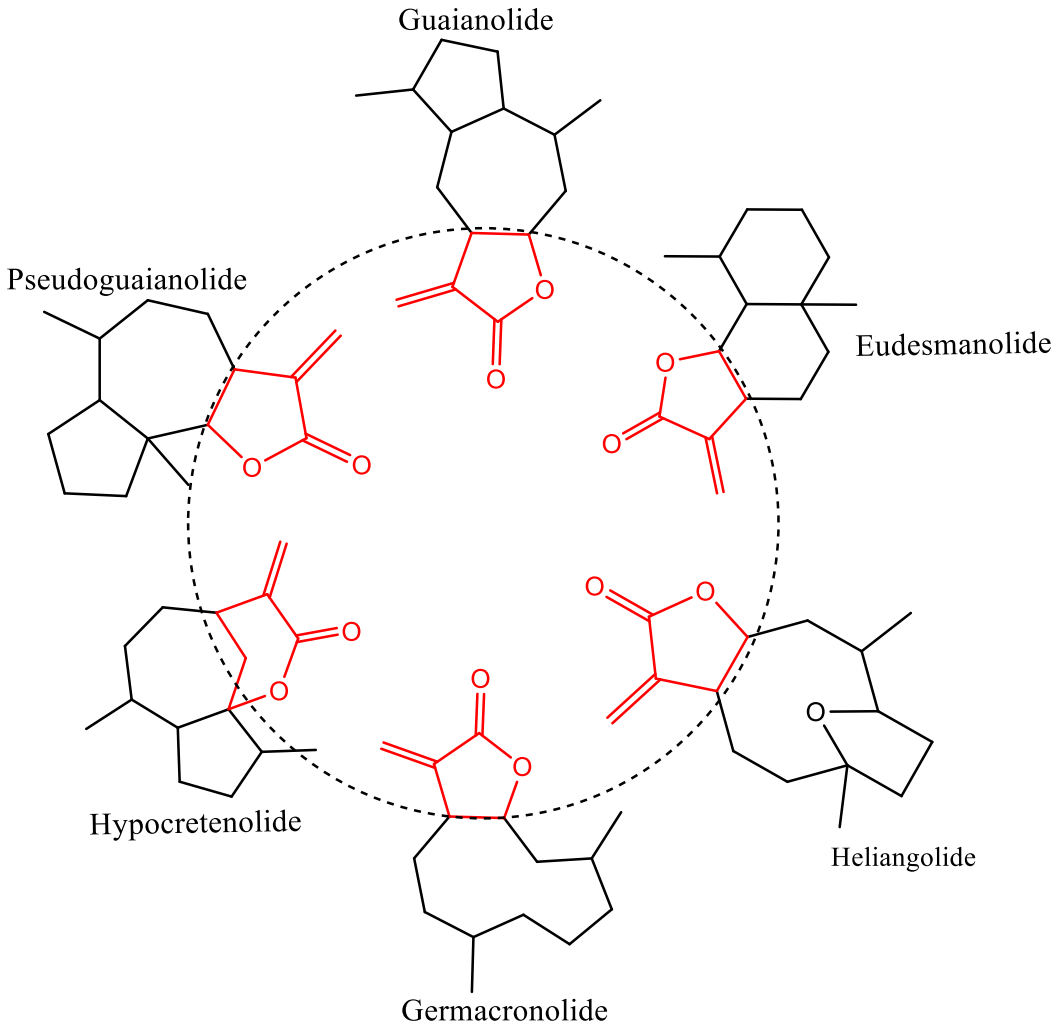

Figure 6.1. Types of sesquiterpene lactones, highlighting the general structure of α-methylene-γ-lactones

Generally, drugs are considered to bind to receptors, and molecules that bind to receptors are usually termed ligands. A drug forms a complex with a biomolecule to serve a biological purpose. When a ligand (potential drug) binds to a protein (receptor), the protein

undergoes a conformational change (receptor changes its shape or activity) which in turn leads to a physiological response (either transmitting a signal or directly producing a change inside a cell). A computational approach that is used to predict the preferred binding orientation of one molecule (ligand) to another molecule (receptor/target) to form a stable complex is termed molecular docking. From the results of binding, predictions are made about the energy profiling as well as the binding affinity and stability of the complex (9). The time a ligand spends attached to a receptor or specific protein is a function of the affinity between the ligand and the protein. The higher the affinity, the stronger the ligand will bind to the protein, and the longer the functional modification will last. The lower the affinity, the less likely is the binding or the faster the release from the receptor. Binding occurs through intermolecular forces, such as ionic bonds, hydrogen bonds and Van der Waals forces (10). High-affinity ligand binding results from greater attractive forces between the ligand and its receptor while low-affinity ligand binding involves less attractive force. A ligand can be an agonist (when a ligand directly initiates a response - bind to a receptor and activates the receptor to produce a biological response) or an antagonist (the type that blocks a biological response by binding to and blocking the receptor rather than activating it- in other words, antagonist drugs interfere in the natural operation of receptor protein) (11). Antagonists are sometimes called blockers. A drug binds to a receptor, and that provokes a series of biochemical and physiological changes to produce the observed drug effect. All drugs act by interacting specifically with its receptor. Each receptor only allows a very limited range of molecules to activate a response.

Carbonic anhydrase inhibitors (CAIs) have the potential to cure diseases, and they are becoming very popular as a means of overcoming the problem of antibiotic resistance (12–14). The available CAIs can be divided into four groups: the metal ion binders such as anions, sulfonamides, dithiocarbamates, xanthates; compounds which attach to the zinc-coordinated water molecule or hydroxide ion like phenols, polyamines, thioxocoumarins, sulfocumarins; compounds occluding the active site entrance such as coumarins and their isoesters and compounds binding out of the active site (13,15).

A study described in chapter 4 showed that xerantholide, a SL has anti-gonorrhea activity, which is a motivation to investigate its mechanism of action to find ways to improve activity. The present study aimed to screen various other sesquiterpene lactones that are analogous to xerantholide for potential inhibitory effect on NgCA. The binding effect of these molecules on *Neisseria gonorrhoeae* carbonic anhydrase (NgCA) were investigated. NgCA is an enzyme that catalyse CO_2 hydration to bicarbonate and proton, an essential reaction in the bacteria's physiological and pathological processes.

6.2 Material and methods

6.2.1 Computational methods and Docking

The method used in this section follows the one described in section 5.2.1 with some modifications. Based on energy and Boltzmann distribution criteria, MMFF and PM3 were used to generate 107 conformers from 83 xerantholide SL analogues. From the results of section 5.2.1, the performance of B3LYP/6-311++G(d,p) compares well with other theoretical methods employed in that section (e.g M06-2X and ωB97xd with the same basis set). Therefore, B3LYP/6-311++G(d,p) was used for full geometry optimization (without

symmetry constraints) and frequency calculations of the molecules considered in this section. The frequency calculations enabled characterization of the structures as minima. Table 6.1 list the computer programs that were used to draw and optimize structures as well as analysing some results.

Eighty-three SL structures representing analogues of xerantholide were selected from the literature. These ligands and xerantholide (the lead) were fully optimized as described above, and subsequently docked with NgCA using the AutoDock programme (16). Ten (10) different docked poses were generated for each ligand, scored, and compared to find the best fit ligand. Energy files in LOG format with binding affinity (kcal/mol) values and the pdbqt files with docking conformations of ligands were generated. Acetazolamide (AZM), ethoxzolamide (EZM), as well as tetracycline (Tet), which are known NgCAI and antibiotics with antimicrobial activity against *N. gonorrhoeae* were also docked as reference. Schematics representation of interaction of the ligand and residues inside the binding site of the receptor was generated using AutoDock Python Molecule Viewer (PMV), PyMOL and Discovery studio visualizer (16-19).

Table 6.1 Summary of software used in this section

	Software
Drawing and generating 2D&3D chemical structures.	Spartan ’14, ChemDraw and Gauss View
Gaussian input generation and reading of the outputs.	Spartan'14, Gauss View 3.0, Avogadro
Optimization of the geometry and frequency calculations.	Gaussian 16, Revision B.01, 6-processors HP workstation (supercomputer)
Molecular docking & analysis	AutoDock Vina, PyMOL, Discovery Studio Visualizer

The binding affinities of all studied compounds with carbonic anhydrase active site model, zinc-tris imidazole, ($[ZnIm_3]^{2+}$) were predicted computationally using DFT. The method described in section 5.2.1 was used to calculate the binding free energy (change in Gibbs free energy) of each molecule using their respective total energy of the optimized ligand, active site model and the ligand-$[ZnIm_3]^{2+}$ complex.

6.3 Results and discussion

The 2D structures of the molecules used in molecular docking reported in this section are shown in Figure 6.2 and their reference sources are listed in Table 6.2. The structures were fully optimized and characterized as minima via frequency calculations. Since there is no literature on the inhibition of CA by xerantholide and its analogues, their potential as inhibitors was determined using the binding affinity and the various interactions computed in the docking study.

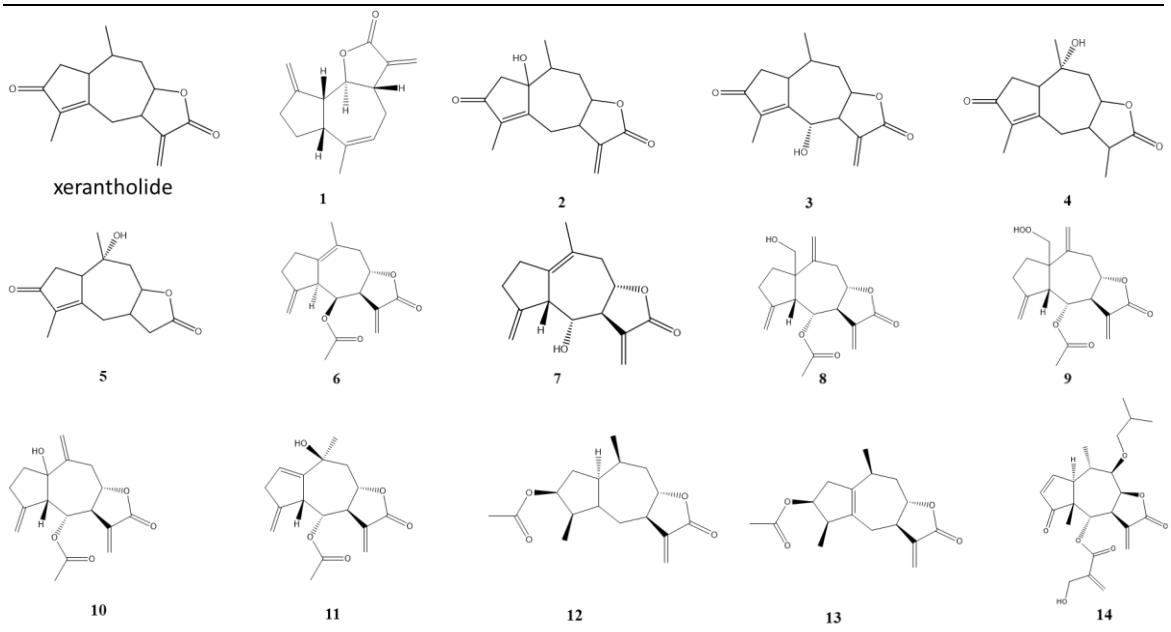

Figure 6.2. Lead compound, xerantholide and its analogues that were used in this study.

Figure 6.2 (Continued)

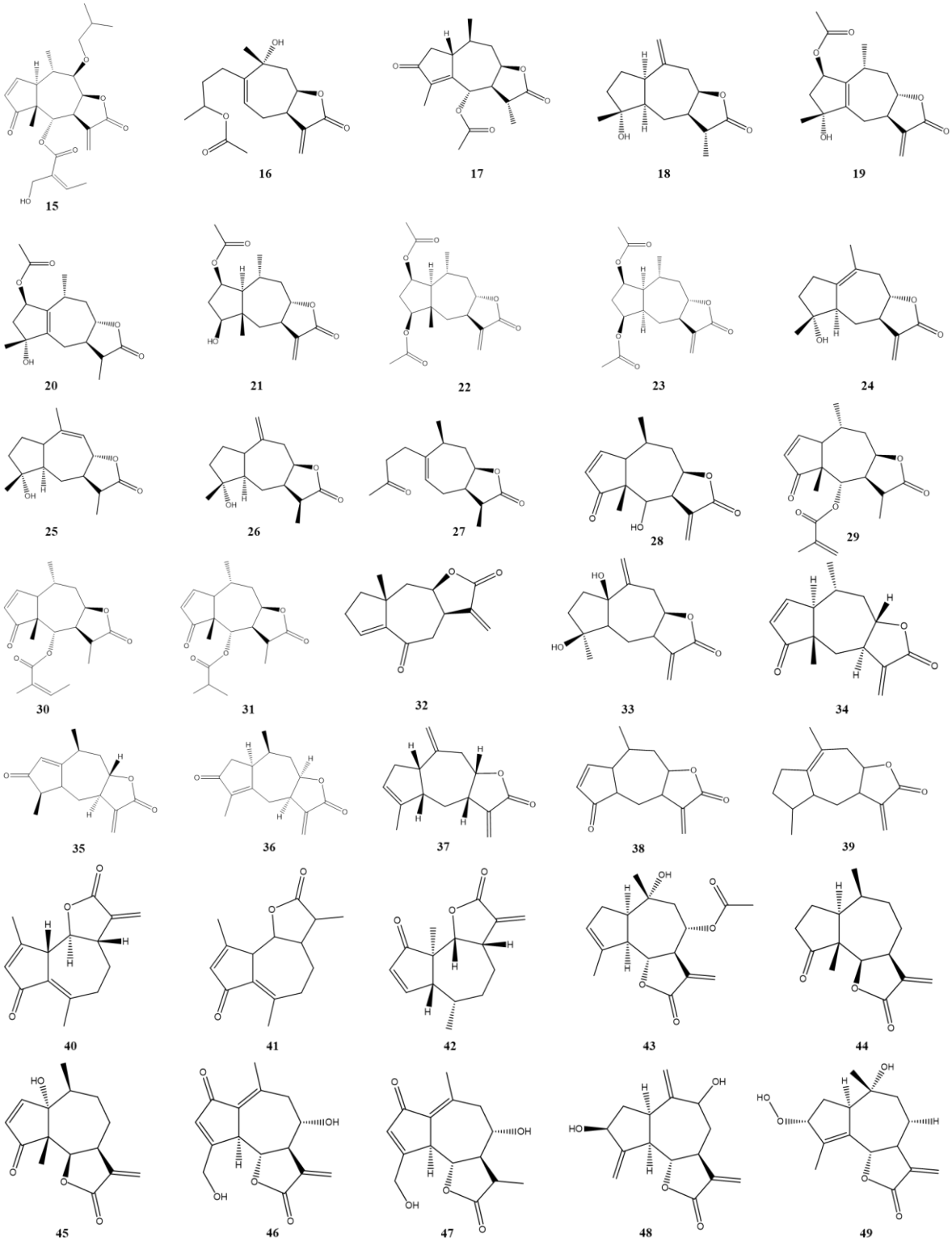

Figure 6.2 (Continued)

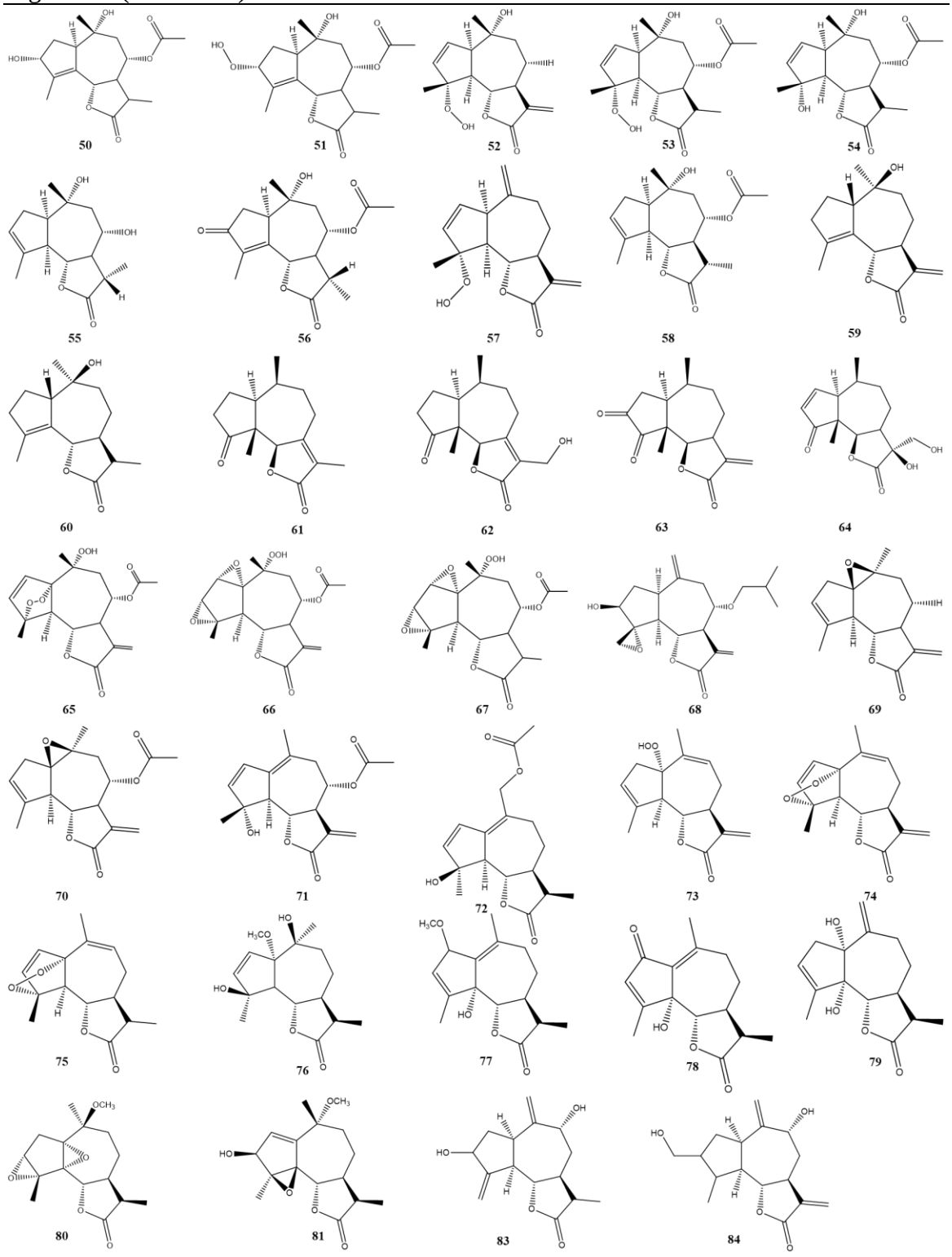

6.3.1 Molecular docking analysis and binding free energy

Docking of each SL ligand returned top ten ranked docked poses in which scoring method took into account both polar and nonpolar interaction of the ligand with the enzyme. The results of the interactions between the target and the inhibitors were predicted, and the binding scores for NgCA with the respective compounds are presented in Table 6.2. The results show that all structures docked with binding affinities ranging from -5.3 to -7.4 kcal/mol and several analogues were close in binding energy, thus the structures with affinity higher than that of the lead compound were selected for further interpretation. It is important to note that comparison of binding affinity was done between the highest ranked poses of each analogue while analysis took into consideration the differences between poses of the same analogue. Figure 6.3 shows that most of the compounds (63 of them) have binding score of -6.0 to -6.5 kcal/mol. None of the molecules gave binding energy below -7.5 kcal/mol. It is noteworthy that the lower the value of the binding score, the better the binding affinity of the ligand to the receptor. Eleven structures (**22**, **40**, **65**, **69**, **70, 71, 72, 73, 74, 76**, **80**) gave lowest ligand-receptor binding score between -7.0 to -7.4 kcal/mol.

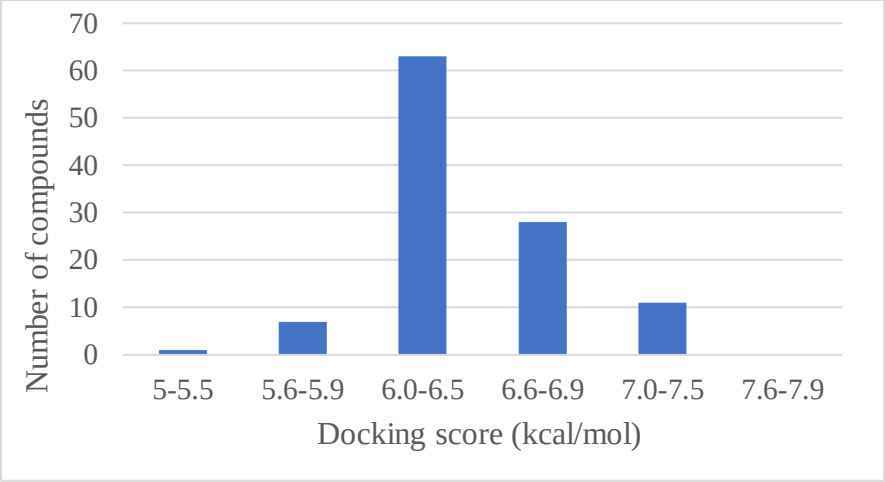

Figure 6.3. Xerantholide sesquiterpene lactone analogues classified according to their binding energies obtained using docking

Of the structures investigated, the highest binding affinity was observed with one of the conformers of structure **76** (conformer a76_c4), with a docking score of -7.4 kcal/mol. Although compound **76** has higher docking score than the lead compound xerantholide, it did not coordinate directly to Zn (II) ion in the active site. The high affinity displayed by **76** can thus be attributed to the multiple H-bond interactions with the amino acid residues in the active site, namely Gln-69, Gln-90, Thr-177, and Thr-178 as shown in Figure 6.4. Additionally, **76** has hydrophobic contribution with Val-113, Val-123, Leu-176 and His-92. Another molecule that did not have Zn (II) ion coordination but with high number of H-bond interaction is **14** interacting with Gln-69, Gln-90, Asn-64, Trp-7 as well as the nonpolar interactions with several other amino acid residues (Table 6.2). Selected analogues are presented in Figure 6.5 to show some types of interactions observed between studied ligands and NgCA. Generally, compounds that gave high score have polar interactions that involve the lactone ring. This is an indication that when the oxygen of the lactone ring is involved in bonding, strong binding to the receptor is very likely. Low values of binding energy were observed with structures that form H-bonds with the receptor.

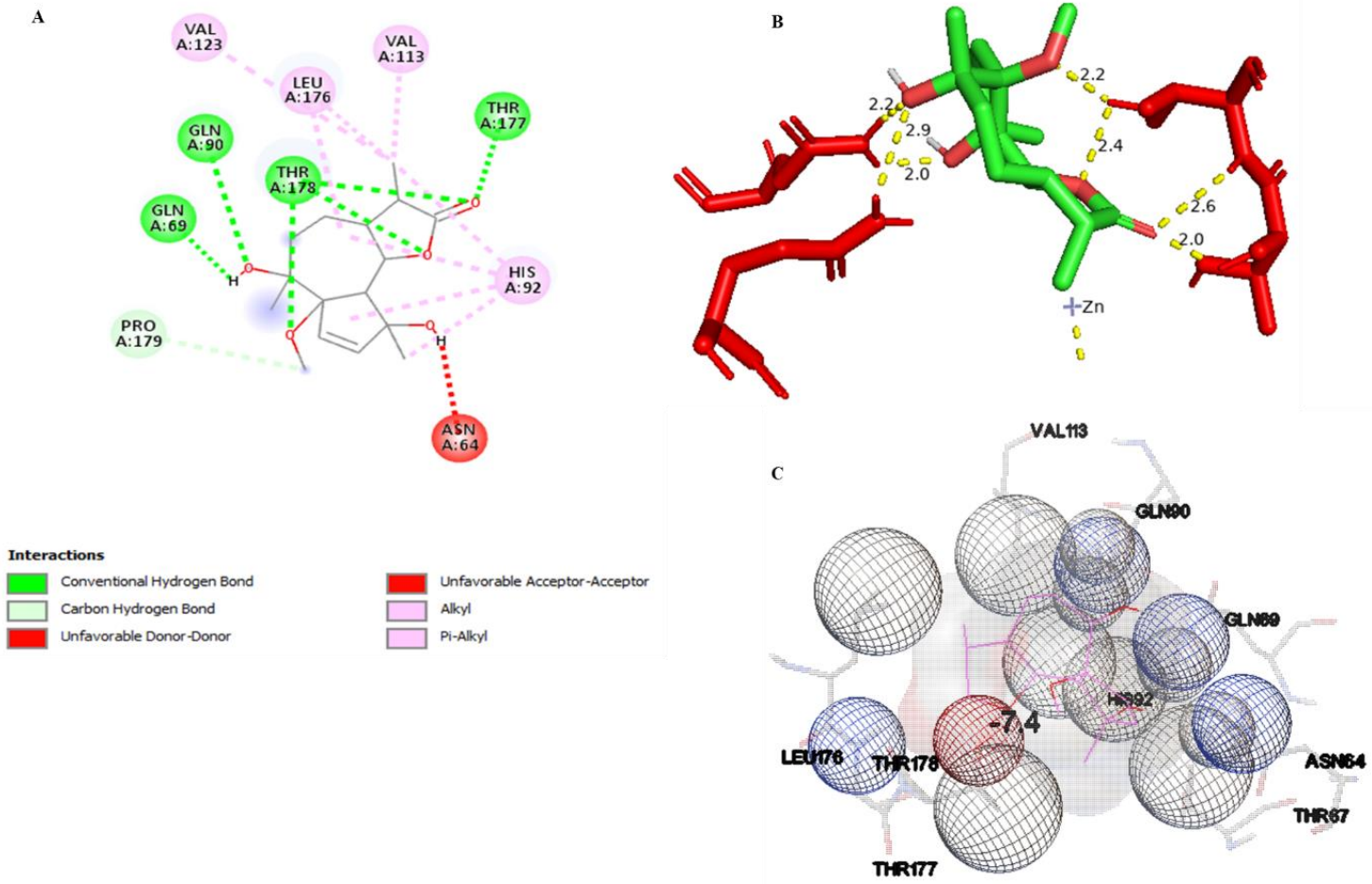

Figure 6.4. Docked pose of compound **76** with NgCA showing (A) 2D structure of amino acids residues interacting with compound **76** (B) bond distance between ligand and amino acids residues (C) amino acids in close proximity with the ligand. Visualized using Discovery studio, PMV and PyMOL.

Table 6.2. Binding affinities and binding interactions of xerantholide and analogues with NgCA determined by molecular docking and DFT method as well as their predicted amino acids involved in polar interaction with the ligand as analysed using PyMoL

Comp.# (Ref.)	Conformer code	Binding energy DFT ΔG° (kcal/mol)	Binding energy Docking (kcal/mol)	# of Polar interaction	Ligand interaction
1 (A)	a1_c1	-34.1	-6.8	4	His-92, Thr-178, Gln-69, Zn, His-111-(Zn)
	a1_c2	-33.9	-6.9	4	His-94, Thr-178, Gln-90, Zn, His-111-(Zn)
10 (C)	a10_c1	-33.8	-5.8	2	Gln-90, His-111-(Zn)
	a10_c2	-33.7	-5.7	4	Gln-69, Asn-64, Trp-7, Thr-178
11 (C)	a11_c1	-36.4	-6.6	3	Thr178, Gln-69, His-111-(Zn)
	a11_c5	-28.8	-6.1	3	Gln-69, Gln-90, Zn
12 (C)	a12_c2	-32.7	-6.9	2	Thr-177, Zn
13 (C)	a13_c3	-32.3	-6.5	2	Gln-90, His-111-(Zn)
14 (C)	a14_c26	-37.2	-6.3	8	Gln-69, Gln-90, Asn-64, Trp-7, His-111-(Zn)
	a14_c33	-26.9	-6.2	7	Gln-69, Gln-90, Asn-64, Trp-7, His-111-(Zn)
	a14_c38	ND	-6.9		Gln-69, Gln-90, Asn-64, Thr-178
15 (C)	a15_c1	ND	-6.5	4	Thr-177, Thr-178, His-111-(Zn)
	a15_c58	-32.8	-6.1	2	Gln-90, His-111-(Zn)
16 (C)	a16_c6	-35.1	-6.4	5	Gln 69, Thr-177, Thr-178, Zn, His-111-(Zn)
17 (C)	a17_c1	-27.9	-6.4	2	Gln-69, Asn-64
18 (C)	a18_c1	-33.6	-6.0	2	Gln-69, Trp-7
19 (C)	a19_c5	-32.4	-6.6	6	Gln-69, Asn-64, Thr-178, His-92, Zn, His-111-(Zn)
2 (B)	a2_c2	-32.3	-6.6	3	Thr-178, Zn, His-111-(Zn)
	a2_c3	ND	-6.6	4	Thr-178, His-92, Zn, His-111-(Zn)
20 (C)	a20_c2	-33.7	-6.3	4	Gln-69, Asn-64, Thr-178, His-111-(Zn)
21 (C)	a21_c1	-34.2	-6.3	4	Asn-64, His-92, Zn, His-111-(Zn)
22 (C)	a22_c1	-33.5	-7.3	3	Asn-64, Zn, His-111-(Zn)
23 (C)	a23_c1	-32.3	-6.6	3	His-92, Thr-178, Zn
24 (C)	a24_c3	-35.2	-6.2	2	Thr-178, Zn
25 (C)	a25_c2	-35.1	-6.6	4	His-92, Thr-178, Zn, His-111-(Zn)
26 (C)	a26_22	-32.8	-6.0	4	Gln-69, Trp-7, Pro-179
	a26_c13	-33.8	-5.8	1	Gln-90
27 (C)	a27_c3	-35.5	-6.4	2	His-92, Zn
28 (D)	a28_c2	-35.6	-6.1	2	Gln-69
29 (D)	a29_c1	-33.4	-6.1	5	Gln-69, Asn-64, His-66, Trp-7, Thr-178
3 (B)	a3_c1	-31.8	-6.2	2	Gln-90, Thr-178
	a3_c2	-33.7	-6.2	5	Gln-69, Asn-64, Pro179, Trp-7, Thr-5
	a3_c3	-32.0	-6.4	2	Gln-90, Thr-178

Comp.# (Ref.)	Conformer code	Binding energy DFT ΔG° (kcal/mol)	Binding energy Docking (kcal/mol)	# of Polar interaction	Ligand interaction
30 (D)	a30_c1	-34.5	-6.4	5	Gln-69, Gln-90, Thr-178, His-111-(Zn)
31 (D)	a31_c1	-33.3	-6.1	5	Gln-69, Asn-64, Trp-7, Thr-178, His-66
32 (C)	a32_c1	-30.2	-6.0	5	Gln-90, Thr-177, Thr-178, Zn, His-111-(Zn)
33 (C)	a33_c2	ND	-6.6	5	Gln-69, Asn-64, Trp-7, His-66
34 (A)	a34_c1	-31.2	-6.2	4	Thr-178, His-92, Zn, His-111-(Zn)
35 (A)	a35_c1	-29.0	-6.1	2	Thr178, Zn
	a35_c2	-31.2	-6.6	3	His-92, Zn, His-111-(Zn)
36 (A)	a36_c1	-29.3	-6.9	4	Thr-177, Thr-178, Zn, His-111-(Zn)
37 (A)	a37_c1	-33.8	-6.4	2	Asn-64, His-111-(Zn)
38 (A)	a38_c1	-31.0	-6.2	2	His-66, Trp-7
39 (A)	a39_c1	-34.4	-6.1	1	Thr-178
4 (B)	a4_c1	ND	-6.3	2	Thr-205, His-111-(Zn)
40 (A)	a40_c1	ND	-7.3	3	Thr-178, Zn, His-111-(Zn)
41 (A)	a41_c1	-26.5	-6.4	3	His-92, Zn, His-111-(Zn)
42 (A)	a42_c1	-41.7	-6.3	3	Gln-69, Gln-90
43 (C)	a43_c1	-32.5	-6.8	4	Gln-69, Gln-90, Asn-64, Zn
44 (C)	a44_c1	-37.6	-6.3	3	Gln-69, Gln-90, Asn-64
45 (C)	a45_c2	-43.1	-6.4	3	Gln-69, Gln-90, Asn-64, Leu-176, His-66
46 (C)	a46_c4	-35.0	-6.4	4	Gln-69, Thr-177, Thr-178, His-111-(Zn)
47 (C)	a47_c5	ND	-6.3	2	His-92, Zn
48 (C)	a48_c15	-33.9	-6.5	5	Gln-69, Thr-178, His-92, Zn, His-111-(Zn)
	a48_c9	-34.5	-6.5	5	Gln-69, Thr-178, His-92, Zn, His-111-(Zn)
49 (C)	a49_c28	-35.5	-6.8	6	Pro-179, Thr-178, His-92, Zn,
5 (B)	a5_c1	-30.3	-6.4	4	Gln-69, Thr-178, Zn, His-111-(Zn)
50 (C)	a50_c4	-32.5	-6.8	5	Gln-69, Gln-90, Thr-177, Thr-178, His-111-(Zn)
51 (C)	a51_c27	-33.9	-6.7	5	Gln-69, Gln-90, Thr-177, Thr-178, His-111-(Zn)
52 (C)	a52_c24	-39.9	-6.1	5	Thr-178, His-92, Zn, His-111-(Zn)
53 (C)	a53_c21	-37.9	-6.6	7	Gln-69, Asn-64, His-92, Zn, His-111-(Zn)
54 (C)	a54_c2	-34.1	-6.2	5	Gln-69, Trp-7, Thr-178, His-66
55 (C)	a55_c7	-36.9	-6.5	4	Gln-69, Pro-179, His-111-(Zn)
56 (C)	a56_c3	-	-	-	Gln-69, Trp-7, His-66, His-111-(Zn)
57 (C)	a57_c5	-36.5	-6.7	6	Thr-178, His-92, Zn, His-111-(Zn)
58 (C)	a58_c2	-31.2	-6.7	4	Gln-90. Asn-64, Thr-178, His-111-(Zn)
	a58_c4	-30.5	-6.4	3	Asn-64, Pro-179, Thr-178
59 (C)	a59_c1	-36.2	-6.3	2	Gln-69, Asn-64

Comp.# (Ref.)	Conformer code	Binding energy DFT ΔG° (kcal/mol)	Binding energy Docking (kcal/mol)	# of Polar interaction	Ligand interaction
	a59_c3	-32.3	-6.3	1	Gln-90
6 (C)	a6_c1	-33.8	-6.7	3	Thr-178, His-92, Zn
	a6_c2	-33.6	-6.4	2	Gln-90, His-111-(Zn)
60 (C)	a60_c2	-35.8	-6.7	2	Gln-90, Asn-64
	a60_c4	ND	-6.1	1	Gln-90
61 (C)	a61_c1	-42.6	-6.4	3	Gln-69, Gln-90
62 (C)	a62_c2	ND	-6.3	3	Gln-69, Gln-90
63 (C)	a63_c1	-36.7	-6.7	3	Gln-69, Gln-90
64 (C)	a64_c1	-34.9	-5.9	5	Gln-69, Gln-90, Asn-64, Thr-178
	a64_c9	-37.5	-6.3	5	Gln-69, Gln-90, Asn-64
65 (C)	a65_c14	-29.9	-7.3	2	Gln-90, Zn
66 (C)	a66_c1	-35.8	-6.3	5	Gln-69, Gln-90, Trp-7, His-66
67 (C)	a67_c2	-31.9	-6.2	5	Gln-69, Gln-90, Trp-7, His-66
68 (C)	a68_c30	-36.7	-6.4	4	Gln-69, Thr-178, His-92, Zn
	a68_c60	ND	-6.5	5	Gln-69, Thr-178, His-92, Zn, His-111-(Zn)
69 (C)	a69_c1	-33.1	-7.2	4	Gln-90, Thr-178, Zn, His-111-(Zn)
	a69_c2	ND	-6.3	1	Gln-69
7 (C)	a7_c1	-34.9	-6.5	3	Gln-90, Zn, His-111-(Zn)
	a7_c4	-36.9	-6.6	3	Gln-90, Zn, His-111-(Zn)
70 (C)	a70_c2	-32.4	-7.3	4	Gln-69, Thr-178, His-92, Zn
71 (C)	a71_c2	-37.0	-7.3	4	Asn-64, Thr-177, Thr178, His-111-(Zn)
72 (C)	a72_c3	-36.1	-7.1	6	Gln-69, Gln-90, Thr-178, Zn, His-111-(Zn)
73 (C)	a73_c1	-32.5	-7.0	3	Thr-178, Zn, His-111-(Zn)
74 (C)	a74_c1	-28.5	-7.0	4	Thr-178, His-92, Zn, His-111-(Zn)
75 (C)	a75_c1	-28.8	-6.9	4	Thr-178, Asn-64
76 (C)	a76_c4	-36.3	-7.4	8	Gln-69, Gln-90, Asn-64, Thr-67, Thr-177, Thr-178, His-92, Leu-176, Val-113, His-111-(Zn)
77 (C)	a77_c3	-32.9	-6.2	5	Gln-69, Thr-178, Zn, His-111-(Zn)
78 (C)	a78_c2	-28.7	-6.7	4	Thr-178, Zn, His-111-(Zn)
79 (C)	a79_c2	-36.7	-6.3	5	Thr-178, His-92, Zn, His-111-(Zn)
	a79_c4	-30.2	-6.1	3	Gln-69, Asn-64, His-111-(Zn)
8 (C)	a8_c2	-31.8	-5.9	3	Tyr-9, Thr-10, His-111-(Zn)
80 (C)	a80_c2	-35.8	-7.3	5	Thr-177, Thr-178, Zn, His-111-(Zn)
81 (C)	a81_c1	-29.2	-6.5	3	Gln-69, Asn-64, Zn
83 (C)	a83_c16	-32.8	-6.1	3	Trp-7, Pro-179, His-111-(Zn)
	a83_c9	-33.3	-6.1	4	Gln-69, Asn-64, Thr-178, His-111-(Zn)

Comp.# (Ref.)	Conformer code	Binding energy DFT ΔG° (kcal/mol)	Binding energy Docking (kcal/mol)	# of Polar interaction	Ligand interaction
84 (C)	a84_c34	-40.4	-6.0	3	Thr-178, His-92, Zn
9 (C)	a9_c6	-33.6	-6.0	3	Gln-90, Trp-7, His-66
	azm	ND	-5.7	5	Gln-69, Asn-64, Thr-177, Thr-178, His-111-(Zn)
	ezm	ND	-5.3	6	Asn-64, Thr-177, Thr-178, His-92, Zn, His-111-(Zn)
	tet	ND	-6.6	6	Gln-90, Asn-64, Trp-7, Pro-179, Thr-178, His-111-(Zn)
Lead (Isolated)	xer_c1	-28.5	-6.8	4	Thr-178, His-92, Zn, His-111-(Zn)
	xer_c2	-32.9	-5.9	1	His-111-(Zn)

References: A=PubChem, B = (18), C = (17), D = (19). ND = not determined

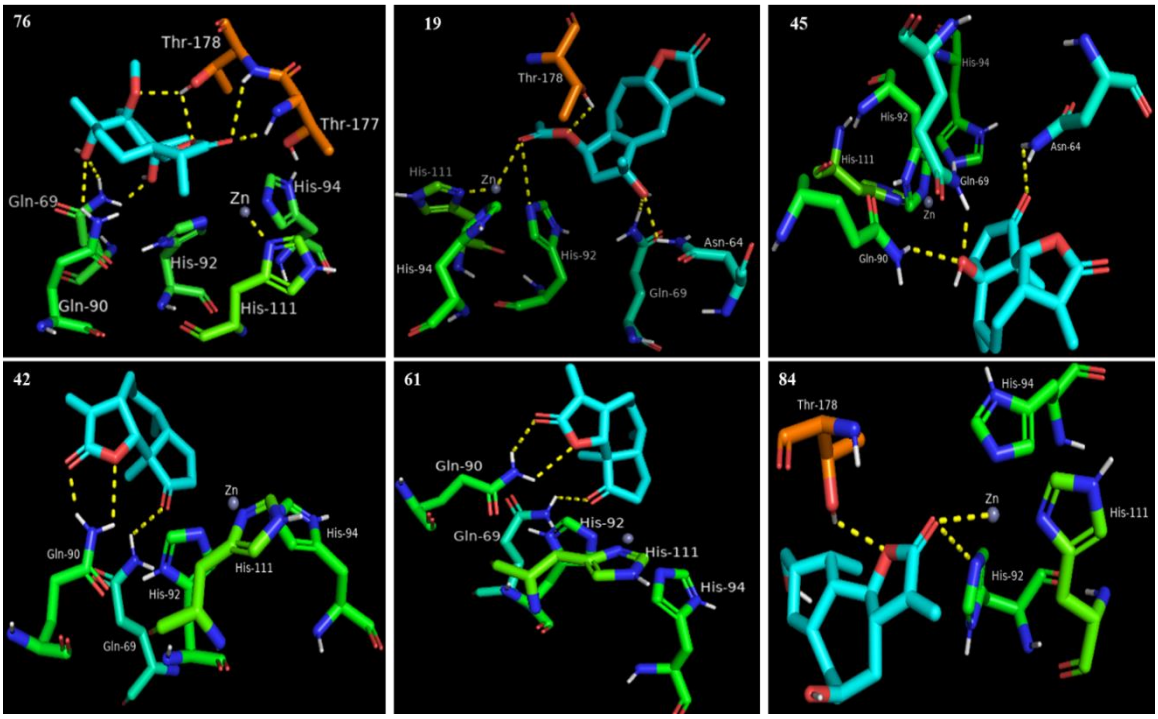

Figure 6.5. Molecular interactions between NgCA and selected analogues. Hydrogen bond contacts (yellow dotted lines) visualized in PyMOL

The amino acid residues that formed hydrogen bonds with most of the compounds studied were Gln-69, Gln-90, Asn-64, Thr-178, and His-92. These residues are catalytically important for NgCA (Huang et al. 1998). Binding of these compounds to the mentioned residues specifically inhibits the proton transfer step in the hydrolysis of CO_2 to HCO_3^-. Different poses of the same molecule interact differently with the target leading to different binding energies. For compound **45**, the docking results show that although pose 1 has the lowest binding score (-6.4 kcal/mol), it attached to the enzyme outside the active site pocket forming only 1 hydrogen bond and an alkyl bond (Figure 6.6). Pose 3 proved to form up to 5 hydrogen bonds, however it also bound outside the pocket. Pose 7 of structure **45** was the best pose which bound to the enzyme inside the pocket, having 3 hydrogen bonds interactions between the ligand and amino acid residues Gln-69, Gln-90 and Asn-64. None

of the poses formed coordination with Zn (II) ion and only pose 3 showed interactions through the lactone ring (Figure 6.6). The high binding energy thus can be attributed to the hydrogen bonds observed based on the selected conformation that aligned best with the model.

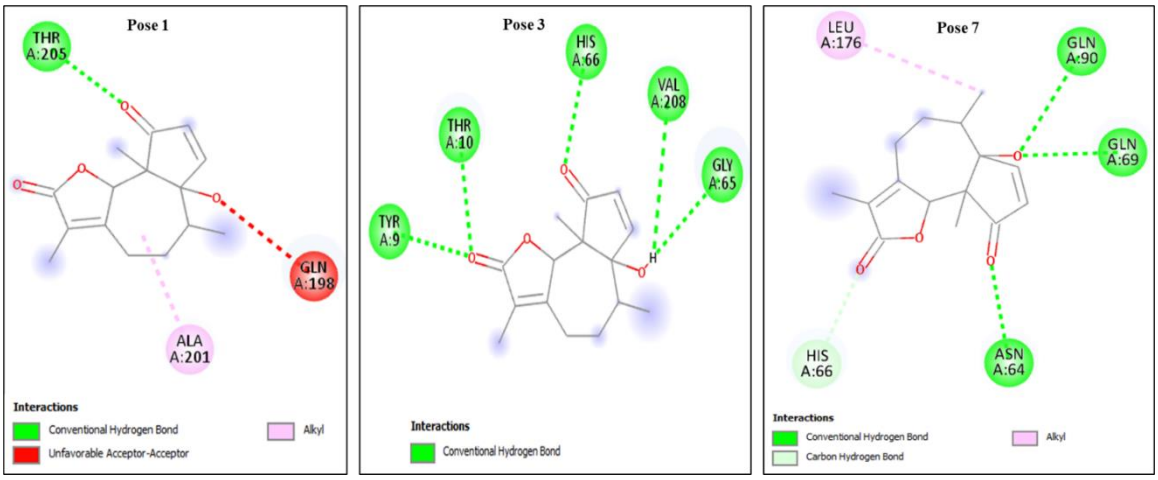

Figure 6.6. Interaction of structure 45 with NgCA depicting the difference in interactions between poses, the type of bonds and the amino acid residues involved. Visualized using Discovery studio

Another factor that was observed in the docking study is the role played by the substituent groups in the binding of SLs to NgCA. The eleven structures (**22**, **40**, **65**, **69**, **70, 71, 72, 73, 74, 76**, **80**) which gave lowest ligand-receptor binding score ≤ -7.0 kcal/mol have epoxides, esters, and peroxides groups in addition to the lactone ring. This supports the study by Fisher (8) who reported that the functional groups mentioned above enhanced the activity of the lactone group. These groups increase the polar interactions that contribute to the stability of the complex. Other analogues' low binding score can thus be linked to unfavourable interactions within the hydrophobic regions.

Nineteen of the analogues (**1, 12, 14, 22, 36, 40, 43, 49, 50, 65, 69, 70, 71, 72, 73, 74, 75, 76, 80**) that were studied have docking score equal to or higher than that of the lead

compound, xerantholide (Table 6.2). Based on the docking scores, these compounds exhibit potential as NgCA inhibitors with better binding than the lead compound. The interactions of five analogues (**1, 2, 25, 34,74**) with NgCA were very similar to that of xerantholide in docking scoring values and the interaction type. They involve the polar interaction of the lactone ring with His-92, Thr-178, His-111 and Zn (II) ion coordination with slightly different H-bond distances (Figure 6.7). The carbonyl oxygen in the lactone ring interacts with Zn (II) ion of the active site and at the same time with His-92 while the oxygen in the lactone ring interacts with Thr-178 thereby enhancing the stability of the ligand-enzyme complex. Other analogues that showed interaction similar to xerantholide but with additional H-bonds are compounds **19, 48, 52, 57, 68, 79** and **84**. All these compounds formed polar bonds involving the lactone ring.

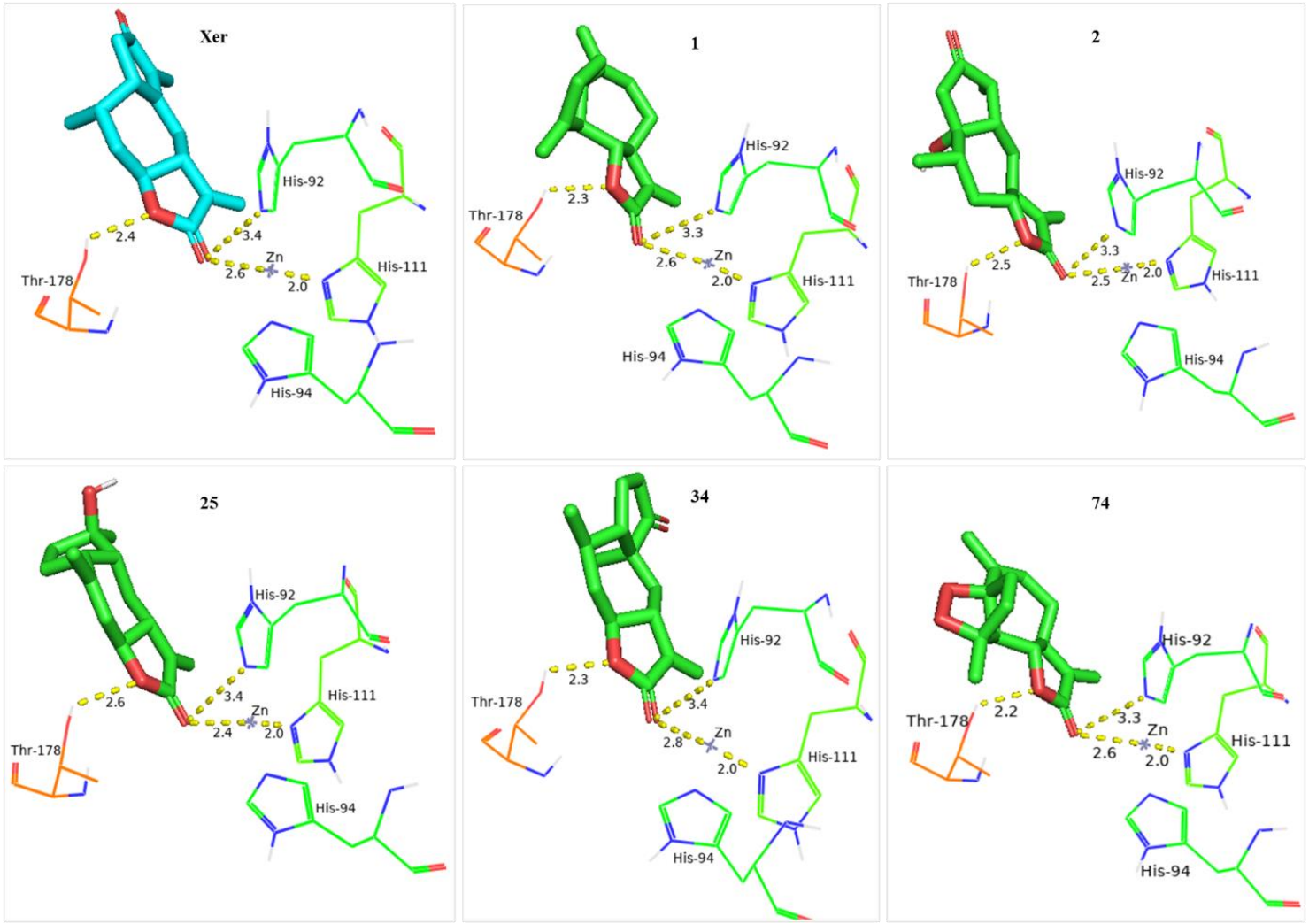

Figure 6.7. Xerantholide and selected analogues binding to NgCA showing similarity in the polar interactions (yellow dotted lines) and the amino acid residues involved and the bond distance. Visualized using PyMOL

Docking analysis of structures **17** and **41** show that although they interact with amino acids in the binding pocket of the enzyme, the interaction is not through the lactone ring, thus giving low binding score. This highlights the importance of this group in binding to the enzyme. Compound **41** coordinates with Zn (II) ion but only through the second keto group which is located away from the lactone ring. No H-bond interactions were observed with structure **41,** while **17** shows two H-bonds and no metal-acceptor bonding (Figure 6.8).

Over half of the compounds studied (47 compounds) were capable of forming interactions with the zinc cation and coordinating through the oxygen atom of the lactone ring. The binding score of AZM to hCA reported by (10) is -6.711 kcal/mol as obtained using Glide docking. This study reports the binding score obtained for the interaction of xerantholide and its analogues with NgCA to be -6.8 to 7.4 kcal/mol. It could be inferred that on the basis of binding, xerantholide and its analogues probably achieved higher or comparable activities to the reference AZM and EZM NgCA inhibitors. The molecular docking analysis of this study shows that xerantholide and several of its analogues formed hydrogen bonding, hydrophobic contacts such as pi-alkyl, alkyl and other nonspecific interactions. The studied molecules also show potential as NgCA inhibitors by binding to the active site with specific interactions involving Zn (II) ion and the imidazole moieties. These results highlight the potential of xerantholide and some of its analogues to have the ability to inhibit the activity of NgCA.

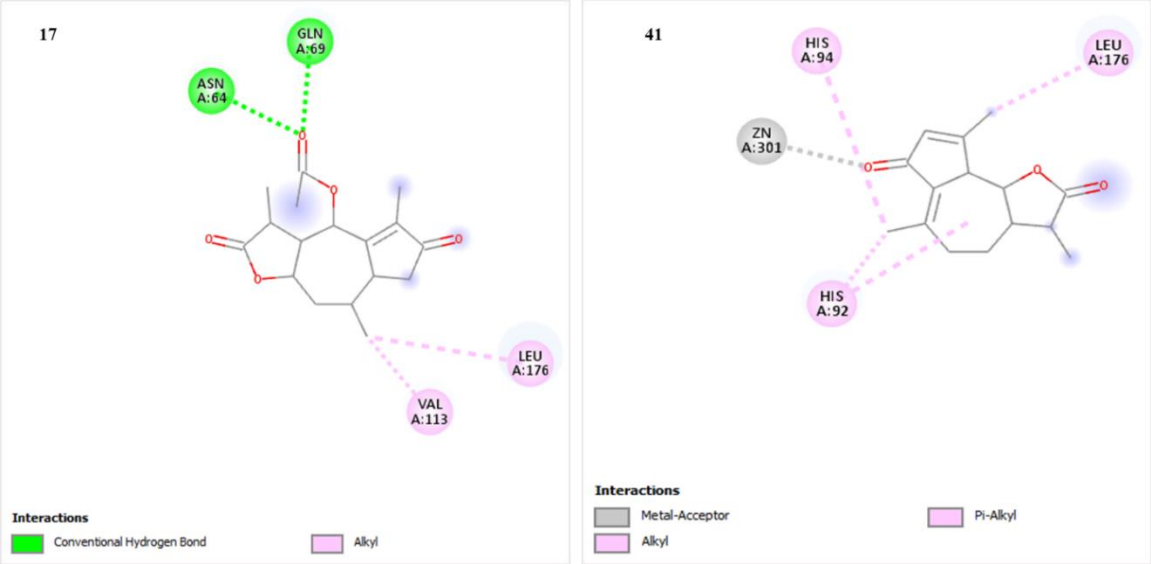

Figure 6.8. Interaction of compound 17 and compound 41 with NgCA. Visualized using Discovery studio

6.3.2 DFT study of the interaction of xerantholide and its analogues with $[ZnIm_3]^{2+}$ model of the active site

Considering that docking has its limitations (such as water molecules are removed before docking, entropic factor is not taken into consideration and MM force fields are used which is not good for calculating electronic properties), a method that takes into consideration some of these factors was used in active site modelling study, namely DFT calculations. The DFT binding free energy (ΔG°) shown in Table 6.2 was calculated using total energy obtained from the computational binding of the analogues with $[ZnIm_3]^{2+}$. Of the 83 molecules that were complexed with $[ZnIm_3]^{2+}$ and submitted for DFT calculations, 77 converged successfully. The interaction energy computed for all ligand-$[ZnIm_3]^{2+}$ complexes ranged from -26.45 to -43.11 kcal/mol with compound **45**-$[ZnIm_3]^{2+}$ complex giving the lowest binding energy of -43.11 kcal/mol, thus showing strong interaction with

the active site of NgCA. About 99% of the structures studied exhibited lower binding energy values and higher affinity for NgCA when compared to the lead structure.

Comparison of docking scores to computed ligand-$[ZnIm_3]^{2+}$ binding free energy, shows an agreement in trend. The observed trend is presented in Figure 6.7 where only compounds with docking score equal to or higher than xerantholide were considered (**1, 12, 22, 36, 43, 49, 50, 65, 69, 70, 71, 72, 73, 74, 75, 76, 80**). The plot shows that compounds with docking score higher than xerantholide also have DFT binding free energy values that are below the value calculated for xerantholide, thus suggesting good binding of these compounds to NgCA.

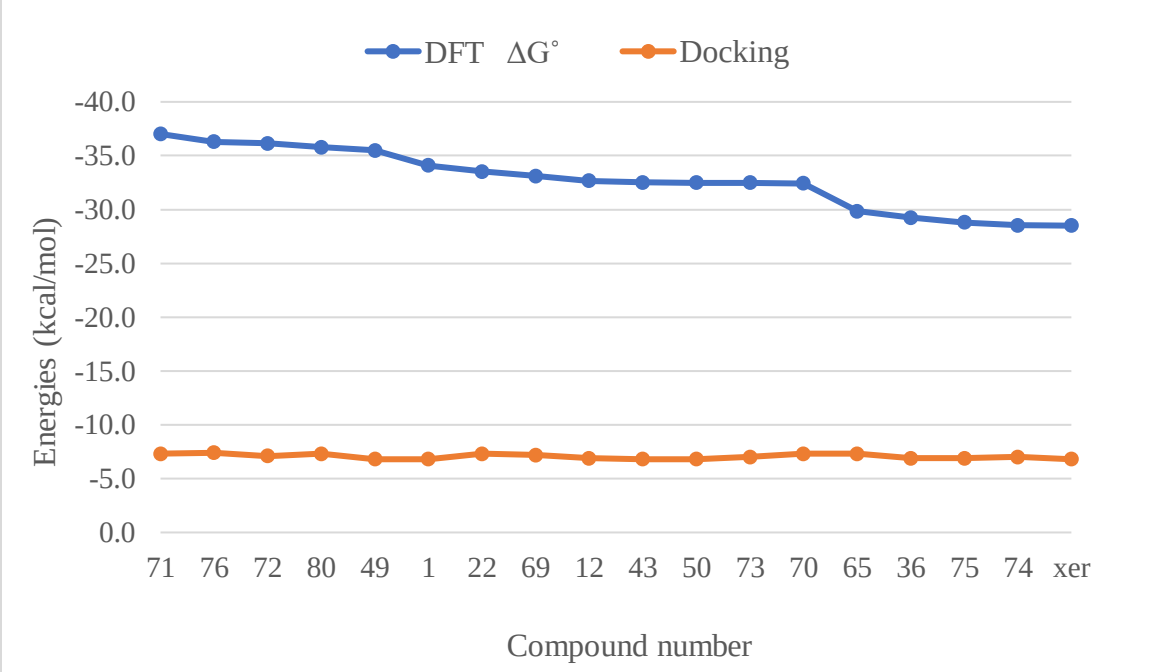

Figure 6.9. Comparison of the binding affinity of xerantholide and its sesquiterpene lactone analogues to NgCA by DFT modelling vs docking

Four of the ligand-$[ZnIm_3]^{2+}$ complexes (**42**, **45**, **61** and **84**) have binding free energy below -40 kcal/mol being lower compared to xerantholide with the binding energy of -28.50 kcal/mol (Table 6.2). However, these compounds gave docking score of -6.3, -6.4, -6.4, -6.0 kcal/mol for **42**, **45**, **61** and **84** respectively, values that are slightly lower than that of xerantholide. The high binding affinity can be attributed to the observed zinc (II) ion coordination in **84** as well as the H-bonds seen in docking analysis for all four. Although Zn (II) ion coordination of **42**, **45**, and **61** was not observed with docking analysis, the DFT model study suggest that this interaction is possible as seen in Figure 6.10. The calculated ΔG° validates their potentials as NgCA inhibitor.

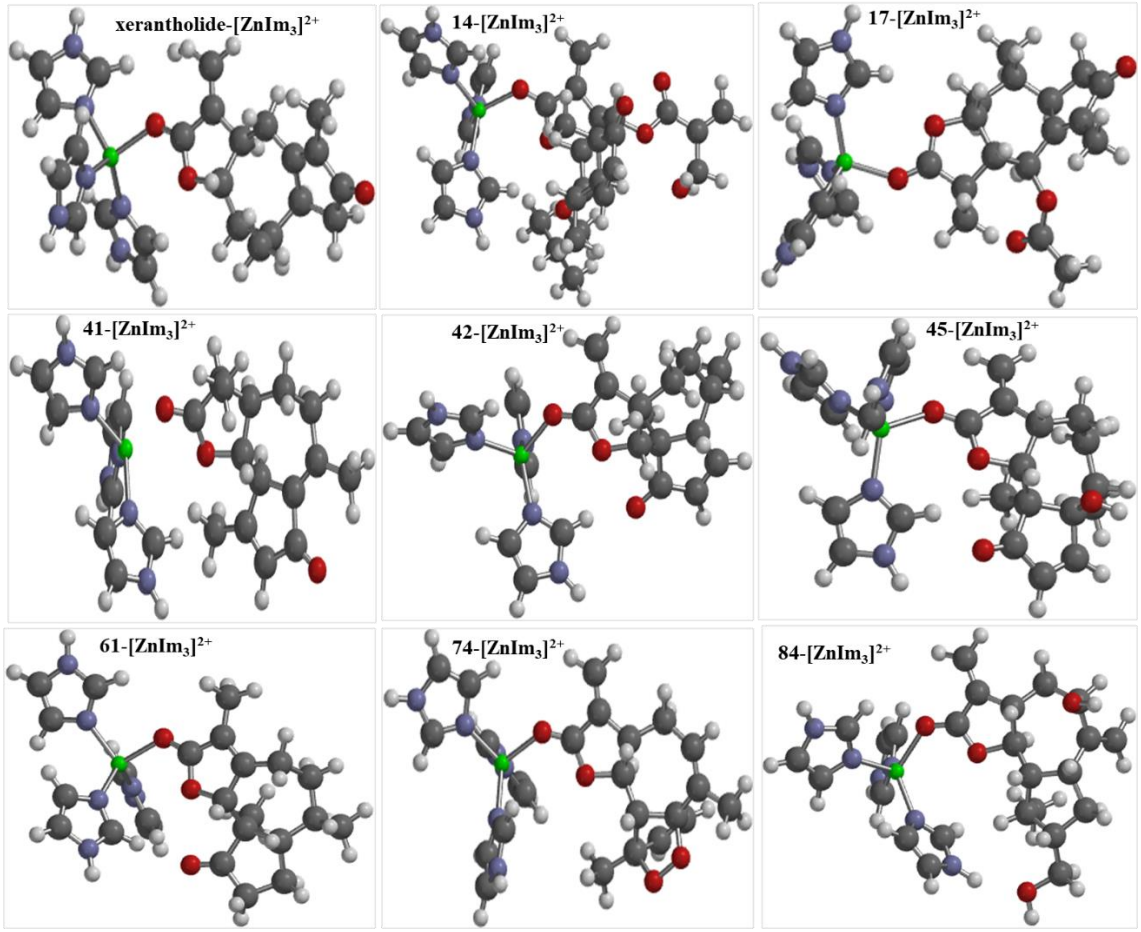

Figure 6.10. Optimized structures of ligands (analogues and lead) complexed with zinc-tris imidazole as calculated using DFT

Like in docking results, DFT calculations also showed that compounds that gave the lowest binding energy, between -37.0 to -43.1 kcal/mol also had esters, peroxides, epoxides and ketone groups as substituents. For example, eight structures (**11, 12, 28, 41, 43, 44, 49,** and **69**) did not form coordination with the Zn (II) ion in the model structure but gave docking scores equal to or higher than that of xerantholide. The high ranking can therefore be linked to the presence of the mentioned functional groups in these structures. This highlights the importance of these functional groups in the SL's potential to bind to NgCA. $[ZnIm_3]^{2+}$ complex with compounds **76** and **14** gave binding free energies of -36.28 and -37.20

kcal/mol respectively, values that support the observed high docking scores for these compounds. Structures **17** and **41** were the only two that gave binding free energy higher than the lead compound with -27.9 and -26.45 kcal/mol respectively. The low binding energy observed for compound **41** is most likely because it did not have zinc (II) ion coordination with the model, which is in agreement with the docking analysis that also showed that the interaction of this compound is not through the lactone ring. Based on the docking and model study, several compounds (**1, 12, 22, 36, 43, 49, 50, 65, 69, 70, 71, 72, 73, 74, 75, 76, 80**) are superior to xerantholide in terms of interaction with NgCA.

6.4 Conclusion

This study established that xerantholide and several of its analogues had the potential to bind NgCA's active site with lower binding energy. Hydrogen bonding, van der Waals, and hydrophobic interactions dominate the ligand-receptor interactions. Over 50% of the SL analogues coordinate to Zn (II) ion of the receptor through the lactone ring that yield stable complexes. The high number of hydrogen bond interactions observed in several ligand-enzyme complexes is indicative of strong inhibitor binding. The results also show that the lactone ring in the sesquiterpene structure is essential in the binding of the ligands with NgCA. Structures having functional groups such as epoxides, peroxides, esters, and ketones showed better binding affinity due to increased polar interactions. The high binding affinity values suggest that these SLs offer a potential inhibitory activity towards NgCA and thus are good candidates for *in-vitro* studies. Docking and modelling study give basis to investigate *in-vitro* the NgCA inhibition potential of compounds **1, 12, 22, 36, 43, 49, 50, 65, 69, 70, 71, 72, 73, 74, 75, 76,** and **80**.

6.5 References

1. Ivanescu B, Miron A, Corciova A. Sesquiterpene lactones from *Artemisia* Genus: Biological activities and methods of analysis. J Anal Methods Chem. 2015;2015.

2. Awouafack MD, Tane P, Kuete V, Eloff JN. Sesquiterpenes from the medicinal plants of Africa. Medicinal plant research in Africa: Pharmacology and Chemistry. Elsevier Inc.; 2013. 33–103

3. Gach K, Janecka A. α-Methylene-γ-lactones as a novel class of anti-leukemic agents. Anti-cancer agents Med Chem. 2014;14(5):688–94.

4. Luo HJ, Wang JZ, Deng WQ, Zou K. DFT calculations and docking study on sesquiterpene lactones: Inhibition of aromatase. Procedia Environ Sci. 2011;8(November):446–50.

5. Alhassan AM, Malami I. *In silico* screening of sesquiterpene lactones as aldose reductase inhibitors. Niger J Basic Appl Sci. 2021;28(2):64–9.

6. Possart K, Herrmann FC, Jose J, Costi MP, Schmidt TJ. Sesquiterpene lactones with dual inhibitory activity against the trypanosoma brucei pteridine reductase 1 and dihydrofolate reductase. Molecules. 2022;27(1):1–14.

7. Chadwick M, Trewin H, Gawthrop F, Wagstaff C. Sesquiterpenoids lactones: Benefits to plants and people. Int J Mol Sci. 2013;14(6):12780–805.

8. Fischer NH, Lu T, Cantrell CL, Castañeda-Acosta J, Quijano L, Franzblau SG. Antimycobacterial evaluation of germacranolides in honour of professor G.H. Neil Towers 75th birthday. Phytochemistry. 1998;49(2):559–64.

9. Agarwal S, Mehrotra R. An overview of molecular simulation. JSM Chem. 2016;4(2):1024.

10. Barua H, Bhagat N, Toraskar (mrs.) M. P. Study of binding interactions of human carbonic anhydrase Xii. Int J Curr Pharm Res. 2016;9(1):118.

11. Berg KA, Clarke WP. Making sense of pharmacology: Inverse agonism and functional selectivity. Int J Neuropsychopharmacol. 2018;21(10):962–77.

12. Supuran CT. Bacterial carbonic anhydrases as drug targets: Toward novel antibiotics? Front Pharmacol. 2011; (July):1–6.

13. Nocentini A, Hewitt CS, Mastrolorenzo MD, Flaherty DP, Supuran CT. Anion inhibition studies of the α-carbonic anhydrases from *Neisseria gonorrhoeae*. J Enzyme Inhib Med Chem. 2021;36(1):1061–6.

14. Cuffaro D, Nuti E, Rossello A. An overview of carbohydrate-based carbonic anhydrase inhibitors. J Enzyme Inhib Med Chem. 2020;35(1):1906–22.

15. Alhashimi M, Mayhoubo A, Seleem MN. Repurposing salicylamide for combating multidrug-resistant *Neisseria gonorrhoeae*. Antimicrob agents Chemother. 2019;63(November):e01225-19.

16. Morris GM, Ruth H, Lindstrom W, Sanner MF, Belew RK, Goodsell DS, et al. Software news and updates AutoDock4 and AutoDockTools4: Automated docking with selective receptor flexibility. J Comput Chem. 2009;30(16):2785–91.

17. Trott O, Olson AJ. Software News and Update-AutoDock Vina: Improving the speed and accuracy of docking with a new scoring function, efficient optimization, and multithreading. J Comput Chem. 2009;31(2):455–61.

18. Schrödinger L, DeLano W. PyMOL Molecular Graphics System. Schrödinger, LLC; 2020. Accessed 8 June 2022, <http://www.pymol.org/pymol>.

19. BIOVIA DS. Discovery Studio Visualizer,. San Diego: Dassault Systèmes; 2019.

CHAPTER 7: QUANTITATIVE STRUCTURE PROPERTY RELATIONSHIP (QSPR) AND PREDICTION OF BIOLOGICAL ACTIVITY OF XERANTHOLIDE AND ITS SESQUITERPENE LACTONE ANALOGUES

Abstract

Xerantholide and some of its sesquiterpene lactone (SL) analogues have been shown to bind *Neisseria gonorrhoeae* carbonic anhydrase (NgCA) with affinity comparable or better than those of standard NgCA inhibitors like acetazolamide (AZM). In this Chapter, using multilinear regression (MLR) analysis, models were developed to find the relationship between the binding affinities computed for the SLs-Zn$[Im_3]^{2+}$ complex (Chapter 6) and molecular descriptors derived for the SLs. The best model consisted of six descriptors and proved to have good predictive ability. The statistical indicators associated with the best model are R (0.789), R^2 (0.623), AdjR^2 (0.578), F (14.02), BIC (241). The generated model showed that the binding affinity of the SLs-Zn$[Im_3]^{2+}$ complex was highly influenced by properties such as minimum electrostatic potential (MinElPot), hydrogen bond donor, HOMO, LUMO, logS and P-Area with MinElpot being the most correlated descriptor. Investigation of the prediction of activity spectra for substances (PASS) indicated that these molecules exhibit good probability of possessing biological activities such as antibacterial, antiparasitic, neoplastic antifungal and anti-inflammatory.

Keywords: Binding affinity, QSPR, model, multiple linear regression, PASS

7.1 Introduction

Models are expressions and simplifications of real life that contain specific assumptions reliable enough to give chemically meaningful results, and they vary widely in their comprehensiveness, quality, and utility (1). The high level of computer technology has allowed an increase in the size and number of systems that can be studied, as well as the degree of accuracy of the models on a reasonable time scale. Accurate results are obtained with more complex models at the cost of added computational expense. Common methods of virtual screening are molecular docking, pharmacophore modelling, quantitative structure-activity/property relationship (QSAR/QSPR), and prediction of activity spectrum for substances (PASS).

QSAR studies describe the relationship between the structural descriptors of a molecule or its physicochemical properties and biological activities by means of statistical tools (2). The traditional QSAR/QSPR approach was developed to relate structure or physicochemical properties of molecules to the biological activity or a chosen response variable (dependant variable). It is one of the most widely used computational methods which helps in the design of drugs and prediction of drug activities. QSAR/QSPR model works on the assumption that the numerical value of a specified biological activity or properties such as the binding affinity or toxicity of a set of molecules depend on the structure of these molecules (3). In medicinal Chemistry, the QSAR/QSPR knowledge is used to modify chemical structures in order to influence a drug's activity. The established relationship between the molecular structure and the biological activity or property (the model) can then be used in the prediction, interpretation and assessment of new compounds

with desired activities/properties while cutting on time and cost involved in compound synthesis and new product development. QSAR/QSPR is perhaps the most accurate and effective method to use when the receptor structure is not known, having the advantage of small amount of calculation and good predictive ability (1).

QSAR/QSPR analysis reveals the importance of the physical and chemical properties of the different functional substituents that lead to biological activity of the extracted compounds. For each chemical compound, a series of chemical parameters known as descriptors are calculated. Physicochemical and topological parameters are usually selected and correlated to biological activities (5). The most common studied physicochemical properties are hydrophobicity, electronic, and steric properties (2–4). Some of the physicochemical properties used in building QSAR/QSPR models are listed and explained in Table 7.1. Various QSAR/QSPR approaches are used depending on the type of target property values, descriptors, variables selection and the optimization algorithms used to relate the descriptors to the target properties in order to generate statistically significant model. After the model(s) generation, validation of models is done to check the accuracy and performance, a process that ascertains that the model is suitable for its intended purpose. Common 2D and 3D methods are based on multiple linear regression (MRL), principal component analysis (PCA), artificial neural networks (ANN) and hypothetical active site lattice (HASL) (6,7). A number of conditions must be satisfied for a classical QSAR/QSPR model to be developed and be applicable. The compounds under study should be chemically similar with same mechanism of action and it should be possible to relate biological activity to the physicochemical properties being considered.

There must be a good selection of descriptors that have an influence on the activity of the compounds. Generally, steps that are followed for QSAR modelling are: compound representation, identification or creation of measured properties, generation of molecular descriptors, development of the model(s), model validation and analysis (8). Statistical parameters such as R, R^2, adjusted R^2, standard error of estimates are usually used to measure how well a model can predict the activity of molecules.

The importance of model validation cannot be overemphasized because classical QSAR/QSPR models depend highly on the number of compounds used in the model as well as the number and type of descriptors selected. Validation methods must include both internal and external validations after a model have been developed in order to make sure the model is accurate and can be used for predictions. Internal validation methods involve using the data that created the model (training set) while external validation uses data that is separate from the one used to generate the model. Common internal validation methods employed include the least squares fit (R^2), adjusted (adjR^2), leave one-out method (LOO, Q^2), leave many-out method (LMO, Q^2), y-randomization method, and hold-out cross validation which evaluate the stability of the model. External validation is done to test the predictive power of a QSAR model where R^2 and the slope of observed vs predicted activity is considered. A model is said to have a good predictive power if R^2 predicted is more than or equal to 0.6 (8).

Table 7.1. Physicochemical properties explained

Properties	**Explanation**
Polarizability (α)	The ability of the molecule to form instantaneous dipoles through electron cloud distortion.
Polar surface area (PSA); hydrophobic surface area	The sum of surfaces of polar atoms (oxygen, nitrogen and attached hydrogen). It provides useful information about specific receptor binding interactions.
Hydrogen donor/acceptor	Hydrogen bond donating/accepting ability.
Energy of highest occupied molecular orbital/Energy of lowest unoccupied molecular orbital (E_{HOMO}-E_{LUMO})	The energy difference between HOMO and LUMO (ΔE_{H-L}) can be used to predict the strength and kinetic stability of transition metal and molecular complexes. HOMO and LUMO also indicate areas having possible electrophilic and nucleophilic interaction in a molecule.
Lipophilicity (logP)	It is related to the partition coefficient (P), a ratio which describes the relative distribution of a molecule in non-polar and aqueous medium. It is an important parameter that gives an indication of a drug's ability to dissolve in non-polar medium.
Hydrophobicity constant (π)	Substituent constant indicating the influence of individual substituents on overall partitioning behavior.
Electronic inductive factor (F)	This is a collective measure of the total electronic effects of a substituent on a phenyl ring. This allows to determine the electronic nature of substituents on a phenyl ring in the drug molecule, either electron withdrawing or electron donating.
Molecular volume (V_m)	This may be calculated using the sum of van der Waals atomic volumes; indicates general size of a molecule.
Dipole moment (DM) (δ)	Is directly related to the charge distribution in a molecule.
Molar refractive (MR)	Represents steric (size and shape) effect.
Heat capacity (C)	The amount of energy required to change a substance's temperature by a given amount.
Entropy (S_e)	The degree of disorder or randomness in the system. It is a measure of the unavailable energy in a closed system.
Electronegativity (χ)	Ability of an atom (or group) to attract shared electrons.
Chemical hardness (η)	Related to the stability of the molecule $\eta = (E_{LUMO} - E_{HOMO})/2$

Reference: (9,10)

PASS (prediction of activity spectra for substances) is a computer program which predicts the biological activity spectrum for a compound based on its structural formula. The tool can predict numerous toxicities including mutagenicity, carcinogenicity, teratogenicity and

embryotoxicity and probability of thousands of biological activities of a compound (11). It has an average prediction accuracy of 95%. The principle of PASS is that the biological activity of a compound equates to its structure therefore similar structures display similar activity. PASS is an analysis of the structure-activity relationship in comparison to training set, containing information on the structure and biological activity of more than 300000 organic compounds. It predicts the probability of a biological activity for a new compound, by estimating the similarity and differences of the new compound to already known compounds (with well-known biological activities present in the training set of 300000 compounds). The higher the Pa (active) with low Pi (inactive), the better the chance of experimentally finding a given activity. If only compounds with Pa>90% are selected, the probability of false positive prediction is insignificant but one risk missing about 90% of actually active compounds. On the other hand, the lower the Pa value, the higher the probability of false positives predictions. It is not a good idea to limit the selection of compounds to those with higher Pa value especially in the case of new compounds, because compounds with higher Pa may prove to be analogues of known pharmacological agents. For example, if *P*a > 0.7, It is very likely to find experimental activity and but the chance that such a compound is an analogue of a known pharmaceutical agent is also high. If 0.5 < Pa < 0.7, the chances for detecting experimental activity will be lower but the compounds will be less similar to known pharmaceutical agents (11-13).

For $Pi < Pa < 0.5$, the chances of detecting experimental activity will be even lower but if the prediction is confirmed, the compound found might be a new compound (12,13). The prediction can help to determine which biological activities should be initially tested

experimentally and which compounds have the highest probability for displaying the required types of activity. Although these predictions are helpful, they do have limitations and so it would be incorrect to draw conclusions that a compound has biological activity based only on computer predictions. The computer prediction results have to be confirmed either by direct experimental testing *in-vitro* or *in-vivo* or by referring to published literature data.

This study aimed at analysing the relationship between selected physicochemical properties of xerantholide SLs analogues and the binding affinity of these molecules to NgCA, by performing QSPR studies through which models can be generated for the prediction of binding affinities of similar compounds.

7.2 Material and methods

7.2.1 QSPR (descriptors)

Optimization and vibration frequency calculations of xerantholide and its analogues were done as described in section 5.2.1. Of the 83 compounds used in this study, some were eliminated if one descriptor value was not available for the structure or the mode of binding to the model did not involve the lactone ring based on the study reported in chapter 6. The modelling set thus comprised of 73 compounds. Therefore, physicochemical parameters of 73 compounds were computed for classical QSPR study (Hansch analysis) using structures fully optimized at the B3LYP/6-311++G(d,p) level. Initially, a total of 26 molecular descriptors covering a wide range of properties were computed. These properties were related to molecular interactions and represented by constitutional, thermodynamic,

electronic, spatial and topological parameters. Some of the descriptors (logP, logarithm of the aqueous solubility (logS), XLOGP3) were obtained using ALOGPS 2.1 and E-DRAGON 1.0 software, while other descriptors (dipole moment, polarizability, heat capacity, entropy, molar mass, E_{HOMO}, E_{LUMO}, polar surface area (PSA), hydrogen bond donor (HBD) and hydrogen bond acceptor (HBA), Area, volume, ovality, minimum electrostatic potential (MinElPot), maximum electrostatic potential (MaxElPot), polar area (75), Acc. Polar area (75), Acc. Area, inductive effect (F) and resonance effect (R)) were computed using Spartan '14 programme (14). Calculated standard Gibbs free energy (ΔG°) of the reactions for the formation of the SLs-NgCA complexes were converted to the binding constant K_a. Logarithm of the dissociation constant ($K_d = 1/K_a$; log K_d) was the physicochemical property that was used as the dependent variable, whereas parameters describing structural and physicochemical properties were used as the independent variables. The equation below was used to calculate K_a from which logK_d was computed as shown above:

$$\Delta G^{\circ} = -RT\ln K_a \qquad \text{(eqn. 7.1)}$$

where ΔG° is the Gibbs free energy of binding, also known as standard free energy change of interaction, R is the universal gas constant (8.314 J. $K^{-1}mol^{-1}$) or (1.987 cal $mol^{-1}K^{-1}$), T is the absolute temperature in kelvin, and lnK is the natural log of the equilibrium constant K_a.

Equation 7.1 was rearranged to calculate binding constant K_a as follows:

$$\ln K_a = -\frac{\Delta G^{\circ}}{RT}; \qquad K_a = e^{-\frac{\Delta G^{\circ}}{RT}} \qquad \text{(eqn. 7.2)}$$

7.2.2 Model generation

Before model development, the data was cleaned. First, intercorrelation between descriptors was checked whereby decision was made that a model will not include any pair of descriptors with correlation coefficient greater than 0.7. Next, variance inflation factor (VIF) was also used to identify multi-collinearity among the independent variables. A model with descriptors having VIF greater than 10 was not considered. VIF for the regression coefficient was calculated as: VIF = $1/(1-Rx)$, where Rx is the coefficient obtained when descriptor x is correlated with the other descriptors. Consequently, the total number of descriptors that were determined to significantly contribute to the prediction of $\log K_d$ was 12 (logS, XlogP3, HOMO, LUMO, HBD, Min ElPot, P-Area, Acc. P-Area, PSA, Volume, Acc. Area and H-L gap). Relationship between binding affinity of the compounds and the selected descriptors were modelled using multiple linear regression (MLR) analysis initially applying the step wise, forward and backward feature selection in SPSS program (version 27) to screen possible descriptors combinations.

To construct the QSPR models, the dataset of 73 compounds was divided into training set and test set at a ratio of 4:1 applying the random selection method using SPSS version 27. The training set was used to develop the QSPR models, while the test set was used to validate the developed models. The backward selection method was used to build the models in which a model is constructed starting with all candidate variables and stepwise removing the least significant variables (variables with largest p-value) one after the other until no further variables can be deleted without a statistically significant loss of fit. This

allows the level of significance of each descriptor to be determined. To get the best regression model, all possible combination of descriptors were considered. The model selection and justification were initially based on correlation coefficient (R^2), adjusted R^2 as well as the significance level (F-value and p-value). Only models with R^2 value greater than 0.6 and consisting of predictor variables with $p < 0.05$ were selected to ensure statistical reliability. The QSPR model was developed in the following form:

$$Y = b_1x_1 + b_2x_2 + b_3x_3 \ldots + b_0 \qquad \text{(eqn. 7.3)}$$

Where Y is the calculated (also referred to in this chapter as observed) $\log K_d$ (dependent variable), b_1, b_2... are the regression coefficients, x_1, x_2... are independent variable (descriptors) and b0 is the regression constant.

7.2.3 Model validation

The models were validated using internal and external validation methods. Statistical calculations using SPSS, MS Excel and R programmes were performed to assess the goodness of the fits and significance of the developed models. To assess the models' goodness of fit, the correlation coefficient (R), squared correlation coefficient (R^2), adjusted squared correlation coefficient ($AdjR^2$), Fischer's value (F-test) and standard error of estimates (s) were calculated as well as the p-value. For p-values ≤ 0.05, the parameter is significant. The R^2 values obtained from the regression analysis provide information on how well the physicochemical parameters present in the equations explain the variation in binding affinity of the ligand to the target. Cross validation using the out of sample validation was done to check how predicted $\log K_d$ values compare with observed $\log K_d$ (calculated $\log K_d$) values using training set. Observed logKd was obtained using equation

7.2 while predicted logKd was obtained using equation 7.3 for training set compounds, then compare the predicted and observed data.

The standard error of estimate for the test set was also compared to the standard error estimate for the training set. The closer the values are to each other, the better the model. Residuals were also calculated and the models that gave higher residuals were eliminated. Furthermore, the difference between R^2 and adjusted R^2 was checked to avoid overfitting which is a fictitious or misleading improvement in the prediction of the dependent variable as more independent variables are included. When the difference between R^2 and adjusted R^2 is less than 0.3, it is an indication that the number of descriptors involved in the model is acceptable (8). External validation using test set compounds followed to assess the generalization of the selected models. The final performance was assessed in the computing and programming environment R using the k-fold method to compare the different models and arrange them using the Bayesian information criterion (BIC) and Akaike information criterion (AIC). Table 7.2 lists the threshold of statistical parameters that can be used for a stable, reliable, predictable QSAR model (8). The developed models were used to predict $logK_d$ of the compounds that were not part of the training set to obtain validation correlation coefficient q^2. MS Excel 365 version 2201 was used to draw scatter plots.

Table 7.2. Minimum recommended value for significant QSAR/QSPR model

Name and symbol	Value
Coefficient of determination R^2	≥0.6
Coefficient of determination for external test set R^2	≥0.6
Confidence interval at 95% confidence level P (95%)	<0.05
Cross validation coefficient R^2 (Q^2)	≥0.5
Validation coefficient R2 test (q^2)	≥0.5
Difference between R^2 and Q^2	≤0.3
Minimum number of external test set (compounds)	≥5
Difference between R^2 and adjR^2	<0.3

7.2.4 Biological activity spectrum estimation

The computer program PASS was used to estimate *in silico* the most probable selected pharmacological effects that could be expected for each analogue and lead structure. This program can predict over 4000 types of biological activity with the mean prediction accuracy of 95% (12). PASS results are given as a list of biological activity with probabilities to be active (Pa) and to be inactive (Pi) calculated for each activity. The list is arranged in descending order of Pa-Pi; therefore, more probable activities are at the top of the list. Only activities with Pa>Pi are considered as probable for a particular compound. The method is based on prediction of activity based on chemical structure and this represents a theoretical estimation of general potential of the compound (13). The 2D structures of xerantholide and its analogues were drawn using ChemBioDraw Ultra 12.0 and saved as a MOL file, submitted to the PASS online program. Probable activities were selected at the cut-off value of Pa>0.5. All the compounds were analysed for antibacterial and antiparasitic effects.

7.3 Results and discussion

7.3.1 QSPR (Dataset structure)

The QSPR analysis was done using computed binding constant, K_a for the binding of xerantholide and its analogues to NgCA active site model, zinc-tris imidazole ($[ZnIm_3]^{2+}$). This analysis aimed to describe the binding ability of xerantholide and its analogues by relating the interaction energy that was based on Gibbs free energy to a set of molecular descriptors that explain important properties related to chemical structure of drug molecules. The Gibbs free energy was converted to $\log K_d$ as described in section 7.2.1.1. The data set used for QSPR analysis is presented in Table 7.3 where the test compounds are marked with letter "a". The structures of molecules on which the modelling was done are given in Table 7.8. The initial dataset was randomly divided into 58 training set and 15 test set compounds. QSPR Models were generated using the training set by MLR method and models were validated using the test set data.

Table 7.3. Values of descriptors for 73 molecules based on DFT calculations and ALOGPS 2.1

Compd #	MOL_ID	$logK_d$	logS	XlogP3	HOMO (au)	LUMO (au)	H-L gap (Δϵ)	HBD	Vol (Å3)	PSA (Å2)	Acc Area (Å2)	Min ElPot (kJ/mol)	P-Area(75) (Å2)	Acc. P-Area(75)
1	a1_c2	-24.866	-3.06	2.57	-0.249	-0.062	-0.187	0	251.23	21.751	167.93	-207.77	46.51	32.94
2	a2_c2	-23.679	-1.73	1.37	-0.260	-0.061	-0.199	1	269.22	54.922	168.12	-200.75	102.6	69.45
3	a3_c1	-23.339	-1.66	1.46	-0.258	-0.076	-0.182	1	268.81	54.938	168.98	-191.79	127.7	80.57
5	a5_c1[a]	-22.241	-1.34	0.89	-0.254	-0.039	-0.215	1	254.99	55.029	158.98	-197.79	126.8	83.40
6	a6_c2[a]	-24.615	-2.81	3.3	-0.247	-0.06	-0.187	0	300.01	41.442	191.32	-204.89	68.94	50.47
7	a7_c1	-25.598	-2.25	2.92	-0.245	-0.059	-0.186	1	258.12	39.754	171.40	-209.91	66.09	45.49
8	a8_c2	-23.337	-2.61	1.36	-0.266	-0.063	-0.203	1	324.49	58.475	195.39	-197.43	108.4	74.70
9	a9_c6	-24.661	-2.48	2.34	-0.269	-0.064	-0.205	1	333.58	70.997	201.31	-197.59	124.9	88.58
10	a10_c1	-24.767	-1.83	1.88	-0.263	-0.06	-0.203	1	307.30	59.285	188.48	-205.77	91.64	67.13
11	a11_c1	-26.721	-1.91	1.89	-0.26	-0.058	-0.202	1	307.52	59.202	191.06	-211.13	99.62	71.86
12	a12_c2	-23.965	-2.93	2.93	-0.277	-0.061	-0.216	0	307.84	42.482	193.85	-204.64	79.35	61.03
13	a13_c3	-23.697	-2.93	2.93	-0.245	-0.063	-0.182	0	304.00	42.503	195.71	-205.18	77.54	57.96
14	a14_c26	-27.284	-2.75	2.55	-0.258	-0.074	-0.184	1	428.03	80.148	250.57	-203.15	113.2	72.83
15	a15_c58	-24.019	-2.98	2.91	-0.258	-0.075	-0.183	1	446.06	71.582	249.95	-190.48	131.6	77.46
16	a16_c6	-25.707	-2.38	1.96	-0.261	-0.061	-0.2	1	323.52	60.386	212.55	-212.48	106.2	75.58
17	a17_c1[a]	-20.470	-1.90	1.96	-0.259	-0.067	-0.192	0	310.85	55.713	192.15	-189.87	133.4	85.59
18	a18_c1	-24.613	-2.53	2.3	-0.26	-0.022	-0.238	1	267.21	40.990	165.47	-208.06	64.04	44.78
19	a19_c5	-23.743	-2.01	1.71	-0.264	-0.065	-0.199	1	312.13	62.149	199.49	-203.12	108.7	76.47
20	a20_c2	-24.681	-2.01	1.71	-0.261	-0.029	-0.232	1	315.50	62.013	193.00	-202.33	101.2	73.75
21	a21_c1	-25.097	-1.98	1.92	-0.275	-0.061	-0.214	1	314.75	60.169	191.73	-208.95	107.5	72.50
22	a22_c1[a]	-24.591	-2.52	2.3	-0.279	-0.064	-0.215	0	355.92	60.765	219.76	-202.91	127.2	88.63
23	a23_c1[a]	-23.703	-2.28	1.91	-0.28	-0.064	-0.216	0	338.74	61.795	209.43	-199.36	143.5	96.10
24	a24_c3	-25.820	-2.53	2.3	-0.246	-0.06	-0.186	1	262.51	42.006	169.74	-207.27	65.81	46.97
25	a25_c2	-25.708	-2.53	2.3	-0.252	-0.062	-0.19	1	263.20	41.207	171.82	-206.57	76.52	49.51
26	a26_c13	-24.775	-2.53	2.3	-0.26	-0.026	-0.234	1	267.01	40.930	164.32	-207.97	83.32	52.84
27	a27_c3	-26.045	-2.92	2.99	-0.25	-0.034	-0.216	0	274.28	36.478	182.04	-206.70	94.17	67.99

Compd #	MOL_ID	$logK_d$	logS	XlogP3	HOMO (au)	LUMO (au)	H-L gap (Δε)	HBD	Vol (Å3)	PSA (Å2)	Acc Area (Å2)	Min ElPot (kJ/mol)	P-Area(75) (Å2)	Acc. P-Area(75)
28	a28_c2	-26.120	-1.34	1.54	-0.271	-0.086	-0.185	1	264.35	50.514	167.19	-211.34	124.1	81.18
29	a29_c1	-24.516	-2.33	2.88	-0.262	-0.077	-0.185	0	342.00	55.193	204.78	-205.15	110.1	70.95
30	a30_c1	-25.321	-2.61	3.24	-0.261	-0.076	-0.185	0	359.95	54.925	218.63	-208.04	104.5	66.85
31	a31_c1	-24.443	-2.33	2.88	-0.262	-0.077	-0.185	0	346.05	56.302	199.54	-203.98	109.3	69.46
32	a32_c1 [a]	-22.131	-2.02	2.44	-0.263	-0.077	-0.186	0	240.01	36.875	160.80	-197.52	92.46	66.57
34	a34_c1 [a]	-22.860	-2.43	2.51	-0.26	-0.074	-0.054	0	257.31	36.979	166.22	-201.19	107.1	71.24
35	a35_c1	-21.279	-2.39	2.55	-0.255	-0.071	-0.184	0	258.60	37.181	168.66	-193.53	126.8	80.24
36	a36_c1	-21.451	-2.39	2.55	-0.255	-0.072	-0.183	0	257.94	36.792	170.74	-195.24	110.9	73.93
37	a37_c1	-24.799	-4.17	3.9	-0.248	-0.063	-0.185	0	252.20	22.164	170.04	-208.41	48.43	36.31
38	a38_c1	-22.709	-2.05	2.12	-0.262	-0.074	-0.188	0	240.09	37.026	161.82	-200.05	117.1	78.01
39	a39_c1 [a]	-25.261	-4.17	3.9	-0.239	-0.059	-0.18	0	255.12	22.262	167.09	-211.16	38.39	29.09
41	a41_c1	-19.397	-2.30	2.74	-0.248	-0.072	-0.176	0	257.64	33.907	174.81	-197.41	97.37	63.98
42	a42_c1	-30.566	-2.36	2.7	-0.252	-0.067	-0.185	0	257.12	36.765	158.51	-236.00	107.7	72.37
45	a45_c2 [a]	-31.621	-1.41	1.45	-0.259	-0.08	-0.179	1	264.01	52.878	159.11	-225.10	90.87	63.62
46	a46_c4	-25.644	-0.97	0.36	-0.254	-0.08	-0.174	2	268.11	69.785	181.84	-183.06	120.0	85.68
48	a48_c9	-25.311	-0.97	1.58	-0.266	-0.061	-0.205	2	266.94	60.461	170.06	-203.86	78.68	56.31
50	a50_c4	-23.820	-1.39	0.73	-0.258	-0.024	-0.234	2	322.90	80.617	196.19	-199.73	117.1	80.77
51	a51_c27	-24.866	-1.58	0.78	-0.256	-0.025	-0.231	2	331.99	93.096	201.44	-192.79	113.7	78.06
52	a52_c24	-29.239	-1.60	1.12	-0.258	-0.067	-0.191	2	279.51	71.987	172.69	-197.78	108.8	67.70
53	a53_c21 [a]	-27.780	-1.59	0.53	-0.26	-0.025	-0.235	2	331.73	91.714	197.46	-191.55	130.7	84.64
54	a54_c2	-24.996	-1.42	0.48	-0.263	-0.025	-0.238	2	322.55	78.574	191.52	-184.39	116.3	77.01
55	a55_c7	-27.095	-1.38	1.51	-0.257	-0.032	-0.225	2	272.96	53.895	164.40	-203.39	89.12	56.71
57	a57_c5	-26.752	-2.48	2.53	-0.257	-0.065	-0.192	1	267.97	53.750	173.07	-202.72	86.52	58.32
58	a58_c2	-22.356	-1.91	1.89	-0.245	-0.025	-0.114	1	315.61	56.532	195.69	-199.54	98.68	61.85
59	a59_c1	-26.512	-2.41	2.48	-0.239	-0.056	-0.183	1	262.70	38.244	168.06	-211.23	52.66	36.07
60	a60_c2	-26.289	-2.41	2.48	-0.235	-0.021	-0.214	1	266.79	38.325	167.07	-212.44	53.10	35.65
61	a61_c1	-31.216	-2.36	2.7	-0.251	-0.051	-0.2	0	261.66	36.625	165.27	-235.34	101.6	65.88

Compd #	MOL_ID	$logK_d$	logS	XlogP3	HOMO (au)	LUMO (au)	H-L gap (Δε)	HBD	Vol (Å3)	PSA (Å2)	Acc Area (Å2)	Min ElPot (kJ/mol)	P-Area(75) (Å2)	Acc. P-Area(75)
63	a63_c1	-26.879	-1.47	1.72	-0.25	-0.109	-0.141	0	264.62	50.309	165.06	-200.59	153.1	94.84
65	a65_c14	-21.897	-1.69	0.51	-0.259	-0.073	-0.186	1	327.45	89.246	199.29	-181.61	136.6	99.77
66	a66_c1	-26.253	-1.29	-0.49	-0.271	-0.072	-0.199	1	325.74	87.447	193.02	-194.55	157.99	103.26
67	a67_c2 [a]	-23.402	-1.29	-0.49	-0.272	-0.028	-0.244	1	329.91	87.637	192.37	-195.08	156.68	98.24
68	a68_c30	-26.935	-2.82	2.16	-0.259	-0.061	-0.198	1	347.58	58.334	210.62	-197.62	71.64	47.99
70	a70_c2 [a]	-23.780	-2.06	1.65	-0.248	-0.063	-0.185	0	305.93	52.236	199.21	-198.76	96.96	67.81
71	a71_c2	-27.147	-1.95	1.71	-0.231	-0.067	-0.164	1	307.39	58.982	201.55	-184.36	97.08	70.36
72	a72_c3	-26.508	-2.18	1.46	-0.237	-0.044	-0.193	1	311.46	58.946	198.96	-184.16	93.66	66.11
73	a73_c1 [a]	-23.819	-2.38	2.52	-0.246	-0.065	-0.181	1	268.00	51.285	178.22	-200.72	75.93	52.89
74	a74_c1	-20.933	-2.55	2.28	-0.244	-0.068	-0.176	0	259.11	41.939	172.19	-189.39	88.48	62.99
75	a75_c1	-21.120	-2.55	2.28	-0.243	-0.038	-0.205	0	262.96	41.796	169.66	-191.77	92.33	63.23
76	a76_c4 [a]	-26.612	-2.50	0.55	-0.265	-0.027	-0.238	2	301.18	61.619	174.43	-201.17	69.57	45.91
77	a77_c3	-24.118	-2.10	2.22	-0.253	-0.028	-0.225	1	290.15	45.773	179.23	-204.51	58.99	38.65
78	a78_c2	-21.048	-1.29	1.68	-0.253	-0.076	-0.177	1	264.97	52.161	174.08	-190.33	85.61	61.32
79	a79_c4	-22.126	-1.34	1.41	-0.25	-0.023	-0.227	2	269.20	53.715	166.55	-182.22	56.92	39.69
80	a80_c2	-26.257	-2.07	0.51	-0.268	-0.024	-0.244	0	293.05	47.221	179.81	-229.33	102.00	64.84
81	a81_c1	-21.391	-1.71	0.57	-0.263	-0.031	-0.232	1	294.85	57.560	174.53	-188.81	101.01	66.48
83	a83_c9 [a]	-24.399	-1.47	1.58	-0.265	-0.029	-0.236	2	270.75	60.348	167.06	-204.27	71.82	51.54
84	a84_c34	-29.625	-2.31	1.77	-0.272	-0.069	-0.203	2	288.33	60.181	176.35	-190.80	105.31	69.24
lead	xer_c1	-20.903	-2.39	2.55	-0.256	-0.07	-0.186	0	258.07	37.060	171.23	-192.09	117.83	77.37

[a] = test set compounds; compd # = compound numbering corresponding to structures shown in Chapter 6, Figure 6.2

7.3.2 QSPR model and quality

Eighteen QSPR models were developed, of which four were selected to be good based on BIC, AIC, and other statistical parameters. The resulting 18 models are shown in Table 7.4 with their statistics. The best four models are all good models in predicting the dissociation constant of the studied compounds. The internal and external validation parameters of these models conformed to the minimum standard for a stable, reliable, predictable QSAR model as described by (8), see Table 7.3. Five of the 12 selected descriptors were common in all the models that were developed, and they are a combination of thermodynamic (logS), constitutional (HBD), and electronic (MinElPot, E_{HOMO}, E_{LUMO}) properties of molecules. These are important properties in the study of compounds' biochemical compounds. Their presence in all developed models emphasized their importance in the interaction of xerantholide and its SL analogues to NgCA.

Prediction of aqueous solubility (LogS) of a molecule is important in order to evaluate the likelihood of a drug's bioavailability, an important factor in ADMET (absorption, distribution, metabolism, elimination, and toxicity). Table 7.3 shows that the predicted logS values of all except two compounds (**37** and **39**) fall within the range of water-soluble compounds which is 0 to -4 (15). MinElPot gives an indication of how a molecule interacts with approaching protons or positive centres and can be used to understand the relative polarity of a molecule. High positive potential energy occurs when repulsive interaction occurs due to regions in the molecule having low electron density which repels the proton (blue). Negative potential energy occurs as a result of a proton approaching a negative region giving attractive interaction (red). The analogues have MinElPot values ranging

between -181 to -235 kJ/mol (Table 7.3). E_{HOMO} and E_{LUMO} for molecules gives useful information on the stability of the molecule. High HOMO energy gives an indication that the molecule is a soft nucleophile and low HOMO energy is a hard nucleophile while high LUMO energy is observed for hard electrophiles and low LUMO energy for soft electrophiles. HOMO and LUMO energies of selected molecules are presented in Figure 7.1. HBD play an important role in influencing the H-bonding interaction of the molecule at the active site.

In all these equations it is observed that the logarithmic value of dissociation constant, $logK_d$ of the studied molecules depend theoretically on positive logS, energy value of LUMO and MinElPot, while it depends negatively on energy value of HOMO and hydrogen bond donor as indicated by their coefficients. This means compounds with high values of logS, E_{LUMO} and MinElPot will increase the value of $logK_d$, thus K_d increases and that lead to high dissociation. The model predicts that compounds with high values of these descriptors (logS, LUMO and MinElPot) reduce the stability of SL-NgCA complex. On the other hand, all the models suggest that increase in E_{HOMO} and HBD will result in the decrease in the value of $logK_d$ implying strong binding which increases the complex stability. Of the 4 selected best models, only model 18 had an additional descriptor that has a positive coefficient (XlogP3) which also suggest compounds with high XlogP3 values can destabilize the complex. The other 3 models, though having one descriptor that is not common, the coefficient for the additional descriptor is negative for all (Eqn 7.4-7.7 and Table 7.4).

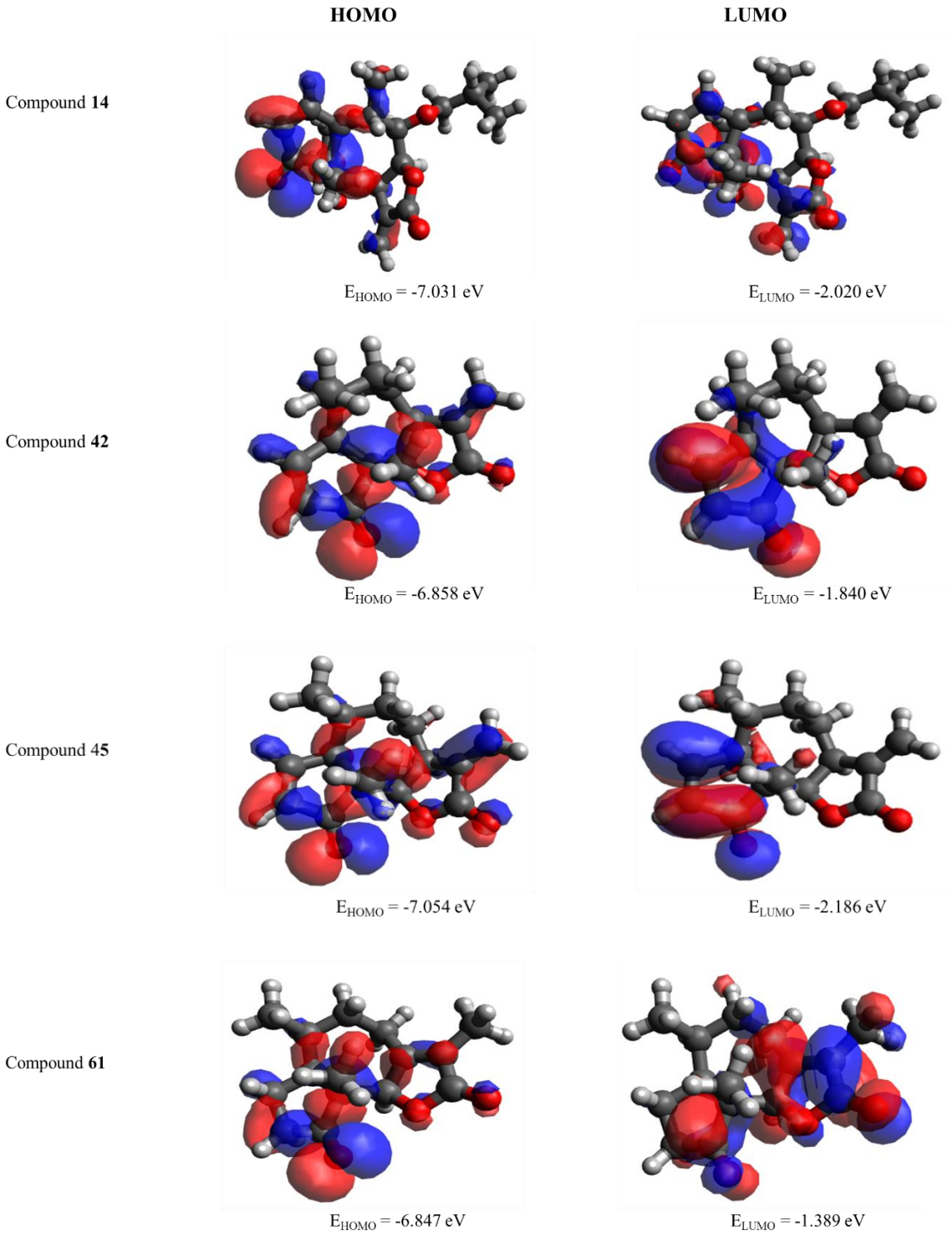

Figure 7.1. HOMO-LUMO diagram of selected SLs analogues of xerantholide

The selected best four QSPR models built using MLR method is represented by the equations below:

Model 1

$\log K_d$ = 4.304 + 1.363*logS – 68.198*HOMO + 31.599*LUMO – 3.033*HBD + 0.180*MinElP – 0.032*P-Area (eqn. 7.4)

n_{train} = 58 R = 0.789 R^2 = 0.623 AdjR^2 = 0.578

Model 2

$\log K_d$ = 4.825 + 1.337*logS – 68.030*HOMO + 32.683*LUMO – 3.022*HBD + 0.182*MinElP – 0.048*Acc-P-Area (eqn. 7.5)

n_{train} = 58 R = 0.786 R^2 = 0.618 AdjR^2 = 0.573

Model 6

$\log K_d$ = 4.296 + 0.908*logS – 59.613*HOMO + 39.678*LUMO – 2.196*HBD – 0.044*PSA + 0.179*MinElP (eqn. 7.6)

n_{train} = 58 R = 0.780 R^2 = 0.609 AdjR^2 = 0.562

Model 18

$\log K_d$ = 3.707 + 1.677*logS – 55.350*HOMO + 50.389*LUMO – 2.583*HBD + 0.179*MinElP + 1.025*XlogP3 (eqn. 7.7)

n_{train} = 58 R = 0.781 R^2 = 0.610 AdjR^2 = 0.564

Table 7.4. Models developed

#	Hansch equation of the model	R	R^2	AdjR^2	F	R^2 test
1	$logK_d$ = 4.304±6.591 + 1.363±0.510logS – 68.198±25.292HOMO + 31.599±12.317LUMO – 3.033±0.460HBD + 0.180±0.021MinElP – 0.032±0.012P-Area	0.789	0.623	0.578	14.02	0.697
2	$logK_d$ = 4.825±6.633 + 1.337±0.514logS – 68.030±25.655HOMO + 32.683±12.311LUMO – 3.022±0.463HBD + 0.182±0.022MinElP – 0.048±0.019Acc-P-Area	0.786	0.618	0.573	13.76	0.704
3	$logK_d$ = 2.653±6.624 + 1.347±0.505logS – 96.856±32.015HOMO + 49.457±17.415LUMO – 3.016±0.455HBD + 0.180±0.021MinElP + 22.186±15.451H-Lgap – 0.034±0.012P-Area	0.798	0.637	0.587	12.56	0.651
4	$logK_d$ = -2.201±7.934 + 1.486±0.606logS – 82.824±27.164HOMO + 37.304±12.583LUMO – 3.003±0.497HBD + 0.178±0.022MinElP – 0.035±0.022Vol – 0.050±0.022AccP-Area + 0.072±0.045AccArea	0.798	0.637	0.578	10.76	0.678
5	$logK_d$ = 2.490±6.585 + 1.803±0.617logS – 97.859±31.831HOMO + 54.066±17.687LUMO – 2.912±0.460HBD + 0.187±0.022MinElP + 19.407±15.512H-Lgap + 0.614±0.484XlogP3 – 0.028±0.013P-Area	0.806	0.649	0.592	11.33	0.671
6	$logK_d$ = 4.296±6.712 + 0.908±0.464logS – 59.613±24.961HOMO + 39.678±11.903LUMO – 2.196±0.489HBD – 0.044±0.021PSA + 0.179±0.022MinElP	0.780	0.609	0.562	13.21	0.725
7	$logK_d$ = 3.847±6.634 + 1.553±0.625logS – 65.841±24.986HOMO + 46.460±12.573LUMO – 2.276±0.486HBD – 0.032±0.022PSA + 0.186±0.022MinElP + 0.753±0.496XlogP3	0.791	0.626	0.573	11.95	0.726
8	$logK_d$ = 4.296±6.628 + 1.293±0.524logS – 69.929±25.570HOMO + 32.966±12.560LUMO – 2.768±0.613HBD – 0.018±0.027PSA + 0.182±0.022MinElP – 0.025±0.016P-Area	0.791	0.626	0.573	11.94	0.723
9	$logK_d$ = 1.429±6.930 + 1.512±0.620logS – 64.262±24.905HOMO + 41.392±11.837LUMO – 2.019±0.499HBD – 0.085±0.035PSA + 0.180±0.022MinElP + 0.030±0.020Acc-Area	0.790	0.624	0.572	11.87	0.692
10	$logK_d$ = 4.682±6.674 + 1.254±0.533logS – 69.100±25.854HOMO + 34.121±12.578LUMO – 2.736±0.640HBD – 0.019±0.029PSA + 0.184±0.022MinElP – 0.035±0.027Acc-P-Area	0.788	0.621	0.568	11.72	0.726
11	$logK_d$ = 2.871±6.782 + 0.860±0.464logS – 83.386±31.590HOMO + 55.698±17.699LUMO – 2.131±0.490HBD – 0.047±0.020PSA + 0.179±0.022MinElP + 19.153±15.720HLgap	0.787	0.620	0.567	11.65	0.687

#	Hansch equation of the model	R	R^2	AdjR^2	F	R^2 test
12	$logK_d$ = 4.312±6.731 + 1.247±0.614logS – 59.168±25.037HOMO + 39.465±11.939LUMO – 2.092±0.506HBD – 0.070±0.036PSA + 0.181±0.022MinElP + 0.009±0.010Vol	0.784	0.614	0.560	11.37	0.712
13	$logK_d$ = 3.902±6.584 + 1.812±0.650logS – 74.122±25.571HOMO + 39.743±13.466LUMO – 2.768±0.608HBD – 0.010±0.027PSA + 0.188±0.022MinElP – 0.022±0.016P-Area + 0.661±0.497XlogP3	0.799	0.639	0.580	10.83	0.716
14	$logK_d$ = 2.662±6.724 + 1.456±0.631logS – 85.719±31.355HOMO + 59.631±17.773LUMO – 2.213±0.489HBD – 0.035±0.022PSA + 0.185±0.022MinElP + 0.688±0.499XlogP3 + 16.450±15.703HLgap	0.796	0.634	0.574	10.61	0.702
15	$logK_d$ = 4.218±6.639 + 1.746±0.652logS – 72.670±25.829HOMO + 41.079±13.601LUMO – 2.702±0.637HBD – 0.013±0.029PSA + 0.189±0.022MinElP + 0.654±0.505XlogP3 – 0.029±0.028Acc-P-Area	0.796	0.634	0.574	10.60	0.727
16	$logK_d$ = 1.992±6.949 + 1.797±0.680logS – 67.384±25.085HOMO + 45.833±12.613LUMO – 2.133±0.511HBD – 0.063±0.041PSA + 0.185±0.022MinElP + 0.552±0.543XlogP3 + 0.020±0.022Acc-Area	0.795	0.632	0.572	10.52	0.703
17	$logK_d$ = 3.882±6.700 + 1.604±0.673logS – 65.282±25.360HOMO + 45.928±12.931LUMO – 2.241±0.517HBD – 0.040±0.043PSA + 0.186±0.022MinElP + 0.701±0.556XlogP3 + 0.002±0.011Vol	0.791	0.626	0.565	10.26	0.726
18	$logK_d$ = 3.707±6.707 + 1.677±0.626logS – 55.350±24.195 HOMO + 50.389±12.417LUMO – 2.583±0.443HBD + 0.179±0.022MinElP + 1.025±0.465XlogP3	0.781	0.610	0.564	13.29	0.727

The±value = unstandardized coefficients±standard error of coefficients

Model 1 was chosen to be the best model based on p-value <0.05 for all descriptors in the model, R, R^2, root mean squared error (RMSE), and F-values obtained with the descriptor in that model. The model consists of 6 descriptors. This model was therefore used to calculate the predicted $logK_d$ of the molecules. The correlation matrix of descriptors included in model 1 and the statistic for this model is shown in Table 7.5 and Table 7.6,

respectively. Table 7.5 shows that MinElPot have the best correlation with $logK_d$ revealing that the binding of these molecules is strongly dependent on the distribution of charge in the molecule. This is significant because electrostatic potential gives an indication of the positive and negative charged region in a molecule which plays an important role in determining the ligand-receptor interaction. The VIF values for each descriptor in model 1 as shown in Table 7.6 are all low, with the highest value being 2.273 and p-value at 95% confidence level less than 0.05 which confirms that these descriptors are statistically significant and support that the models are not biased. This shows that there is a relationship between the selected descriptors which were used to build this model and the binding affinity of the molecules. The model gives an indication that the dissociation constant for the molecules to NgCA could be explained by electronic factors such as E_{HOMO}, E_{LUMO}, and minimum electrostatic potential.

Table 7.5. Pearson's correlation coefficient for the descriptors used in QSPR model 1

	Inter-correlation						
	$logK_d$	**logS**	**HOMO**	**LUMO**	**HBD**	**Min ElPot**	**P-Area**
$logK_d$	1.000						
logS	0.011	1.000					
HOMO	0.034	-0.2	1.000				
LUMO	0.03	0.043	0.138	1.000			
HBD	-0.222	0.595	-0.155	0.323	1.000		
Min ElPot	0.516	0.295	0.081	-0.086	0.361	1.000	
P-Area	0.028	0.408	-0.425	-0.429	0.001	0.250	1.000

Table 7.6. Statistics for model 1

Descriptor	**t-Test**	**Significance (p)**	**Tolerance**	**VIF**
Intercept	0.653	0.517		
logS	2.672	0.010	0.473	2.116
HOMO	-2.696	0.009	0.710	1.408
LUMO	2.565	0.013	0.697	1.434
Hydrogen bond donor	-6.599	0.000	0.440	2.273
Min ElPot (kJ/mol)	8.388	0.000	0.716	1.396
P-Area(75) (Å2)	-2.598	0.012	0.476	2.103

The R^2 calculated using model 1 (eqn 7.4) shows that the model explains 62.3% of the variability in the observed $logK_d$, which indicate that there is a good relationship between the descriptors used in the model and $logK_d$ of the molecules under study. Schmidt (16) also reported R^2 value of 0.61 for a QSAR model developed on some sesquiterpene lactones with antiprotozoal activity against *Trypanosoma brucei rhodesiense*, and R^2 = 0.41 for cytotoxicity. Five of the structures included in this study (**17**, **21**, **22**, **28** and **31**) were also in Schmidt (16)'s study. Table 7.7 confirms that model 1 was the best model as the calculated BIC and AIC of this model was the lowest of all the developed models.

Table 7.7. Bayesian information criterion and Akaike information criterion data used to order models from most to least stable

Model #	CV (5-fold) mean square	AIC (1)	AIC (2)	BIC
1	3.01	58.3	225	241
2	2.96	59	226	242
6	3.03	60.4	227	244
18	3.3	60.2	227	243

Validation of the model using test set data revealed that model 1 is capable of making reliable predictions of binding energy of new compounds. R^2 test (q^2) was higher (0.6967), a value greater than 0.6 which indicates that the model is valid with good predictive power. Furthermore, the residual values for each compound calculated using model 1 are low for both the training and test set compounds. The low residual value confirms that there is high agreement between the observed (computed) and predicted $logK_d$, which is an indication that the model generated has a good predictive ability. The observed $logK_d$ and predicted $logK_d$ as well as the residuals for each compound are given in Table 7.8. All the residual values were within the limit boundary of ±3 of cross-validated residuals.

Table 7.8. Calculated and predicted $logK_d$ of training set molecules using model 1

Compd #	MOL_ID	$logK_d$ observed	$logK_d$ predicted	Residual
1	a1_c2	-24.87	-23.73	-1.134
2	a2_c2	-23.68	-24.70	1.021
3	a3_c1	-23.34	-24.41	1.067
7	a7_c1	-25.60	-26.85	1.252
8	a8_c2	-23.34	-25.14	1.805
9	a9_c6	-24.66	-25.35	0.687
10	a10_c1	-24.77	-25.15	0.387
11	a11_c1	-26.72	-26.62	-0.096
12	a12_c2	-23.96	-22.10	-1.864
13	a13_c3	-23.70	-24.39	0.689
14	a14_c26	-27.28	-27.41	0.126
15	a15_c58	-24.02	-26.06	2.045
16	a16_c6	-25.71	-27.75	2.040
17	a18_c1	-24.61	-24.64	0.029
19	a19_c5	-23.74	-25.56	1.817
20	a20_c2	-24.68	-24.24	-0.439
21	a21_c1	-25.10	-25.65	0.556
24	a24_c3	-25.82	-26.71	0.891
25	a25_c2	-25.71	-26.58	0.874
26	a26_c13	-24.77	-25.37	0.594
27	a27_c3	-26.05	-23.92	-2.125
28	a28_c2	-26.12	-26.80	0.683
29	a29_c1	-24.52	-23.89	-0.627
30	a30_c1	-25.32	-24.65	-0.674
31	a31_c1	-24.44	-23.65	-0.791
35	a35_c1	-21.28	-22.70	1.419
36	a36_c1	-21.45	-22.53	1.080
37	a37_c1	-24.80	-25.52	0.722
38	a38_c1	-22.71	-22.72	0.009
41	a41_c1	-19.40	-22.84	3.446
42	a42_c1	-30.57	-29.77	-0.796
46	a46_c4	-25.64	-25.08	-0.563
48	a48_c9	-25.31	-26.08	0.773
50	a50_c4	-23.82	-26.52	2.697
51	a51_c27	-24.87	-25.59	0.720
52	a52_c24	-29.24	-27.55	-1.691
54	a54_c2	-25.00	-23.46	-1.533
55	a55_c7	-27.09	-26.59	-0.505
57	a57_c5	-26.75	-25.89	-0.857

Compd #	MOL_ID	$logK_d$ observed	$logK_d$ predicted	Residual
58	a58_c2	-22.36	-24.49	2.132
59	a59_c1	-26.51	-27.19	0.679
60	a60_c2	-26.29	-26.59	0.300
61	a61_c1	-31.22	-29.02	-2.197
63	a63_c1	-26.88	-25.10	-1.778
65	a65_c14	-21.90	-22.74	0.839
66	a66_c1	-26.25	-24.36	-1.898
68	a68_c30	-26.94	-24.70	-2.234
71	a71_c2	-27.15	-24.04	-3.106
72	a72_c3	-26.51	-23.07	-3.435
74	a74_c1	-20.93	-21.60	0.668
75	a75_c1	-21.12	-21.27	0.153
77	a77_c3	-24.12	-23.92	-0.197
78	a78_c2	-21.05	-22.63	1.586
79	a79_c4	-22.13	-21.89	-0.240
80	a80_c2	-26.26	-25.54	-0.714
81	a81_c1	-21.39	-21.32	-0.070
84	a84_c34	-29.63	-26.25	-3.370
xer	xer_c1	-20.90	-22.05	1.150

Compounds **14**, **42**, **45**, **52**,**59** and **61** fits properly with model 1 because their predicted $logK_d$ using this model was lower ($logK_d$ < -27.0) than that of the lead compound ($logK_d$ = -22.05). This suggest that these compounds form stable complexes with NgCA. Low $logK_d$ values for these compounds can be associated to their low MinElPot values (Table 7.3). The compound that gave the lowest predicted $logK_d$ value (-31.62) is compound **45,** a structure that satisfy the condition of model 1 in that it has low values of logS, LUMO and MinElPot with high values of HOMO and consisting of at least one HBD. This prediction is supported by the results obtained with docking analysis that showed that **45** interacts with NgCA inside the pocket forming 3 H-bonds. DFT calculations of the interaction with zinc-tris imidazole is also in agreement showing that **45** has the lowest free

energy of binding (-43.11kcal/mol). A combination of these three computational analyses (QSPR, docking and DFT study with NgCA model) suggesting favourable values for compound **45**, is an indication that this molecule has a very good potential as NgCA inhibitor. Other molecules with favourable QSPR prediction supported by docking and DFT study are compounds **42** and **61** having low $\log K_d$ (-30.57 and -29.02), low binding energy (-41.67 and -42.56 kcal/mol) and good binding score (-6.3 and -6.4 kcal/mol), respectively.

The plots of predicted $\log K_d$ against observed $\log K_d$ for the training and test sets is presented in Figure 7.2-7.4. A linear relationship was observed with correlation coefficient (R^2) value of 0.6225 for training set and R^2 = 0.6967 for test set which are above the accepted QSAR minimum value. The high R^2 value indicate that model 1 is of good quality. The statistical parameters comparison shows that there is no significant difference between the coefficients obtained in training set and that obtained in test set data. Figure 7.8 shows that the points from both training and test sets are scattered around the diagonal line indicating that the model fits well. The plots also show that the predicted $\log K_d$ obtained with the test set data is close to the observed $\log K_d$ which confirms the reliability of the training set. The plot of standardized residuals against observed $\log K_d$ as presented in Figure 7.5 shows that the range of residuals values is within an acceptable limit of ±2 on residual activity axis, thus no computational inaccuracy is suspected in the model.

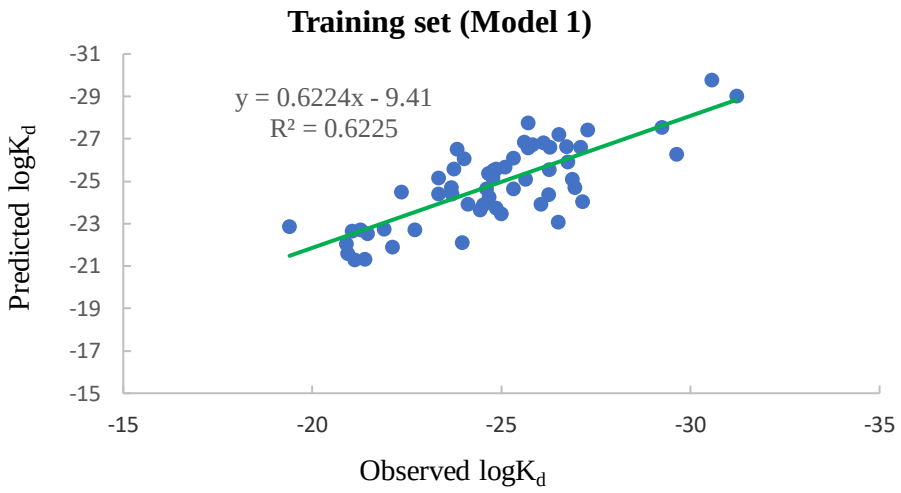

Figure 7.2. Plot of observed versus predicted $logK_d$ of the training set using model 1.

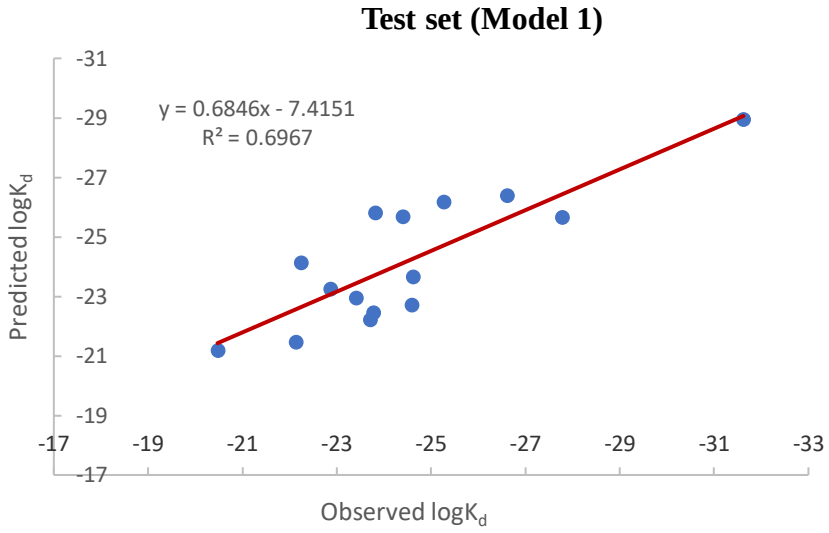

Figure 7.3. Plot of observed against predicted $logK_d$ of the test set using model 1.

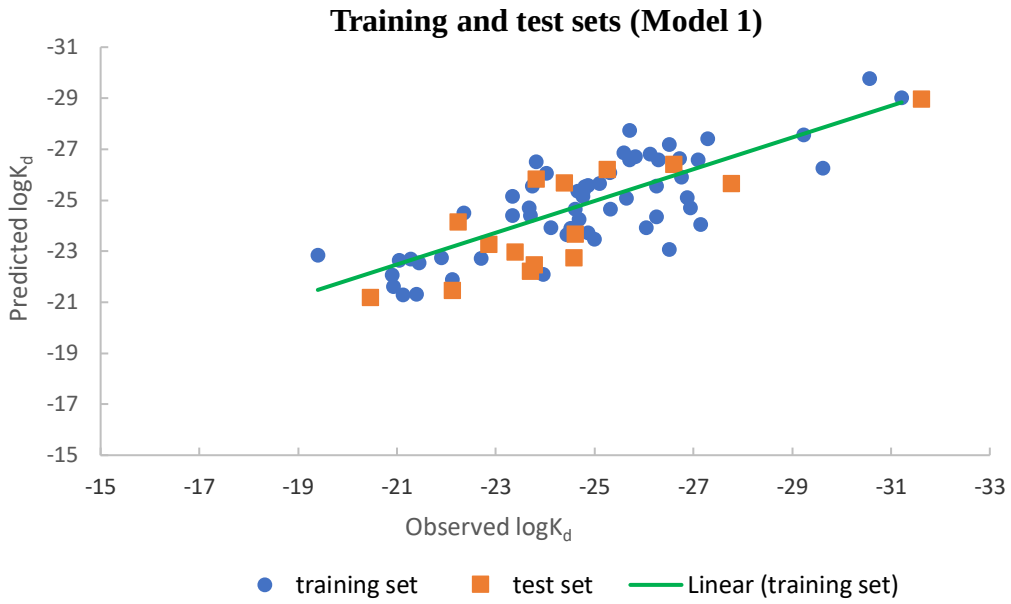

Figure 7.4. Comparison of training and test set plots.

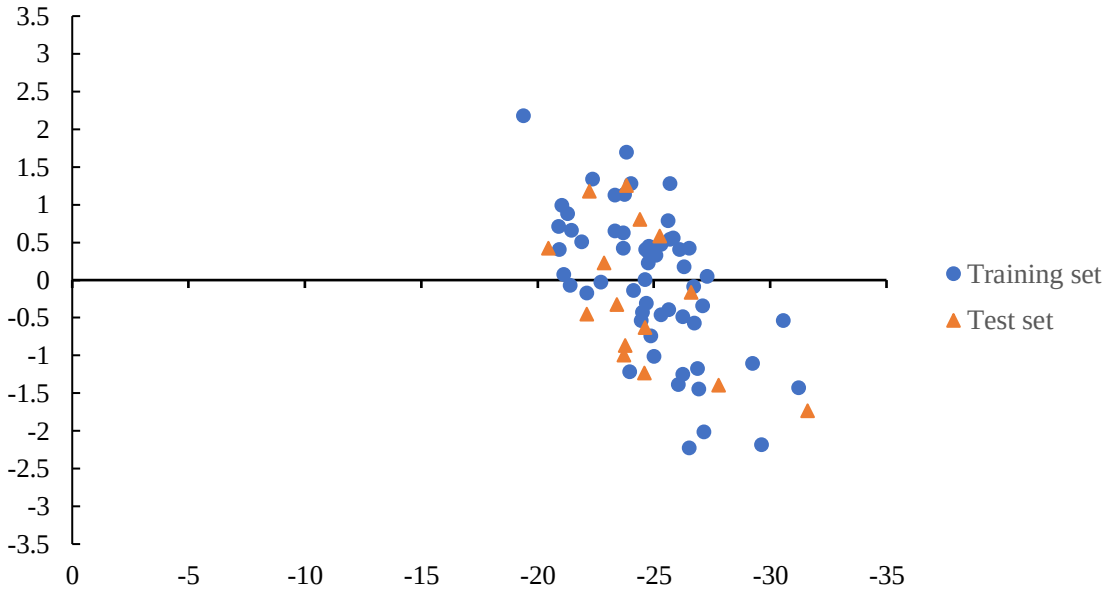

Figure 7.5. Plot of standardized residual activity against observed $logK_d$

7.3.3 PASS studies

The biological activities of all 83 compounds on *N. gonorrhoeae* were estimated by generating PASS probabilities of effects such as antibacterial, antifungal, antiparasitic, anti-inflammatory, antieczema, antineoplastic, and dermatologic. Structures with biological prediction probability of Pa ≥ 0.5 were considered. Table 7.10 shows the structures and their antibacterial activity probability values. Over 60% of the structures showed prediction of antibacterial activity, the biological activity closely related to anti-gonococcal activity. Analogue **19** gave the highest probability of antibacterial activity with Pa = 0.616, followed by analogue **20** with Pa = 0.602. The selected predicted activities for other disease models are presented in Figure 7.6. The results show that beside antibacterial activity, the studied compounds also have potential to be used for other biological activities such as antimalaria, anticancer, anti-inflammatory as well as for skin conditions. All structures were predicted to have antineoplastic activity with Pa value greater than 0.8. This highlights the potential of these compounds for drug repurposing. Table 7.9 shows which structures were predicted for the specified biological activity. Analogue 23 was predicted to have all the selected biological activities and it had Pa = 0.6 for antibacterial activity. The three compounds (**19**, **20** and **23**) that were predicted to have good antibacterial activity, all have an ester as a substituent group in the structure. This observation agrees with what Schmidt (16) reported, whereby they linked the presence of a reactive α,β-unsaturated carbonyl group of sesquiterpenes to biological activity. Other analogues that are reported to have good affinity to NgCA (Chapter 5 of this dissertation) such as **12**, **19**, **70**, and **74** also had biological activities with Pa ≥ 0.5 for all selected activities except dermatologic. This correlation between biological activities and binding

affinity can be a basis for exploring the potential of these analogues as potential anti-gonococcal agents.

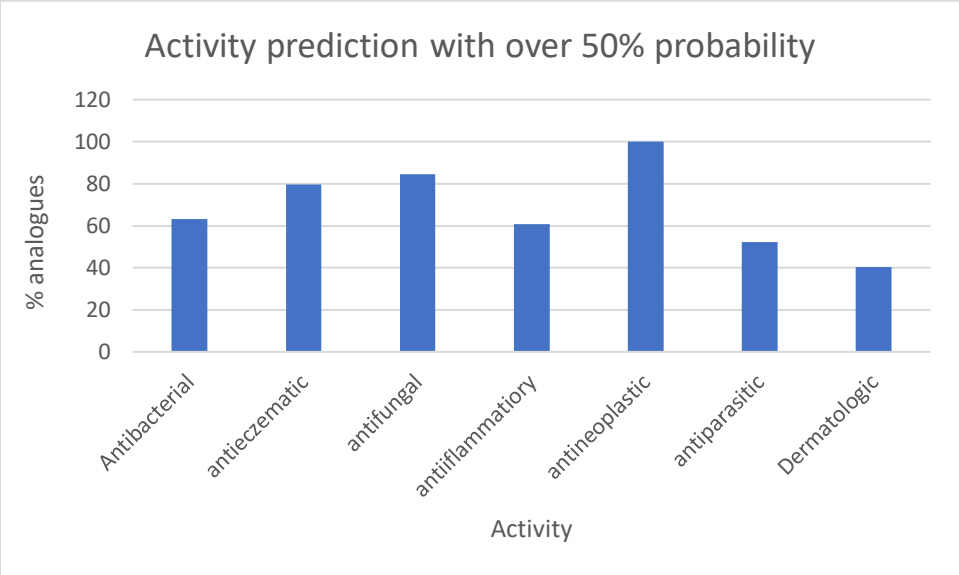

Figure 7.6. Predicted biological activity effect with Pa>50% of xerantholide and its analogues

Table 7.9. Biological effects predicted with Pa>50 and structure IDs of corresponding compounds

Activity	**Analogue number**
Antibacterial	2, 3, 4, 5, 6, 7, 11, 12, 13, 15, 17, 18, **19**, **20**, 21, 22, **23**, 24, 25, 26, 27, 28, 29, 30, 31, 32, 35, 36, 37, 38, 39, 40, 41, 43, 46, 47, 50, 54, 55, 56, 58, 60, 68, 70, 71, 72, 74, 75, 76, 80, 81, 83, xer
Antieczematic	1, 2, 3, 6, 7, 8, 9, 10, 11, 12, 13, 14, 15, 16, 17, 18, **19**, 21, 22, **23**, 24, 26, 27, 29, 30, 31, 32, 33, 34, 35, 36, 37, 38, 39, 40, 41, 42, 44, 45, 46, 47, 48, 50, 54, 55, 56, 57, 58, 59, 60, 61, 62, 63, 68, 69, 70, 71, 72, 73, 74, 76, 77, 78, 79, 81, 83, xer
Antifungal	1, 2, 4, 5, 6, 10, 11, 12, 13, 14, 15, 16, 17, 18, **19**, **20**, 21, 22, **23**, 24, 25, 26, 27, 28, 29, 30, 31, 32, 33, 34, 35, 36, 37, 38, 39, 40, 41, 42, 43, 44, 45, 46, 47, 48, 50, 54, 55, 56, 57, 58, 59, 60, 63, 64, 65, 66, 67, 68, 70, 71, 72, 74, 75, 76, 77, 78, 79, 80, 81, 83, xer
Anti-inflammatory	1, 2, 3, 4, 5, 6, 7, 10, 11, 12, 13. 16, 18, **19**, 21, 22, **23**, 24, 25, 26, 27, 32, 33, 34, 35, 36, 37, 38, 39, 40, 41, 42, 44, 45, 46, 48, 59, 60, 62, 63, 69, 70, 71, 72, 73, 74, 79, 80, 81, 83, xer
Antineoplastic*	1, 2, 3, 4, 5, 6, 7, 8, 9, 10, 11, 12, 13, 14, 15, 16, 17, 18, **19**, **20**, 21, 22, **23**, 24, 25, 26, 27, 28, 29, 30, 31, 32, 33, 34, 35, 36, 37, 38, 39, 40, 41, 42, 43, 44, 45, 46, 47, 48, 49, 50, 51, 52, 53, 54, 55, 56, 57, 58, 59, 60, 61, 62, 63, 64, 65, 66, 67, 68, 69, 70, 71, 72, 73, 74, 75, 76, 77, 78, 79, 80, 81, 83, 84, xer
Antiparasitic	2, 3, 4, 5, 7, 10, 12, 13, 17, 18, **19**, **20**, 21, 22, **23**, 24, 25, 26, 27, 28, 29, 30, 31, 32, 33, 34, 35, 36, 37, 38, 39, 41, 42, 70, 71, 74, 75, 77, 78, 79, 80, 81, 83, xer
Dermatologic	1, 3, 5, 8, 13, 18, 21, 22, **23**, 24, 26, 28, 32, 34, 35, 36, 37, 39, 42, 44, 48, 50, 55, 56, 58, 59, 60, 61, 62, 63, 64, 68, 83, xer

*Predicted with Pa>0.8. Other activities predicted with Pa>0.5 probability
All analogue ID numbers start with “a”

Table 7.10. Antibacterial activity predictions of the studied molecules and their structures

Anologue # (source/Ref)	**2D Structure**	**Antibacterial activity Pa**	**Anologue # (source)**	**2D Structure**	**Antibacterial activity Pa**
Lead structure	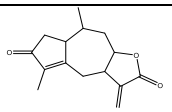	0.517	**11** (17)	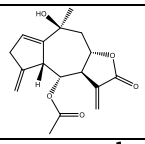	0.512
1 (PubChem)	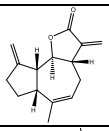	0.455	**12** (17)	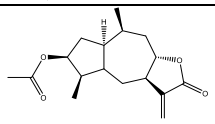	0.577
2 (18)	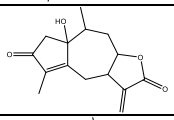	0.501	**13** (17)	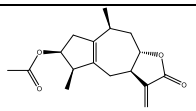	0.542
3 (18)	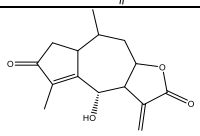	0.532	**14** (17)	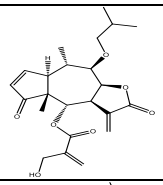	0.467
4 (18)	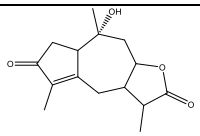	0.575	**15** (17)	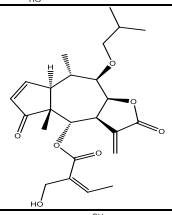	0.559
5 (18)	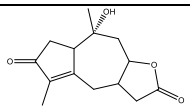	0.551	**16** (17)	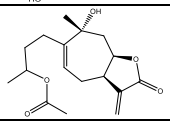	0.424
6 (17)	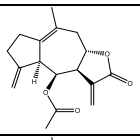	0.539	**17** (17)	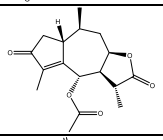	0.534
7 (17)	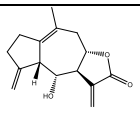	0.573	**18** (17)	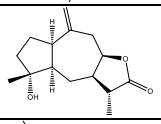	0.562
8 (17)	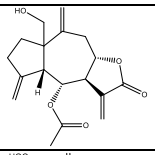	0.412	**19** (17)	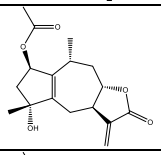	0.616
9 (17)	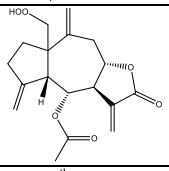	0.213	**20** (17)	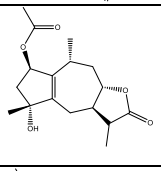	0.602
10 (17)	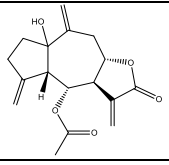	0.415	**21** (17)	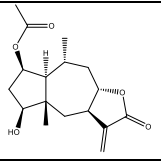	0.524

Anologue # (source/Ref)	2D Structure	Antibacterial activity Pa	Anologue # (source)	2D Structure	Antibacterial activity Pa
22 (17)	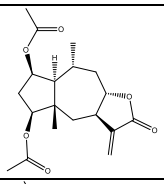	0.514	**33** (17)	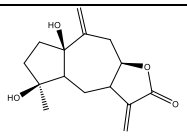	0.425
23 (17)	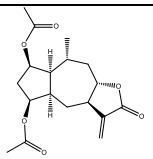	0.597	**34** (PubChem)	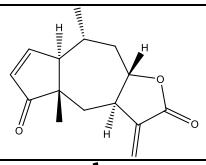	0.435
24 (17)	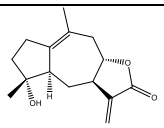	0.561	**35** (PubChem)	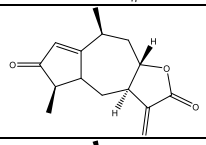	0.509
25 (17)	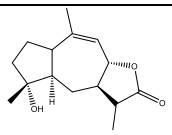	0.538	**36** (PubChem)	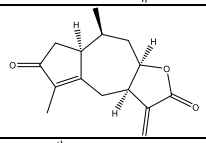	0.517
26 (17)	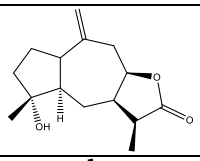	0.562	**37** (PubChem)	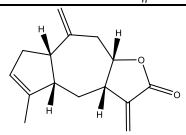	0.509
27 (17)	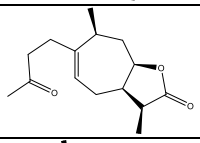	0.479	**38** (PubChem)	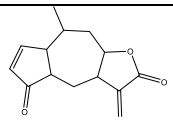	0.565
28 (19)	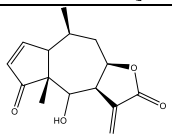	0.513	**39** (PubChem)	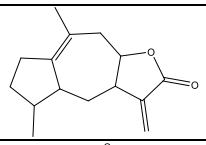	0.471
29 (19)	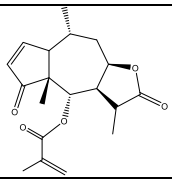	0.498	**40** (PubChem)	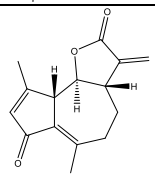	0.471
30 (19)	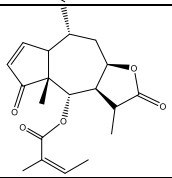	0.537	**41** (PubChem)	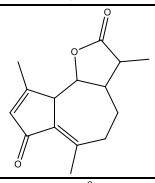	0.485
31 (19)	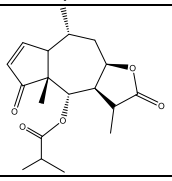	0.506	**42** (PubChem)	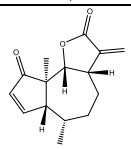	0.375

Anologue # (source/Ref)	2D Structure	Antibacterial activity Pa	Anologue # (source)	2D Structure	Antibacterial activity Pa
32 (17)	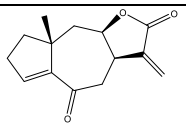	0.463	**43** (17)	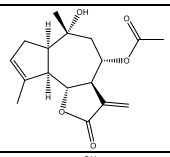	0.476
44 (17)	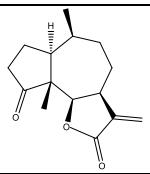	-	**55** (17)	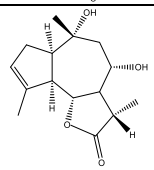	-
45 (17)	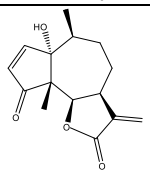	0.292	**56** (17)	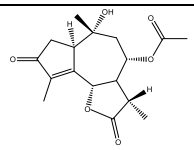	0.552
46 (17)	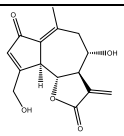	0.493	**57** (17)	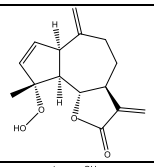	0.323
47 (17)	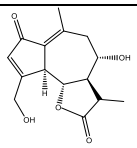	0.521	**58** (17)	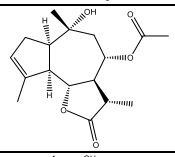	0.503
48 (17)	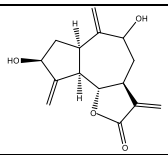	0.338	**59** (17)	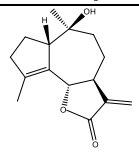	0.407
49 (18)	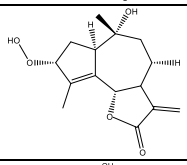	0.163	**60** (17)	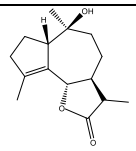	0.457
50 (17)	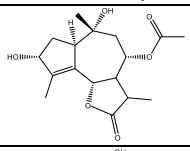	0.523	**61** (17)	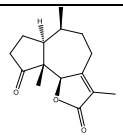	0.227
51 (17)	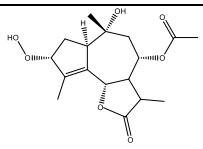	0.335	**62** (17)	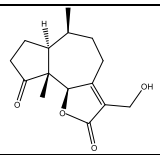	0.233
52 (17)	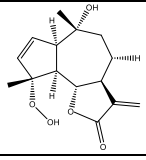	0.29	**63** (17)	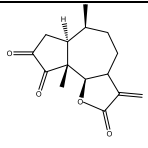	0.337

Anologue # (source/Ref)	2D Structure	Antibacterial activity Pa	Anologue # (source)	2D Structure	Antibacterial activity Pa
53 (17)	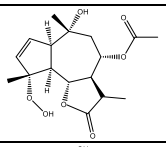	0.445	**64** (17)	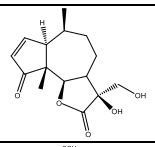	0.192
54 (17)	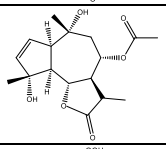	0.541	**65** (17)	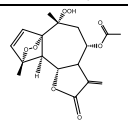	0.326
66 (17)	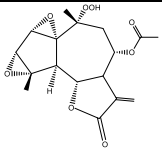	0.405	**76** (17)	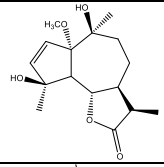	0.458
67 (17)	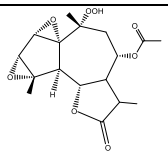	0.442	**77** (17)	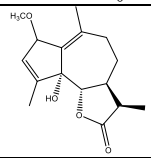	0.431
68 (17)	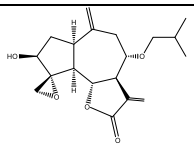	0.450	**78** (17)	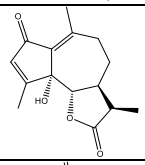	0.402
69 (17)	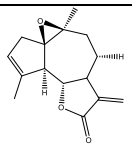	0.399	**79** (17)	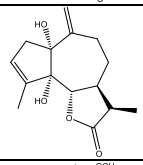	0.398
70 (17)	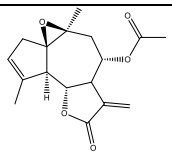	0.573	**80** (17)	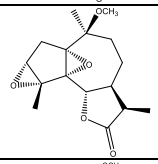	0.561
71 (17)	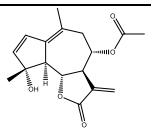	0.488	**81** (17)	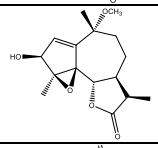	0.569
72 (17)	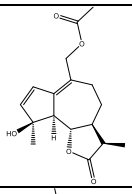	0.454	**83** (17)	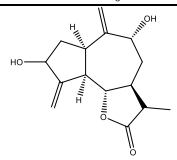	0.496
73 (17)	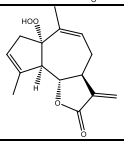	0.246			
74 (17)	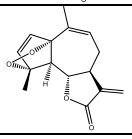	0.479			

Anologue # (source/Ref)	2D Structure	Antibacterial activity Pa	Anologue # (source)	2D Structure	Antibacterial activity Pa
75 (17)	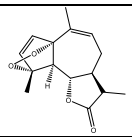	0.493			

- = no prediction obtained

7.4 Conclusion

A total of 18 QSPR models were developed which are valid for predicting the binding affinity of the studied molecules to NgCA through calculation of $\log K_d$ for protein-ligand complexes. Four of these models 1, 2, 6 and 18 were ranked to be good based on BIC and AIC criterion. The statistical parameters of these models indicate that they are valid and therefore can be used for predicting binding affinity of xerantholide derivatives. Model 1 being ranked best of the 18 models, with coefficient of the prediction R = 0.789 and R^2 = 0.623 produced a six parameters equation. The developed models suggest that structural features that strongly influence the binding of xerantholide and its analogues to NgCA are logS, HOMO, LUMO, HBD, MinElpot and P-Area, thus the binding affinity of xerantholide and analogues can be predicted based on these descriptors. The best selected model is also highly predictive giving $\log K_d$ that is consistent with the observed results that were obtained from DFT calculations of the ligand-receptor complex models. Compounds **42**, **45** and **61** satisfy the condition of model 1 as they gave lower predicted logKd when calculated with this model. PASS predictions also highlight the potential of the studied compounds to have not only antibacterial activity but also other biological activities. The results in this study can be a basis for selecting xerantholide analogues to be optimized as new anti-gonococcal agents, thereby reduce the time and cost of experimental work.

7.5 References

1. Lin X, Li X, Lin X. A review on applications of computational methods in drug screening and design. Molecules. 2020;25(6):1–17.

2. Devillers J. No-free-lunch molecular descriptors in QSAR and QSPR. In: Devillers J, Balaban A., editors. Topological indices andrelateddescriptos in QSAR and QSPR. The Netherlands: Gordon and Breach Science Publishers; 1999. p. 1–20.

3. Ivanciuc O. 3D QSAR models. In: Diudea M V., editor. QSPR/QSAR Studies by Molecular Descriptors. Huntington, New York: Nova Science Publishers; 2001. p. 233–80.

4. Patrick GL. An introdcution to medicinal chemistry. 5th ed. Oxford University Press; 2013.

5. Hazra A, Mondal C, Chakraborty D, Halder AK, Bharitkar YP, Mondal SK, et al. Towards the development of anticancer drugs from andrographolide: semisynthesis, bioevaluation, QSAR analysis and pharmacokinetic studies. Curr Top Med Chem. 2015;15:1013–26.

6. Roy K, Kar S, Das R. Statistical Methods in QSAR / QSPR. In: A Primer on QSAR/QSPR modeling: Fundamental concepts. Switzerland: Springer International Publishing; 2015. p. 37–59.

7. Chtita S, Bouachrine M, Lakhlifi T. Basic approaches and applications of {QSAR}/{QSPR} methods. Rev Interdiscip. 2016;1(September).

8. Veerasamy R, Rajak H, Jain A, Sivadasan S, Varghese CP, Agrawal RK. Validation of QSAR Models - Strategies and Importance. Int J Drug Des Disocovery. 2011;2(3):511–9.

9. Albo Hay Allah MA, Balakit AA, Salman HI, Abdulridha AA, Sert Y. New Heterocyclic Compound as Carbon Steel Corrosion Inhibitor in 1 M H_2SO_4, High Efficiency at Low Concentration: Experimental and Theoretical Studies. Journal of Adhesion Science and Technology. 2022; 1-24

10. Prasanna S, Doerksen RJ. Topological Polar Surface Area: A Useful Descriptor in 2D-QSAR. Curr Med Chem. 2009;16(1):21–41.

11. Gatnik MF, Worth AP. Review of software tools for toxicity prediction. JRC Scientific and Technoical Reports. 2010: EUR 24489 EN

12. Filimonov DA, Lagunin AA, Gloriozova TA, Rudik A V., Druzhilovskii DS, Pogodin P V., et al. Prediction of the biological activity spectra of organic

compounds using the pass online web resource. Chem Heterocycl Compd. 2014;50(3):444–57.

13. Lagunin A, Filimonov D, Poroikov V. Multi-Targeted Natural Products Evaluation Based on Biological Activity Prediction with PASS. Curr Pharm Des. 2010;16(15):1703–17.

14. Spartan'14 V1.1.0. Tutorial and User ' s Guide Preliminary Edition. Irvine: Wavefunction, Inc; 2013.

15. Sorkun MC, Khetan A, Er S. AqSolDB, a curated reference set of aqueous solubility and 2D descriptors for a diverse set of compounds. Sci Data. 2019;6(1):1–8.

16. Schmidt TJ, Nour AMM, Khalid SA, Kaiser M, Brun R. Quantitative structure - Antiprotozoal activity relationships of sesquiterpene lactones. Molecules. 2009;14(6):2062–76.

17. Awouafack MD, Tane P, Kuete V, Eloff JN. Sesquiterpenes from the Medicinal Plants of Africa. Medicinal Plant Research in Africa: Pharmacology and Chemistry. Elsevier Inc.; 2013. 33–103 p.

18. Staneva JD, Todorova MN, Evstatieva LN. Sesquiterpene lactones as chemotaxonomic markers in genus Anthemis. Phytochemistry. 2008;69(3):607–18.

19. Chaturvedi D. Sesquiterpene lactones : Structural diversity and their biological activities. Oppor Chall Scope Nat Prod Med Chem. 2011;661(2):313–34.

CHAPTER 8: SUMMARY AND CONCLUSION

Gonorrhea is a global problem and a solution to overcome antimicrobial agent resistance is needed. This study revealed that plants and their secondary metabolites are good potential sources of antimicrobial agents. These natural sources can thus help to solve the anti-gonococcal resistance problem. The first step in discovering medicinal compounds from plants is through screening of plants that are ethnomedicinally used or via random screening of plants. In this study several plant species were shown to exhibit anti-gonococcal activity at varying degrees. One of the isolated compounds with proven anti-gonococcal activity, xerantholide also showed potential as an enzyme (NgCA) inhibitor, paving a way to investigate other plant compounds as enzyme inhibitors. This mode of action is significant because it is different from the mode of action applied by the existing gonorrhea drugs. Since drug discovery process is long, costly and involve several stages (1), computational methods are usually applied to reduce time and cost spent in finding drug compounds. In this study docking analysis, DFT calculations, QSPR and PASS analysis were done to determine the mode of action, binding affinity and find sesquiterpene lactones that are potentially active against *N. gonorrhoeae*. This research fits well into the sustainable development goals (SDGs), goal 3 (good health and well-being) and goal 12 (Responsible consumption and production). Since gonorrhea is a global health threat, addressing the problem will reduce long term effects such as infertility, disseminated gonococcal infections and even maternal death, that result from untreated infections. Awareness on the sustainable use of plants in managing the disease teach communities to find ways of not overusing the valuable plants. This study had five objectives that contribute to the effort of finding new and alternative anti-gonorrhea agents.

8.1 Screening plants for anti-gonococcal activity

The first objective was achieved in which 13 selected plants that are used in Namibia to treat gonorrhea were identified and screened, not only for anti-gonococcal activity but also for other microorganisms known to cause common diseases as a way of testing antimicrobial broad-spectrum potential and opening room for drug repurpose. Six crude extracts of the thirteen plants screened exhibited anti-gonococcal activity with low MIC (2.5-5 mg/mL), therefore the results in this study support the traditional use of these plants for treatment of gonorrhea. The most active extracts were obtained from *Ziziphus mucronata, Strychnos cocculoides, Tribulus terrestris, Indigofera hofmanniana, Tallinum* sp., and *Pechuel-loeschea leubnitziae*.

8.2 Isolation and characterization of bioactive compounds

The second objective was also achieved whereby two compounds (xerantholide and hiptagin) were successfully isolated from two of the plant species whose crude extracts exhibited good anti-gonococcal activity, namely *P. leubnitziae* and *I. hofmanniana*. The activity observed for the former, was attributed to the isolated xerantholide, a sesquiterpene lactone, which was characterized by x-ray diffraction analysis. Though isolated in good yield, the compound from *I. hofmanniana,* hiptagin, did not show anti-gonococcal activity, therefore the activity of this plant is from another compound which was not isolated. These results as demonstrated with TLC confirms that plant crude extracts indeed contain a mixture of diverse groups of compounds which may or may not be active against selected microorganisms. To obtain a pure compound that has activity, several steps were followed such as bioassay guided fractionation, TLC, column chromatography, x-ray diffraction,

and NMR analysis. It is also important to note that some compounds show activity against certain microbes when they work in synergy with other compounds.

8.3 DFT study of the geometry and electronic structure of xerantholide

Using molecular mechanics, several conformations of xerantholide and those of its analogues were computed. Based on the computed steric energies and Boltzmann distribution criteria, the most stable conformers of these compounds were selected, and full geometry optimization carried out using density functional theory (DFT). In one set of the DFT calculations on xerantholide, the ionization energy, adiabatic detachment energies, and chemical reactivity indices were computed using the B3LYP variant of DFT with the 6-311++G(d,p) basis sets. In another set of calculations, the interaction of xerantholide with NgCA was studied using a model of the enzyme's active site. For the latter calculations, the B3LYP, B3LYP-D2, M06-2X, ωB97xd density functionals were employed in conjunction with the 6-311++G(d,p), 6-311++G(2d,p), 6-311++G(2df,2p) and Aug-CC-pVTZ one-particle basis sets. Objective 3 was thus achieved as the structure of xerantholide was optimized and its properties determined.

8.4 Molecular docking and modelling of xerantholide and analogues with NgCA

Molecular docking and modelling of the active site of NgCA using Zn-tris (imidazole) was performed and the analysis revealed the potential of xerantholide and its analogues as a NgCA inhibitor as these compounds attached inside the binding pocket of the enzyme. Since all structures bound to the active site of the enzyme and most of them forming

coordination with Zn (II) ion and several amino acid residues, the result is a basis for performing *in-vitro* NgCA inhibition studies of these compounds.

8.5 QSPR and PASS of xerantholide and analogues

The theoretical interaction energies were subsequently used in a QSPR study in order to relate binding energies to specific descriptors of the analogues. Finally, a PASS analysis was conducted to determine the biological activities of the compounds. Eighteen models we successfully developed and the best model of them was used in predicting the binding affinity of xerantholide and analogues to NgCA. The six descriptors that contribute significantly to the interaction of of studied sesquiterpene lactones with NgCa were shown to be, logS, HOMO, LUMO, H-bond donor, minimum electrostatic potential, and P-Area. Good correlation coefficient (R^2), F, t and low residual values confirmed the reliability and predictive ability of this model, thus can be used to predict the activity of sesquiterpene lactones analogues to xerantholide. Additionally, PASS results confirmed the potential of the studied compounds to have antibacterial activity. These results suggest that the studied sesquiterpene lactones are promising anti-gonococcal agents and that the plants are promising sources of antibacterial sources which are suitable for further investigation.

8.6 Recommendations

- Extracts from several plants exhibited anti-gonococcal activity, therefore compounds responsible for this activity must be isolated and characterized.
- Xerantholide was found to be active against *N. gonorrhoeae* and previous studies reported its toxicity against mammalian cell (2), studies that look into the ADMET

of this compound is recommended to establish the suitable concentration that will be medicinally beneficial while toxicity is minimized. QSAR studies is also recommended so as to adjust the structure to improve efficacy and reduce toxicity.

- An *in-vivo* antibacterial study is recommended in order to confirm the *in-vitro* anti-gonococcal activity of xerantholide reported in this study. This will also reveal the therapeutic effect of this drug and suitable dose.
- Xerantholide, a SL has been proven to inhibit the growth of *N. gonorrhoeae*, thus there is basis to explore other SLs. Repurposing of SLs experimentally should thus be done to find compounds with anti-gonococcal activity with enzyme inhibition mechanism of action.
- Since some plants are used in combination, it is recommended that studies on the synergistic effect of some extracts and compounds be done.
- Aqueous extracts must be studied since water is traditionally used in extraction.
- Molecular docking results suggest that xerantholide bind well to NgCA, co-crystallization of this compound to NgCA should be done to ascertain binding.
- Extracts from the studied plant extracts should be tested against other pathogens that are linked to STIs to establish whether they have activity other than anti-gonococcal activity.

8.7 References

1. Prakash N, Devangi P. Drug Discovery. J Antivirals Antiretrovir. 2010;2(4):063–8.

2. Kadhila NP, Sekhoacha M, Tselanyane M, Chinsembu KC, Molefe-Khamanga DM. Determination of the antiplasmodial activity, cytotoxicity and active compound of Pechuel-loeschea leubnitziae O. Hoffm. (Asteraceae) of Namibia. SN Appl Sci. 2020;2(8).

APPENDIX LIST

Appendix 1. Ethical clearance

ETHICAL CLEARANCE CERTIFICATE

Ethical Clearance Reference Number: SOS-0016 Date: 25 October 2021

This Ethical Clearance Certificate is issued by the University of Namibia Ethics Committee (REC) in accordance with the University of Namibia's Research Ethics Policy and Guidelines. Ethical approval is given in respect of undertakings contained in the Research Project outlined below. This Certificate is issued on the recommendations of the ethical evaluation done by the ethics committee.

Title of Project:	CHARACTERIZATION AND QUANTITATIVE STRUCTUREACTIVITY RELATIONSHIP (QSAR) STUDIES OF ACTIVE COMPOUNDS FROM SELECTED NAMIBIAN MEDICINAL PLANTS USED FOR THE TREATMENT OF GONORRHEA
Student:	MOOLA M. NYAMBE
Student Number:	200028170
Supervisor(s):	PROF CROFFAT CHINSEMBU (UNIVERSITY OF NAMIBIA)

Centre for Research Services Take note of the following:

7. Any significant changes in the conditions or undertakings outlined in the approved Proposal must be communicated to the ethics committee. An application to make amendments may be necessary.
8. Any breaches of ethical undertakings or practices that have an impact on ethical conduct of the research must be reported to the ethics committee
9. The Principal Researcher must report issues of ethical compliance to the ethics committee (through the Chairperson) at the end of the Project or as may be requested by the ethics committee
10. The ethics committee retains the right to:
11. Withdraw or amend this Ethical Clearance if any unethical practices (as outlined in the Research Ethics Policy) have been detected or suspected,
12. Request for an ethical compliance report at any point during the course of the research.

The ethics committee wishes you the best in your research.

Appendix 2. Sample collection permit

NCRST
NATIONAL COMMISSION ON RESEARCH SCIENCE & TECHNOLOGY

AUTHORIZATION OF RESEARCH PROJECTS

Authorization is hereby granted in terms of section 21 of the RST Act No. 23 of 2004, to:

Name: Moola Maritha Nyambe

Address: 1 Haseweb street, Cimbebasia,
Windhoek,
Namibia

Coworkers: Prof. K.C Chinsembu

Certificate Number (if applicable): N/A **Authorization No:** AN20181004

Type of research

Non Commercial research and the use of the resources be limited to what is specified in the proposal

Title of Research authorized:

Characterization and quantitative structure-activity relationship (QSAR) studies of active compounds from selected Namibian medicinal plants used for the treatment of gonorrhoea.

Locality:

All regions of Namibia

Duration: 15 February 2019-28 February 2020

Research/Sample collection conditions:

See page 2 under research/collection condition where applicable.

Yours sincerely,

National Commission on Research Science & Technology
15 FEB 2019
P/Bag 13253
Windhoek, Namibia
CEO Office

Ms. Enid Keramen
Acting Chief Executive Officer

Head Office:
ERF 490, Platinum Street - Prosperita, Windhoek
Private Bag 13253, Windhoek
+264 61 431 7000
+264 61 216 531
www.ncrst.na
info@ncrst.na

Innovation Hub:
Cnr Louis Raymond & Grant Webster Street
Olympia, Windhoek
+264 61 431 7099
+ 246 61 235 758

RESEARCH/COLLECTING PERMIT CONDITIONS

****

Specific Conditions

1. Prior informed consent must be obtained in writing from community representatives in the areas of the research.
2. The specimens and their derivatives may be used for the purposes of this study only and may not be patented, commercialised, donated or sold to a third party without the written consent of the Ministry of Environment and Tourism.
3. The traditional knowledge accessed remains the property of the community and shall not be shared and used without the consent of the community. Where benefits are derived from knowledge of the communities, these benefits are to be shared in a fair and equitable way with the communities.
4. For *Sesamothamnus guerichii*, a protected species, permission is granted to collect leaves not exceeding 500g.
5. For export of biological and genetic resources and their derivatives, an export permit should be obtained from the Ministry of Environment and Tourism.
6. Digital sequencing of genetic information of plants and their derivatives is strictly prohibited under this project.
7. All applicants and institutions cited in the applications are subjected to these terms and conditions.

The research permit does not exempt the holder(s) from complying with any other requirements under the Access to Biological and Genetic Resources and Associated Traditional Knowledge Act (Act No. 2 of 2017), its Regulations or any other legislation

General Conditions

1. You must report to the Park Chief warden and / or Regional Office of the Ministry of Environment and Tourism prior to arrival in fieldwork area, and must present your permit.
2. This permit does NOT entitle the holder to free entry to the protected areas or state land outside protected areas.
3. For Field work in National Parks you have to make arrangement with park management in advance prior to arrival in fieldwork area.
4. Voucher specimens should be deposited with National Museum of Namibia.
5. If you would like to export samples of specimens you must loan them from the National Museum of Namibia.
6. To conduct research work in the rhinos and elephants range all persons listed on the permit must be in possession of a police clearance certificate.
7. The permission of the land owner / communal Authority is required to work/collect on private lands/communal areas.
8. The permission of the concession holder is required to work/collect in concession areas.
9. No commercial filming will be permitted without prior approval by the Ministry of Environment and Tourism under this permit.
10. Duplicates of publications and / or final report should be made available to the Ministry of Environment and Tourism and also the final report.
11. The specimens and their derivatives may be used for the purposes of this study only and may not be patented, commercialised, donated or sold to a third party without the written consent of the Ministry of Environment and Tourism.
12. All results (raw materials) or technology derived directly or indirectly from this research must be made available free of charge without reservations to the Ministry of Environment and Tourism.
13. A report on the work conducted under this permit must be submitted to the Ministry of Environment and Tourism not later than one month after the expiry of this permit as well as to regional office in whose area research was conducted.
14. Applications for renewal of this permit must reach this office at least three months prior to the expiry of this permit.
15. Habitat destructive collecting methods must not to be used.
16. Veterinary restriction may apply in the case of movement of samples and it is the applicants' responsibility to obtain such permits.
17. Foreign (or destination) wildlife import, and veterinary import permits may be required.
18. CITES import permit from the country of the destination is required for the application of export permit for CITES – listed species.
19. All field teams must be in possession of the permit and permit copy must accompany the transport of specimens.
20. You are subject to all conditions listed on the entry permit to any of the protected areas, unless specifically exempted.
21. Failure to adhere to the conditions will lead to cancellation of the research permit.
22. It is your responsibility to make the necessary contacts and arrangements as specified above.

Appendix 3. Plant Identification report

Ministry of Agriculture, Water and Forestry

National Herbarium of Namibia (WIND)

Identification Report

Report No.: 413

30 January 2020

Collector/s: Nyambe, M.M.
Address: Ms Moola Nyambe
UNAM

Number	ID cat.	Identification
001	1	Gomphocarpus fruticosus (L.) W.T.Aiton subsp. fruticosus
002	1	Pechuel-loeschea leubnitziae (Kuntze) O.Hoffm.
003	1	Laggera decurrens (Vahl) Hepper & J.R.I.Wood
004	1	Ziziphus mucronata Willd. subsp. mucronata
005	1	Tribulus terrestris L.
006	1	Gymnanthemum amygdalinum (Delile) Sch.Bip. ex Walp.
007	1	Talinum sp.
008	1	Senna occidentalis (L.) Link

Comment:

Curator
National Herbarium of Namibia (WIND)

Identification categories: 1. Certain identification 2. Closest to 3. Certain to genus only 4. Unable to identify

Private Bag 13184, Windhoek Tel: +264 - 61 - 202 - 2021 Fax: +264 - 61 - 259 - 153 e-mail: Frances.Chase@mawf.gov.na 1

Ministry of Agriculture, Water and Forestry

National Herbarium of Namibia (WIND)

Identification Report

Report No.: 2021/420

12 March 2021

Collector/s: Moola M. Nyambe
Address: Madume Ndemfayo Avenue
Tel: 061 206 4330
Cell:0812020273
Windhoek

Number	ID cat.	Identification
009	1	Indigofera hofmanniana Schinz
010	1	Strychnos cocculoides Baker
011	1	Neorautanenia mitis (A.Rich.) Verdc.

Comment: 03: Sterile, non-Indigenous lawn species. Thus we are unable to provide positive identification.

Curator
National Herbarium of Namibia (WIND)

Identification categories: 1. Certain identification 2. Closest to 3. Certain to genus only 4. Unable to identify

Appendix 4. Supplementary file for X-ray diffraction analysis

The supplementary file for x-ray data can be accessed using the link below:

https://ars.els-cdn.com/content/image/1-s2.0-S0254629922000242-mmc1.pdf

4/27/2021 SUP File Extension - What is it? How to open a SUP file?

FILExt since 2000 Zoom Share Print View another file

♀ - 1 -

GP10 P 21 21 21 R = 0.04 : Apr 26 17:29:20 2021

==========
SUPPLEMENTARY MATERIAL
==========

BELONGING TO THE PAPER

by

Contents
==========

https://filext.com/file-extension/SUP 1/16

Appendix 5. NMR spectra of hiptagin, a compound isolated from *Indigofera hofmanniana*

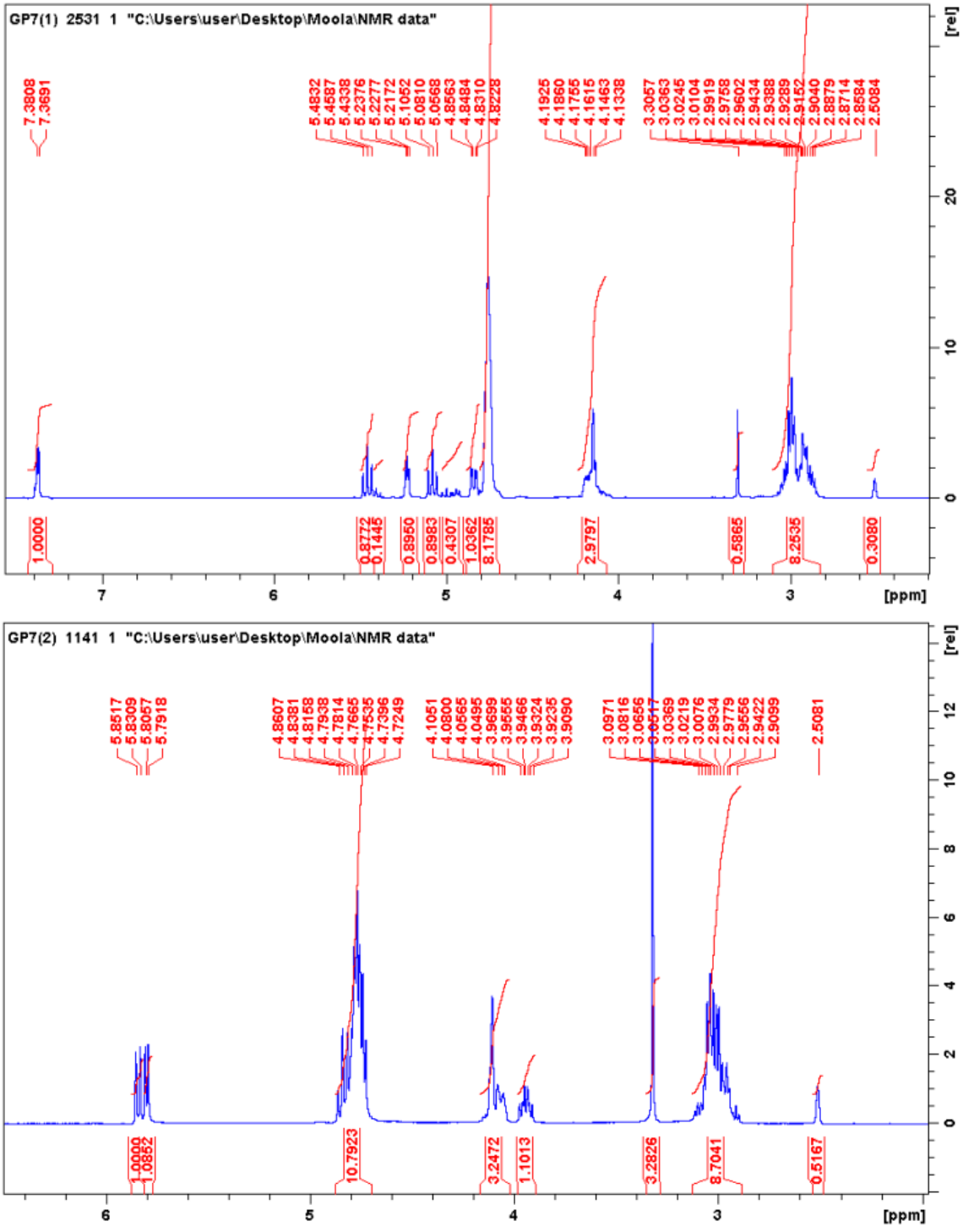

^{1}H spectrum of GP7(1) and GP7(2) in DMSO

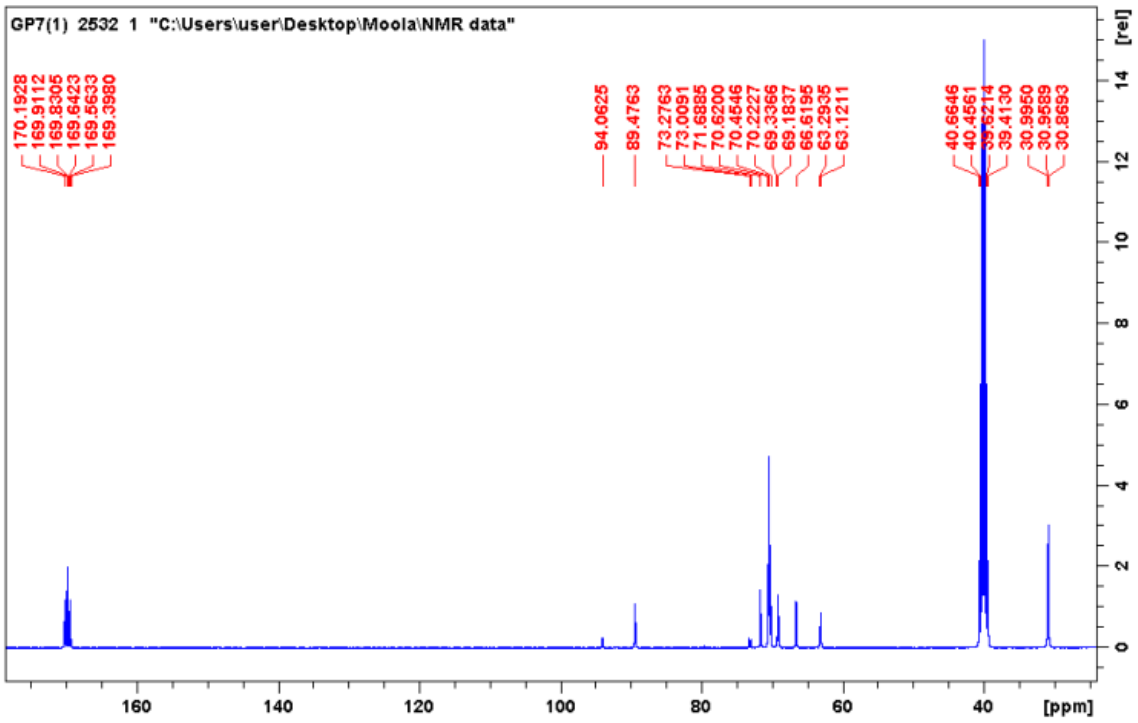

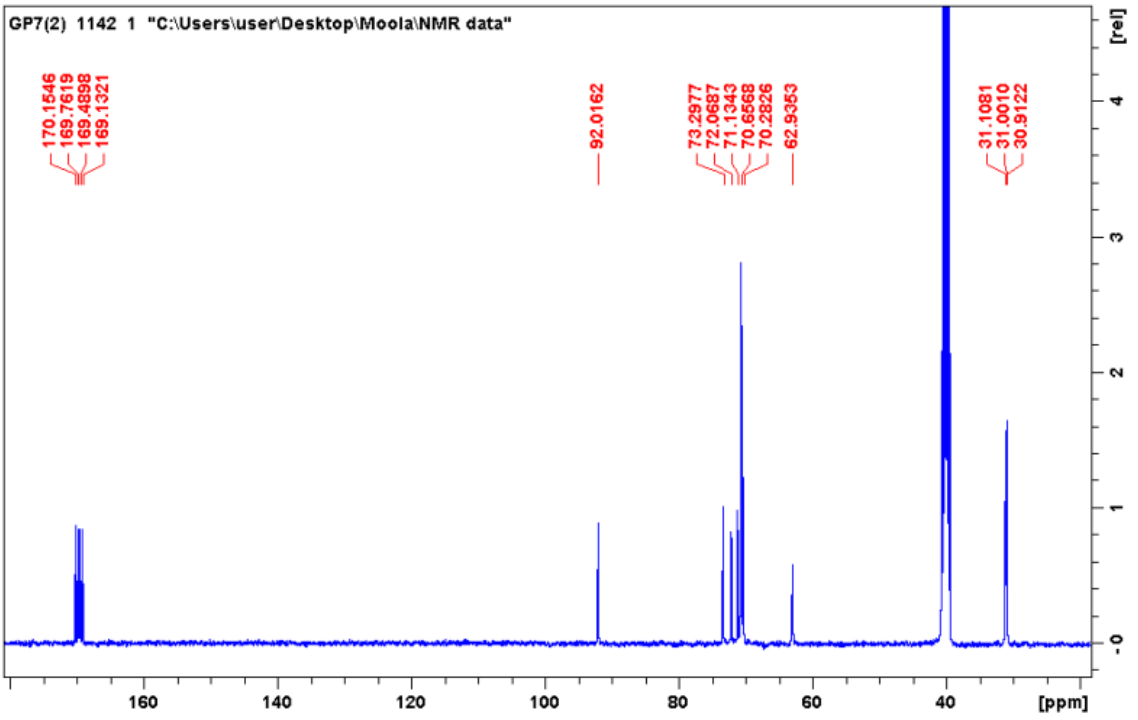

^{13}C spectra of GP7(1) and GP7(2) in DMSO

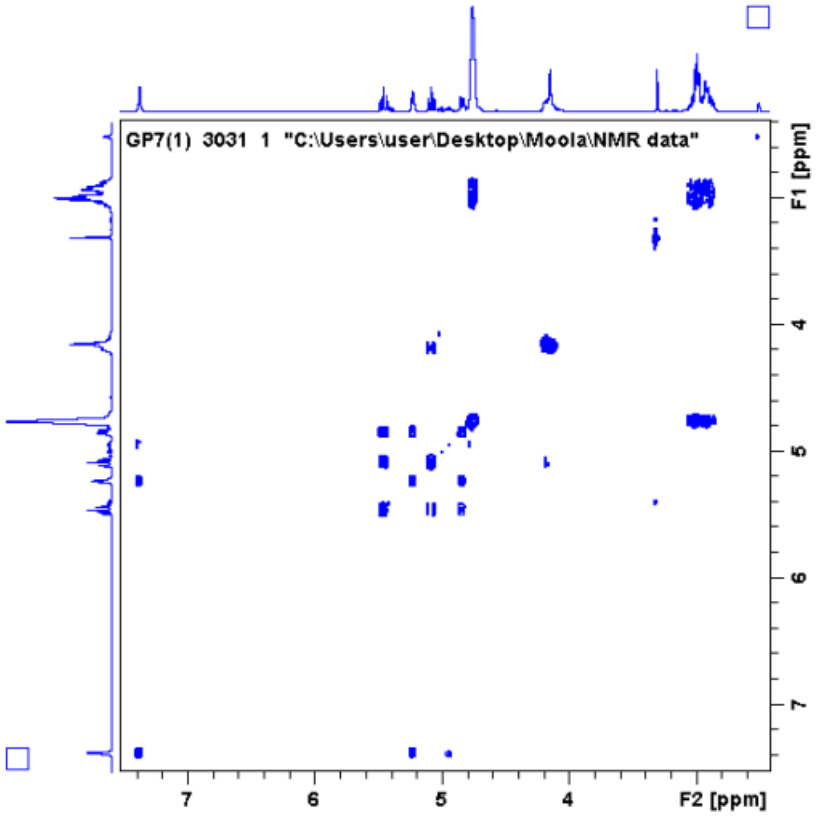

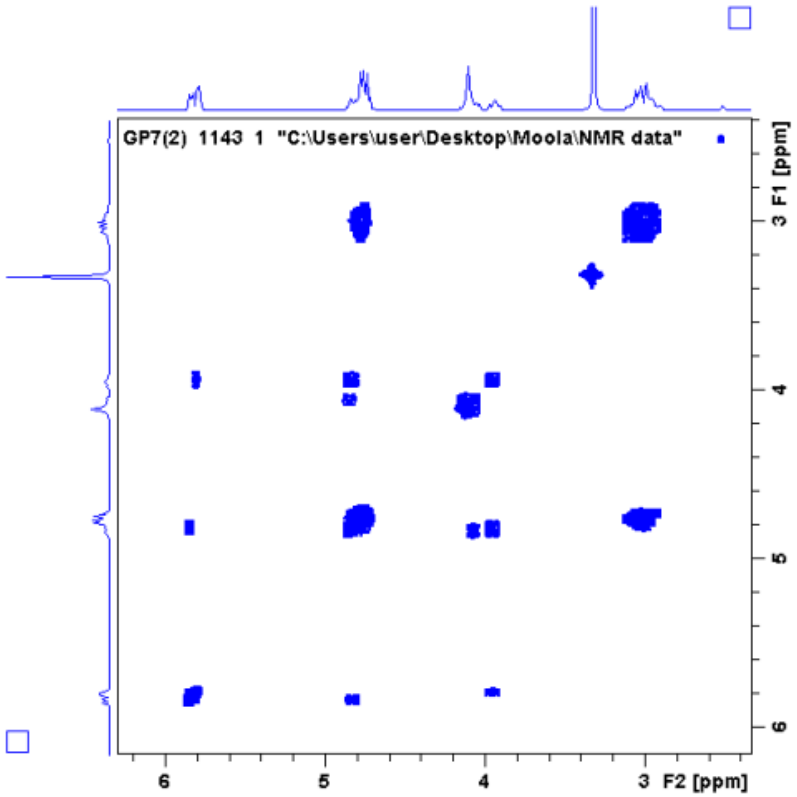

COSY spectra of GP7(1) and GP7(2) in DMSO

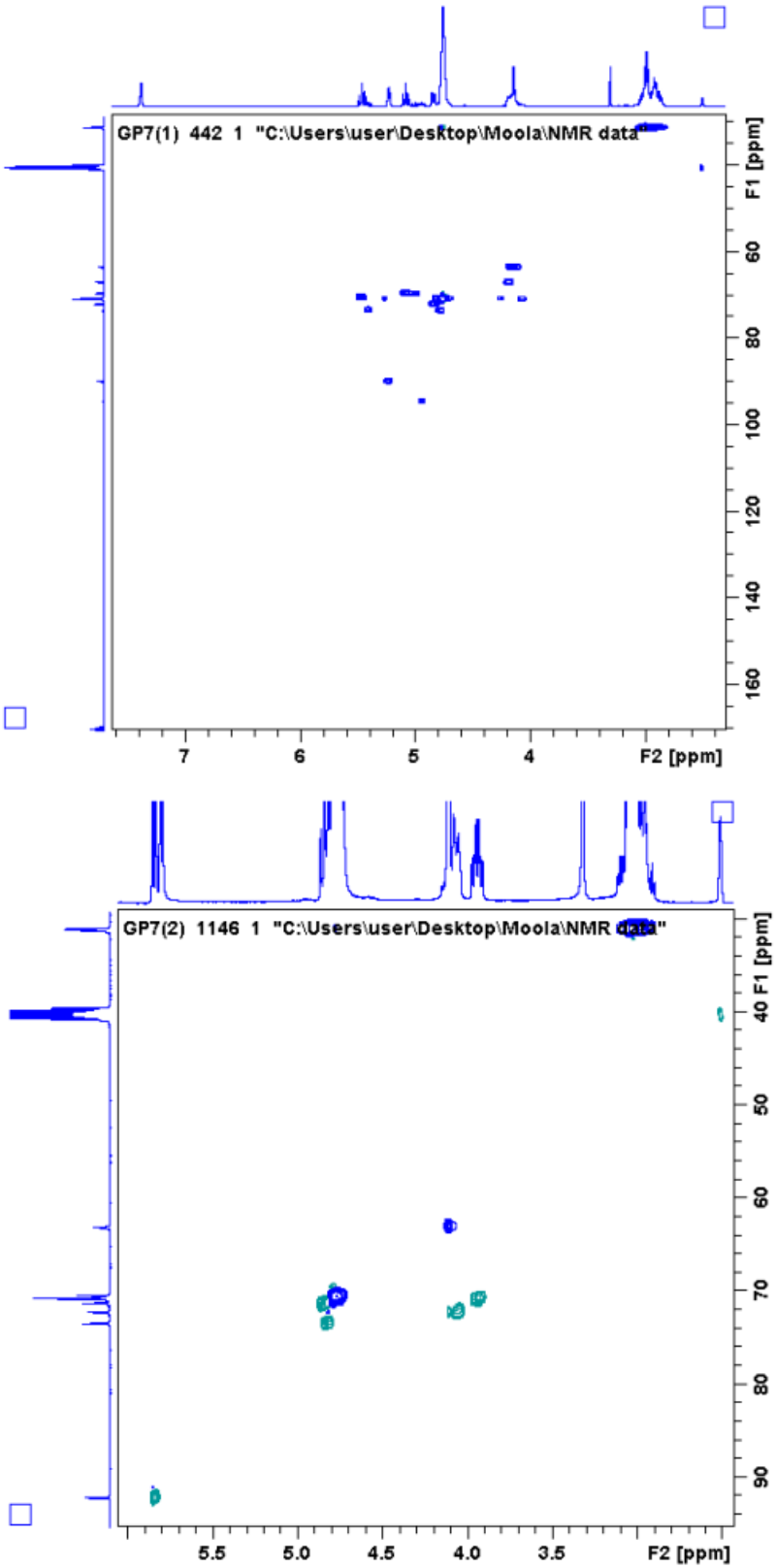

HSQC Spectrum of GP7(1) and GP7(2) in DMSO

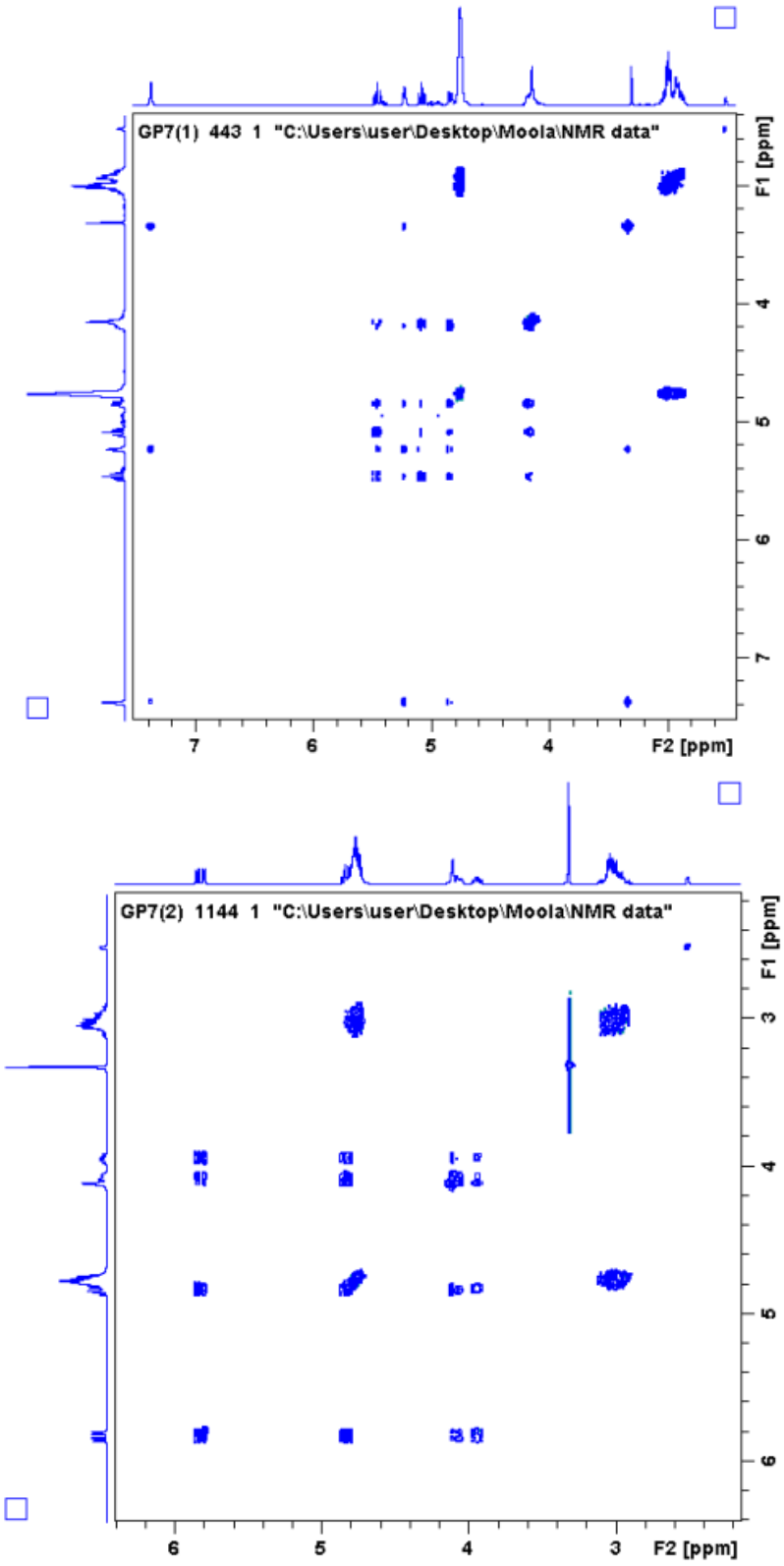

TOCSY Spectrum of GP7(1) in DMSO

Appendix 6. Supplementary material for Chapter 5

Table SP1. Total energies including zero-point energy, Gibb's free energy, of xerantholide conformers, transition state structure and interaction energies of conformer 1 with zinc-tris imidazole, calculated at B3LYP, M062x, and wB97xd levels using six basis sets.

Total Energy (a.u)		Total Energy+ZPE (a.u)	Total Energy + Gibbs (a.u)	Total Energy (a.u)	Total Energy+ZPE (a.u)	Total Energy + Gibbs (a.u)	Total Energy of Reactants (a.u)
conformer 1 (S1)	**conormer 2 (S2)**	**S1**	**S1**	**$[ZnIm_3]^{2+}$**	**[ZnIm3]$^{2+}$**	**[ZnIm3]$^{2+}$**	**S1+[ZnIm3]$^{2+}$**
-808.130405	-808.124019	-807.827300	-807.871515	-2457.441565	-2457.219759	-2457.267642	-3265.565584
-808.299887	-808.293694	-807.997858	-808.042279	-2457.751304	-2457.530190	-2457.578030	-3266.044998
-808.323828	-808.317729	-808.022773	-808.067296	-2457.777451	-2457.556583	-2457.604450	-3266.095180
-808.343356	-808.337123	-808.042232	-808.086563	-2457.791251	-2457.570530	-2457.618495	-3266.128374
-808.370573	-808.364283	-808.069019	-808.113324	-2457.822340	-2457.600837	-2457.648707	-3266.186623
-808.398115	-808.391808	-808.096801	-808.141065	-2457.991110	-2457.769800	-2457.817692	-3266.382919
-808.383971		-808.083650	-808.128120	-2457.805399	-2457.585136	-2457.633282	-2457.805399
-808.430864		-808.130018	-808.174500	-2457.850344	-2457.629430	-2457.677509	-2457.850344
-807.787742	-807.781097	-807.481316	-807.525443	-2457.099976	-2456.875421	-2456.923643	-3264.881073
-807.975257	-807.968700	-807.669436	-807.712128	-2457.432902	-2457.208835	-2457.256953	-3265.401603
-807.992437	-807.985951	-807.687537	-807.731747	-2457.454526	-2457.230950	-2457.279087	-3265.440478
-808.014397	-808.007806	-807.709682	-807.754054	-2457.470649	-2457.247348	-2457.295696	-3265.478455
-808.039012	-808.032412	-807.734178	-807.778394	-2457.499349	-2457.275449	-2457.323605	-3265.531760
-808.074461	-808.067855	-807.769672	-807.813796	-2457.661267	-2457.437631	-2457.485826	-3265.729122
-807.893538	-807.886591	-807.586358	-807.630361	-2457.232048	-2457.006968	-2457.054760	-3265.118639
-808.054941	-808.048234	-807.749080	-807.793445	-2457.533364	-2457.309142	-2457.357060	-3265.581597
-808.077640	-808.071014	-807.772664	-807.816894	-2457.558325	-2457.334544	-2457.384257	-3265.629340
-808.097168	-808.090458	-807.792249	-807.836345	-2457.572235	-2457.348538	-2457.396514	-3265.662693
-808.122335	-808.115565	-807.817042	-807.861190	-2457.601904	-2457.377480	-2457.424991	-3265.717470
-808.149109	-808.142360	-807.843851	-807.887911	-2457.771520	-2457.547216	-2457.594886	-3265.913881

Methods	Total Energy of Reactants+ZPE (a.u)	Total Energy of Reactants + Gibbs (a.u)	Total Energy of Complex (a.u)	Total Energy of Complex +ZPE (a.u)	Total Energy of Complex+ Gibbs (a.u)	Transition_State Energy (a.u)	Transition_State Energy+ZPE (a.u)	Transition_State Energy+Gibbs (a.u)
B3LYP	**S1+[ZnIm3]$^{2+}$**	**S1+[ZnIm3]$^{2+}$**	**S1_[ZnIm3]$^{2+}$**	**S1_[ZnIm3]$^{2+}$**	**S1_[ZnIm3]$^{2+}$**			
6-31+G(d)	-3265.047059	-3265.139157	-3265.636808	-3265.111034	-3265.185920	-808.108012	-807.804353	-807.847809
6-311+G(d)	-3265.528048	-3265.620309	-3266.115456	-3265.591510	-3265.666189			
6-311++G(d,p)	-3265.579356	-3265.671746	-3266.165501	-3265.642667	-3265.717229	-808.301691	-808.000050	-808.043602
6-311++G(2d,p)	-3265.612762	-3265.705058	-3266.198045	-3265.675289	-3265.749949			
6-311++G(2df,2p)	-3265.669856	-3265.762031	-3266.256205	-3265.732257	-3265.806940	-808.348403	-808.046268	-808.089776
Aug-CC-pVTZ	-3265.866601	-3265.958757	-3266.452436			-808.375963	-808.074062	-808.117595
B3LYP(disp)	-3265.668786	-3265.761402	-3266.264386	-3265.742472	-3265.815649			
B3LYP(disp)	-3265.759448	-3265.852009	-3266.355171	-3265.832151	-3265.905704			
M062x								
6-31+G(d)	-3264.356737	-3264.449086	-3264.966663	-3264.434613	-3264.508964			
6-311+G(d)	-3264.878271	-3264.969081	-3265.485979	-3264.955035	-3265.029453			
6-311++G(d,p)	-3264.918487	-3265.010834	-3265.524727	-3264.995259	-3265.069757			
6-311++G(2d,p)	-3264.957030	-3265.049750	-3265.561918	-3265.032824	-3265.107354			
6-311++G(2df,2p)	-3265.009627	-3265.101999	-3265.614895	-3265.085052	-3265.159213			
Aug-CC-pVTZ	-3265.207303	-3265.299622	-3265.813010					
wB97xd								
6-31+G(d)	-3264.593326	-3264.685121	-3265.200383	-3264.667091	-3264.741649			
6-311+G(d)	-3265.058222	-3265.150505	-3265.662840	-3265.131801	-3265.205999			
6-311++G(d,p)	-3265.107208	-3265.201151	-3265.710422	-3265.180415	-3265.253871			
6-311++G(2d,p)	-3265.140787	-3265.232859	-3265.743191	-3265.213482	-3265.287205			
6-311++G(2df,2p)	-3265.194522	-3265.286181	-3265.797698	-3265.267064	-3265.341212			
Aug-CC-pVTZ	-3265.391067	-3265.482797	-3265.993664					

Anion	Total Energy (a.u)	Total Energy + ZPE (a.u)	Total Energy + Gibbs (a.u)					
B3LYP								
6-31+G(d)	-808.153179	-807.854925	-807.899226					
6-311++G(d,p)	-808.347482	-808.051223	-808.095649					
Aug-CC-pVTZ	-808.420505	-808.123992	-808.168357					
CATION								
B3LYP								
6-31+G(d)	-807.810756	-807.510170	-807.555018					
6-311++G(d,p)	-808.003020	-807.704653	-807.749483					
Aug-CC-pVTZ	-808.078828	-807.780139	-807.825016					

Table SP2. Bond length (Å), bond angles (˚) of xerantholide conformers, anion and transition state structure

		conformer 1 (S1)			conformer 2 (S2)			anion
	x-ray	B3LYP	M062x	wB97	B3LYP	M062x	wB97	B3LYP
Bond length								
O1 - C8	1.478	1.455	1.442	1.442	1.454	1.441	1.441	1.439
O1 - C12	1.355	1.364	1.355	1.353	1.365	1.356	1.354	1.408
O2-C12	1.211	1.199	1.193	1.195	1.199	1.192	1.195	1.221
O3-C3	1.227	1.215	1.206	1.209	1.214	1.206	1.208	1.238
C1-C2	1.543	1.544	1.539	1.537	1.541	1.535	1.534	1.548
C1-C5	1.513	1.527	1.523	1.520	1.529	1.523	1.521	1.529
C1-C10	1.551	1.560	1.552	1.552	1.552	1.541	1.542	1.563
C2-C3	1.505	1.525	1.522	1.520	1.525	1.522	1.520	1.529
C3-C4	1.467	1.479	1.482	1.478	1.484	1.486	1.483	1.449
C4-C5	1.343	1.350	1.342	1.342	1.351	1.343	1.343	1.373
C4-C14	1.486	1.497	1.494	1.493	1.496	1.492	1.492	1.500
C5-C6	1.502	1.510	1.506	1.504	1.505	1.501	1.500	1.502
C6-C7	1.520	1.528	1.521	1.521	1.557	1.550	1.550	1.530
C7-C8	1.528	1.542	1.538	1.536	1.542	1.539	1.537	1.540
C7-C11	1.505	1.508	1.502	1.501	1.506	1.501	1.500	1.507
C8-C9	1.507	1.518	1.514	1.514	1.530	1.524	1.523	1.522
C9-C10	1.537	1.544	1.536	1.537	1.545	1.538	1.538	1.545
C10-C15	1.521	1.537	1.531	1.531	1.535	1.529	1.528	1.537
C11-C12	1.479	1.499	1.499	1.497	1.501	1.502	1.499	1.447
C11-C13	1.319	1.330	1.326	1.325	1.330	1.325	1.325	1.372
C1-H1	1.000	1.097	1.096	1.097	1.100			
C2-H2A	0.990	1.092	1.093	1.092	1.095			
C2-H2B	0.990	1.094	1.091	1.093	1.091			
C6-H6A	0.990	1.098	1.098	1.098	1.091			
C6-H6B	0.990	1.097	1.096	1.097	1.096			
C7-H7	1.000	1.099	1.099	1.099	1.097			
C8-H8	1.000	1.096	1.097	1.097	1.094			
C9-H9A	0.990	1.094	1.094	1.094	1.095			
C9-H9B	0.990	1.096	1.096	1.096	1.095			
C10-H10	1.000	1.096	1.095	1.096	1.096			
C13-H13A	0.950	1.084	1.084	1.085	1.084			
C13-H13B	0.950	1.084	1.084	1.085	1.084			
C14-H14A	0.980	1.095	1.093	1.094	1.095			
C14-H14B	0.980	1.095	1.091	1.095	1.091			
C14-H14C	0.980	1.091	1.094	1.091	1.094			
C15-H15A	0.980	1.093	1.093	1.093	1.094			
C15-H15B	0.980	1.093	1.092	1.093	1.093			
C15H15C	0.980	1.093	1.093	1.093	1.094			

		conformer 1 (S1)			Conformer 2 (S2)			anion	TS
	x-ray	B3LYP	M062x	wB97	B3LYP	M062x	wB97	B3LYP	B3LYP
Bond angle									
C8-O1-C12	109.2	110.7	110.7	110.8	110.5	110.3	110.4	108.8	111.1
C2-C1-C5	103.0	103.4	103.3	103.2	103.5	103.6	103.5	103.2	101.8
C2-C1-C10	111.8	113.0	112.0	112.5	117.0	116.4	116.5	112.5	114.8
C5-C1-C10	116.2	115.7	114.0	114.4	115.8	115.1	115.3	115.1	117.8
C1-C2-C3	105.7	105.8	105.6	105.7	104.9	104.5	104.8	105.9	104.9
O3-C3-C2	125.4	126.0	126.3	126.1	126.1	126.5	126.2	124.6	126.4
O3-C3-C4	126.2	126.4	126.2	126.4	126.1	125.8	126.1	128.0	126.4
C2-C3-C4	108.4	107.7	107.5	107.5	107.8	107.8	107.7	107.4	107.1
C3-C4-C5	109.3	109.9	109.6	109.7	109.5	109.1	109.2	111.3	109.0
C3-C4-C14	122.8	121.8	122.0	122.4	120.1	119.9	120.3	121.9	120.7
C5-C4-C14	128.0	128.3	128.4	127.9	130.4	131.0	130.4	126.8	130.1
C1-C5-C4	113.4	112.9	113.1	113.1	112.4	112.7	112.7	111.2	113.0
C1-C5-C6	124.2	124.0	123.9	123.9	121.2	120.4	120.6	124.6	120.7
C4-C5-C6	122.3	123.1	123.1	123.0	126.4	126.9	126.7	124.1	126.0
C5-C6-C7	115.9	115.6	114.9	115.2	112.4	111.4	111.5	114.9	112.4
C6-C7-C8	114.2	114.2	114.2	114.1	113.6	114.1	114.0	112.4	109.7
C6-C7-C11	115.1	116.8	115.9	116.4	118.1	117.6	117.9	116.6	117.1
C8-C7-C11	101.1	101.3	100.8	101.0	101.3	100.5	100.7	101.7	102.5
O1-C8-C7	104.5	105.0	105.1	105.2	105.0	105.0	105.1	105.9	106.0
O1-C8-C9	109.0	109.1	108.8	109.1	110.1	110.0	110.2	109.0	108.3
C7-C8-C9	116.0	115.9	115.6	115.6	115.4	114.8	115.0	115.6	116.7
C8-C9-C10	112.8	114.9	114.5	114.6	114.2	113.9	114.0	115.0	121.4
C1-C10-C9	112.7	113.3	113.4	113.4	115.4	115.0	115.0	113.4	120.5
C1-C10-C15	112.4	113.1	112.0	112.4	111.3	110.6	110.9	113.0	114.3
C9-C10-C15	112.7	112.5	112.4	112.5	110.6	110.3	110.5	112.3	106.4
C7-C11-C12	106.9	106.8	106.6	106.6	106.7	106.3	106.4	108.9	107.2
C7-C11-C13	130.2	131.0	131.3	130.9	130.9	131.6	131.1	127.1	130.5
C12-C11-C13	122.8	122.3	122.1	122.5	122.4	122.1	122.5	124.5	122.2
O1-C12-O2	121.5	122.8	123.3	123.0	122.8	123.3	123.0	119.6	122.8
O1-C12-C11	109.2	108.3	108.1	108.2	108.3	108.2	108.3	109.0	108.5
O2-C12-C11	129.4	128.9	128.6	128.8	128.9	128.5	128.7	131.3	128.7

		conformer 1 (S1)			Conformer 2 (S2)			TS
	x-ray	B3LYP	M062x	wB97	B3LYP	M062x	wB97	B3LYP
Dihedral angle								
C12-O1-C8-C7	-26.4	-23.9	-25.0	-24.1	-24.3	-26.5	-25.5	-18.3
C12-O1-C8-C9	-151.0	-148.8	-149.4	-148.8	-149.1	-150.5	-150.0	-144.4
C8-O1-C12-O2	-170.0	-171.7	-171.0	-171.7	-171.5	-170.3	-171.0	-173.5
C8-O1-C12-C11	11.2	8.9	9.4	8.8	9.2	10.3	9.6	6.9
C5-C1-C2-C3	3.9	5.2	9.6	8.5	-13.8	-14.9	-14.1	20.0
C10-C1-C2-C3	-121.7	-120.5	-113.5	-115.3	-142.4	-142.2	-141.7	-108.5
C2-C1-C5-C4	-1.2	-4.3	-7.5	-6.8	11.1	11.6	11.1	-16.7
C2-C1-C5-C6	176.9	174.4	173.1	173.3	-168.2	-166.2	-166.6	157.8
C10-C1-C5-C4	121.4	119.7	114.3	115.7	140.4	139.7	139.4	109.7
C10-C1-C5-C6	-60.5	-63.7	-65.2	-64.2	-38.9	-38.1	-38.2	-75.8
C2-C1-C10-C9	-164.3	-164.0	-164.5	-164.3	73.3	69.9	70.5	139.7
C2-C1-C10-C15	67.0	66.4	67.0	66.8	-53.8	-55.8	-55.7	11.0
C5-C1-C10-C9	77.8	77.2	78.7	78.4	-49.1	-51.5	-51.1	19.9
C5-C1-C10-C15	-50.9	-52.4	-49.8	-50.6	-176.2	-177.2	-177.3	-108.8
C1-C2-C3-O3	175.2	176.4	171.9	173.2	-168.5	-167.5	-168.3	165.7
C1-C2-C3-C4	-5.2	-4.7	-8.9	-7.8	12.6	14.0	13.2	-17.8
O3-C3-C4-C5	-175.8	-178.9	-176.3	-177.2	175.0	174.2	174.7	-175.7
O3-C3-C4-C14	4.4	2.0	3.8	3.2	-5.1	-6.7	-6.4	7.6
C2-C3-C4-C5	4.6	2.2	4.6	3.8	-6.1	-7.3	-6.8	7.8
C2-C3-C4-C14	-175.1	-176.9	-175.4	-175.9	173.7	171.9	172.2	-168.9
C3-C4-C5-C1	-2.1	1.4	2.0	2.0	-3.3	-2.9	-2.9	6.0
C3-C4-C5-C6	179.8	-177.2	-178.6	-178.1	175.9	174.7	174.6	-168.1
C14-C4-C5-C1	177.7	-179.6	-178.1	-178.3	176.9	178.1	178.3	-177.7
C14-C4-C5-C6	-0.5	1.8	1.4	1.6	-3.9	-4.3	-4.2	8.2
C1-C5-C6-C7	-1.5	-1.9	1.4	0.5	62.0	65.8	65.6	42.0
C4-C5-C6-C7	176.4	176.6	-178.1	-179.4	-117.2	-111.6	-111.7	-144.3
C5-C6-C7-C8	62.7	64.7	64.2	64.3	16.6	12.0	12.1	47.9
C5-C6-C7-C11	179.1	-177.5	-179.3	-178.7	134.9	129.4	129.9	164.1
C6-C7-C8-O1	153.9	154.4	154.2	154.0	156.0	157.6	157.0	146.6
C6-C7-C8-C9	-86.1	-85.1	-85.9	-85.6	-82.6	-81.5	-81.6	-92.7
C11-C7-C8-O1	29.7	28.0	29.2	28.4	28.4	30.8	29.8	21.5
C11-C7-C8-C9	149.7	148.6	149.1	148.8	149.8	151.7	151.1	142.2
C6-C7-C11-C12	-147.3	-147.8	-147.7	-147.5	-148.0	-149.3	-148.9	-137.8
C6-C7-C11-C13	28.8	31.4	30.0	30.9	31.8	29.5	30.4	41.5
C8-C7-C11-C12	-23.7	-23.2	-23.9	-23.4	-23.3	-24.9	-24.3	-17.7
C8-C7-C11-C13	152.3	156.1	153.8	155.0	156.5	154.0	155.0	161.6
O1-C8-C9-C10	-171.7	-174.8	-175.6	-175.0	151.9	153.8	154.4	158.5
C7-C8-C9-C10	70.9	66.9	66.5	66.7	33.3	35.7	35.8	39.0
C8-C9-C10-C1	-65.9	-63.9	-63.2	-63.3	52.6	52.1	51.7	7.3
C8-C9-C10-C15	62.7	66.9	65.2	65.5	180.0	177.9	178.1	139.4
C7-C11-C12-O1	8.8	10.2	10.4	10.4	10.1	10.6	10.6	7.6
C7-C11-C12-O2	-169.8	-169.2	-169.2	-169.1	-169.3	-168.8	-168.8	-171.9
C13-C11-C12-O1	-167.6	-169.2	-167.5	-168.2	-169.8	-168.4	-168.8	-171.7
C13-C11-C12-O2	13.8	11.5	12.9	12.3	11.0	12.2	11.9	8.7